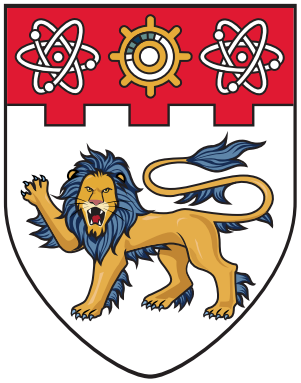

NANYANG TECHNOLOGICAL UNIVERSITY

SINGAPORE

MAGNETO-FLUIDIC MATERIALS AND SYSTEMS FOR ENERGY APPLICATIONS

PATTANAIK MEKAP SUBHASISH

SCHOOL OF MATERIALS SCIENCE AND ENGINEERING

2020

MAGNETO-FLUIDIC MATERIALS AND SYSTEMS FOR ENERGY APPLICATIONS

PATTANAIK MEKAP SUBHASISH

SCHOOL OF MATERIALS SCIENCE AND ENGINEERING

A thesis submitted to the Nanyang Technological University in partial fulfilment of the requirement for the degree of Doctor of Philosophy

2020

Statement of Originality

I hereby certify that the work embodied in this thesis is the result of original research, is free of plagiarised materials, and has not been submitted for a higher degree to any other University or Institution.

07.09.2020

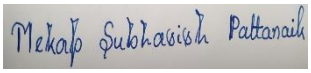

…… . . . . . .

Date Pattanaik Mekap Subhasish

Supervisor Declaration Statement

I have reviewed the content and presentation style of this thesis and declare it is free of plagiarism and of sufficient grammatical clarity to be examined. To the best of my knowledge, the research and writing are those of the candidate except as acknowledged in the Author Attribution Statement. I confirm that the investigations were conducted in accord with the ethics policies and integrity standards of Nanyang Technological University and that the research data are presented honestly and without prejudice.

08.09.2020 Raju V. Ramanujan

. . . . ……..

Date Raju V. Ramanujan

Authorship Attribution Statement

This thesis contains materials from 4 papers, out of which one is published in the following peer-reviewed journal in which I am listed as an author. Rest three manuscripts are under preparation.

1. A self-regulating multi-torus magneto-fluidic device for kilowatt level cooling. *Energy Conversion and Management*, *198*, 111819.

The content of Chapter 4 is published as "Pattanaik, M. S., Varma, V. B., Cheekati, S. K., Prasanna, G., Sudharsan, N. M., & Ramanujan, R. V. (2019). A self-regulating multi-torus magneto-fluidic device for kilowatt level cooling. *Energy Conversion and Management, 198*, 111819. DOI: 10.1016/j.enconman.2019.111819

The contributions of the co-authors are as follows:

- Prof R. V. Ramanujan came up with the initial project direction and edited the manuscript drafts.
- I prepared the manuscript. The manuscript was revised by Prof. R. V. Ramanujan.
- I developed the multi-torus magneto-fluidic cooling device and performed all the experimental study at the School of Materials Science and Engineering, NTU and at the SHARE lab, CREATE, NUS.
- V. B. Varma provided some experimental direction in the beginning and helped in revising the manuscript.
- S. K. Cheekati and G. Prasanna assisted in the numerical simulation.
- Prof. N. M. Sudharsan guided me through the analytical calculations and numerical simulation.

06 September 2020

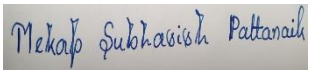

. . . . . .

Date

. . . . . .

Pattanaik Mekap Subhasish

Abstract

Magnetic cooling (MC) is a thermal management passive heat pump technology based on the thermomagnetic convection (TMC) of a ferrofluid (FF). Thermomagnetic convection is the phenomenon of convective heat transfer by the motion of a FF, induced by the combined effect of thermal gradient and the local variation in the fluid's magnetization, in the presence of an external magnetic field. TMC results from the temperature dependent magnetization of a differentially heated FF, which results in a non-uniform magnetic volume force. Such heat pumps do not need any external power, are vibration free, noiseless and require minimum maintenance. Hence, they offer enhanced reliability, low maintenance cost, little or no external energy requirement, and are environmentally friendly.

Such magnetic cooling (MC) technology can replace conventional liquid-based cooling technologies due to the absence of mechanical moving parts and its capability to self-regulate over a range of heat load temperatures and power values. Earlier research on MC systems have been intended for cooling microscale and small-scale devices. However, large scale applications of MC systems are still a challenge due to limitations such as device length scale, flow channel diameter, device geometry, form factor, heat load power, temperature, FF volume, and low boiling point carrier fluid. Also, there are no experimental and numerical investigations on the effect of device and FF parameters on MC.

Hence, the aim of this research is to investigate the cooling performance of large-scale MC devices, capable of cooling high power heat loads and transferring waste heat over long distance. Experimental and numerical study of enhanced thermomagnetic cooling performance based on device and ferrofluid parameters are also studied.

The major research findings of this thesis work are the demonstrations of the capability of novel passive magnetic cooling (MC) systems to cool high power heat loads and to transfer waste heat over longer distances. This work also reported device and ferrofluid (FF) parameters which can significantly increase the cooling performance. This work identified the optimum combination of device configuration, magnet position, and FF properties for magnetic cooling of the heat load. The research findings are further described in the subsequent paragraphs.

A multi-torus MC device, capable of kilowatt level cooling, has been fabricated and its cooling performance assessed. The heat load temperature drop improved from 148˚C to 214˚C when heat load power was increased from 0.5 kW to 1 kW, respectively, demonstrating the self-regulating nature of the device. The heat load cooling performance was evaluated for various magnet positions. Simulated surface velocity vector plots revealed ferrofluid vortices near the heat load, resulting in enhanced mixing of hot and cold ferrofluid, leading to improved cooling. The present device offers lower thermal resistance per unit length and lower ferrofluid thermal resistance per unit volume of FF compared to conventional heat pipes.

The effect of device characteristics and properties on the cooling performance was also investigated. The effect of thermal conductivity of the tube of the device and device geometry on the cooling profile was determined. We developed several racetrack shaped magnetic cooling devices with low device footprint and high thermal conductivity. A hybrid copper-silicone device exhibited highest temperature drop of 123°C for a heat flux value and initial heat load temperature of 3.47 kW/m^2 and 197°C., respectively. The complete copper device cooled the heat load even when the magnet was placed away from the heat load region. Interestingly, the extent of cooling was higher for a hybrid device with higher silicone content.

Magnetic cooling devices with simple geometry can transfer heat over long distances. An 8 m long racetrack MC device was developed for the first time, and its cooling performance was studied. The extent of heat load cooling was examined over a wide range of heat flux values. This device transported heat from devices with heat flux values of up to 8.85 kW/m^2. The drop in temperature is up to 41°C for a heat load temperature of 197 °C. The local Nusselt number exhibited a maximum near the magnet, enhancing heat load cooling.

The performance metrics, non-dimensional parameters, and heat load cooling were calculated to analyze the TM cooling performance of various ferrite and metallic based FF. The resultant magnetic pressure, friction factor, power transferred, and the exergy loss were derived as a function of magnetic and thermophysical parameters to predict the performance of FF based MC devices. Numerical simulations were performed to investigate the effect of magnetic properties of the nanoparticles viz., bulk saturation

magnetization, Curie temperature, pyro magnetic coefficient, and initial magnetic susceptibility on the cooling performance. Ferrite ferrofluids prepared from γ-Fe_2O_3, Fe_3O_4, and $CoFe_2O_4$ exhibited superior cooling. For metallic/alloy-based ferrofluids, FeCo ferrofluid exhibited the best cooling performance followed by Fe and FeNi ferrofluids. Bulk saturation magnetization of the suspended magnetic nanoparticles in the FF and the viscosity of the FF were the parameters which significantly enhanced the convective heat transfer and the heat load cooling. These results can be used to select the optimum ferrofluid for enhanced TM cooling.

The novelties of this thesis work are manifold. We developed a multi-torus MC device to cool heat loads having power and temperature as high as up to 1 kW and 580°C, respectively. Secondly, circular and race-track shaped MC devices having different form factors were developed for the first time from copper, silicone, and hybrid (copper + silicone) tubes. The hybrid and copper-based racetrack shaped MC device yielded significant heat load cooling of 121°C and 113°C, respectively, for an initial heat load temperature of 200°C. An 8 m perimeter length racetrack shaped MC device was developed, and its cooling performance was evaluated for the first time. The long-distance heat transfer and cooling performance was investigated for a wide range of heat load power density and temperature values, relevant to low-grade or medium-grade waste heat values. Finally, the device performance was modelled with respect to the magnetic properties of suspended MNP and the thermophysical properties of the FF. It was predicted that Fe_3O_4, $CoFe_2O_4$, and FeCo ferrofluids should exhibit the best cooling performance.

These experimental and numerical investigations are useful to find the conditions for obtaining the best cooling performance. Two large-scale MC systems were developed and investigated for their use in cooling of high-power heat loads and transferring waste heat over long distances. The performance can be further improved by using a low viscosity, and highly magnetic FF. A hybrid MC device, due to the presence of larger thermal gradient regions, can improve the cooling performance significantly. These developed self-regulating, and passive magnetic cooling devices may meet specific industrial and household cooling needs, increasing their efficiency, service life and reliability.

Lay Summary

The global energy crisis is a major challenge of the present world. Moreover, a significant fraction of the input energy gets wasted in the form of heat, vibration, and noise. Waste heat can have an adverse impact on the reliability, efficiency, and service life of many systems. Conventional cooling systems have low efficiency and utilize additional energy for the removal of the waste energy. Therefore, a passive thermal management technique is the need of the hour. Magnetic cooling is one such passive cooling technique that relies on the principle of thermomagnetic convection. To develop magnetic cooling solutions for large-scale cooling applications, they must be able to carry high amount of waste heat away from the heat load to the heat sink and should be able to transfer the heat over long distances. Taking these factors into consideration, we have developed several magnetic cooling devices capable of cooling high power and high temperature heat loads.

A multi-torus magnetic cooling device, capable of cooling kW level heat loads was designed and its cooling performance was investigated. This device can passively cool a 1 kW heat load from an initial temperature of 580°C to 366°C. Simulations also revealed that ferrofluid vortices give rise to enhanced cooling due to the disruption of a thermal boundary layer near the heat load.

To improve the cooling, the performance was tested against a range of device parameters viz., tube material, device geometry, form factor and device footprint. Hybrid racetrack magnetic cooling devices made up of both copper and silicone tubes were designed and exhibited superior cooling performance due to the presence of larger thermal gradient regions. The all-copper racetrack device offered faster cooling rate, whereas the hybrid racetrack device gave rise to improved temperature drop. Due to the superior thermal conductivity of copper, the all-copper device exhibited cooling even for positions of the magnet away from the heat load. Based on these results, an 8 m long magnetic cooling device was developed using copper tubes and its cooling performance was investigated. This device transported heat from devices with heat flux values of up to 8.85 kW/m^2. The drop in temperature is up to 41°C for a heat load temperature of 197 °C.

To study the effect of ferrofluid parameters on magnetic cooling, the performance metrics, non-dimensional parameters, and heat load cooling were calculated for various ferrite and

metallic/alloy based ferrofluids. Ferrite ferrofluids prepared from γ-Fe_2O_3, Fe_3O_4, and $CoFe_2O_4$ exhibited superior cooling. For metallic/alloy-based ferrofluids, FeCo ferrofluid exhibited the best cooling performance followed by Fe and FeNi ferrofluids. Bulk saturation magnetization of the suspended magnetic nanoparticles and the viscosity of the ferrofluid enhanced the heat transfer and cooling significantly.

Acknowledgements

First and foremost, I would like to express my solemn appreciation to my supervisor Prof. Raju V. Ramanujan for his constant support, thorough guidance, motivation, enthusiasm, and encouragement throughout the PhD work. He has provided me the valuable time and inspired me at all phases. His belief and confidence helped me develop as an independent researcher.

I would like to thank the financial support of the National Research Foundation, Prime Minister's Office, Singapore through its Campus of Research Excellence and Technological Enterprise (CREATE) program on Nanomaterials for Energy and Water Management (NEW). I am very thankful to all the staff members in CREATE who helped me in the smooth conduction of the research, irrespective of the time.

Besides my supervisor, I would like to thank Dr. Vijay, Dr. Varun, Dr. Harshida, Dr. Vinay, and Dr. Liping for their insightful inputs, encouragement, and for their hard-posed questions, which helped me widen my research perspective. I would also like thank Suneel, and Prasanna for their salient inputs in my research work. I would also like to appreciate my fellow lab mates Dr. Jessie Wang, Dr. Deepak, Dr. Tan Xiao, Dr. Yaoying, Dr. Sankara, and Dr. Zviad for their love and support. In addition, I thank my friends, and seniors from other labs for their indirect support during my time at MSE, NTU.

My sincere thanks also go to the School of Materials Science and Engineering, Nanyang Technological University for providing me the required sophisticated facilities for carrying out my research. I am grateful to the faculty members of school of MSE who shared million worth of funny and fruitful moments, be it during colloquiums, seminars, MSE Day, or Friday Tea sessions. I am also thankful to the ever cheering, frisky and helping staffs of MSE Gan Ji Li, Patrick, Wilson, Nelson, Poh Tin, Swee Kuan, Derrick, YY, Alan, Sam, Teddy, Liu Weiling, and Pio for their continual assistance.

I would like to dedicate all my success to my parents, my family members, my fiancée, and in laws for constantly believing in me and supporting me in all possible manner, and providing me the personal space to work freely. I would also like to thank all my teachers, my friends, and my past institutions for bestowing on me the courage and the capability

for research. Last but not the least, my heartfelt gratitude to the juggernaut, the almighty “Lord Jagganath”, for his blessings that laid the foundation towards a bigger journey.

Table of Contents

Table Captions

Figure Captions

Abbreviations

Acronym	Expansion
EHD	Electrohydrodynamics
FF	Ferrofluid
FHD	Ferrohydrodynamics
LOC	Lab-on-a-Chip
MC	Magnetic cooling
MEMS	Magneto electromechanical system
MF	Magnetic fluid
MHD	Magnetohydrodynamics
MNP	Magnetic nanoparticle
MR	Magnetorheological
TM	Thermomagnetic
TMC	Thermomagnetic convection

Chapter 1

Introduction

Current technology demands better passive cooling methods to tackle the problem of device overheating and consequent performance degradation. Thermomagnetic convection is a promising passive heat transfer technique which utilizes a magnetic fluid as a heat transfer medium. It has the potential to cool many devices and systems. Such systems include electronic chips, CPUs, data servers, battery cabinets, solar panels, and industrial machines. A magnetic fluid, also known as a ferrofluid, is a stable colloidal dispersion of coated magnetic nanoparticles in a carrier fluid. Due to the temperature and magnetic field dependence of magnetization of the ferrofluid, the motion of the ferrofluid can be controlled and manipulated by a temperature gradient and an external magnetic field. However, practical applications of this technique are still a challenge. The present thermomagnetic convection based magnetic cooling devices operate over short distances and can only cool low thermal power loads. Hence, the development of novel magnetic cooling systems for cooling of kW power range heat loads is addressed. Cooling with the heat load and the heat sink separated by several metres has also been studied. The present work also investigated lower cost hybrid magnetic cooling devices for improved thermomagnetic cooling. A simulation-based ranking was performed by considering several metallic and soft ferrite materials based ferrofluids. The cooling performance was assessed as a function of nanoparticle saturation magnetization, pyro-magnetic coefficient, volume fraction and ferrofluid thermophysical properties.

This chapter includes the motivation, significance, problem statement, objective, and novelty of this work.

1.1 Overview

The global energy crisis is a major challenge due to diminishing non-renewable energy resources, limited utilization of alternative renewable forms of energy, low energy efficiency, increasing demand for energy due to the soaring population and expectations of a higher standard of living [1, 2]. A significant fraction of input energy that is provided to devices and systems is lost to the surroundings as heat, vibration, and noise, amplifying the energy challenge. According to energy data from Lawrence Livermore National Laboratory, a significant fraction of total energy in the United States is wasted due to inefficient industrial processes and equipment [3, 4]. Waste heat is a by-product from heat engines and systems, as predicted by the laws of thermodynamics [5]. The rapid depletion of fossil fuels, global warming and high energy costs are major factors which drive R&D on the capture and reuse of waste heat. Ideally, waste heat should be utilized in other processes as an energy input instead of being allowed to dissipate to the ambient [6].

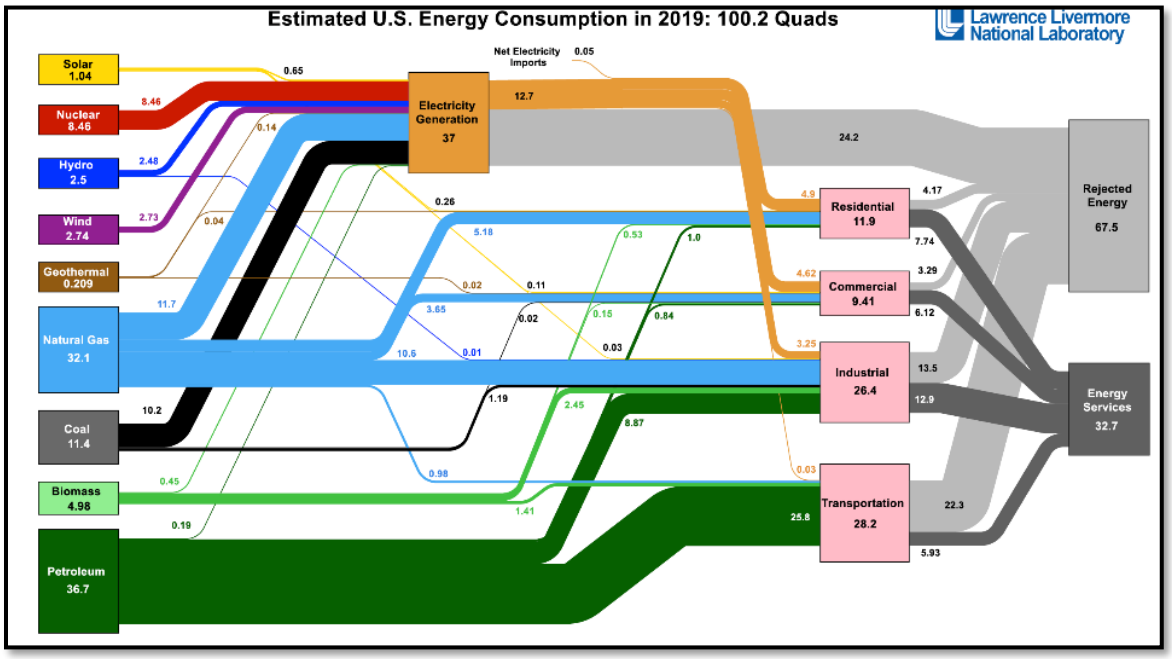

Figure 1.1. Statistical data on the estimated U.S. energy consumption showing input energy to different industrial sectors and the total fraction of utilized and rejected energy, produced by Lawrence Livermore National Laboratory [3].

According to the second law of thermodynamics heat engines produce a certain amount of waste heat, either low-grade, medium-grade or high-grade waste heat (**Figure 1.2**(a)) [6].

Figure 1.2(b) represents the overall energy consumption and amount of waste heat in the United States with and without a heat recovery system [6]. Waste heat is produced in, e.g., power generation units, industrial operations, vehicles, electronic components, and biological processes. **Figure 1.3** shows the amount of waste heat generated from various industrial sectors and the corresponding temperature range [7]. Based on the waste heat temperature range, it can be classified into 3 categories, viz., low-grade (<100°C), medium-grade (100°C-400°C), and high-grade (>400°C) waste heats. A major fraction of the waste heat falls in the low-, and medium-grade category (**Figure 1.3**). Thus, recovery of waste heat can have a significant impact in addition to the increased reliability, efficiency, and service life of the systems.

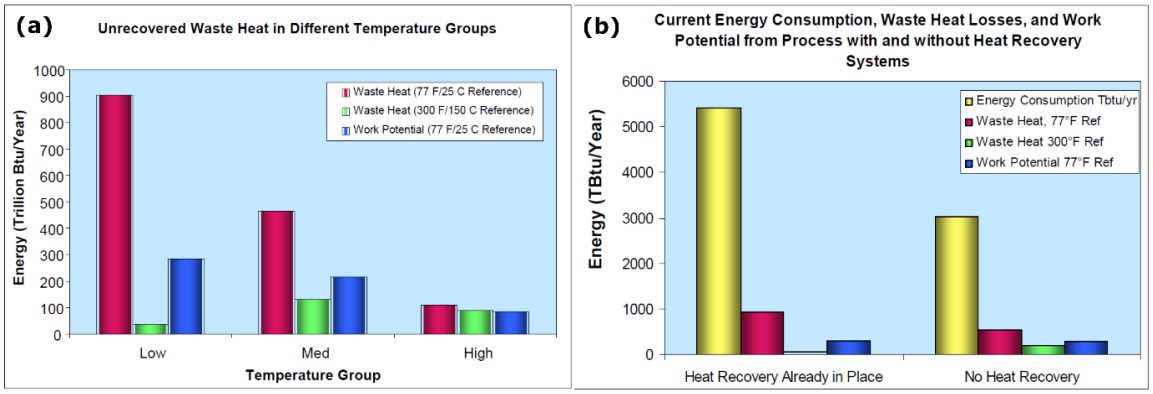

Figure 1.2. (a) Unrecovered waste heat in low-, medium-, and high-grade temperature ranges, (b) overall energy consumption, waste heat loss with and without the heat recovery system [6].

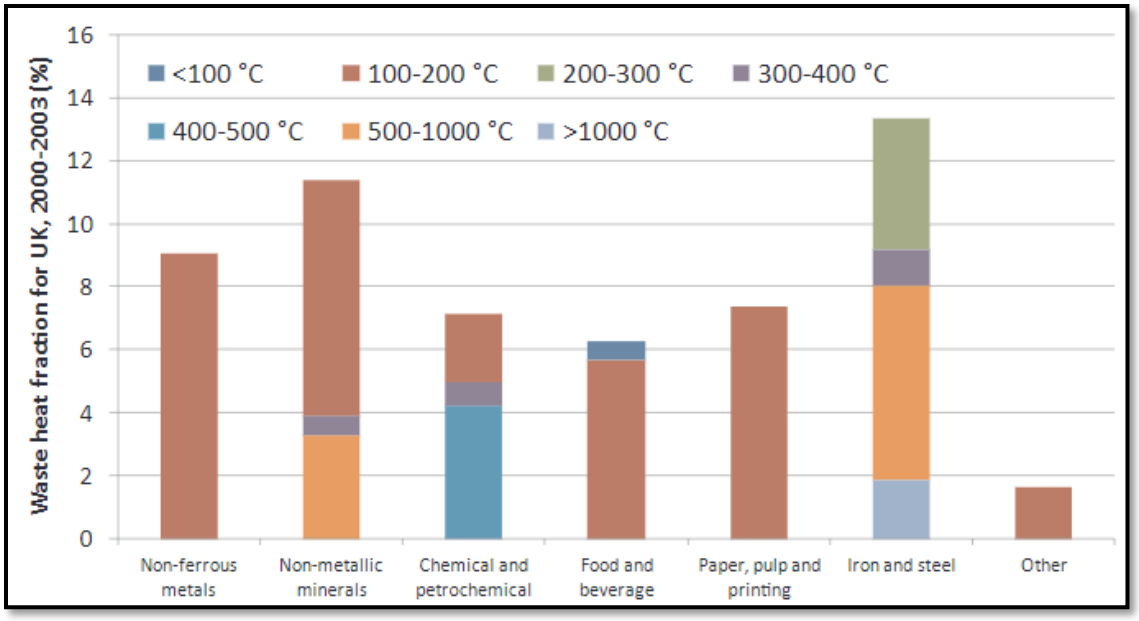

Figure 1.3. Fraction of waste heat and the temperature level of various industries in the UK [7].

Cooling of such waste heat loads can be either active or passive [8]. Active cooling systems can generally cool heat loads faster than passive cooling systems since active cooling systems rely on external energy, e.g., a fan to enhance heat transfer. Active cooling methods include cooling using forced air by a fan, forcing liquid on the top of hot surfaces using an external pump, or thermoelectric devices. However, the major disadvantage of an active cooling mechanism is its requirement of external power, resulting in higher cost [8, 9], vibration, noise, and maintenance [9]. On the other hand, passive cooling systems do not require external energy, are silent, vibration free and require low maintenance [8]. The driving force in such passive systems result from the difference in the temperature-dependent properties of a fluid or material under a thermal gradient [10, 11]. This thermal gradient is a natural consequence of the temperature difference between heat load temperature and heat sink temperature. The cooling rate in the passive cooling systems can be improved by the addition of heat spreaders and heat sinks in the region of heat load and heat sink, respectively, to increase convective and radiative heat transfer. Natural convection-based cooling is a classic example of a passive cooling technique. Other passive cooling systems include heat pipes [12-14], cooling using phase change materials [15, 16], and magnetic cooling using the thermomagnetic convection of a magnetic fluid [17-19].

Fresh water scarcity is another major concern due to population growth, inefficient water management, and polluted water resources [20, 21]. According to the World Wildlife Organization, around 2.7 billion people face water scarcity at least for a month every year [21]. Apart from human consumption and farming, water is heavily used in diverse industrial sectors such as power generation, oil and gas extraction, water-based cooling applications, production, manufacturing, mining etc. This results in the disappearance of wetlands and degradation of ecosystems.

Water is used extensively in various active cooling applications, e.g., data centers [22], computer CPUs [23], photovoltaics [24], magnetorheological brakes [25], and lowering building temperatures by water evaporation cooling [26]. However, the loss of water due to its evaporation is a major concern as it worsens water shortage. Moreover, water-cooling systems require mechanical pumps for water circulation. Hence, they are noisy and associated with mechanical vibration. Metal fins may be utilized to reject heat at a faster rate to the ambient, adding to manufacturing cost and system complexity [27]. Pressure drop is another issue. Water cooling systems need to be replaced by suitable alternatives to alleviate the water crisis problem and overcome other challenges.

Hence, new strategies need to be developed to remove waste heat and eliminate water waste in cooling systems. Better management of energy and water resources are major factors for sustainable development [28]. A potential solution is the utilization of the thermomagnetic convection (TMC) of a ferrofluid (FF), under the effect of a thermal gradient and a magnetic field, as a passive heat transfer method [29]. A ferrofluid (FF) possesses fluidic as well as magnetic properties [29, 30]. The use of FF for cooling applications is due to their ease of manipulation and enhancement of their heat and mass transfer characteristics by externally applying a magnetic field.

1.2 Motivation

There is growing interest in passive liquid cooling technology to replace active cooling technology. About 20-50% of input energy in industrial sectors is discharged as waste heat [31], reducing reliability and service life [6]. Examples of liquid cooling are spray coolers [32] and micro jet cooling devices [33]. However, liquid cooling systems suffer from vibration and noise as they use mechanical pumps. Hence new liquid transport systems

have been implemented. A membrane-based actuation pump was developed, based on the principle of electrostatic actuation, to control fluid flow by periodically applying and removing electrostatic potential across the silicon electrodes through check valves [34]. Other actuator types viz. thermo-pneumatic actuators [35, 36], magnetic actuators [37, 38], and piezoelectric actuators [39, 40] were also developed using membrane based actuation for driving the fluid along a flow duct. Since all these actuator type pump systems rely on check valves, there is a great risk of fatigue and choking of the valves.

Conventional heat pipes and thermosyphons have been extensively utilized as passive heat transfer systems having high effective thermal conductivity [12, 13]. They are based on the evaporation-condensation cycle of a working fluid. However, the cooling performance of these systems is limited due to pressure fluctuations, start-up failure, flow choking due to higher vapor velocity, entrainment limit, boiling in the wick structure, viscous limit, gravity dependence, complex geometrical requirement and evaporation section sensitivity to the power density at the heat load [41, 42]. Hence, conventional heat pipes are not suitable for long-distance heat transfer.

Flow due to the interaction of a fluid with an external electromagnetic field is promising as it does not use a mechanical pump, thus avoiding various issues associated with the conventional flow systems discussed earlier. Fluids can be categorized mainly into three branches based on their interaction with the electromagnetic field [43].

- Electrohydrodynamics (EHD): This deals with the effects arising due to an electric force. It works on the principle of the Coulomb force acting on free charged particles. However, the magnitude of the effects in EHD based actuators is limited by the low electrical conductivity of fluids, which limits flow speed [44].
- Magnetohydrodynamics (MHD): It is the study of the interaction between an external magnetic field and an electrically conductive fluid. However, MHD systems rely on very high electrical conductivity fluid unlike EHD [44]. Utilizing these systems in cooling applications is not feasible due to the requirement of high magnetic field strength, such as those produced in superconducting magnets [45].
- Ferrohydrodynamics (FHD): It deals with the motion of the fluid induced by magnetic polarization forces. In FHD, there is no requirement of current flow

within the fluid, hence the fluid need not be electrically conducting. In FHD, the fluids used are known as ferrofluids. The body force in FHD is due to the temperature and field dependent magnetization of FF resulting from a thermal gradient and external magnetic field gradient.

Ferrofluids possess both fluidic and magnetic behavior, which gives the additional advantage of controlling the motion of a FF by an external magnetic field [29, 30]. Before suspension, magnetic nanoparticles (MNP) are coated with a long-chain surfactant layer to prevent particle agglomeration due to magnetic dipolar interactions and van der Walls interactions [46]. This coating imparts colloidal stability to the magnetic nanoparticles in the carrier fluid.

Thermomagnetic convection (TMC) is the phenomenon of convective heat transfer by the motion of a FF induced by the combined effect of thermal gradient and the local variation in the fluid's magnetization in the presence of an external magnetic field [46]. The notable feature of TMC is the temperature dependence of the fluid's magnetization, which induces a non-uniform magnetic volume force. The cooler fluid near the magnetic field experiences a stronger magnetic volume force compared to the hotter fluid due to its higher magnetization, thus giving rise to convective motion of fluid. This flow of FF can be controlled by tuning the magnetic properties of the magnetic nanoparticles, heat load temperature, heat flux as well as the strength and orientation of the externally applied magnetic field [47]. Notably, such heat pumps based on TMC do not need any external energy input to move the FF along the flow channel. The temperature gradient and magnetic field gradient from a permanent magnet or an electromagnet are sufficient to sustain flow. Therefore, these systems are self-driven [48]. As no mechanical moving parts are involved, there is almost no vibration or noise. Hence, magnetic cooling heat pumps can overcome the problems associated with other cooling mechanisms, with enhanced reliability, low maintenance cost, little or no external energy requirement and environmentally benign.

Figure 1.4(a, a') represent the number of citations and number of publications for the "**ferrofluid**" search string from the Web of Science. The statistics related to the present work, which is associated with the convection of ferrofluid, is shown in **Figure 1.4(b, b')**. The search string used was "**ferrofluid/magnetic fluid & convection**". It can be observed

that the interest in these fields has been increasing rapidly over the past two decades. Hence, it motivates us to investigate the magnetic cooling systems for enhanced cooling.

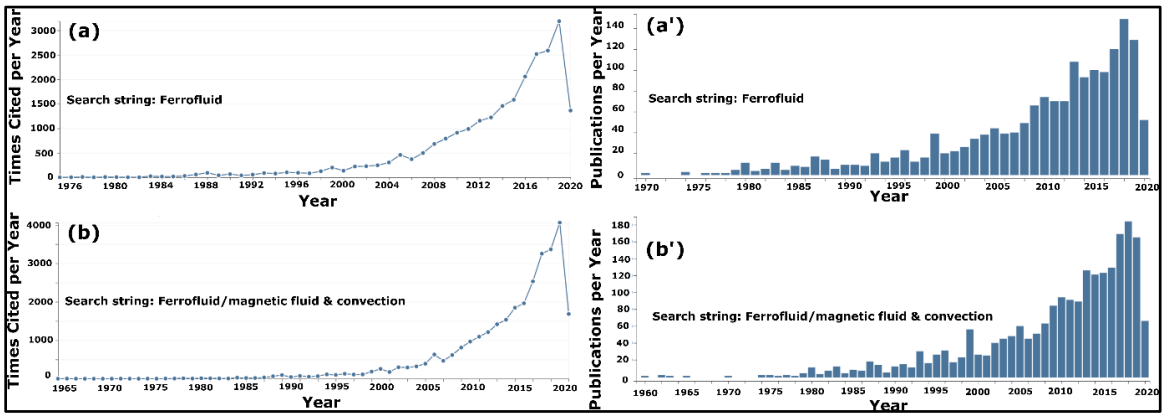

Figure 1.4. (a) Number of citations per year, and the (a') number of publications per year for the ferrofluid search string. (b) Number of citations per year, and (b') number of publications per year related to the search string ferrofluid or magnetic fluid and convection (Web of Science).

1.3 Problem Statement

The reliability of magnetic cooling (MC) devices is limited by several factors such as choice of FF, volume concentration of magnetic nanoparticles in the FF, thermal conductivity of the solid phase in the FF, viscosity of the FF, boiling point of the carrier fluid, Curie temperature of the magnetic solid phase, types of tube materials, characteristic length of the tube material, and strength of the magnet used. For enhanced TM cooling, the magnetic nanoparticle must possess high saturation magnetization, be either soft ferromagnetic or superparamagnetic, and possess high pyro magnetic coefficient [49]. The carrier fluid should have low viscosity [49]. The FF should possess high thermal conductivity and should remain magnetic over a wide temperature range. The thermal conductivity of the tube material and the design of the magnetic cooling device are also important. Hence, the FF magnetic and thermophysical parameters, magnetic cooling device design, and applied magnetic field strength and position etc. can be optimized to achieve enhanced thermomagnetic cooling performance using a magnetic cooling heat pump.

Magnetic cooling (MC) based on the thermomagnetic effect of a ferrofluid has the potential to replace existing liquid-based cooling technologies due to the absence of mechanical

moving parts and its capability to self-regulate over a range of heat load temperatures and power values. However, current magnetic heat pumps generally operate a low heat load power values, power density, and heat load temperature values [44, 50]. Previous reports focused on miniature devices for microfluidic applications, e.g., in magneto electromechanical systems (MEMS) and lab-on-chip (LOC) devices [51-54]. Moreover, the MC devices used a variety of tube materials and tube geometries for their investigations. The effect of tube material thermal conductivity and flow tube geometry on the thermomagnetic cooling of the heat load has not yet been investigated.

There are a few reports of long MC devices utilizing two-phase boiling heat transfer of a binary temperature sensitive FF [19, 55]. However, there are no reports on a long MC heat pipe based on single-phase heat transfer of a FF. Soft-ferrite based FF are usually used as the heat transfer medium in MC device due to their ease of preparation and better colloidal stability [17, 56]. FF having higher saturation magnetization may result in enhanced cooling. However, there are very few reports on the synthesis and application of metallic/alloy based FF for thermal management and heat load cooling in an MC device [57, 58]. There are no simulation studies and ranking of the effect of magnetic nanoparticle properties and FF thermophysical properties on the cooling performance. Hence, experimental, numerical, and analytical investigations of the magnetic cooling performance using TMC of a single-phase FF were carried out.

The limitations of some MC devices reported earlier and the advantages of the MC devices considered in the present work are listed in **Table 1.1**.

Table 1.1. Area of study, the focus of study and limitations of earlier magnetic cooling devices.

Study area	Previous reports	Limitations
Heat load power/temperature	Small-scale cooling for MEMS and LOC application [51-54]	Lower heat load power and lower heat load temperature
Magnetic field type and position	Permanent magnet [17, 18] and electromagnet [19, 54]	No investigation on magnet position on cooling, energy

		requirement for electromagnet, use of multiple magnets
FF temperature profile	Wall temperatures were measured [59, 60]	No experimental investigation
Thermal conductivity of flow tube	Tube having single thermal conductivity [57, 58, 61-63]	No experimental and simulation study on the effect of tube material thermal conductivity
Tube geometry	A single geometry type [17, 58]	No experimental and simulation study on the effect of tube geometry
Device length scale	Small device length [53, 64, 65]	No experimental or simulation study on the cooling performance of long MC heat pipe
FF carrier medium	Water-based or low-boiling oil-based FF [17, 53, 54]	No experimental and simulation study on the cooling performance of a high-boiling oil-based FF
FF MNP type and its magnetic properties	Soft ferrite based FF [17, 18] and few alloy-based FF [57, 58]	No ranking of both ferrite and metallic/alloy based MNP's properties on the simulated results of MC performance
FF thermophysical properties	Lower thermal conductivity [17] and higher viscosity [57, 58]	No simulation results on the effect of FF thermophysical properties on the MC performance

1.4 Hypothesis

Magnetic cooling heat pumps have been studied as passive heat transfer systems. Their performance depends on the magnetic and thermophysical properties of a FF, design of the device such as device length, tube cross sectional area, flow tube geometry, and operation over a range of heat load powers and temperatures. We seek to test if we can develop a MC device for cooling of kW level and high temperature heat loads using a multi-torus device design and larger tube cross section for enhanced heat transfer.

We also hypothesize that the performance can be enhanced by tuning the tube material thermal conductivity, specifically by developing a hybrid MC device consisting of both lower and higher thermal conductivity tubes. We also seek to develop a long MC device based on single-phase thermomagnetic heat transfer of the FF.

Most MC devices utilize ferrite based FF as the heat transfer medium [17, 18]. Very few results are available on the synthesis and utilization of metal based FF [57, 58]. Hence, simulations of ferrite and metallic/alloy-based FF were carried out and they are ranked based on their cooling performance.

1.5 Novelty

Previous literature on the MC devices focused mainly on micro-scale, and small-scale low power devices for cooling waste heat from heat loads operating below 100°C [17, 18, 64, 66, 67]. Multiple magnets were used to improve the cooling performance [68, 69]. However, this results in a large device footprint [70, 71].

Hence, we developed a novel multi-torus MC device having larger heat load interface area to cool kilowatt level heat loads. The heat load power and temperature were as high as 1 kW and 580°C, respectively. For the first time, a larger flow tube diameter of 25 mm was used. For 1 kW heat load power, the heat load was cooled by 214°C. We also calculated the effective thermal resistance of the multi-torus MC device and compared the values with conventional heat pipes.

The flow tube material and geometry were considered as two device design-based parameters and the cooling performance was evaluated as a function of those parameters. Circular and race-track shaped MC devices having different form factors were developed

for the first time from copper, silicone, and hybrid (copper + silicone) tubes. The effect of tube thermal conductivity on the performance was studied. The hybrid and copper-based racetrack shaped MC device yielded significant heat load cooling of 121°C and 113°C, respectively, for an initial heat load temperature of 200°C.

An 8 m long racetrack shaped MC device based on the single-phase heat transfer of the FF was developed and its cooling performance was evaluated for the first time. The long-distance heat transfer and cooling performance was investigated for a wide range of heat load power density and temperature values, relevant to low-grade or medium-grade waste heat values. This MC device can effectively transport heat from devices with waste heat flux values of up to 8.85 kW/m^2 and cool the system significantly by up to 41°C for an initial heat load temperature of 197 °C.

Finally, the device performance was numerically investigated with respect to the magnetic properties of suspended MNP and the thermophysical properties of the FF. Several soft ferrites and metallic/alloy-based MNP were considered and the effect of saturation magnetization, Curie temperature, and pyro magnetic coefficient on the TM cooling performance was studied. Based on the simulation results, the FF were ranked by their cooling performance and the cooling results for the best FF was compared with conventional heat pipes. This work identifies the optimum combination of device configuration, magnet position, and FF properties for magnetic cooling of the heat load. The novelties of this thesis are listed in **Table 1.2**.

Overall, the novelties and their underlying physics can be summarized for each chapter. Chapter 04 investigates the cooling performance of a novel multi-torus MC device for various magnet positions and range of heat load power values. Use of multiple magnets in MC device can tune the applied magnetic field gradient for enhanced cooling. However, it increases the device footprint. Hence, we studied the effect of the variation of magnetic field gradient with respect to the heat load center by varying the position of the magnet. The variation in magnet position triggers the heat load cooling by forming the FF vortices at different regions of the heat load, thus giving rise to a particular trend in the obtained cooling.

Chapter 05 reports the superiority of hybrid MC device over copper and silicone devices in terms of the heat load cooling magnitude. The combined effect of thermal gradient and magnetic field gradient gives rise to the TMC of FF. The enhancement in any one or both parameters result in enhanced heat load cooling. The magnetic field gradient can be controlled by changing the position and orientation of the permanent magnet with respect to the heat load. Similarly, the thermal gradient can be enhanced by creating a junction of two materials having dissimilar thermal conductivity along the flow channel. In the present study, a highly thermally conductive copper tube was joined to a silicone tube having a relatively lower thermal conductivity, thus creating a copper-silicone hybrid hot-cold junction near the heat load region. This gives rise to a larger thermal gradient region, and hence superior heat load cooling.

Chapter 06 investigates the capability of long MC device for heat transfer over longer distances. Without even using any mechanical pump, the volume force resulting from the applied magnetic field, helps in driving the FF over the longer flow channel length. The effect of device perimeter for the long MC devices on the cooling performance was investigated. We reported that the cooling does not vanish even for the highest device perimeter (20 m) as the minimum cooling is achieved due to the formation of FF vortices.

The thermomagnetic cooling is majorly governed by the FF parameters. However, there were no simulation studies focusing entirely on the effect of various FF parameters on the cooling performance. Hence, in Chapter 07, we included several studies, which accounts for the effect of FF parameters on MC performance. The underlying physics can be traced to the dependence of thermomagnetic volume force on the susceptibility, magnetization, and the pyromagnetic coefficient of the FF. We also derived several parameters as functions of FF magnetic and thermophysical parameters, which can help in selecting the suitable FF for cooling application.

Table 1.2. Novelty of this thesis work.

Sl. No.	Thesis results	Novelty of this work
1.	A self-regulating multi-torus magneto-fluidic device for kilowatt level cooling	Multi-torus device design Heat load power up to 1 kW Heat load temperature up to 580°C 214°C heat load cooling for highest heat load power and temperature Lower thermal resistance
2.	High Conductivity, Low Footprint, High Cooling, Passive Magneto-fluidic Devices	Effect of device form factor on cooling Effect of tube thermal conductivity (copper and silicone) on cooling Hybrid device design (copper + silicone)
3.	Magnetic cooling device for long distance heat transfer by thermomagnetic convection of ferrofluid	8 m long racetrack shaped magnetic cooling device Cooling performance evaluation based on the single-phase thermomagnetic convection of ferrofluid Local and average Nusselt number as a function of heat flux Numerical investigation of long magnetic cooling device
4.	Ranking of soft-ferrite and metallic/alloy based ferrofluid based on their performance	Ranking of ferrofluid based on the heat load cooling performance

1.6 Significance

Magnetic cooling (MC) based on the thermomagnetic (TM) effect is an attractive cooling technology [17]. The performance can be optimized by tuning the strength, position, and orientation of the externally applied magnetic field. Due to the presence of MNP, the thermal conductivity of the FF increases by applying an external magnetic field, and the effect can be attributed to the formation of chainlike structures within the FF [72, 73]. The absence of mechanical moving parts in the MC system minimizes vibration and noise. Hence, this cooling technology provides a potential solution to improve the reliability and service life of heat engines and many other modern devices. It has the potential to eliminate the need of water-cooling technology by evaporation. The MC device can be considered for large distance passive heat transfer [56].

Aims and Objectives

The aim is concerned with the experimental design and performance analysis of a magnetic cooling device for kW level applications as well as numerical modelling of the thermomagnetic effect to provide deeper understanding and performance optimization.

The specific objectives of this thesis are;

- To develop a large-scale multi-torus MC device for cooling the heat loads dissipating waste heat in the kilowatt range.
- To develop silicone, copper, and hybrid MC devices and to study the effect of geometry, device form factor, and effective thermal conductivity of the device on the heat load cooling performance.
- To evaluate the long-range thermal transport and TM cooling performance of an 8 m long race-track shaped MC device for a range of heat load power density and temperature values.
- To numerically investigate the thermomagnetic flow profile, isothermal contour plots, Nusselt number and velocity profile of the MC devices using finite element analysis.
- To rank soft ferrite and metallic/alloy nanoparticle-based FF based on their cooling performance estimated using numerical simulation.

Finally, the optimum configuration of device geometry, magnet position and FF will be elucidated.

The science behind these aforementioned objectives are as follows.

- Higher surface area of the cooling device can carry higher amount of waste heat from the heat load. Hence, multi-torus MC device was designed with the silicone tube having an internal diameter of 25 mm.
- Apart from magnetic field gradient, thermal gradient also affects the magnetic cooling. This can be attributed to the change in the themo-magnetic volume force with a change in the temperature distribution of the ferrofluid across the flow channel. The temperature distribution of the ferrofluid affects the magnetization. Hence, we studied the effect of device thermal conductivity in greater detail in chapter 05.
- Long range thermal transport using magnetic cooling device was never investigated owing to the limitations in the available thermomagnetic volume force that can drive the FF through the flow channel. However, by slight modification of the flow channel geometry to racetrack shape, reduced the drag force significantly due to the absence of any sharp corners. The detailed investigations were reported in chapter 06.
- MC device cooling performance strongly depends on the FF magnetic and thermophysical parameters. Hence, we investigated by numerical simulation, and analytical calculation, the effect of ferrofluidic parameters on the cooling performance. The detailed analyses were reported in chapter 07.

1.7 Organization of the Thesis

The present thesis report is organized into 8 chapters, including 4 results chapters, as described below.

- **Chapter 1** provides an overview of MC technology. It also summarizes the motivation, problem statement, hypothesis, objective and scope, novelty, and significances.

- **Chapter 2** provides a literature review starting with the development of FF research and the principle of TMC. The preparation, properties, stability requirement, and selected applications of FF are also summarized. The theoretical background and previous literature are summarized.
- **Chapter 3** describes the experimental methods to develop the MC device designs. The modelling methods to simulate the TM effect of the FF using COMSOL Multiphysics are also described along with the governing equations, boundary conditions and meshing details.
- **Chapter 4** delineates the TM cooling performance of a multi-torus MC device for kilowatt level heat load cooling. The cooling performance and FF temperature profile was investigated for various magnet positions with respect to the heat load. The TM effect was simulated using a single-phase 2D finite element model of the multi-torus MC device.
- **Chapter 5** examines the effect of device thermal conductivity, geometry, and form factor on the heat load cooling. The effect of hybrid MC device (made by joining highly thermally conductive copper tube with silicone tube having lower thermal conductivity) and the ratio of the copper to silicone length in the hybrid device on the heat load cooling for different magnet positions were investigated over a range of heat load power density and temperature values. The results were verified using 2D numerical simulations.
- **Chapter 6** presents the design, performance, and simulation of the longest magnetic cooling device developed so far, based on the single-phase TMC of FF. An 8 m long MC device was built, and its cooling performance was tested over a range of heat flux values. The simulated temperature profiles, velocity vector plots were analyzed to understand the MC performance.
- **Chapter 7** focuses on the effect of material parameters on the TM cooling performance of the MC device. It reports the simulation results on the effect of magnetic properties of nanoparticles viz., saturation magnetization, Curie temperature, pyro magnetic coefficient, nanoparticle volume fraction, and the thermophysical properties of FF viz., thermal conductivity, and viscosity on heat

load cooling. Several ferrite and metallic/alloy based MNP were considered for the simulations and ranked based in their cooling performance.

- **Chapter 8** is a summary of the thesis and possible future directions.

References

[1] S. Bilgen, "Structure and environmental impact of global energy consumption," *Renewable and Sustainable Energy Reviews*, vol. 38, pp. 890-902, 2014.

[2] E. D. Coyle and R. A. Simmons, *Understanding the global energy crisis*. Purdue University Press, 2014.

[3] L. L. N. Laboratory. *Energy flow charts-LLNL flow charts*. Available: https://flowcharts.llnl.gov/commodities/energy, [Accessed on: 22 May 2020].

[4] B. Insider. *The world wastes more energy than it uses every year*. Available: https://www.businessinsider.com/worlds-dirty-energy-comes-from-oil-wasted-2015-11?IR=T, [Accessed on: 3 January 2019].

[5] R. K. Das and C. Subramanian, "Thermal Analysis of Waste Heat Recovery Unit Using the Exhaust Gas Emitted From Internal Combustion Engine," *International Journal of Advances in Science Engineering and Technology*, vol. 4, no. 2, pp. 28-33, 2016.

[6] I. Johnson, W. T. Choate, and A. Davidson, "Waste heat recovery. Technology and opportunities in US industry," BCS, Inc., Laurel, MD (United States)2008.

[7] M. Papapetrou, G. Kosmadakis, A. Cipollina, U. La Commare, and G. Micale, "Industrial waste heat: Estimation of the technically available resource in the EU per industrial sector, temperature level and country," *Applied Thermal Engineering*, vol. 138, pp. 207-216, 2018.

[8] N. Zaharia. *Passive Cooling vs. Active Cooling – What's the Difference?* Available: https://www.simscale.com/blog/2017/01/active-and-passive-cooling, [Accessed on: 6 January 2019].

[9] P. S. Szabo and W.-G. Früh, "The transition from natural convection to thermomagnetic convection of a magnetic fluid in a non-uniform magnetic field," *Journal of Magnetism and Magnetic Materials*, vol. 447, pp. 116-123, 2018.

[10] K. Deepak, M. Pattanaik, and R. V. Ramanujan, "Figure of merit and improved performance of a hybrid thermomagnetic oscillator," *Applied Energy*, vol. 256, p. 113917, 2019.

[11] K. Deepak, V. Varma, G. Prasanna, and R. V. Ramanujan, "Hybrid thermomagnetic oscillator for cooling and direct waste heat conversion to electricity," *Applied Energy*, vol. 233, pp. 312-320, 2019.

[12] H. N. Chaudhry, B. R. Hughes, and S. A. Ghani, "A review of heat pipe systems for heat recovery and renewable energy applications," *Renewable and Sustainable Energy Reviews*, vol. 16, no. 4, pp. 2249-2259, 2012.

[13] M. Mochizuki, R. Singh, T. Nguyen, and T. Nguyen, "Heat pipe based passive emergency core cooling system for safe shutdown of nuclear power reactor," *Applied thermal engineering*, vol. 73, no. 1, pp. 699-706, 2014.

[14] M. F. Remeli, L. Tan, A. Date, B. Singh, and A. Akbarzadeh, "Simultaneous power generation and heat recovery using a heat pipe assisted thermoelectric generator system," *Energy Conversion and management*, vol. 91, pp. 110-119, 2015.

[15] A. Castell, I. Martorell, M. Medrano, G. Pérez, and L. F. Cabeza, "Experimental study of using PCM in brick constructive solutions for passive cooling," *Energy and Buildings*, vol. 42, no. 4, pp. 534-540, 2010.

[16] R. Sabbah, R. Kizilel, J. Selman, and S. Al-Hallaj, "Active (air-cooled) vs. passive (phase change material) thermal management of high power lithium-ion packs: Limitation of temperature rise and uniformity of temperature distribution," *Journal of Power Sources*, vol. 182, no. 2, pp. 630-638, 2008.

[17] V. Chaudhary, Z. Wang, A. Ray, I. Sridhar, and R. V. Ramanujan, "Self pumping magnetic cooling," *Journal of Physics D: Applied Physics*, vol. 50, no. 3, p. 03LT03, 2016.

[18] W. Lian, Y. Xuan, and Q. Li, "Characterization of miniature automatic energy transport devices based on the thermomagnetic effect," *Energy Conversion and Management,* vol. 50, no. 1, pp. 35-42, 2009.
[19] H. Yamaguchi and Y. Iwamoto, "Energy transport in cooling device by magnetic fluid," *Journal of Magnetism and Magnetic Materials,* vol. 431, pp. 229-236, 2017.
[20] E. Drioli, A. Ali, and F. Macedonio, "Membrane distillation: Recent developments and perspectives," *Desalination,* vol. 356, pp. 56-84, 2015.
[21] WWF. *Water Scarcity: Threat, world wildlife fund*. Available: https://www.worldwildlife.org/threats/water-scarcity, [Accessed on: 23 May 2020].
[22] T. Brunschwiler, B. Smith, E. Ruetsche, and B. Michel, "Toward zero-emission data centers through direct reuse of thermal energy," *IBM Journal of Research and Development,* vol. 53, no. 3, pp. 11: 1-11: 13, 2009.
[23] Z. Ping, C. Guangming, L. Jiulong, Y. Zhigang, and Z. Libing, "Compositive water-cooling system applied to computer chip," *JOURNAL-XIAN JIAOTONG UNIVERSITY,* vol. 39, no. 11, p. 1207, 2005.
[24] S. Odeh and M. Behnia, "Improving Photovoltaic Module Efficiency Using Water Cooling," *Heat Transfer Engineering,* vol. 30, no. 6, pp. 499-505, 2009.
[25] D. M. Wang, Y. F. Hou, and Z. Z. Tian, "A novel high-torque magnetorheological brake with a water cooling method for heat dissipation," *Smart Materials and Structures,* vol. 22, no. 2, 2013.
[26] G. Tiwari, A. Kumar, and M. Sodha, "A review—cooling by water evaporation over roof," *Energy conversion and Management,* vol. 22, no. 2, pp. 143-153, 1982.
[27] M. Crawford. *Magnetic Nanofluid Improves Cooling*. Available: https://www.asme.org/engineering-topics/articles/nuclear/magnetic-nanofluid-improves-cooling, [Accessed on: 25 April 2019].
[28] P. S. Lee and X. Chen, "Nanomaterials for energy and water management," *Small,* vol. 10, no. 17, pp. 3432-3, Sep 10 2014.
[29] I. Nkurikiyimfura, Y. Wang, and Z. Pan, "Heat transfer enhancement by magnetic nanofluids—A review," *Renewable and Sustainable Energy Reviews,* vol. 21, pp. 548-561, 2013.
[30] S. Odenbach, *Ferrofluids: magnetically controllable fluids and their applications*. Springer, 2008.
[31] R. Bradley, "Batteries that capture low-grade waste heat," *Scientific American,* vol. 311, no. 6, p. 53, 2014.
[32] Y. Zhang, L. P. Pang, Y. Q. Xie, S. C. Jin, M. Liu, and Y. B. Ji, "Experimental Investigation Of Spray Cooling Heat Transfer On Straight Fin Surface Under Acceleration Conditions," *Experimental Heat Transfer,* vol. 28, no. 6, pp. 564-579, 2014.
[33] Y. Han, B. L. Lau, and X. Zhang, "Package-level microjet-based hotspot cooling solution for microelectronic devices," *IEEE Electron Device Letters,* vol. 36, no. 5, pp. 502-504, 2015.
[34] R. Zengerle, A. Richter, and H. Sandmaier, "A micro membrane pump with electrostatic actuation," in *Micro Electro Mechanical Systems, 1992, MEMS'92, Proceedings. An Investigation of Micro Structures, Sensors, Actuators, Machines and Robot. IEEE*, 1992, pp. 19-24: IEEE.
[35] C. G. Cooney and B. C. Towe, "A thermopneumatic dispensing micropump," *Sensors and Actuators A: Physical,* vol. 116, no. 3, pp. 519-524, 2004.
[36] D. H. Jun, W. Y. Sim, and S. S. Yang, "A novel constant delivery thermopneumatic micropump using surface tensions," *Sensors and Actuators A: Physical,* vol. 139, no. 1-2, pp. 210-215, 2007.

[37] C. H. Ahn and M. G. Allen, "Fluid micropumps based on rotary magnetic actuators," in *Micro Electro Mechanical Systems, 1995, MEMS'95, Proceedings. IEEE*, 1995, p. 408: IEEE.

[38] C. Yamahata, C. Lotto, E. Al-Assaf, and M. A. M. Gijs, "A PMMA valveless micropump using electromagnetic actuation," *Microfluidics and Nanofluidics,* vol. 1, no. 3, pp. 197-207, 2004.

[39] N.-T. Nguyen and T.-Q. Truong, "A fully polymeric micropump with piezoelectric actuator," *Sensors and Actuators B: Chemical,* vol. 97, no. 1, pp. 137-143, 2004.

[40] J.-H. Park, K. Yoshida, and S. Yokota, "Resonantly driven piezoelectric micropump: fabrication of a micropump having high power density," *Mechatronics,* vol. 9, no. 7, pp. 687-702, 1999.

[41] J. v. Es and H. J. van Gerner, "Benefits and Drawbacks of Using Two-Phase Cooling Technologies in Military Platforms," 2011.

[42] H. Jouhara, A. Chauhan, T. Nannou, S. Almahmoud, B. Delpech, and L. C. Wrobel, "Heat pipe based systems-Advances and applications," *Energy,* vol. 128, pp. 729-754, 2017.

[43] R. E. Rosensweig, *Ferrohydrodynamics*. Courier Corporation, 2013.

[44] Y. Xuan and W. Lian, "Electronic cooling using an automatic energy transport device based on thermomagnetic effect," *Applied Thermal Engineering,* vol. 31, no. 8-9, pp. 1487-1494, 2011.

[45] O. M. Al-Habahbeh, M. Al-Saqqa, M. Safi, and T. Abo Khater, "Review of magnetohydrodynamic pump applications," *Alexandria Engineering Journal,* vol. 55, no. 2, pp. 1347-1358, 2016.

[46] P. S. B. Szabo, M. Beković, and W.-G. Früh, "Using infrared thermography to investigate thermomagnetic convection under spatial non-uniform magnetic field," *International Journal of Thermal Sciences,* vol. 116, pp. 118-128, 2017.

[47] R. Ganguly, S. Sen, and I. K. Puri, "Thermomagnetic convection in a square enclosure using a line dipole," *Physics of Fluids,* vol. 16, no. 7, pp. 2228-2236, 2004.

[48] M. Bahiraei and M. Hangi, "Automatic cooling by means of thermomagnetic phenomenon of magnetic nanofluid in a toroidal loop," *Applied Thermal Engineering,* vol. 107, pp. 700-708, 2016.

[49] J. Singh Mehta, R. Kumar, H. Kumar, and H. Garg, "Convective heat transfer enhancement using ferrofluid: a review," *Journal of Thermal Science and Engineering Applications,* vol. 10, no. 2, 2018.

[50] L. Zhou, Y. Xuan, Q. Li, and W. Lian, "A new miniaturized engine based on thermomagnetic effect of magnetic fluids," *Frontiers of Energy and Power Engineering in China,* vol. 3, no. 2, pp. 160-166, 2009.

[51] M. Ghasemian, Z. N. Ashrafi, M. Goharkhah, and M. Ashjaee, "Heat transfer characteristics of Fe3O4 ferrofluid flowing in a mini channel under constant and alternating magnetic fields," *Journal of Magnetism and Magnetic Materials,* vol. 381, pp. 158-167, 2015.

[52] A. Hatch, A. E. Kamholz, G. Holman, P. Yager, and K. F. Bohringer, "A ferrofluidic magnetic micropump," *Journal of Microelectromechanical systems,* vol. 10, no. 2, pp. 215-221, 2001.

[53] L. J. Love *et al.*, "Ferrofluid Field Induced Flow for Microfluidic Applications," *IEEE/ASME Transactions on Mechatronics,* vol. 10, no. 1, pp. 68-76, 2005.

[54] S. Pal, A. Datta, S. Sen, A. Mukhopdhyay, K. Bandopadhyay, and R. Ganguly, "Characterization of a ferrofluid-based thermomagnetic pump for microfluidic applications," *Journal of Magnetism and Magnetic Materials,* vol. 323, no. 21, pp. 2701-2709, 2011.

[55] H. Yamaguchi and T. Bessho, "Long distance heat transport device using temperature sensitive magnetic fluid," *Journal of Magnetism and Magnetic Materials,* vol. 499, p. 166248, 2020.

[56] M. Khairul, E. Doroodchi, R. Azizian, and B. Moghtaderi, "Thermal performance analysis of tunable magnetite nanofluids for an energy system," *Applied Thermal Engineering,* vol. 126, pp. 822-833, 2017.

[57] V. Chaudhary and R. V. Ramanujan, "Magnetocaloric properties of Fe-Ni-Cr nanoparticles for active cooling," *Scientific reports,* vol. 6, no. 1, pp. 1-9, 2016.

[58] V. Sharma, S. Pattanaik, H. Parmar, and R. V. Ramanujan, "Magnetocaloric properties and magnetic cooling performance of low-cost Fe 75− x Cr x Al 25 alloys," *MRS Communications,* vol. 8, no. 3, pp. 988-994, 2018.

[59] F. Fadaei, A. M. Dehkordi, M. Shahrokhi, and Z. Abbasi, "Convective-heat transfer of magnetic-sensitive nanofluids in the presence of rotating magnetic field," *Applied Thermal Engineering,* vol. 116, pp. 329-343, 2017.

[60] M. A. Khairul, E. Doroodchi, R. Azizian, and B. Moghtaderi, "Thermal performance analysis of tunable magnetite nanofluids for an energy system," *Applied Thermal Engineering,* vol. 126, pp. 822-833, 2017.

[61] M. Goharkhah, M. Ashjaee, and M. Shahabadi, "Experimental investigation on convective heat transfer and hydrodynamic characteristics of magnetite nanofluid under the influence of an alternating magnetic field," *International Journal of Thermal Sciences,* vol. 99, pp. 113-124, 2016.

[62] M. Goharkhah, A. Salarian, M. Ashjaee, and M. Shahabadi, "Convective heat transfer characteristics of magnetite nanofluid under the influence of constant and alternating magnetic field," *Powder Technology,* vol. 274, pp. 258-267, 2015.

[63] S. A. Zonouzi *et al.*, "Experimental investigation of the flow and heat transfer of magnetic nanofluid in a vertical tube in the presence of magnetic quadrupole field," *Experimental Thermal and Fluid Science,* vol. 91, pp. 155-165, 2018.

[64] W. Lian, Y. Xuan, and Q. Li, "Design method of automatic energy transport devices based on the thermomagnetic effect of magnetic fluids," *International Journal of Heat and Mass Transfer,* vol. 52, no. 23-24, pp. 5451-5458, 2009.

[65] L. J. Love, J. F. Jansen, T. McKnight, Y. Roh, and T. J. Phelps, "A Magnetocaloric Pump for Microfluidic Applications," *IEEE Transactions on Nanobioscience,* vol. 3, no. 2, pp. 101-110, 2004.

[66] R. Ganguly, S. Sen, and I. K. Puri, "Heat transfer augmentation using a magnetic fluid under the influence of a line dipole," *Journal of Magnetism and Magnetic Materials,* vol. 271, no. 1, pp. 63-73, 2004.

[67] Q. Li, W. Lian, H. Sun, and Y. Xuan, "Investigation on operational characteristics of a miniature automatic cooling device," *International Journal of Heat and Mass Transfer,* vol. 51, no. 21-22, pp. 5033-5039, 2008.

[68] M. Asfer, B. Mehta, A. Kumar, S. Khandekar, and P. K. Panigrahi, "Effect of magnetic field on laminar convective heat transfer characteristics of ferrofluid flowing through a circular stainless steel tube," *International Journal of Heat and Fluid Flow,* vol. 59, pp. 74-86, 2016.

[69] M. Goharkhah and M. Ashjaee, "Effect of an alternating nonuniform magnetic field on ferrofluid flow and heat transfer in a channel," *Journal of Magnetism and Magnetic Materials,* vol. 362, pp. 80-89, 2014.

[70] M. Bahiraei and M. Hangi, "Flow and heat transfer characteristics of magnetic nanofluids: A review," *Journal of Magnetism and Magnetic Materials,* vol. 374, pp. 125-138, 2015.

[71] A. Kumar and S. Subudhi, "Preparation, characteristics, convection and applications of magnetic nanofluids: A review," *Heat and Mass Transfer,* vol. 54, no. 2, pp. 241-265, 2017.

[72] J. Philip, P. D. Shima, and B. Raj, "Enhancement of thermal conductivity in magnetite based nanofluid due to chainlike structures," *Applied Physics Letters*, vol. 91, no. 20, 2007.

[73] J. Philip, P. D. Shima, and B. Raj, "Evidence for enhanced thermal conduction through percolating structures in nanofluids," *Nanotechnology*, vol. 19, no. 30, p. 305706, Jul 30 2008.

Chapter 2

Literature Review

Thermomagnetic convection is the convective heat transfer of a ferrofluid from a hotter region to a colder region due to the combined effect of a thermal gradient and a magnetic field gradient. Magnetic cooling, governed by the principle of thermomagnetic convection, possesses several advantages over other conventional active and passive cooling techniques. The present chapter outlines the chronological development in ferrofluid research, the synthesis procedures, and types of ferrofluid. Subsequently, the stability requirements of the ferrofluid, its thermophysical properties and various applications of ferrofluids are described. The modelling and experimental investigations of magnetic cooling devices has been elucidated.

2.1 Magnetic Fluid

A magnetic fluid (MF), also termed as ferrofluid (FF), is a stable colloidal suspension of nanometer size magnetic particles in a carrier fluid medium [1]. These magnetic nanoparticles (MNP) are usually ferrites or alloys of iron, nickel, and cobalt. A ferrofluid differs from a magnetorheological (MR) fluid, in which the suspended magnetic particles are of micron size, the particle volume fraction is usually higher. One key aspect of FF is that it can retain its flow even after attaining magnetic saturation, hence it behaves like a liquid magnet, whereas a MR fluid experiences great changes in rheological properties under the application of a large magnetic field.

A ferrofluid is usually electrically non-conducting. Exceptions are some recently developed FF containing graphene or carbon nanotubes along with the MNP. A stable ferrofluid usually implies that the size of the suspended MNP should be less than 15 nm in diameter [2]. The MNP also need to be capped by long chain surfactant molecules to prevent their agglomeration even under large magnetic fields. Brownian motion resulting from thermal agitation keeps the MNP suspended in the dispersion fluid. A typical FF contains less than 20% volume fraction of coated magnetic particles [2]. In the absence of an external magnetic field, the magnetic moments of the MNP are randomly oriented in a FF. Hence, the FF possesses no net magnetization. The MNP in the FF are often superparamagnetic. Under the influence of a magnetic field, the MNP orient along the field direction and the FF behaves like a liquid magnet. The extent of FF magnetization depends on the type (metallic, alloy or ferrite) and concentration of MNP constituents in the FF, the strength and orientation of the applied magnetic field, and the temperature of the ferrofluid. The motion of a FF can be controlled by changing the magnitude and direction of application of an external magnetic field. As the FF can be remotely manipulated in a wireless fashion, it has a multitude of applications in targeted drug delivery [3, 4], hyperthermia [5, 6], droplet microfluidics [7], particle synthesis [8], energy harvesting [9, 10] and waste heat recovery [11-14].

2.1.1 Chronological development of ferrofluid research

Research on ferrofluids can be dated back to the 1930s [15, 16]. Ferrofluid research subsequently increased in the 1960s due to industrial manufacture of ferrite-based FF [17].

FF research has continued due to applications in materials science, mechanical engineering, biotechnology, and biomedical engineering. The chronological development in ferrofluid research is summarized below.

- Neuringer and Rosensweig presented a phenomenological treatment of the fluidic and thermodynamic response of MF under the influence of a non-uniform magnetic field [18].
- Papell invented a MF by dispersing MNP in a low viscous carrier liquid for its use as a propellant in no gravity condition in a space shuttle [19].
- Cowley and Rosensweig studied the interfacial stability of a FF by deriving the condition for the critical magnetization level for the onset of instability between a magnetic and non-magnetic fluid layer [20].
- Hall et al.[21] studied the effect of an applied magnetic field on the viscosity of a FF by applying Stokes' theorem to the steady-state motion of the FF.
- Kaiser et al.[22] discussed applications utilizing FF e.g., in viscous dampers in satellites, energy conversion devices, accelerometers, specific gravity analyzer and treatment of cranial aneurysms.
- Krueger et al.[23] investigated the hydrostatic flow profile of a FF surrounding a current-carrying wire oriented along the vertical direction.
- Perry et al.[24] observed surface instability in FF by applying a strong periodic magnetic field gradient along a direction tangential to the FF interface.
- Berkovsky et al.[25]studied experimentally and numerically convective heat transfer characteristics of a vertical FF layer.
- Byrne calculated the force and torque on a magnet immersed inside a FF [26].
- Tanahashi et al.[27] derived equations to describe the steady state flow of a MF in a circular pipe due to a magnetic field parallel to the flow direction.
- Stiles et al.[28] proposed a theory on the influence of axial magnetic field to stabilize cylindrical Couette flow of MF.

2.1.2 Preparation and types of ferrofluid

A stable ferrofluid is prepared by dispersing coated super-para or soft-ferro/ferrimagnetic nanoparticles in a carrier fluid such as water or organic oil [9]. The FF is prepared in three

steps: (a) synthesis of MNP, (b) surface coating using long-chain polymer/s to avoid interparticle interactions, and (c) dispersion of the coated MNP in a suitable carrier fluid. A FF is synthesized by either physical or chemical methods of preparation [2]. There are basically two types of FF viz., metallic/alloy-based and soft ferrite-based FF. Metallic or alloy-based nanoparticles for FF were prepared by methods such as reduction of metal salts, high-temperature reductive decomposition, thermal decomposition of metal carbonyls, and high-energy ball milling [29]. Metal oxide based FF utilize synthesis of MNP by methods such as sonochemical synthesis [30, 31], reverse-micelle [32, 33], co-precipitation [34-37], hydrothermal synthesis [12], sol-gel [38], thermal decomposition [39, 40], phase-transfer[41] and ball-milling [42].

Previously, the top-down physical approach was followed to obtain magnetic particles in the nanometer size range, e.g., the use of surfactant assisted high energy ball milling. Using this physical technique, FF was made by Papell in the early 1960's [19]. The FF was prepared by grinding commercially available micron-sized magnetite particles in a ball mill, subsequently coating the resultant nanoparticles in oleic acid, and dispersing them in heptane. Due to the difficulty in synthesis of alloy-based multicomponent MNP and FF with precise composition control using chemical methods, such FF were often prepared using high energy ball milling [11, 13]. Chaudhary et al.[11] synthesized Fe-Ni-Cr MNP using high energy ball milling under argon atmosphere, coated them using a mixture of oleic acid and ammonium hydroxide solution, and subsequently dispersed the coated nanoparticles in oleic acid. Sharma et al.[13] synthesized Fe-Cr-Al MNP and oil-based FF using surfactant-assisted ball milling under argon atmosphere using oleic acid as both the surfactant and carrier fluid. Other physical methods of preparation of metallic FF include inert gas condensation [43]. Hai et al.[43] prepared iron and cobalt based-FF using inert gas condensation for MNP synthesis, followed by dispersion in a mixture of oil and surfactant.

Very few reports focused on the synthesis of metallic or alloy MNP-based FF using chemical methods. Miguel et al.[44] prepared Fe-based colloidal suspensions for use as a contrast agent for magnetic resonance imaging. Fe nanoparticles were synthesized using a laser pyrolysis technique followed by surface stabilization and dispersion in dextran under alkaline environment. However, the Fe nano powders exhibited a core-shell nanostructure

with an iron-oxide shell. Bao et al.[45] prepared water-based cobalt nanoparticle based FF, using hydrophobic cobalt nanoparticles synthesized by thermal decomposition using a phase transfer technique. Salgueiriño-Maceira et al.[46] prepared water-based FF from oleic acid and oleyl amine capped Fe-Pt nanoparticles, which were initially dispersed in hexane. Bönnemann et al.[47] synthesized air stable Fe and Fe-Co FF using the thermolysis of carbonyl salts in the presence of trialkyl aluminum. Mild oxidation was deliberately performed to create a thin oxide shell around the metallic core for easy surface capping and dispersion in oil medium. **Table 2.1** summarizes the literature on the preparation method, dispersant and carrier fluid medium, and target applications of metallic/alloy-based FF.

Table 2.1. Summary of magnetic nanoparticle types, nanoparticle synthesis method used, surfactant and carrier fluid used for the preparation of metallic/alloy-based ferrofluid, and their intended target application.

Reference	MNP type	Synthesis method	Surfactant used	Carrier fluid	Targeted application
Chaudhary et al[11].	Fe-Ni-Cr	High energy ball milling	Ammonium oleate	Oleic acid	Thermal management
Sharma et al.[13]	Fe-Cr-Al	High energy ball milling	Oleic acid	Oleic acid	Thermal management
Hai et al.[43]	Fe & Co	Inert gas condensation	Octoil	Brij-92	Drug targeting & hyperthermia
Miguel et al.[44]	Fe	Laser pyrolysis	Dextran	Sodium hydroxide & dextran	Magnetic resonance imaging
Bao et al.[45]	Co	Thermal decomposition	Aminododecanoic acid	Water	Biomedical application
Maceira et al.[46]	FePt	Thermal decomposition	Oleic acid & oleyl amine	Water	Drug targeting

Bönnemann et al.[47]	Fe & FeCo	Thermal decomposition	Oleic acid & cashew nut shell liquid	Toluene & kerosene	Biomedical application

Most of the metallic oxide-based FF preparation follows the bottom-up approach using a chemical method for the synthesis of magnetic colloids. Precise control of the MNP size, composition, magnetization, and Curie temperature can be achieved using the bottom-up approach [2]. Magnetite is the preferred choice of MNP for FF preparation due to its ease of synthesis and the wide temperature span over which it remains magnetized. Substituted ferrite-based FF using M-Fe_2O_4 (M=Co, Mn, Ni, Zn, Mg) have also been considered due to their tunable Curie temperature and their magnetic properties. Some of the literature on the synthesis and application of soft ferrite-based FF is summarized below.

Vuong et al.[48] synthesized stable magnetite FF for hyperthermia and MRI applications. Magnetite nanoparticles were synthesized using the thermal decomposition method. The phase transfer process was followed to prepare water-based FF by removing organic solvents. Lazič et al.[6] prepared water-based FF (from coprecipitation synthesized magnetite nanoparticles) to study the effect of photon and electron irradiation for hyperthermia applications. Goharkhah et al.[49] synthesized water-based magnetite FF to investigate its convective heat transfer performance. Magnetite was synthesized by the coprecipitation method and dispersed in DI-water through the addition of tetramethylammonium hydroxide (TMAH). Pîslaru-Dănescu et al.[50] synthesized transformer oil-based FF (using oleic acid capped superparamagnetic Fe_3O_4 nanoparticles prepared by the coprecipitation route) for its use as a coolant in power transformers. Zaibudeen et al.[51] studied the performance of a non-enzymatic sensor for detection of urea using a magnetite FF based oil-in-water microemulsion. MNP were synthesized using the coprecipitation method. The emulsion was functionalized by a triblock copolymer for urea detection.

Çelik et al.[52] synthesized cobalt ferrite nanoparticles via chemical reduction route for its application in magnetic hyperthermia. The as-synthesized nanoparticles were capped using a mixture of oleic acid and oleyl amine and dispersed separately in phenyl, benzyl and octyl ether. Arulmurugan et al.[53] prepared ferrofluid, using Co-Zn ferrite nanoparticles, for

energy conversion by TMC. The MNP were synthesized using the chemical coprecipitation method, followed by coating using ammonium oleate and dispersion in heptane. The Curie temperature and saturation magnetization of the as-synthesized nanoparticles were tuned by zinc substitution. Chaudhary et al.[12] synthesized ammonium oleate coated Mn-Zn ferrite based FF in an aqueous medium for low grade thermal management applications. The hydrothermal technique was used for the synthesis of Mn-Zn ferrite nanoparticles. Gadolinium substituted Mn-Zn ferrite nanoparticles were synthesized using the chemical coprecipitation method and subsequently dispersed in distilled water for MF hyperthermia applications [54].

Halbreich et al.[55] synthesized maghemite nanoparticle-based FF using the chemical coprecipitation method to prepare MNP, followed by dispersion of the resultant MNP in nitric acid. Ghasemi et al.[56] prepared oil-based maghemite FF, using the chemical coprecipitation method to prepare MNP, to study its magneto-viscous effect. Polikarpov et al.[57] synthesized water-based maghemite FF using a chemical method. **Table 2.2** summarizes the literature on the preparation method, dispersant and carrier fluid medium and applications of ferrite-based FF. It can be inferred from **Table 2.1** and **Table 2.2** that the synthesis of metallic/alloy-based and soft ferrite-based MNP are mostly performed by the thermal decomposition and coprecipitation technique, respectively. Thermal decomposition of metal precursors is performed at elevated temperature in the presence of surfactant molecules and under argon or argon/H_2 atmosphere to prevent agglomeration and oxidation of the nanoparticles. The coprecipitation method is widely used for the synthesis of ferrites due to its ease of production, low-cost, facile particle size control, relatively low reaction temperatures, good composition control, less hazardous precursors, reduced time for the reaction, and scalability [3, 58].

Table 2.2. Summary of magnetic nanoparticle types, nanoparticle synthesis method used, surfactant and carrier fluid used for the preparation of ferrite-based ferrofluid, and target application.

Reference	MNP type	Synthesis method	Surfactant used	Carrier fluid	Targeted application

Papell[19]	Fe_3O_4	High energy ball milling	Oleic acid	Heptane	Propellant in space shuttle
Vuong et al.[48].	Fe_3O_4	Thermal decomposition	Oleic acid & oleyl amine	Water	Hyperthermia & MRI
Lazič et al.[6].	Fe_3O_4	Coprecipitation	Oleic acid	Water	Hyperthermia
Goharkhah et al.[49]	Fe_3O_4	Coprecipitation	Tetramethylammonium hydroxide	Water	Thermal management
Pîslaru-Dănescu et al.[50]	Fe_3O_4	Coprecipitation	Oleic acid	Transformer oil	Thermal management
Zaibudeen et al.[51]	Fe_3O_4	Coprecipitation	Oleic acid	Water	Biosensor
Çelik et al.[52]	$CoFe_2O_4$	Chemical reduction	Oleic acid & oleyl amine	Ether	Hyperthermia
Arulmuruga n et al.[53]	Co-Zn ferrite	Coprecipitation	Ammonium oleate	Heptane	Thermal management
Chaudhary et al.[12].	Mn-Zn ferrite	Hydrothermal	Ammonium oleate	Water	Thermal management
Jadhav et al.[54]	Gd-substituted Mn-Zn ferrite	Coprecipitation	No information	Water	Hyperthermia
Halbreich et al.[55]	γ-Fe_2O_3	Coprecipitation	No information	Nitric acid	Biomedical application

Ghasemi et al.[56]	γ-Fe_2O_3	Coprecipitation	Oleic acid	Kerosene	No information
Polikarpov et al.[57]	γ-Fe_2O_3	Chemical method	Electrostatic stabilization	Water	No information

2.2 Stability Requirements of Ferrofluid

The stability of a ferrofluid depends on various aspects [59]: (a) FF consist of MNP with high surface energies, hence they are thermodynamically unstable, (b) nanoparticles in the FF experience thermal Brownian motion, keeping the FF in stable suspension against gravitational sedimentation, (c) MNP may agglomerate due to magnetic dipolar interactions and van der Waals interactions and then sediment, (d) no chemical reaction should occur between the nanoparticles or between the carrier fluid and nanoparticles. MNP suspended in a carrier fluid experience several effects. Some of these effects favor stable suspensions while the rest increase particle agglomeration and settling. Therefore, aggregation and settling of particles are two crucial factors defining the stability of a ferrofluid.

Magnetic nanoparticles in the FF experience thermal, magnetic and gravitational effects [2]. The energy per MNP under these different energies are,

$$Thermal\ energy = kT \tag{2.1}$$

$$Magnetic\ energy = \mu_0 MHV \tag{2.2}$$

$$Gravitational\ energy = \Delta\rho V g L \tag{2.3}$$

where, k is Boltzmann's constant, T is absolute temperature, μ_0 is the free space magnetic permeability, M is the nanoparticle magnetization, H is the strength of externally applied magnetic field, V is the volume of the nanoparticle, which is equal to $\pi d^3/6$ for a spherical particle of diameter d, $\Delta\rho$ is the density difference of the solid and fluid phases in the FF, g is gravitational acceleration, and L is the height of the particle above zero potential in the gravitational field.

2.2.1 Stability under external magnetic field

Under the effect of an external magnetic field gradient, magnetic nanoparticles experience an attractive force towards stronger magnetic field regions, while thermal motion acts against the magnetic force to impart random motion to the nanoparticles across the fluid volume [2]. Stability against particle agglomeration is supported by a high ratio of thermal energy to magnetic energy,

$$\frac{Thermal\ energy}{Magnetic\ energy} = \frac{kT}{\mu_0 MHV} \tag{2.4}$$

The maximum allowable nanoparticle size that can be dispersed in carrier fluid to avoid sedimentation can be assessed by using the Odenbach formula [60];

$$d \leq \left({}^{6kT}/_{\mu_0 MHV}\right)^{1/3} \tag{2.5}$$

2.2.2 Stability in gravitational field

The gravitational force acts on the center of mass of the particle and pulls it down while thermal energy favors the uniform dispersion of particles in the carrier fluid [2]. The relative influence of gravitational field and magnetic field is given by the ratio

$$\frac{Gravitational\ energy}{Magnetic\ energy} = \frac{\Delta \rho g L}{\mu_0 MH} \tag{2.6}$$

But the gravitational energy is almost 100 times weaker than the magnetic energy [2]. Therefore, particle segregation due to gravitational effect is unlikely to happen for ferrite nanoparticles.

2.2.3 Stability against particle agglomeration

As the concentration of magnetic nanoparticles in the ferrofluid is high, frequent collisions occur between the nanoparticles [2]. Hence, there is a very high chance of nanoparticle agglomeration. When particles encounter each other, the magnetic dipole-dipole interaction energy is given by [2],

$$E_{dd} = \frac{1}{12}\mu_0 M^2 V \tag{2.7}$$

Thermal agitation works against the agglomeration of nanoparticles and this effect of reducing agglomeration can be assessed by the ratio

$$\frac{Thermal\ energy}{Dipole-dipole\ interaction\ energy} = \frac{12kT}{\mu_0 M^2 V} \quad (2.8)$$

Again, the particle size can be deduced, and the inequality can be given by

$$d \leq \left({}^{72kT}/_{\pi\mu_0 M^2}\right)^{1/3} \quad (2.9)$$

Apart from magnetic dipolar interactions, electric dipole-dipole interactions can also affect particle agglomeration [2]. Considering all the energy terms that affect stability, magnetic nanoparticles ranging up to 10 nm in size can be used for preparation of stable ferrofluids [2].

2.3 Thermophysical properties of ferrofluid

The thermophysical properties of FF are thermal conductivity and viscosity. The thermal transport of FF depends greatly on the thermophysical properties and is affected by the magnitude and direction of the applied magnetic field [61]. Hence, the thermophysical properties under applied magnetic field can be strongly anisotropic. Both the thermal conductivity and viscosity of the FF are higher than the base fluid value both without as well as in the presence of an external magnetic field. The effect of various factors on the thermal conductivity and viscosity of the FF are discussed in the following subsections. The thermophysical properties of a FF also depend on several other factors such as nanoparticle volume concentration, size and type of magnetic nanoparticle, properties of carrier fluid, surfactant coating type, and temperature [9].

2.3.1 Thermal conductivity

Water or oil is usually used as the liquid phase coolant for waste heat removal from devices and systems. Recently, the potential of a stable suspension of nanoparticles to enhance the thermal conductivity of the base fluid, improving heat transfer, has been investigated. This thermal conductivity enhancement in the base fluid was studied by the addition of either metallic nanoparticles or their oxide such as Al_2O_3, Cu, CuO, TiO_2, Ag, graphene and carbon nanotubes [14]. However, the addition of highly thermally conductive nanoparticles to the base fluid does not always result in substantial enhancement of the thermal conductivity of resultant suspension [62]. These investigations opened up the opportunity for the use of MNP in a base fluid, especially under the application of an externally applied

magnetic field. The improvement in the thermal conductivity of a stable FF is represented as the ratio of the thermal conductivity of the FF (κ_{ff}) to the thermal conductivity of the carrier fluid (κ_{cf}).

2.3.1.1 Theoretical background for the enhancement of ferrofluid thermal conductivity

Thermal conductivity of FF tends to increase significantly under an applied magnetic field. Two mechanisms are proposed for the enhancement of the thermal conductivity of FF, namely, Brownian motion and MNP chain formation [63, 64]. Brownian motion is the random zigzag movement of small particles in the carrier fluid due to collision with the fluid molecules. The Brownian motion can contribute to FF thermal conductivity enhancement in two ways: (a) heat transport through the FF due to the diffusion of MNP, and (b) micro-convection of carrier fluid around the MNP [65, 66]. The theory of Brownian motion as the factor for enhancing thermal conductivity of the FF has not gained much interest as it overestimated the thermal conductivity [14].

Magnetic nanoparticle chain formation due to dipolar interactions in the presence of an external magnetic field has received interest as the main mechanism behind the thermal conductivity enhancement of FF [63, 67]. The presence of nanoparticle aggregates provides effective low thermally resistive path for faster heat conduction compared to the carrier fluid thermal conductivity. MNP tend to assemble in the direction of the applied magnetic field and form 1-D chains, 2-D aggregates and 3-D superlattices, depending on the strength and orientation of magnetic field [14].

Theoretical models for the thermal conductivity improvement have been developed by many researchers. The Maxwell formula [68] (equation (2.10)) is extensively used to evaluate the thermal conductivity of solid-liquid mixtures, but it doesn't consider the shape of the solid particles [69].

$$\frac{k_{nf}}{k_{bf}} = \left[\frac{k_p + 2k_{bf} + 2\left(k_p - k_{bf}\right)\Phi}{k_p + 2k_{bf} - \left(k_p - k_{bf}\right)\Phi}\right] \qquad (2.10)$$

Hamilton et al. [70] modified Maxwell's formula by including the effect of shape for calculating the thermal conductivity (equation (2.11)).

$$k_{nf} = k_{bf}\left[\frac{k_p + (n-1)k_{bf} - (n-1)\Phi\left(k_{bf} - k_p\right)}{k_p + (n-1)k_{bf} + \Phi\left(k_{bf} - k_p\right)}\right] \quad (2.11)$$

In these formulae, Φ represents nanoparticle volume fraction in the FF; k_p, k_{bf} and k_{nf} represent the thermal conductivities of particle, base fluid, and FF respectively, while n represents the shape of the nanoparticle [69].

2.3.2 Viscosity

The viscosity of a ferrofluid tends to increase under the application of an external magnetic field, this phenomenon is called the magnetoviscous effect [1]. The reason for such an effect can be attributed to the hindered motion of the FF due to the alignment of the tiny magnetic dipoles along the direction of the applied magnetic field. Rosensweig [71] discovered the magnetoviscous effect in concentrated magnetite FF. McTague [72] studied this effect in a dilute cobalt nanoparticle based FF. They observed an increase in the viscosity of the FF with an increase in the applied magnetic field strength. McTague also observed larger increment in the FF viscosity when the magnetic field was applied in a direction parallel to the flow of FF than the perpendicular case.

2.3.2.1 Theoretical study of viscosity of ferrofluid

Viscosity affects the application of FF [69, 73]. The presence of magnetic agglomerates affects the viscosity [74]. FF with larger particles result in a sharp increase in viscosity in the presence of a magnetic field due to the magnetoviscous effect, whereas FF having finer particle size of ~10nm do not display much contribution to the magnetoviscous effect [74]. Einstein's equation [75] relates viscosity to the nanoparticle volume fraction;

$$\eta_{nf} = \eta_f(1 + 2.5\Phi) \quad (2.12)$$

The above correlation is best suited for low volume fraction of particles and considers the effect of Brownian motion of particles in the base fluid [69]. Kunitz has accounted for the case of higher particle concentration of up to 50% and developed an empirical formula to describe the viscosity of the stable suspension (equation (2.13)) [76]. Here, Φ is the particle volume concentration; η_{nf}, η_f are the viscosities of the FF and the base fluid, respectively. These models are applicable when there is no applied magnetic field [69]. Rosensweig estimated the viscosity variation of FF, as a function of external magnetic field for different ratios of hydrodynamic stress to magnetic stress, using the dimensional analysis technique

[77]. For the values of this ratio above 10^{-4}, the viscosity does not vary with magnetic field while for values between 10^{-6} and 10^{-4}, it does vary with applied field. Ilg et al.[78] studied the anisotropy in the observed viscosity of a FF using molecular simulation. They observed different viscosity coefficients of the FF at different orientation of the magnetic field with respect to the flow direction as a function of magnetic field strength and volume concentration of nanoparticles in the FF.

$$\eta_{nf} = \eta_f \left(1 + 0.5\Phi\right) \Big/ (1 - \Phi)^4 \qquad (2.13)$$

2.4 Applications of Ferrofluids

Ferrofluids possess both fluidic and magnetic behavior, hence the dynamics of the FF can be tuned by applying an external magnetic field. The thermal properties of FF such as thermal conductivity, viscosity, and heat capacity along with the magnetic properties can be tuned by an external magnetic field. Hence, FF finds application in various fields of biotechnology, biomedical engineering, and mechanical engineering [1, 2, 79]. FF is used in multitude of applications viz., targeted drug delivery, hyperthermia, magnetic seal, materials synthesis, energy harvesting, micro robotics, optical filters, micromechanical sensors , magneto-optical filters, optical switches, optical limiters and magneto-optical waveguides, biosensors, and thermal management systems [79-83]. Energy harvesting and thermal management are the two major applications of FF, which utilize the conversion of waste energy for energy management. These two applications are described in the following subsections.

2.4.1 Energy harvesting

Ferrofluids contain superparamagnetic or single domain soft ferro/ferrimagnetic nanoparticles which can act as tiny magnetic dipoles under an external magnetic field. Hence, they develop magnetic flux lines around a given volume of the FF under the application of an external magnetic field. If the magnetic flux can be made time varying and cut the surface of a coil perpendicularly, a voltage is generated owing to Faraday's law of electromagnetic induction. The time variation of magnetic flux can be achieved by utilizing natural energy sources such as vibrational energy, wind energy, tidal energy, and thermal gradient. Hence, the FF are a potential fluid medium for vibrational energy

harvesting systems. Energy harvesting refers to the conversion of environmental energy to electrical energy [84]. FF-based energy harvesters are useful to power sensors in sophisticated medical instruments, buildings, meteorological and archaeological monitoring , military applications, and industrial equipment [9]. The harvested electrical energy can be used to power sensor networks in remote places to avoid regular maintenance and replacement issues. Vibrational energy harvesters utilizing FF, unlike solar energy harvesters, can provide electrical power throughout the year due to the abundance of vibrational energy sources [9].

The magnitude of the harvested energy depends on the time-varying flux linkage passing perpendicular through the coil around the harvester, which depends on the frequency of the energy that induces the FF vibration. Yun et al.[10] developed a FF-based energy harvester system by passing air bubbles at different rates through the FF column (**Figure 2.1**). The movement of air droplets through the FF at a certain frequency disturbs the temporalmagnetic flux linked with the coil. They developed a numerical model to study the effect of drag force, interfacial tension, buoyancy, and electromagnetic forces on the magnitude of harvested energy.

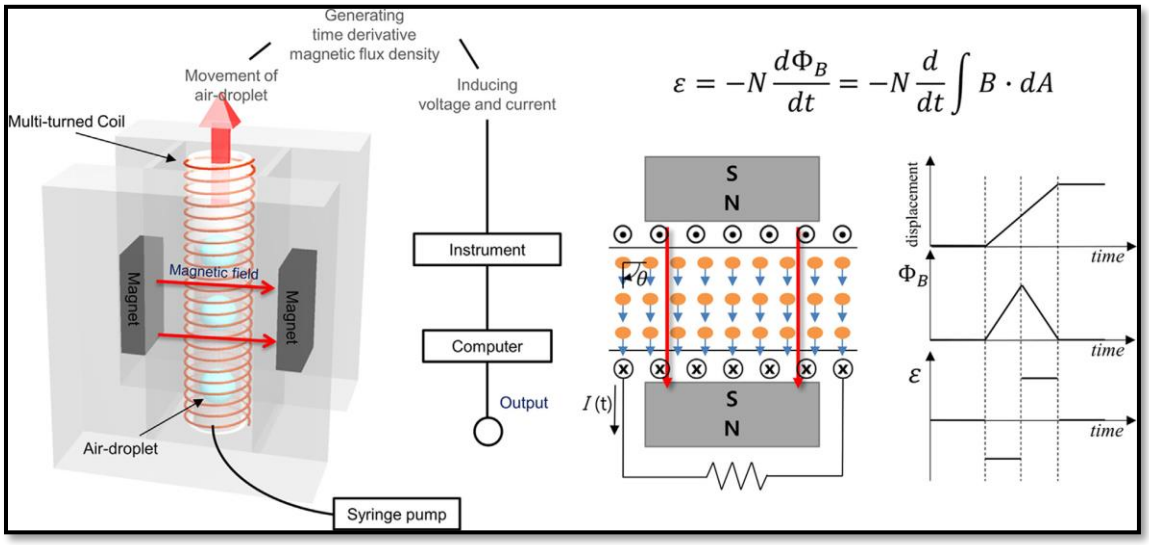

$$\varepsilon = -N\frac{d\Phi_B}{dt} = -N\frac{d}{dt}\int B \cdot dA$$

Figure 2.1. Schematic and working principle of ferrofluid-based energy harvester based on air droplet motion through the ferrofluid [10].

Bibo et al.[85] investigated an electromagnetic energy harvester for converting mechanical vibration to electrical power resulting from the sloshing motion of FF. The schematic of

such an energy harvester is shown in **Figure 2.2**. Due to the fluidic behavior of FF, it can be filled inside containers of any shape. The MNP can respond to very small acceleration, giving rise to electrical power ranging from μW to mW range with a potential of being scalable [86].

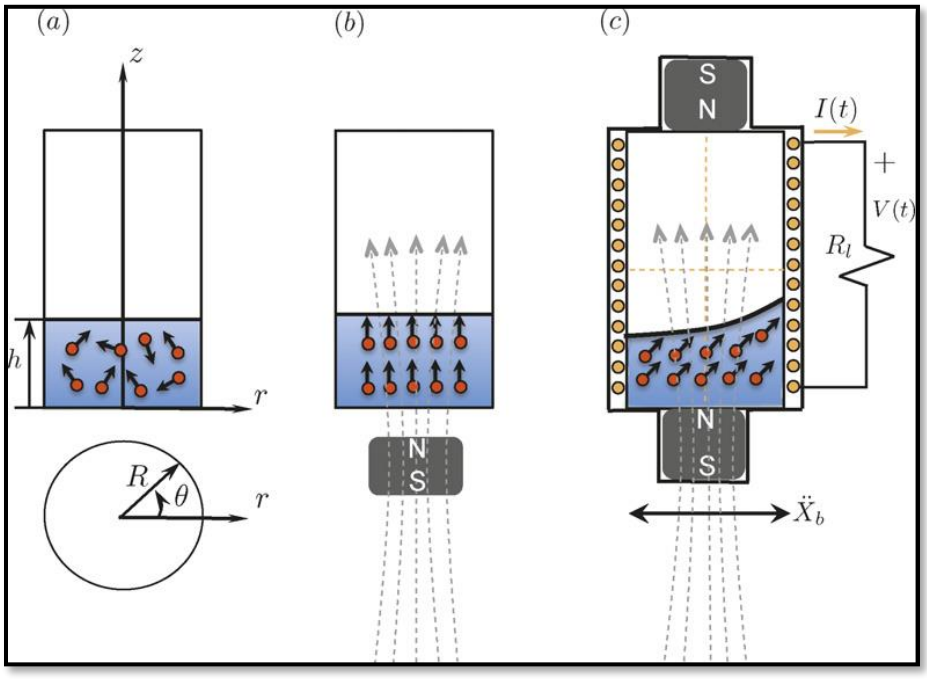

Figure 2.2. Concept of electromagnetic energy harvester utilizing the sloshing motion of ferrofluid in the presence of an applied magnetic field [85].

Recent literature reported the use of a solid thermomagnetic alloy for energy harvesting owing to Faraday's law of electromagnetic induction [87, 88]. Deepak et al. devised a multifunctional hybrid TM oscillator for cooling the heat load as well as harvesting energy from waste heat (**Figure 2.3**). They reported voltage and current generation of 10 V and 15 mA per oscillation cycle. In another work, they demonstrated an enhancement in energy harvesting by replacing the rigid spacer with a flexible spacer (**Figure 2.4**) [87]. A 32% increment in oscillation frequency was reported due to the use of flexible spacer, resulting in 18% enhancement in the voltage harvested. They also derived the figure of merit of the hybrid thermomagnetic oscillator considering device parameters with magnetic properties of the alloy.

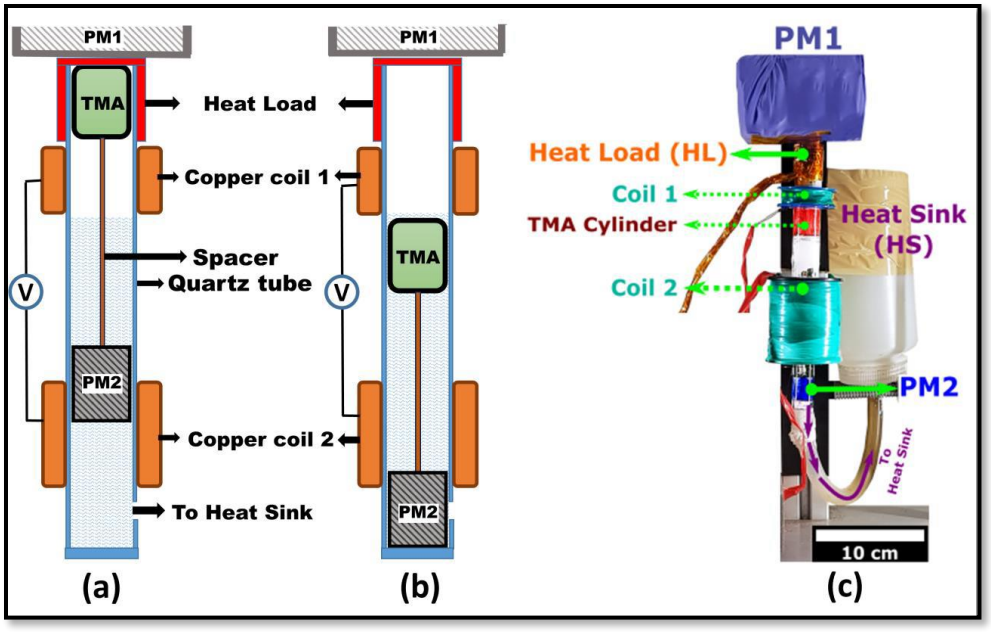

Figure 2.3. Schematic of the hybrid thermomagnetic oscillator, representing the position of the MnNiSi based alloy at (a) the heat load, (b) the heat sink, and (c) experimental setup [88].

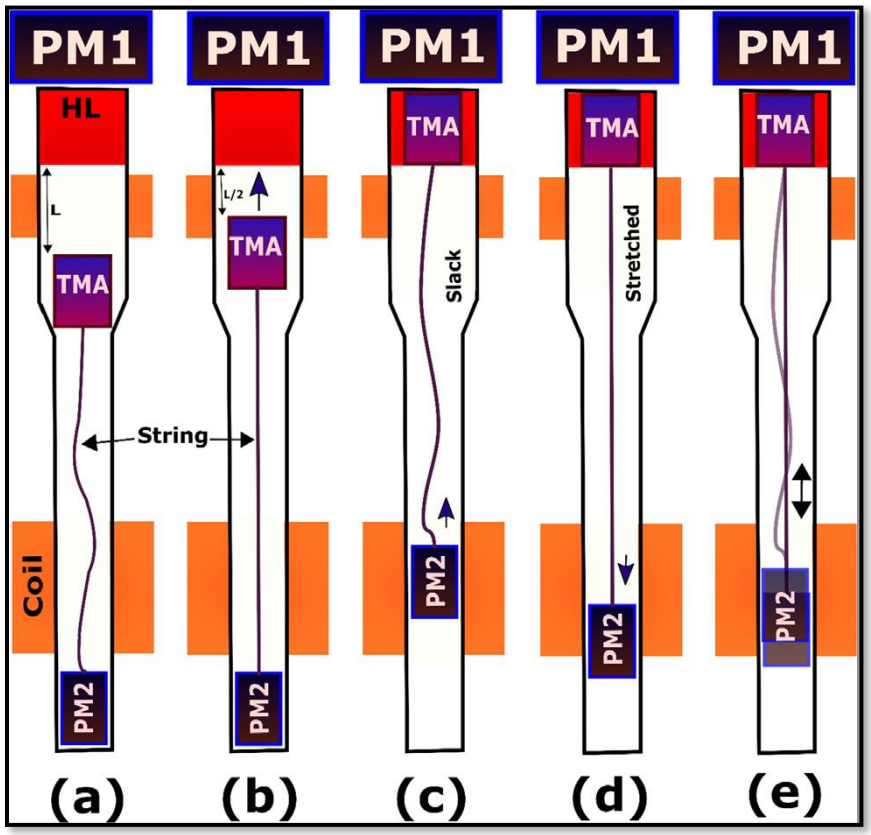

Figure 2.4. Schematic of the hybrid thermomagnetic oscillator with a flexible spacer showing different phases of oscillation [87].

2.4.2 Energy and thermal management

The flow of a FF under the combined effect of thermal and magnetic energy can be controlled by an external magnetic field. The corresponding phenomenon is called thermomagnetic convection [14]. Many experimental and theoretical studies have been performed to assess the conversion efficiency of magnetic and thermal energy to the movement of the FF, which can be used to remove waste heat from devices. This method is used to realize passive heat transfer systems. Moreover, MC devices based on the TM effect are noise free, vibration free, require no or low maintenance, and are self-pumping and self-regulating in nature [12, 89]. The principle along with the experimental and theoretical investigations on MC devices are reported in the next section. **Figure 2.5** represents one such MC device to cool the heat load.

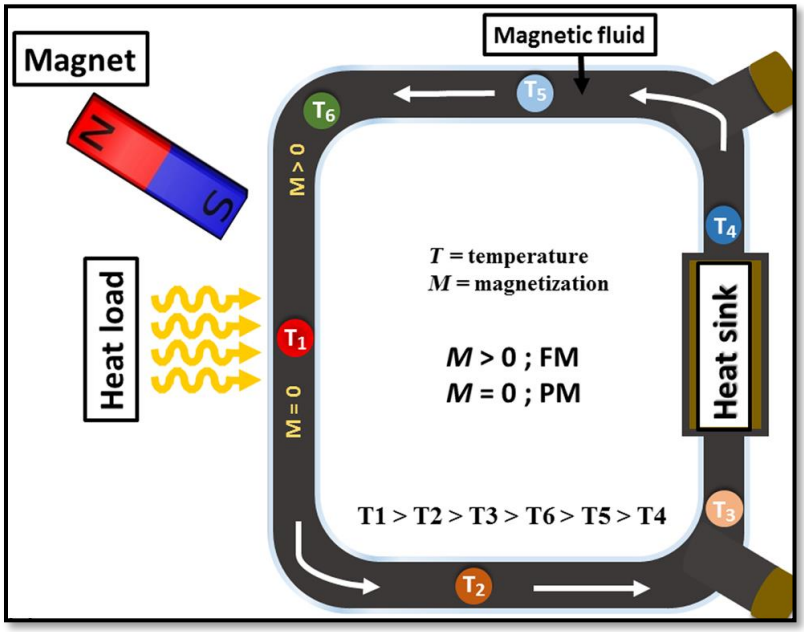

Figure 2.5. Schematic of a magnetic cooling device used to transfer waste heat from a heat load to the heat sink using the thermomagnetic convection of a ferrofluid [13].

2.5 Thermomagnetic Convection of Ferrofluid

A normal fluid, under the effect of a thermal gradient, experiences a variation in its density, which affects the buoyancy of the fluid, this is known as natural convection (**Figure 2.6**(a)).

The gravitational field is the major driving factor for natural convection. Due to the interplay between the thermal gradient and the gravitational field, the denser fluid falls to the bottom portion of the container, while the relatively warmer fluid rises, leading to bulk fluid motion.

In the presence of a thermal gradient, if the normal fluid is replaced by a FF, then the density variation is also accompanied by a variation in the FF magnetization. In such a case, the interplay between the thermal gradient and the externally applied magnetic field leads to the motion of FF, this phenomenon is known as thermomagnetic convection, as shown in **Figure 2.6**(b) (TMC). In TMC, an external magnetic field triggers the stronger movement of colder FF towards the magnet, pushing the warmer FF away from the magnet, due to a differential magnetic Kelvin body force on the FF [90]. Gravity is not a requirement for TMC, which makes it a suitable convection method for thermal management in space shuttles under zero gravity condition [91, 92]. TMC loops do not require any mechanical moving parts for FF flow, instead the fluid flows under the effect of thermal gradient and magnetic field, hence, these systems are self-pumping in nature [92-95]. Moreover, the FF pumping speed through the flow channel gets autotuned due to the change in the effective magnetization gradient as the temperature is varied, hence TMC based cooling systems are self-regulating in nature. A TMC based cooling system is also known as a MC system or a TM cooling device.. These MC systems can recover waste heat from heat engines, household appliances, electrical and mechanical devices, electronic equipment, data servers etc.

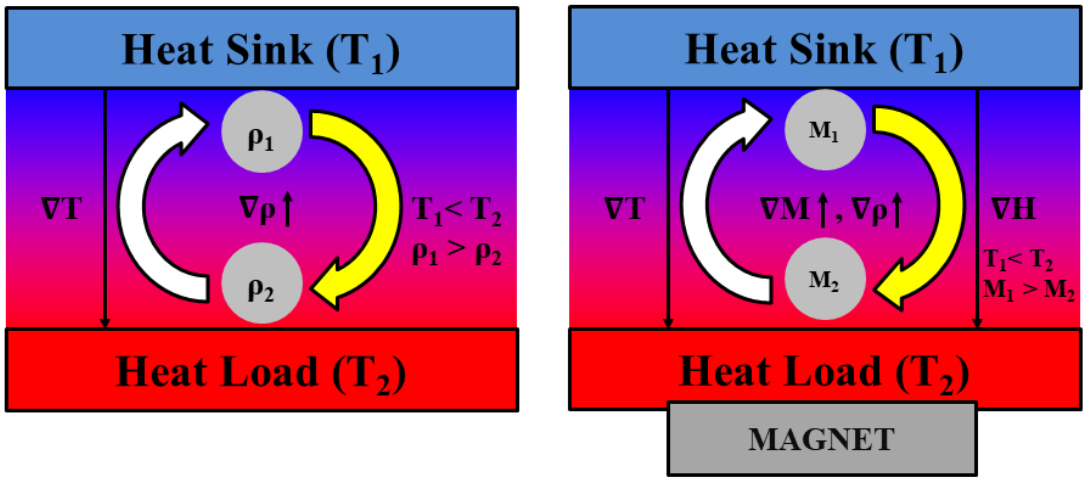

Figure 2.6. Schematic of (a) natural convection (left) of a fluid under the effect of a thermal gradient, and (b) thermomagnetic convection (right) of a ferrofluid in presence of a magnetic field gradient applied parallel to the thermal gradient.

2.5.1 Theoretical background of thermomagnetic convection

Devices based on thermomagnetic convection can be important for passive thermal management. The FF removes heat from the heat load under the influence of an external magnetic field [91]. The dispersed MNP are set in motion by the magnetic field, and transfer part of their kinetic energy to the surrounding carrier fluid, resulting in bulk motion of the fluid [61].

A ferrofluid experiences several forces such as van der Waals force, magnetic dipolar force, gravitational force, drag force and Brownian force. Some of the forces lead to nanoparticle agglomeration due to their attractive nature, while the other forces impart random motion to the nanoparticles. A differentially heated FF subjected to an external magnetic field experiences a non-linear magnetic volume force as a result of the temperature dependence of FF magnetization. This force arises due to the interaction of magnetic moments of the MNP with the applied magnetic field and is known as Kelvin body force. Electromagnetic theory [96] gives the Kelvin body force experienced by a FF having magnetization **M** in a magnetic field of strength **H**,

$$\boldsymbol{F} = \mu_0(\boldsymbol{M}.\boldsymbol{\nabla})\boldsymbol{H} \qquad (2.14)$$

where, μ_0 is the magnetic permeability of the free space. Under an applied magnetic field, the suspended magnetic nanoparticles in a FF take less time to align in the field direction compared to the characteristic time for TMC to commence [61]. Therefore, equation (2.14) can be rewritten as,

$$\boldsymbol{F} = \left(\frac{\mu_0 M}{H}\right)(\boldsymbol{H}.\boldsymbol{\nabla})\boldsymbol{H} \qquad (2.15)$$

where M and H represent the scalar magnitude of magnetization of the material and the strength of magnetic field, respectively. By using the vector identity and further considering the electrically non-conductive nature of the FF, equation (2.15) can be modified as,

$$F = \mu_0 M \boldsymbol{\nabla} H \qquad (2.16)$$

Equation (2.16) clearly reveals that the magnetic field gradient results in a Kelvin body force acting on the FF. The interaction force also depends on temperature, because temperature affects the FF magnetization [2]. Therefore, under a thermal gradient, the FF experiences a TM driving force in the presence of a magnetic field, which causes convective motion of a FF along the flow channel.

2.5.2 Numerical simulation of thermomagnetic convection effect

Numerical simulations were conducted to understand the effect of various parameters such as ferrofluid parameters, thermophysical properties, flow tube geometries, magnitude, and direction of applied magnetic field, and heat flux magnitude on the TMC of a FF. The FF flow and heat transfer characteristics were simulated in the presence of both static and dynamic magnetic fields. The numerical models for the investigation of the TMC of a FF can be mainly divided into two categories:

2.5.2.1 Single phase numerical model

A ferrofluid is a multiphase system, i.e., a solid magnetic MNP suspended in a liquid phase carrier fluid [14]. However, due to the very small size of the magnetic particles and the very small value of slip velocity between the MNP and the carrier fluid, a thermal equilibrium is established between the two phases of the FF [97]. Hence, the physical properties of the FF can be treated as the weighted average value of both the phases (depending on their relative concentration) and can be treated as a single-phase continuum without separately considering the solid and liquid phases. The single-phase numerical model for simulating FF heat transfer is also known as homogeneous model.

Ganguly et al.[98] correlated the heat transfer enhancement due to the TMC of the FF using a single-phase simulation model. They observed the formation of FF vortices near the cold wall and local asymmetry of the thermal boundary layer profiles near the higher magnetic field regions. They also concluded that the heat transfer augmentation greatly depends on the number and the relative distance between the line dipoles.

Goharkhah et al.[99] numerically studied the influence of an alternating non-uniform magnetic field on the laminar thermomagnetic heat transfer of a FF through a flow channel. A total of eight line dipoles were considered along the top and bottom surface of a flow

channel with slight offset position and were simulated to turn the magnetic fields on or off periodically by adding a rectangular wave form to the numerical model. An increase in the heat transfer performance was reported with increasing magnetic field strength and Reynolds number. They observed a sharp increase in local heat transfer coefficient near the alternating magnetic field region.

Ashouri et al.[100] numerically simulated the TMC of a FF, which was filled in a cavity containing the permanent magnet. In the developed 2D single phase model, the side walls are defined as the hotter and colder sides with different temperatures, the top and bottom walls are defined as adiabatic. They observed two counter orienting strong FF circulation loops in the upper and lower half of the cavity. They also investigated the effect of permanent magnet size on the FF TMC and found that the circulation loops increase in size with increasing magnet size. However, an optimum size of the magnet showed better TMC due to the counteracting nature of increase in magnetic field strength, and flow resistance with increasing magnet size.

Sheikholeslami[101] studied the free convective heat transfer of a FF through a porous cavity using a single-phase control volume finite element numerical model. He investigated the effect of various non-dimensional numbers such as Hartmann number, Rayleigh number and Darcy number on the heat transfer characteristics of the FF. He observed that the gradient in temperature increased with increasing Darcy number, Rayleigh number and MNP volume fraction, but reduced with increasing Hartmann number.

Fadaei et al.[97] numerically investigated the forced thermomagnetic heat transfer of a magneto-sensitive nanofluid under rotating magnetic field using a single-phase approach. They studied the effect of varying magnetic field strength, frequency, fluid inlet velocity and viscosity on the convective heat transfer of the FF. They found that the velocity profile changed from parabolic to sinusoidal shape for certain magnetic field parameters. The Nusselt number decreased with increasing inlet fluid velocity for a given magnetic field strength.

Hekmat et al. [102] numerically studied the TMC of water-based Fe_3O_4 FF in a 3D annular region for varying MNP volume fraction and magnetic field gradient. Zanella et al. [103] simulated the effect of FF TMC on the cooling of a transformer with and without the

ferromagnetic core. The presence of a highly permeable core strengthened the effect of magnetic field near that region, giving rise to stronger TM effect. Mousavi et al. [104] numerically investigated the effect of magnetic field on the FF flow behavior inside a helical tube. They obtained ~40% increase in Nusselt number with increasing magnetic field strength.

2.5.2.2 Two-phase numerical model

In the two-phase numerical modelling approach, the solid magnetic nanoparticle phase and the liquid carrier fluid phase are treated as two independent phases having separate sets of conservation equations [14, 97]. Factors such as friction between the two phases, Brownian diffusion, and settling of nanoparticles are also considered in the two-phase approach.

Aminfar et al.[105] used two-phase numerical modelling to study the TMC of a kerosene based Fe_3O_4 FF. They investigated the effect of positive and negative magnetic field gradients on the hydrodynamic and thermal characteristics of the FF in a vertical channel. Their results showed that a negative magnetic field gradient acts like the buoyancy effect, resulting in higher convective heat transfer and pumping power. In another study, Amnifar et al.[106] investigated the hydrodynamic behavior of a sea water based Fe_3O_4 FF in a vertically oriented rectangular duct using a two-phase numerical model. In this model, they considered the electrical conductivity of the FF along with the ferrohydrodynamic phenomena. The effects of non-uniform magnetic field with both positive and negative gradients, uniform transverse magnetic field, and combined non-uniform and uniform magnetic fields on the TMC effect of the FF were studied. They reported that non-uniform magnetic field with a negative magnetic field gradient and uniform transverse magnetic field results in larger Nusselt number and friction factor. For the case of non-uniform magnetic field as well as uniform magnetic field, they observed that by increasing the magnetic field strength of the uniform field, the effect arising due to the non-uniform axial field decreases to a greater extent.

Aursand et al.[107] developed a one-dimensional two-phase model to study the flow behavior of a FF due to TMC. The model employed a nanoparticle model with sets of equations for describing the thermodynamic state of the particles. They also incorporated statistical mechanics to account for the non-uniform MNP size distribution. They reported

that the prediction on the thermomagnetic heat transfer performance of the FF is highly sensitive to the temperature profile of the flow channel.

Sheikholeslami et al. developed a two-phase numerical model to study the forced convective heat transfer of a FF under the effect of a variable magnetic field in a semi-annulus tube. They used a finite element method model using a control volume concept to solve the ferrohydrodynamic governing equations. They studied the effect of various non-dimensional numbers such as Lewis number, Hartmann number and Reynolds number on the thermomagnetic convective heat transfer of a FF. An enhancement in the Nusselt number was observed with increasing Reynolds number and decreasing Lewis and Hartmann number.

Shahsavar et al.[108] numerically investigated the effect of magnetic field on the entropy generation of a Mn-Zn ferrite-based FF in a miniaturized channel using two-phase modelling. They studied the effect of Reynolds number, the strength of the external magnetic field, number of line dipoles and their relative arrangement around the flow channel on the thermal and entropy generation rates. They observed rotating vortices of the FF, which resulted in flow mixing and uniform temperature distribution. They also reported that the entropy generation rate due to friction tends to increase with increasing field strength and decreasing Reynolds number, whereas the total entropy generation rate reduces with increasing magnetic field strength and higher Reynolds number. **Table 2.3** summarizes this literature on the thermomagnetic heat transfer and flow behaviour of a FF using single-phase and two-phase simulation model.

Table 2.3. Summary of literatures on the single-phase and two-phase simulation model to study the thermomagnetic convection of a ferrofluid.

Reference	Simulated geometry	Ferrofluid type	Numerical approach	Major findings
Ganguly et al.[98]	Small rectangular channel	Water/No information	Single-phase	Enhancement in heat transfer depends on the number and placements

				of the magnetic line dipoles.
Goharkhah et al.[99]	Two-dimensional rectangular flow channel	Fe_3O_4/Water	Single-phase	Forced convection of FF enhanced by applying AC magnetic field and higher Reynolds number.
Ashouri et al.[100]	Rectangular cavity	No information	Single-phase	Larger size of magnet improves TM force resulting in higher drag force.
Sheikholeslami [101]	Porous media	Fe_3O_4/Water	Single-phase	Nusselt number enhanced with rise of Darcy number, Rayleigh number, and MNP volume fraction.
Fadaei et al.[97]	Rectangular channel	Fe_3O_4/Water	Single-phase	Higher mixing rate of FF and reduction in thermal boundary layer thickness under rotating magnetic field.
Aminfar et al[105].	Vertical channel	Fe_3O_4/Kerosene	Two-phase	Negative and positive magnetic field gradient augment and suppress the Nusselt number, respectively.
Aminfar et al[106].	Vertical channel	Fe_3O_4/Sea water	Two-phase	Nusselt number and friction factor increased for negative gradient

				axial field but decreased for positive gradient axial field.
Aursand et al.[107]	Rectangular flow channel	Mn-Zn ferrite/Kerosene	Two-phase	FF based cooling provides compactness to the cooling system with improved performance.
Sheikholeslami et al.[109]	Semi-annulus tube	No information	Two-phase	Enhancement in Nusselt number with increase in Reynolds number and decrease in Hartmann number and Lewis number
Shahsavar et al.[108]	Two stationary parallel plates	Mn-Zn ferrite/Tetradecane	Two-phase	Fluid vortices formed under magnetic field, leading to flow mixing. Total entropy generation rate reduced with increasing strength of the magnetic field and higher Reynolds number.

2.5.3 Experimental investigation of thermomagnetic convection effect

Thermomagnetic convection (TMC) based magnetic cooling devices utilizing a ferrofluid as the cooling medium have been developed over a wide range of temperatures, heat load power/heat flux, flow tube diameter, flow tube geometry, flow tube length, range of external pumping power, heat sink temperature, type and strength of external magnetic field and various ferrofluidic properties such as type of MNP, volume concentration of MNP, and carrier fluid medium. Cooling prototypes driven by TMC mainly consists of FF, flow channels, magnetic fields, heat sink, and heat source (**Figure 2.7**). Many researchers have investigated the effect of various factors, e.g., tube geometry [110], heat load power

and power density [110-113], MNP volume fraction in FF [12], magnetic field strength [12, 99, 111-113], heat sink temperature [111-113], inclination of flow channel [114], and position of magnet with respect to heat load [110].Depending on the tube length, tube diameter, a TMC based magnetic cooling device can be subdivided into three categories, viz., micro scale, small scale and large scale. The following subsections describe some experimental investigations of the TM cooling performance of a FF.

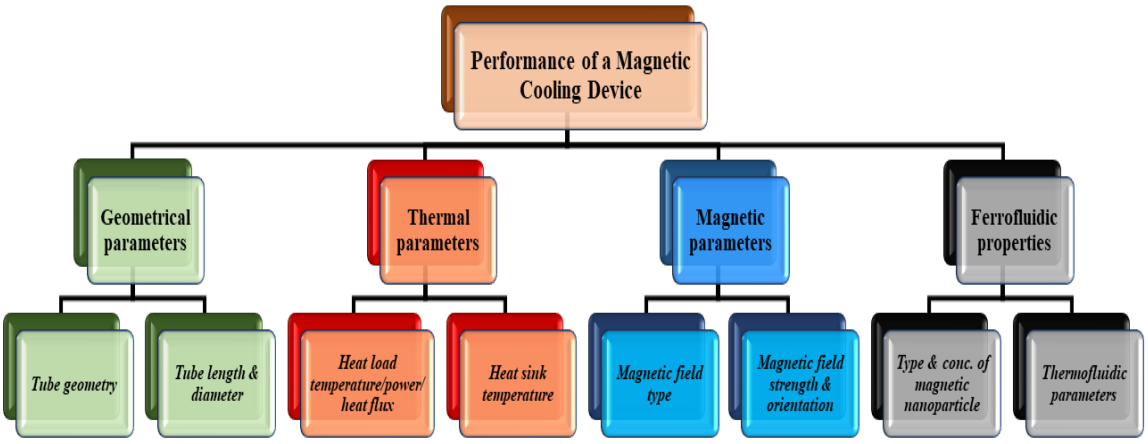

Figure 2.7. Various thermal, magnetic, fluidic, and geometric parameters, which affect the cooling performance of a thermomagnetic convection based magnetic cooling device.

2.5.3.1 Micro scale magnetic cooling devices

Micro scale magnetic cooling devices were mainly investigated for microfluidic applications, e.g., in MEMS and LOC devices. Love et al. [93, 115] compared the experimental results with theoretical models of a ferrofluidic pump system for application in a microfluidic platform. They prepared Mn-Zn ferrite-based FF, using both oil and water as the carrier medium, having a Curie temperature of 150°C. The channel used for the study of this microfluidic pump for lab-on-a-chip (LOC) application was a 2 mm diameter glass tube filled with various FF. They estimated the fluid velocity from the digital camera video output. They measured the displacement using a ruler attached to the flow channel and time from the digital recording. They compared the energy conversion efficiency of both the water and oil-based Mn-Zn ferrite, and oil-based magnetite FF in a MC system. They also demonstrated LOC device cooling using this device.

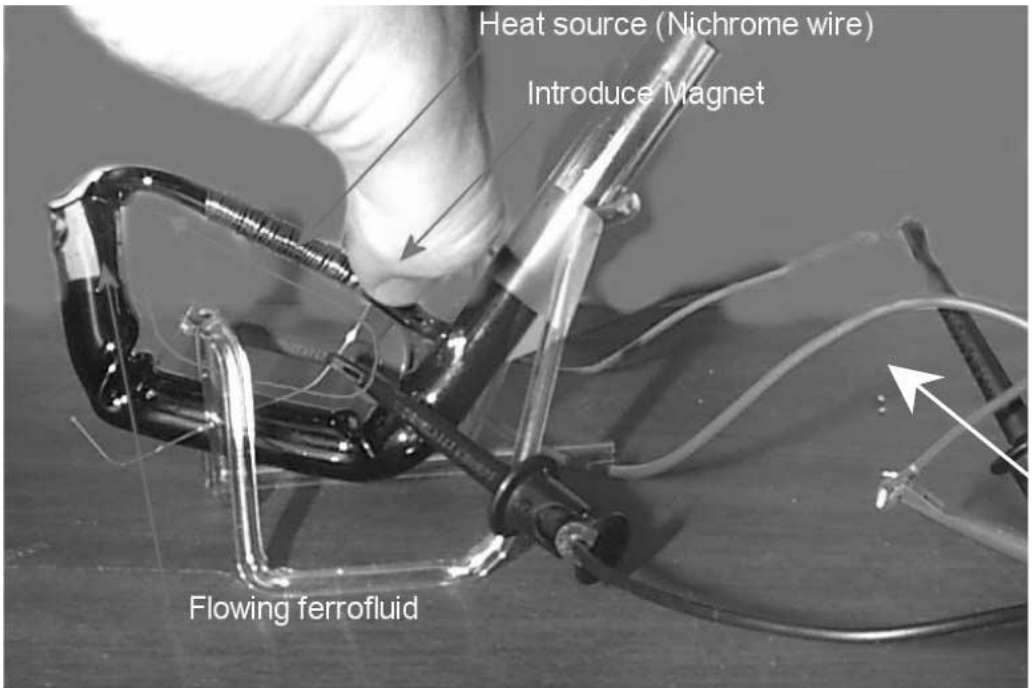

Figure 2.8. Microfluidic magnetocaloric pump for LOC applications [115].

Pal et al. [90] fabricated and experimentally analyzed the performance of a miniaturized thermomagnetic pump targeting MEMS application. They used a glass tube of 2 mm inner diameter to pump the FF under the effect of thermal and magnetic field gradient. They observed an enhancement in the performance of the pump with an increase of either the heat input at the heat load or the external magnetic field strength. They concluded that the TM pump offers better flow rate compared to MHD or field actuated pumps.

2.5.3.2 Small scale magnetic cooling devices

Most of the magnetic cooling devices developed so far are small scale devices. In small scale devices, the flow channel length is less than 1 m, hence they are suitable for cooling of small devices. Lian et al. [112] conducted particle image velocimetry (PIV) measurements to determine the velocity of the ferrofluid in the flow channel. The flow loop was a 75 mm square channel with a depth of 1mm, fabricated as a groove on an aluminum plate (**Figure 2.9**). When two heat loads are used, the flow velocity was found to be higher for a circular geometry compared to both the single heat load case and a square geometry. They also observed FF vortices near the stronger magnetic field regions. Xuan et al. [95] developed a magnetic cooling device for cooling electronic chip using the TMC of a FF.

They found that placement of the permanent magnet near the heat load region resulted in enhanced cooling performance.

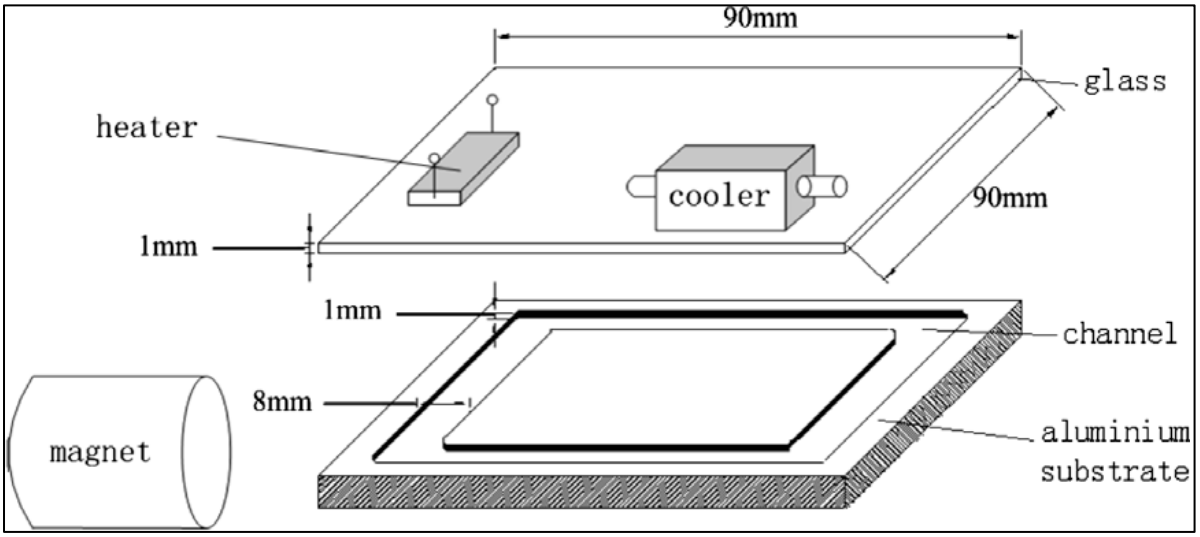

Figure 2.9. Schematic of an automatic heat transport device [112].

Li et al. [111] designed a rectangular cross section magnetic cooling device to examine the effect of external magnetic field strength and power of heat load on the FF flow and heat transfer characteristics. They observed a linear increase in the flow velocity of the FF with increase in the heat load power. Chaudhary et al [116] investigated the magnetic cooling performance of a water-based Mn-Zn ferrite FF using both experiment and simulations. The Mn to Zn molar ratio in the nanoparticle was carefully varied to achieve the desired Curie temperature and the relevant saturation magnetization. They investigated the effect of heat load temperature, the concentration of MNP in the FF and the saturation magnetization of the MNP on the cooling performance of the FF. Cooling was found to increase for larger magnetic field strength and higher MNP volume fraction.

Szabo et al. [117] used infrared thermal imaging to investigate the combined effects of buoyancy force and magnetic force on FF heat transfer due to TMC effect. Heat transfer was analyzed by calculating the Nusselt number and modified Rayleigh number. Zonouzi et al. [118] experimentally investigated the influence of a magnetic quadrupole field on device cooling performance. The local heat transfer coefficient and the pressure drop in the FF for different Reynolds numbers was studied for various axial positions of the quadrupole magnets.

2.5.3.3 Large-scale magnetic cooling devices

Azizian et al.[119] studied the influence of an external magnetic field on the thermomagnetic convective heat transfer and pressure drop of a Fe_3O_4/water FF under laminar flow condition. The flow channel was a stainless-steel tube with an inner diameter of 5.5 mm and the length of the test section was 1 m. The heat transfer was enhanced with an increase in the strength of magnetic field and its gradient. From the simulation, they attributed heat transfer enhancement to MNP agglomeration, resulting in higher momentum and energy transfer. Wang et al.[120] experimentally investigated the influence of external magnetic field orientation and their relative placement on the thermomagnetic convective heat transfer performance of a Fe_3O_4/water FF at a heat load power of 65 W. The heat load section was made from a stainless-steel tube having an inner diameter of 5 mm and length of 1.2 m.

Goharkhah et al.[49] studied the TM heat transfer performance of a Fe_3O_4/water FF under the effect of both constant and alternating magnetic field conditions. The heat load section was an aluminum tube having an internal diameter and length of 9.8 mm and 2.68 m, respectively. They investigated the effect of MNP volume fraction on the thermophysical properties and local heat transfer coefficient of the FF. They attributed the heat transfer enhancement using the constant and alternating magnetic field to nanoparticle chain formation and FF vortices resulting in better flow mixing, respectively. In another work, they examined the effect of varying magnetic field on the heat transfer performance of a Fe_3O_4/water FF [121]. They reported larger heat transfer of FF with increasing magnetic field intensity for a constant value of Reynolds number.

Khairul et al. [122] studied the TMC of a Fe_3O_4/water FF under laminar and turbulent flow conditions as a function of the external magnetic field strength. The MC system used for the investigation has a total channel length more than 3 m. The thermal performance was investigated by studying the effect of pumping power, friction factor, and exergy loss. They reported that the advantages of using FF based heat transfer in MC devices overweighs the disadvantages arising due to the friction factor.

Yamaguchi et al. [114] experimentally studied the performance of a 5 m long magnetic heat transfer system using a temperature-sensitive binary MF (**Figure 2.10**). They reported heat transfer from a

35.8 W heat load using liquid-gas two-phase flow for the horizontal orientation of the device. They observed an enhancement in the heat transport performance and the flow pressure due to the boiling of the low-boiling organic liquid. They reported a maximum thermal energy transfer of 107 W over a distance of 5 m. They also found that the average Nusselt number of the magnetic fluid increases with magnetic field strength. Recently they developed a 10 m long-distance thermal transport device based on liquid-gas two-phase boiling of a temperature-sensitive magnetic fluid for waste heat recovery over a wide temperature range [123].

Table 2.4 summarizes the experimental investigations on the FF TMC based magnetic cooling devices and their categories based on the device length scale along with the study focus.

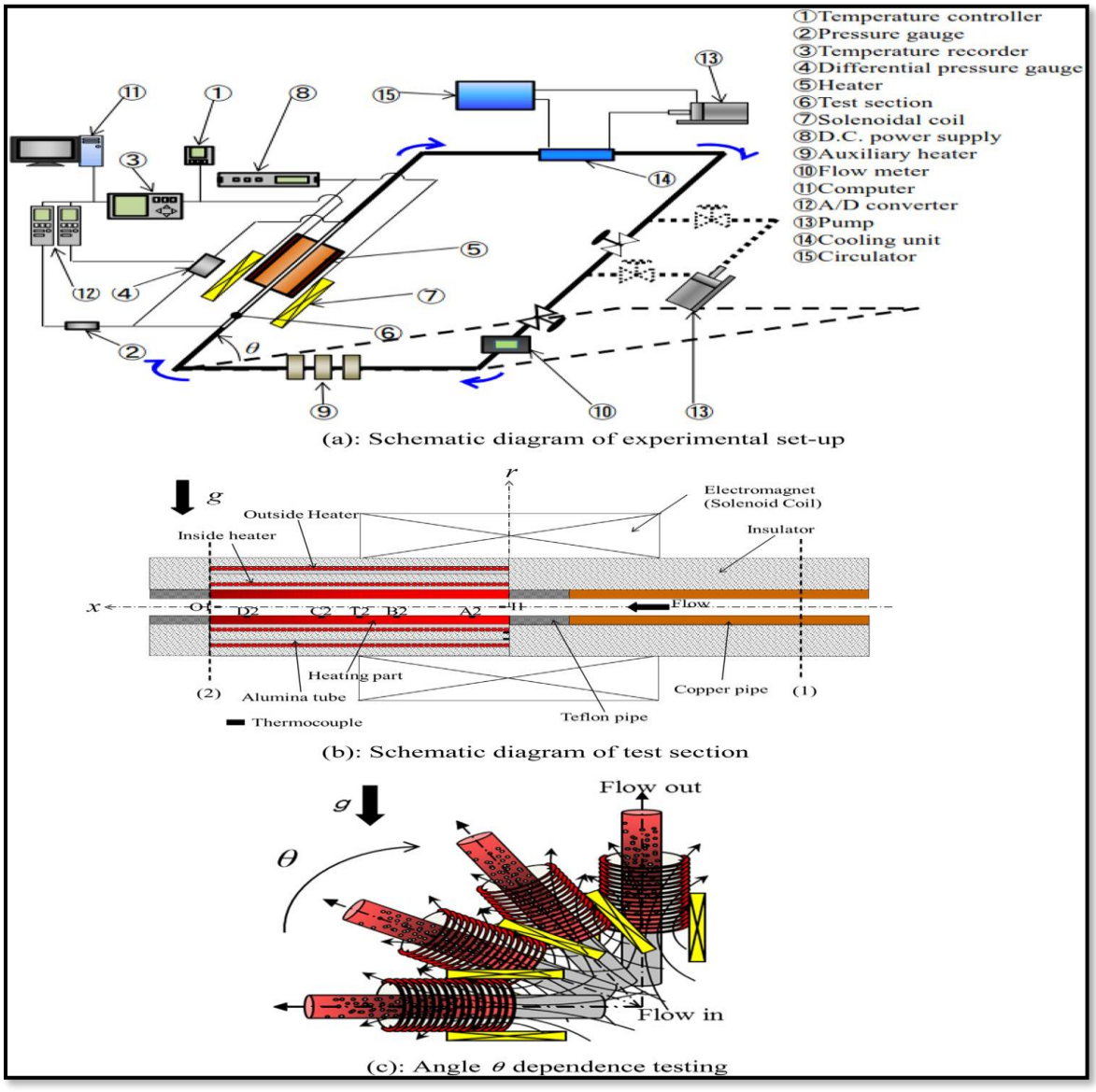

Figure 2.10. Schematic diagram of (a) experimental flow prototype, (b) test section, and (c) inclination angle dependent testing [114].

Table 2.4. Summary of magnetic cooling devices based on the thermomagnetic convection of a ferrofluid. Notations used: L_{tube}: length of the flow tube, d_{tube}: characteristic flow tube length/inner diameter for a rectangular/circular cross section, Pmax: maximum applied heat load power, Q_{max}: maximum applied heat flux, T_{max}: maximum heat load temperature, ΔT: extent of heat load cooling due to thermomagnetic convection, exp: experiment, sim: simulation, NA: no data available.

Ref.	Magnetic cooling device				Device Performance			Category & study focus
	Tube material: Device geometry	Ferrofluid type	L_{tube} (mm)	d_{tube} (mm)	P_{max} (W)/ Q_{max} (kW/m^2)	T_{max} (°C)	ΔT (°C)	
[93, 115]	Glass: straight	Fe_3O_4: oil Mn-Zn ferrite: water & oil	40	2	NA	86	13	Micro scale, Exp+sim
[90]	Glass: straight	Fe_3O_4: oil	110	2	6.2 W	68	NA	Micro scale, Exp
[112]	Aluminum: square	Mn-Zn ferrite: oil	300	8	9 W	68	48	Small scale, Exp
[95]	PMMA: rectangular	Mn-Zn ferrite: oil	460	4	5 W	80	~18	Small scale, Exp
[111]	Glass: rectangular	Mn-Zn ferrite: oil	360	4	3.7 W	77	~25	Small scale, Exp+Sim

[12]	Polymer: circular	Mn-Zn ferrite: water	600	5.2	NA	87	28	Small scale, Exp+Sim
[124]	Perspex: cavity	Commercial	50	50	NA	NA	20	Small scale, Exp +Sim
[118]	Steel: rectangular	Fe_3O_4: water	360	3.7	NA	80	NA	Small scale, Exp
[119]	Steel: rectangular	Fe_3O_4: water	1000	5.5	NA	NA	NA	Large scale, Exp
[49]	Aluminum: rectangular	Fe_3O_4: water	2680	9.8	NA	NA	NA	Large scale, Exp
[121]	Copper: rectangular	Fe_3O_4: water	2500	40	NA	NA	NA	Large scale, Exp
[122]	Steel: rectangular	Fe_3O_4: water	>3000	4.57	NA	NA	NA	Large scale, Exp
[114]	Brass+ copper: rectangular	Mn-Zn ferrite: kerosene+ hexane	5000	10	34.7 kW/m^2	NA	20	Large scale, Exp
[123]	Brass+ copper:	Mn-Zn ferrite:	10000		18 kW/m^2	120	NA	Large scale, Exp

	rectangular	kerosene+hexane					

References

[1] S. Odenbach, "Recent progress in magnetic fluid research," *Journal of physics: condensed matter,* vol. 16, no. 32, p. R1135, 2004.

[2] R. E. Rosensweig, *Ferrohydrodynamics*. Courier Corporation, 2013.

[3] P. Amin and M. Patel, "Magnetic nanoparticles-a promising tool for targeted drug delivery system," *Asian Journal of Nanosciences and Materials,* vol. 3, no. 1, pp. 24-37, 2020.

[4] H. Marie, V. Plassat, and S. Lesieur, "Magnetic-fluid-loaded liposomes for MR imaging and therapy of cancer," *Journal of Drug Delivery Science and Technology,* vol. 23, no. 1, pp. 25-37, 2013.

[5] S. Laurent, S. Dutz, U. O. Häfeli, and M. Mahmoudi, "Magnetic fluid hyperthermia: focus on superparamagnetic iron oxide nanoparticles," *Advances in colloid and interface science,* vol. 166, no. 1-2, pp. 8-23, 2011.

[6] D. Lazič *et al.*, "Investigation of therapeutic-like irradiation effect on magnetic hyperthermia characteristics of a water-based ferrofluid with magnetite particles," *Journal of Magnetism and Magnetic Materials,* vol. 502, p. 166605, 2020.

[7] V. B. Varma, A. Ray, Z. M. Wang, Z. P. Wang, and R. V. Ramanujan, "Droplet Merging on a Lab-on-a-Chip Platform by Uniform Magnetic Fields," *Scientific Reports,* vol. 6, p. 37671, Nov 28 2016.

[8] V. B. Varma, R. G. Wu, Z. P. Wang, and R. V. Ramanujan, "Magnetic Janus particles synthesized using droplet micro-magnetofluidic techniques for protein detection," *Lab Chip,* 10.1039/C7LC00830A vol. 17, no. 20, pp. 3514-3525, Oct 11 2017.

[9] M. A. Khairul, E. Doroodchi, R. Azizian, and B. Moghtaderi, "Advanced applications of tunable ferrofluids in energy systems and energy harvesters: A critical review," *Energy Conversion and Management,* vol. 149, pp. 660-674, 2017.

[10] H. R. Yun, D. J. Lee, J. R. Youn, and Y. S. Song, "Ferrohydrodynamic energy harvesting based on air droplet movement," *Nano Energy,* vol. 11, pp. 171-178, 2015.

[11] V. Chaudhary and R. V. Ramanujan, "Magnetocaloric properties of Fe-Ni-Cr nanoparticles for active cooling," *Scientific reports,* vol. 6, no. 1, pp. 1-9, 2016.

[12] V. Chaudhary, Z. Wang, A. Ray, I. Sridhar, and R. V. Ramanujan, "Self pumping magnetic cooling," *Journal of Physics D: Applied Physics,* vol. 50, no. 3, p. 03LT03, 2016.

[13] V. Sharma, S. Pattanaik, H. Parmar, and R. V. Ramanujan, "Magnetocaloric properties and magnetic cooling performance of low-cost Fe 75− x Cr x Al 25 alloys," *MRS Communications,* vol. 8, no. 3, pp. 988-994, 2018.

[14] I. Nkurikiyimfura, Y. Wang, and Z. Pan, "Heat transfer enhancement by magnetic nanofluids—a review," *Renewable and Sustainable Energy Reviews,* vol. 21, pp. 548-561, 2013.

[15] W. Elmore, "Ferromagnetic colloid for studying magnetic structures," *Physical Review,* vol. 54, no. 4, p. 309, 1938.

[16] W. Elmore, "The magnetization of ferromagnetic colloids," *Physical Review,* vol. 54, no. 12, p. 1092, 1938.

[17] V. Bashtovoy, B. Berkovsky, and A. Vislovich, "Statics of magnetic fluids," in *Introduction to thermomechanics of magnetic fluids*, 1988.

[18] J. L. Neuringer and R. E. Rosensweig, "Ferrohydrodynamics," *The Physics of Fluids,* vol. 7, no. 12, pp. 1927-1937, 1964.

[19] S. Papell, "Low viscosity magnetic fluid obtained by the colloidal suspension of magnetic particles Patent," 1965.

[20] M. Cowley and R. E. Rosensweig, "The interfacial stability of a ferromagnetic fluid," *Journal of Fluid mechanics,* vol. 30, no. 4, pp. 671-688, 1967.

[21] W. H. S. Busenberg, "Viscosity of magnetic suspension," *J. Chem. Phys,* vol. 51, p. 137, 1969.

[22] R. Kaiser and G. Miskolczy, "Some applications of ferrofluid magnetic colloids," *IEEE Transactions on magnetics,* vol. 6, no. 3, pp. 694-698, 1970.
[23] D. A. Krueger and T. B. Jones, "Hydrostatic profile of ferrofluid around a vertical current-carrying wire," *The Physics of Fluids,* vol. 17, no. 10, pp. 1831-1833, 1974.
[24] M. Perry and T. Jones, "Interfacial parametric ferrohydrodynamics," *Journal of Applied Physics,* vol. 46, no. 2, pp. 756-760, 1975.
[25] B. Berkovsky, V. Fertman, V. Polevikov, and S. Isaev, "Heat transfer across vertical ferrofluid layers," *International Journal of Heat and Mass Transfer,* vol. 19, no. 9, pp. 981-986, 1976.
[26] J. Byrne, "Force on a magnet immersed in a ferrofluid," *IEEE Transactions on Magnetics,* vol. 14, no. 5, pp. 560-562, 1978.
[27] T. Tanahashi, T. Sawada, T. Ando, M. Iga, and H. Torii, "A note on the analytical treatment in ferrohydrodynamics," *Bulletin of JSME,* vol. 26, no. 219, pp. 1509-1517, 1983.
[28] P. J. Stiles, M. Kagan, and J. B. Hubbard, "On the Couette-Taylor instability in ferrohydrodynamics," *Journal of colloid and interface science,* vol. 120, no. 2, pp. 430-438, 1987.
[29] V. L. Kolesnichenko, "Synthesis of nanoparticulate magnetic materials," *Magnetic Nanoparticles,* 2009.
[30] Y. Wang, I. Nkurikiyimfura, and Z. Pan, "Sonochemical synthesis of magnetic nanoparticles," *Chemical Engineering Communications,* vol. 202, no. 5, pp. 616-621, 2015.
[31] R. S. Yadav *et al.*, "Impact of sonochemical synthesis condition on the structural and physical properties of MnFe2O4 spinel ferrite nanoparticles," *Ultrasonics sonochemistry,* vol. 61, p. 104839, 2020.
[32] J. Chandradass and K. H. Kim, "Solvent effects in the synthesis of MgFe2O4 nanopowders by reverse micelle processing," *Journal of Alloys and Compounds,* vol. 509, no. 5, pp. L59-L62, 2011.
[33] I. Sharifi, H. Shokrollahi, M. M. Doroodmand, and R. Safi, "Magnetic and structural studies on CoFe2O4 nanoparticles synthesized by co-precipitation, normal micelles and reverse micelles methods," *Journal of Magnetism and Magnetic Materials,* vol. 324, no. 10, pp. 1854-1861, 2012.
[34] I. Gul, A. Maqsood, M. Naeem, and M. N. Ashiq, "Optical, magnetic and electrical investigation of cobalt ferrite nanoparticles synthesized by co-precipitation route," *Journal of alloys and compounds,* vol. 507, no. 1, pp. 201-206, 2010.
[35] S. Joshi, M. Kumar, S. Chhoker, G. Srivastava, M. Jewariya, and V. Singh, "Structural, magnetic, dielectric and optical properties of nickel ferrite nanoparticles synthesized by co-precipitation method," *Journal of Molecular structure,* vol. 1076, pp. 55-62, 2014.
[36] K. Petcharoen and A. Sirivat, "Synthesis and characterization of magnetite nanoparticles via the chemical co-precipitation method," *Materials Science and Engineering: B,* vol. 177, no. 5, pp. 421-427, 2012.
[37] C. Venkataraju, G. Sathishkumar, and K. Sivakumar, "Effect of cation distribution on the structural and magnetic properties of nickel substituted nanosized Mn–Zn ferrites prepared by co-precipitation method," *Journal of Magnetism and Magnetic Materials,* vol. 322, no. 2, pp. 230-233, 2010.
[38] Y. Lu, Y. Yin, B. T. Mayers, and Y. Xia, "Modifying the surface properties of superparamagnetic iron oxide nanoparticles through a sol− gel approach," *Nano letters,* vol. 2, no. 3, pp. 183-186, 2002.
[39] D. Amara, J. Grinblat, and S. Margel, "Solventless thermal decomposition of ferrocene as a new approach for one-step synthesis of magnetite nanocubes and nanospheres," *Journal of Materials Chemistry,* vol. 22, no. 5, pp. 2188-2195, 2012.

[40] C. Ravikumar and R. Bandyopadhyaya, "Mechanistic study on magnetite nanoparticle formation by thermal decomposition and coprecipitation routes," *The Journal of Physical Chemistry C,* vol. 115, no. 5, pp. 1380-1387, 2011.

[41] W. Yu, H. Xie, L. Chen, and Y. Li, "Enhancement of thermal conductivity of kerosene-based Fe3O4 nanofluids prepared via phase-transfer method," *Colloids and surfaces A: Physicochemical and engineering aspects,* vol. 355, no. 1-3, pp. 109-113, 2010.

[42] H. Yin, H. Too, and G. Chow, "The effects of particle size and surface coating on the cytotoxicity of nickel ferrite," *Biomaterials,* vol. 26, no. 29, pp. 5818-5826, 2005.

[43] N. H. Hai *et al.*, "Iron and Cobalt-based magnetic fluids produced by inert gas condensation," *Journal of Magnetism and Magnetic Materials,* vol. 293, no. 1, pp. 75-79, 2005.

[44] O. Bomatí-Miguel *et al.*, "Fe-based nanoparticulate metallic alloys as contrast agents for magnetic resonance imaging," *Biomaterials,* vol. 26, no. 28, pp. 5695-5703, 2005.

[45] Y. Bao, A. Pakhomov, and K. M. Krishnan, "Brownian magnetic relaxation of water-based cobalt nanoparticle ferrofluids," *Journal of applied physics,* vol. 99, no. 8, p. 08H107, 2006.

[46] V. Salgueiriño-Maceira, L. M. Liz-Marzán, and M. Farle, "Water-based ferrofluids from Fe x Pt1-x nanoparticles synthesized in organic media," *Langmuir,* vol. 20, no. 16, pp. 6946-6950, 2004.

[47] H. Bönnemann *et al.*, "Air stable Fe and Fe Co magnetic fluids—synthesis and characterization," *Applied organometallic chemistry,* vol. 19, no. 6, pp. 790-796, 2005.

[48] T. K. O. Vuong *et al.*, "PMAO-assisted thermal decomposition synthesis of high-stability ferrofluid based on magnetite nanoparticles for hyperthermia and MRI applications," *Materials Chemistry and Physics,* vol. 245, p. 122762, 2020.

[49] M. Goharkhah, A. Salarian, M. Ashjaee, and M. Shahabadi, "Convective heat transfer characteristics of magnetite nanofluid under the influence of constant and alternating magnetic field," *Powder Technology,* vol. 274, pp. 258-267, 2015.

[50] L. Pîslaru-Dănescu, A. M. Morega, G. Telipan, M. Morega, J. B. Dumitru, and V. Marinescu, "Magnetic nanofluid applications in electrical engineering," *IEEE Transactions on magnetics,* vol. 49, no. 11, pp. 5489-5497, 2013.

[51] A. Zaibudeen and J. Philip, "Magnetic nanofluid based non-enzymatic sensor for urea detection," *Sensors and Actuators B: Chemical,* vol. 255, pp. 720-728, 2018.

[52] Ö. Çelik, M. M. Can, and T. Firat, "Size dependent heating ability of CoFe 2 O 4 nanoparticles in AC magnetic field for magnetic nanofluid hyperthermia," *Journal of nanoparticle research,* vol. 16, no. 3, p. 2321, 2014.

[53] R. Arulmurugan, G. Vaidyanathan, S. Sendhilnathan, and B. Jeyadevan, "Co–Zn ferrite nanoparticles for ferrofluid preparation: Study on magnetic properties," *Physica B: Condensed Matter,* vol. 363, no. 1-4, pp. 225-231, 2005.

[54] S. Jadhav *et al.*, "Study of structural and magnetic properties and heat induction of gadolinium-substituted manganese zinc ferrite nanoparticles for in vitro magnetic fluid hyperthermia," *Journal of colloid and interface science,* vol. 541, pp. 192-203, 2019.

[55] A. Halbreich *et al.*, "Biomedical applications of maghemite ferrofluid," *Biochimie,* vol. 80, no. 5-6, pp. 379-390, 1998.

[56] E. Ghasemi, A. Mirhabibi, and M. Edrissi, "Magnetoviscous effect in a maghemite ferrofluid," *Journal of nanoscience and nanotechnology,* vol. 11, no. 6, pp. 5285-5291, 2011.

[57] M. Polikarpov, V. Cherepanov, M. Chuev, R. Gabbasov, I. Mischenko, and V. Panchenko, "Magnetically coupled clusters in aggregated maghemite ferrofluid: Mössbauer and magnetization study," *Hyperfine Interactions,* vol. 237, no. 1, p. 48, 2016.

[58] B. Pejjai, M. Reddivari, and T. R. R. Kotte, "Phase controllable synthesis of CuS nanoparticles by chemical co-precipitation method: Effect of copper precursors on the properties of CuS," *Materials Chemistry and Physics*, vol. 239, p. 122030, 2020.
[59] Z. Haddad, C. Abid, H. F. Oztop, and A. Mataoui, "A review on how the researchers prepare their nanofluids," *International Journal of Thermal Sciences*, vol. 76, pp. 168-189, 2014.
[60] S. Thurm and S. Odenbach, "Particle size distribution as key parameter for the flow behavior of ferrofluids," *Physics of Fluids*, vol. 15, no. 6, pp. 1658-1664, 2003.
[61] Q. Li, Y. Xuan, and J. Wang, "Experimental investigations on transport properties of magnetic fluids," *Experimental Thermal and Fluid Science*, vol. 30, no. 2, pp. 109-116, 2005.
[62] T.-K. Hong, H.-S. Yang, and C. Choi, "Study of the enhanced thermal conductivity of Fe nanofluids," *Journal of Applied Physics*, vol. 97, no. 6, p. 064311, 2005.
[63] J. Philip, P. Shima, and B. Raj, "Enhancement of thermal conductivity in magnetite based nanofluid due to chainlike structures," *Applied physics letters*, vol. 91, no. 20, p. 203108, 2007.
[64] T.-H. Tsai, L.-S. Kuo, P.-H. Chen, and C.-T. Yang, "Thermal conductivity of nanofluid with magnetic nanoparticles," *PIERS online*, vol. 5, no. 3, pp. 231-234, 2009.
[65] J. Eapen, R. Rusconi, R. Piazza, and S. Yip, "The classical nature of thermal conduction in nanofluids," *Journal of heat transfer*, vol. 132, no. 10, 2010.
[66] S. Özerinç, S. Kakaç, and A. G. Yazıcıoğlu, "Enhanced thermal conductivity of nanofluids: a state-of-the-art review," *Microfluidics and Nanofluidics*, vol. 8, no. 2, pp. 145-170, 2010.
[67] J. Philip, P. Shima, and B. Raj, "Evidence for enhanced thermal conduction through percolating structures in nanofluids," *Nanotechnology*, vol. 19, no. 30, p. 305706, 2008.
[68] P. D. Shima and J. Philip, "Role of Thermal Conductivity of Dispersed Nanoparticles on Heat Transfer Properties of Nanofluid," *Industrial & Engineering Chemistry Research*, vol. 53, no. 2, pp. 980-988, 2014.
[69] A. Kumar and S. Subudhi, "Preparation, characteristics, convection and applications of magnetic nanofluids: A review," *Heat and Mass Transfer*, vol. 54, no. 2, pp. 241-265, 2017.
[70] R. L. Hamilton and O. Crosser, "Thermal conductivity of heterogeneous two-component systems," *Industrial & Engineering chemistry fundamentals*, vol. 1, no. 3, pp. 187-191, 1962.
[71] R. Rosensweig, R. Kaiser, and G. Miskolczy, "Viscosity of magnetic fluid in a magnetic field," *Journal of Colloid and Interface Science*, vol. 29, no. 4, pp. 680-686, 1969.
[72] J. P. McTague, "Magnetoviscosity of magnetic colloids," *The Journal of Chemical Physics*, vol. 51, no. 1, pp. 133-136, 1969.
[73] M. Bahiraei and M. Hangi, "Flow and heat transfer characteristics of magnetic nanofluids: A review," *Journal of Magnetism and Magnetic Materials*, vol. 374, pp. 125-138, 2015.
[74] S. Odenbach and K. Raj, "The influence of large particles and agglomerates on the magnetoviscous effect in ferrofluids," *Magnetohydrodynamics*, vol. 36, no. 4, pp. 312-319, 2000.
[75] A. Einstein, *Investigations on the Theory of the Brownian Movement*. Courier Corporation, 1956.
[76] M. Kunitz, "An empirical formula for the relation between viscosity of solution and volume of solute," *The Journal of general physiology*, vol. 9, no. 6, pp. 715-725, 1926.
[77] R. E. Rosensweig, R. Kaiser, and G. Miskolczy, "Viscosity of magnetic fluid in a magnetic field," *Journal of Colloid and Interface Science*, vol. 29, no. 4, pp. 680-686, 1969.
[78] P. Ilg, M. Kröger, and S. Hess, "Anisotropy of the magnetoviscous effect in ferrofluids," *Physical Review E*, vol. 71, no. 5, p. 051201, 2005.

[79] S. Odenbach, "Ferrofluids and their applications," *MRS bulletin,* vol. 38, no. 11, pp. 921-924, 2013.
[80] K. Raj and R. Moskowitz, "Commercial applications of ferrofluids," *Journal of Magnetism and Magnetic Materials,* vol. 85, no. 1-3, pp. 233-245, 1990.
[81] J. Roger, J. Pons, R. Massart, A. Halbreich, and J. Bacri, "Some biomedical applications of ferrofluids," *The European Physical Journal Applied Physics,* vol. 5, no. 3, pp. 321-325, 1999.
[82] H. Shokrollahi, "Structure, synthetic methods, magnetic properties and biomedical applications of ferrofluids," *Materials Science and Engineering: C,* vol. 33, no. 5, pp. 2476-2487, 2013.
[83] I. Torres-Díaz and C. Rinaldi, "Recent progress in ferrofluids research: novel applications of magnetically controllable and tunable fluids," *Soft matter,* vol. 10, no. 43, pp. 8584-8602, 2014.
[84] W. Bertsch, J. Azzi, and J. Davidson, "Delayed light studies on photosynthetic energy conversion. I. Identification of the oxygen-evolving photoreaction as the delayed light emitter in mutants of Scenedesmus obliquus," *Biochimica et Biophysica Acta (BBA)-Bioenergetics,* vol. 143, no. 1, pp. 129-143, 1967.
[85] A. Bibo, R. Masana, A. King, G. Li, and M. Daqaq, "Electromagnetic ferrofluid-based energy harvester," *Physics Letters A,* vol. 376, no. 32, pp. 2163-2166, 2012.
[86] I. Sari, T. Balkan, and H. Kulah, "A wideband electromagnetic micro power generator for wireless microsystems," in *TRANSDUCERS 2007-2007 International Solid-State Sensors, Actuators and Microsystems Conference,* 2007, pp. 275-278: IEEE.
[87] K. Deepak, M. Pattanaik, and R. V. Ramanujan, "Figure of merit and improved performance of a hybrid thermomagnetic oscillator," *Applied Energy,* vol. 256, p. 113917, 2019.
[88] K. Deepak, V. Varma, G. Prasanna, and R. V. Ramanujan, "Hybrid thermomagnetic oscillator for cooling and direct waste heat conversion to electricity," *Applied energy,* vol. 233, pp. 312-320, 2019.
[89] M. S. Pattanaik, V. Varma, S. Cheekati, G. Prasanna, N. Sudharsan, and R. V. Ramanujan, "A self-regulating multi-torus magneto-fluidic device for kilowatt level cooling," *Energy Conversion and Management,* vol. 198, p. 111819, 2019.
[90] S. Pal, A. Datta, S. Sen, A. Mukhopdhyay, K. Bandopadhyay, and R. Ganguly, "Characterization of a ferrofluid-based thermomagnetic pump for microfluidic applications," *Journal of Magnetism and Magnetic Materials,* vol. 323, no. 21, pp. 2701-2709, 2011.
[91] S. Odenbach, "Sounding rocket and drop tower experiments on thermomagnetic convection in magnetic fluids," *Advances in Space Research,* vol. 16, no. 7, pp. 99-104, 1995.
[92] H. Yamaguchi, A. Sumiji, S. Shuchi, and T. Yonemura, "Characteristics of thermo-magnetic driven motor using magnetic fluid," *Journal of Magnetism and Magnetic Materials,* vol. 272-276, pp. 2362-2364, 2004.
[93] L. J. Love *et al.*, "Ferrofluid Field Induced Flow for Microfluidic Applications," *IEEE/ASME Transactions on Mechatronics,* vol. 10, no. 1, pp. 68-76, 2005.
[94] H. Matsuki, K. Yamasawa, and K. Murakami, "Experimental considerations on a new automatic cooling device using temperature-sensitive magnetic fluid," *IEEE Transactions on Magnetics,* vol. 13, no. 5, pp. 1143-1145, 1977.
[95] Y. Xuan and W. Lian, "Electronic cooling using an automatic energy transport device based on thermomagnetic effect," *Applied Thermal Engineering,* vol. 31, no. 8-9, pp. 1487-1494, 2011.
[96] D. J. Griffiths, *Introduction to electrodynamics*. Prentice Hall, 1962.

[97] F. Fadaei, A. M. Dehkordi, M. Shahrokhi, and Z. Abbasi, "Convective-heat transfer of magnetic-sensitive nanofluids in the presence of rotating magnetic field," *Applied Thermal Engineering,* vol. 116, pp. 329-343, 2017.

[98] R. Ganguly, S. Sen, and I. K. Puri, "Heat transfer augmentation using a magnetic fluid under the influence of a line dipole," *Journal of Magnetism and Magnetic Materials,* vol. 271, no. 1, pp. 63-73, 2004.

[99] M. Goharkhah and M. Ashjaee, "Effect of an alternating nonuniform magnetic field on ferrofluid flow and heat transfer in a channel," *Journal of Magnetism and Magnetic Materials,* vol. 362, pp. 80-89, 2014.

[100] M. Ashouri and M. B. Shafii, "Numerical simulation of magnetic convection ferrofluid flow in a permanent magnet–inserted cavity," *Journal of Magnetism and Magnetic Materials,* vol. 442, pp. 270-278, 2017.

[101] M. Sheikholeslami, "Numerical simulation of magnetic nanofluid natural convection in porous media," *Physics Letters A,* vol. 381, no. 5, pp. 494-503, 2017.

[102] M. H. Hekmat and K. K. Ziarati, "Effects of nanoparticles volume fraction and magnetic field gradient on the mixed convection of a ferrofluid in the annulus between vertical concentric cylinders," *Applied Thermal Engineering,* vol. 152, pp. 844-857, 2019.

[103] R. Zanella, C. Nore, F. Bouillault, J.-L. Guermond, and X. Mininger, "Influence of thermomagnetic convection and ferrofluid thermophysical properties on heat transfers in a cylindrical container heated by a solenoid," *Journal of Magnetism and Magnetic Materials,* vol. 469, pp. 52-63, 2019.

[104] S. Mousavi, N. Jamshidi, and A. Rabienataj-Darzi, "Numerical investigation of the magnetic field effect on the heat transfer and fluid flow of ferrofluid inside helical tube," *Journal of Thermal Analysis and Calorimetry,* pp. 1-11.

[105] H. Aminfar, M. Mohammadpourfard, and Y. N. Kahnamouei, "A 3D numerical simulation of mixed convection of a magnetic nanofluid in the presence of non-uniform magnetic field in a vertical tube using two phase mixture model," *Journal of Magnetism and Magnetic Materials,* vol. 323, no. 15, pp. 1963-1972, 2011.

[106] H. Aminfar, M. Mohammadpourfard, and F. Mohseni, "Two-phase mixture model simulation of the hydro-thermal behavior of an electrical conductive ferrofluid in the presence of magnetic fields," *Journal of Magnetism and Magnetic Materials,* vol. 324, no. 5, pp. 830-842, 2012.

[107] E. Aursand, M. A. Gjennestad, K. Y. Lervåg, and H. Lund, "A multi-phase ferrofluid flow model with equation of state for thermomagnetic pumping and heat transfer," *Journal of Magnetism and Magnetic Materials,* vol. 402, pp. 8-19, 2016.

[108] A. Shahsavar, R. Ansarian, and M. Bahiraei, "Effect of line dipole magnetic field on entropy generation of Mn-Zn ferrite ferrofluid flowing through a minichannel using two-phase mixture model," *Powder technology,* vol. 340, pp. 370-379, 2018.

[109] M. Sheikholeslami, M. Rashidi, and D. Ganji, "Numerical investigation of magnetic nanofluid forced convective heat transfer in existence of variable magnetic field using two phase model," *Journal of Molecular Liquids,* vol. 212, pp. 117-126, 2015.

[110] W. Lian, Y. Xuan, and Q. Li, "Design method of automatic energy transport devices based on the thermomagnetic effect of magnetic fluids," *International Journal of Heat and Mass Transfer,* vol. 52, no. 23-24, pp. 5451-5458, 2009.

[111] Q. Li, W. Lian, H. Sun, and Y. Xuan, "Investigation on operational characteristics of a miniature automatic cooling device," *International Journal of Heat and Mass Transfer,* vol. 51, no. 21-22, pp. 5033-5039, 2008.

[112] W. Lian, Y. Xuan, and Q. Li, "Characterization of miniature automatic energy transport devices based on the thermomagnetic effect," *Energy Conversion and Management,* vol. 50, no. 1, pp. 35-42, 2009.

[113] L. Zhou, Y. Xuan, Q. Li, and W. Lian, "A new miniaturized engine based on thermomagnetic effect of magnetic fluids," *Frontiers of Energy and Power Engineering in China,* vol. 3, no. 2, pp. 160-166, 2009.
[114] H. Yamaguchi and Y. Iwamoto, "Energy transport in cooling device by magnetic fluid," *Journal of Magnetism and Magnetic Materials,* vol. 431, pp. 229-236, 2017.
[115] L. J. Love, J. F. Jansen, T. McKnight, Y. Roh, and T. J. Phelps, "A Magnetocaloric Pump for Microfluidic Applications," *IEEE Transactions on Nanobioscience,* vol. 3, no. 2, pp. 101-110, 2004.
[116] V. Chaudhary, Z. Wang, A. Ray, I. Sridhar, and R. Ramanujan, "Self pumping magnetic cooling," *Journal of Physics D: Applied Physics,* vol. 50, no. 3, p. 03LT03, 2016.
[117] P. S. Szabo, M. Beković, and W.-G. Früh, "Infrared thermography of wall temperature distribution caused by convection of magnetic fluid," *International Journal of Thermal Sciences,* vol. 134, pp. 129-139, 2018.
[118] S. A. Zonouzi *et al.*, "Experimental investigation of the flow and heat transfer of magnetic nanofluid in a vertical tube in the presence of magnetic quadrupole field," *Experimental Thermal and Fluid Science,* vol. 91, pp. 155-165, 2018.
[119] R. Azizian, E. Doroodchi, T. McKrell, J. Buongiorno, L. Hu, and B. Moghtaderi, "Effect of magnetic field on laminar convective heat transfer of magnetite nanofluids," *International Journal of Heat and Mass Transfer,* vol. 68, pp. 94-109, 2014.
[120] J. Wang, G. Li, H. Zhu, J. Luo, and B. Sundén, "Experimental investigation on convective heat transfer of ferrofluids inside a pipe under various magnet orientations," *International Journal of Heat and Mass Transfer,* vol. 132, pp. 407-419, 2019.
[121] M. Goharkhah, M. Ashjaee, and M. Shahabadi, "Experimental investigation on convective heat transfer and hydrodynamic characteristics of magnetite nanofluid under the influence of an alternating magnetic field," *International Journal of Thermal Sciences,* vol. 99, pp. 113-124, 2016.
[122] M. A. Khairul, E. Doroodchi, R. Azizian, and B. Moghtaderi, "Thermal performance analysis of tunable magnetite nanofluids for an energy system," *Applied Thermal Engineering,* vol. 126, pp. 822-833, 2017.
[123] H. Yamaguchi and T. Bessho, "Long distance heat transport device using temperature sensitive magnetic fluid," *Journal of Magnetism and Magnetic Materials,* vol. 499, p. 166248, 2020.
[124] P. S. Szabo, M. Beković, and W.-G. Früh, "Using infrared thermography to investigate thermomagnetic convection under spatial non-uniform magnetic field," *International Journal of Thermal Sciences,* vol. 116, pp. 118-128, 2017.

Chapter 3

Experimental and Modelling Methods

This chapter discusses the design of magnetic cooling devices developed to cool heat loads over a wide power and temperature range. The components used for these devices are discussed and categorized into three sections viz., magnetic field unit, fluid flow unit, and heat transfer unit. Various designs and their geometrical parameters are given. The thermomagnetic cooling performance of our magnetic cooling devices were numerically verified and validated by a 2D numerical model developed using COMSOL Multiphysics. The governing equations and relevant boundary conditions used for the numerical simulation of the thermomagnetic convection effect are also presented. Finally, the material properties for different ferrite and metallic/alloy-based ferrofluids are provided, these were used to rank the materials based on their modelled cooling performance.

3.1 Overview

The principle of passive thermomagnetic convection (TMC) of a ferrofluid (FF) was used to develop magnetic cooling devices. These devices had a range of the following parameters: (a) size of the device, (b) internal diameter of the flow tubes, (c) geometry of the device, (d) thermal conductivity of tube material, (e) coupling and multiplexing of the tubes, (f) heat load length and area, and (g) magnet positions. The components required to develop the magnetic cooling device, and the instruments used to record the experimental data are discussed.

2D numerical models to elucidate the single-phase FF thermomagnetic (TM) heat transfer were developed for various MC devices. The numerical model was further elaborated through the governing equations, modelling methodology and the boundary conditions. The effect of HL power, strength of magnetic field, and thermophysical properties of FF on flow behavior were simulated. The experimental findings were modelled and compared with the experimental results to optimize the performance. The material parameters being used to rank various ferrite and metallic/alloy-based FF depending on their MC performance is provided. **Figure 3.1** shows the overview of the experimental, modelling, and analytical methods used for this thesis.

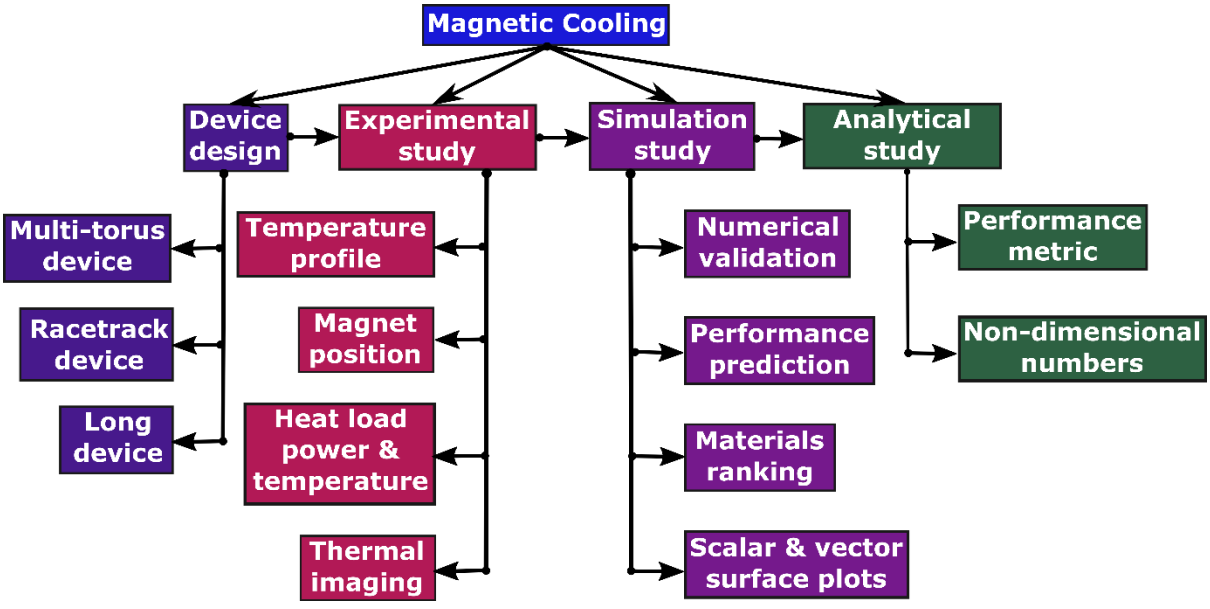

Figure 3.1. Overview of the experimental, modelling, and analytical methods used in this thesis.

3.2 Magnetic Cooling Device Experimental Setup

A MC device requires the integration of several items, e.g., tubes for the flow of FF to remove the waste heat, a permanent magnet to provide the magnetic driving force to the FF, temperature measuring unit to determine the temperature distribution of the heat load and FF along the flow channel, infrared (IR) camera for thermal imaging of the magnetic cooling device, and data acquisition unit. FF is used as the fluidic heat transfer medium in the magnetic cooling device. The constituents of the MC device and the properties of the FF used for this work is described in the following subsections. The device dimensions and the surface temperature/ power/power density of the heat loads were used as input parameters for numerical investigation of the TM flow behavior of the FF.

3.2.1 Components of the magnetic cooling device setup

The main components of the magnetic cooling devices are:(a) magnetic field unit, (b) fluid flow unit, and (c) heat transfer unit.

3.2.1.1 Magnetic field unit

For magnetic pressure driven FF flow along the flow channel, a non-uniform magnetic field was applied near the vicinity of heat load using a permanent magnet. The magnet is a 10cm*5cm*2cm Nd-Fe-B permanent magnet (Lifton Magnets, Singapore) of N50 grade, having a surface magnetic field strength of 0.41 T. A Gaussmeter (Lakeshore, model 410) was used to measure the distribution of magnetic field along the surface of the Nd-Fe-B magnet and along the flow channel. The accuracy of the Gaussmeter is 10^{-5} Tesla.

3.2.1.2 Fluid flow unit

The fluid flow unit of the MC device consists of silicone and copper tubes to form the closed flow loops, as described below. The properties of the silicone and copper tubes is given in **Table 3.1**.

Silicone tubes

Silicone tubes of various internal diameters were connected through T-joints to provide a closed flow loop. Silicone tubing was used to form the flow loops because of its excellent chemical resistance, flexibility, and high degradation temperature. Due to its flexible nature,

the arc lengths of the flow channels were easily adjusted to the desired device geometry, device length and heat load arc length.

Copper tubes

Copper tubes were also used. The use of copper tubes results in an enhancement of heat transfer from the heat load due to its superior thermal conductivity, high degradation temperature. The high thermal conductivity of copper offers effective low-grade waste heat transfer (below 100°C) from the heat load to the FF.

Hybrid tubes

In MC devices, thermal gradient and magnetic field gradient are two important factors. The thermal gradient can be enhanced by creating a junction of two materials having dissimilar thermal conductivity along the flow channel. In the present study, highly thermally conductive copper tube was joined to silicone tube having a relatively lower thermal conductivity, thus creating a copper-silicone hybrid hot-cold junction near the heat load region. This gives rise to a larger thermal gradient region. A hybrid copper-silicone device can improve TM cooling compared to its full copper device counterpart. In addition, use of silicone reduces both cost and the weight of the device.

Table 3.1. Properties of silicone and copper tubing used for this work.

Sr.	Properties	Silicone Tube	Copper Tube
1.	Thermal Conductivity, k ($W.m^{-1}K^{-1}$)	0.2	400
2.	Specific Heat, C_p ($J.kg^{-1}K^{-1}$)	1050	385
3.	Density, ρ ($kg.m^{-3}$)	1100-2300	8960
4.	Melting temperature, T_{melt} (°C)	>450	1085
5.	Optical Property	Translucent	Opaque

3.2.1.3 Heat transfer unit

Heat transfer unit includes (a) the heat load, (b) temperature measurement unit, and (c) surface insulation.

Heat load

Two types of heat loads were used to provide the thermal field gradient, and their TM cooling performance tested. These heat loads simulate a waste heat source for two heat load power regimes. To investigate the TMC effect at lower heat load power/power density values and cool low and medium grade waste heat loads, heater wires (Kanthal wires, Proheat Singapore) having a resistivity of 8.8 Ω/m were wrapped on the tube wall. For the investigation of the MC effect at higher heat load power, higher heat load temperature, and larger surface area heat loads, a hot plate having a maximum power rating of 1.1 kW was used as a heat load. The power and the temperature of the heat load was adjusted using the regulator knob of the hot plate.

Temperature measurement unit

To investigate the heat load, FF temperature at various points around the flow loop was recorded. The temperature measurement unit consists of thermocouple probes and the temperature recorder.

Thermocouple probes

K-type and T-type thermocouples having measurement accuracy values of ±1.5°C and ±0.5°C, respectively were connected at various regions of the flow loop to measure the heat load and FF temperature profiles. T-type thermocouples were used to sense temperatures below 300°C. K-type thermocouples were used to sense the temperature of the kW level heat load (typically >300°C).

Temperature recorder

To record the temperature readings of the heat load and the FF, the thermocouples were connected to the temperature module of a highly sensitive data acquisition system (NI 9213, cDAQ-9178, National Instruments) with a sensitivity value of ±0.02°C. Temperature values were recorded over a fixed time period and subsequently stored in a computer using LabVIEW system engineering software (National Instruments).

Surface insulation

The heat load region of the magnetic cooling device was thermally insulated using a ceramic fiber blanket minimize heat loss to the ambient due to natural convection. A

ceramic fiber blanket was used because of its excellent high temperature stability, low density, and low thermal conductivity.

3.2.2 Ferrofluid

An oil-based audio FF (APG S11N, Ferrotec, Singapore) comprised of Fe_3O_4 nanoparticles dispersed in organic ester oil was used as the heat transfer fluid. It possesses high saturation magnetization, high flash point temperature, high MNP volume fraction and good dispersion stability at high temperatures and strong magnetic fields. The properties of the FF are provided in **Table 3.2**

Table 3.2. Properties of oil-based APG S11N ferrofluid (Ferrotec, Singapore); abbreviations used: - MNP: magnetic nanoparticle, NA: not applicable.

Ferrofluid Properties	Notation	Value or Content
Magnetic nanoparticle	MNP	Fe_3O_4
Carrier fluid	NA	Organic ester oil
Ferrofluid saturation magnetization (mT)	M_s	22
Fe_3O_4 nanoparticle volume fraction (% v/v)	$\mathbb{C}_o$	5-8
Viscosity (mPa.s)	M	85
Density ($kg.m^{-3}$)	P	1150
Thermal conductivity ($W.m^{-1}.K^{-1}$)	K	0.15

3.3 Experimental Designs of Magnetic Cooling Devices

Magnetic cooling devices of various geometrical shapes, sizes, and flow channel internal diameters were prepared from tube materials to investigate the cooling performance. The flow loop was filled with FF and then part of it was placed in contact with the heat load section. An Nd-Fe-B permanent magnet (N50 grade, Lifton Magnets, Singapore) of dimensions 100 mm × 50 mm × 25 mm and saturation magnetic flux density of 0.41 T was used. The permanent magnet was placed near the heat load section to provide the necessary magnetic force field to the FF. During the experiment, the heat load was entirely covered with 12.5 mm thick ceramic wool to minimize heat loss from the heat load. No cooling

means or coolants were used at the heat sink to cool the FF. No external pumps or external energy sources were utilized. Based on the heat load power/heat flux and temperature, heat load surface area and length, three different types of MC devices were developed (as shown in **Figure 3.1.** Overview of the experimental, modelling, and analytical methods used in this thesis.), as described in the following subsection. The design aspects and the device parameters of the magnetic cooling devices are provided in **Table 3.3** and **Table 3.4**, respectively.

Table 3.3. Design aspects of developed magnetic cooling devices.

Magnetic Cooling Device	Geometry	Torus	Tube Material	Heat Load Type
Multi-torus device	Circular: Triple	Triple	Silicone	Planar hot plate
Racetrack device	Racetrack: Single	Single	Copper, Silicone, Hybrid	Radial resistive heating
Long racetrack device	Racetrack: Single	Single	Copper	Radial resistive heating

Table 3.4. Device parameters of the developed magnetic cooling devices. Notations used: L_D: total length of the device, d_i: internal diameter of the flow tube, L: heat load arc length, P_{max}: maximum heat load power, Q_{max}: maximum heat flux at the heat load, T_{max}: maximum heat load temperature.

Magnetic cooling device	L_D (cm)	d_i (mm)	L (cm)	P_{max} (W): Q_{max} (kW/m^2)	T_{max} (°C)
Multi-torus device	176	25	25	1000: 16	580
Racetrack device	130	8.1	30	30: 3.93	200

Long racetrack device	800	8.1	18	40: 8.85	200

3.3.1 Multi-torus magnetic cooling device

A multi-torus MC device was developed for the cooling of kilowatt level heat load, with heat load power and temperature up to 1 kW and 580°C, respectively. Cooling was achieved by a three concentric torus configuration device and larger flow channel diameter of 25 mm. The multi-torus device provided larger surface area for waste heat transfer from the heat load to magnetic cooling device. The multi torus device consists of three concentric torus shaped silicone tubes (**Figure 3.1.** Overview of the experimental, modelling, and analytical methods used in this thesis.**(a)**), forming three flow channels (FC 1, FC2, and FC 3). A hot plate (power rating: 230V×13A) was used to simulate a source of waste heat in the power range of 0.5 kW to 1 kW. The portion of the device in contact with the HL surface (Y= -125 mm to 125 mm), is termed as the heat load section. This section was wrapped with aluminum to efficiently transfer heat from the heat load to the tubes and subsequently to the ferrofluid. The device dimensions are provided in **Table 3.5**.

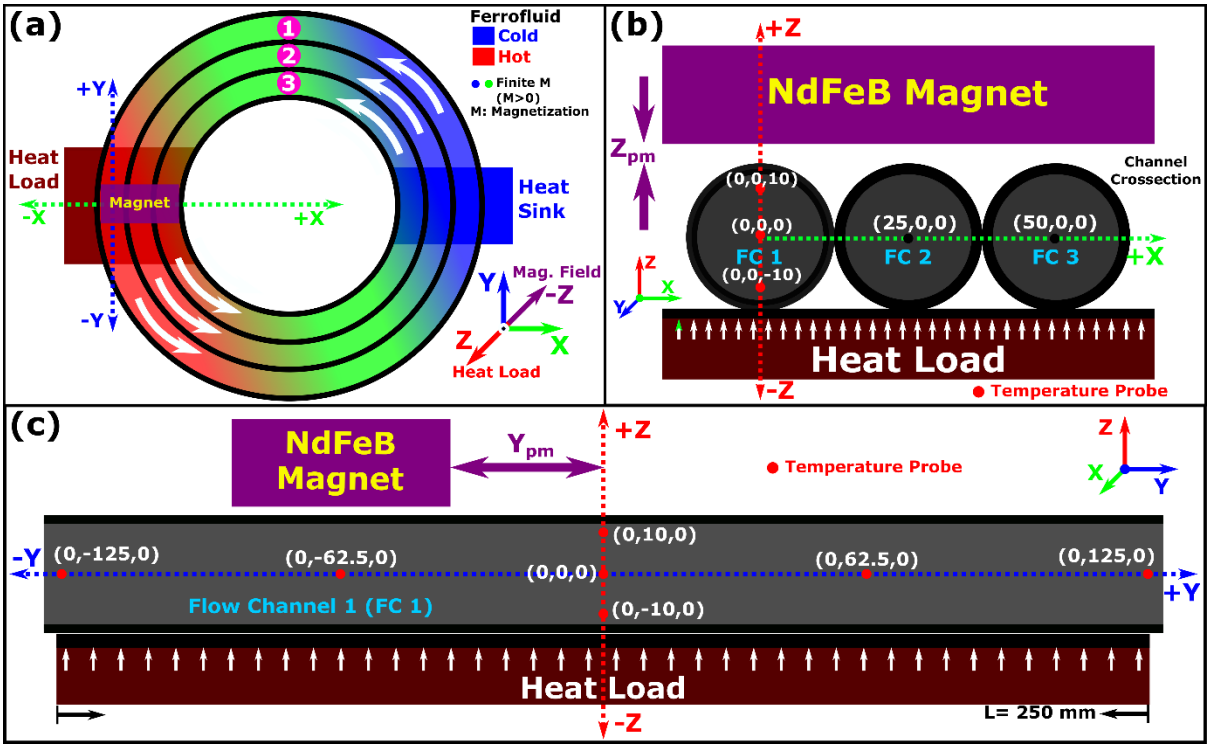

Figure 3.2. Schematic of the multi-torus magnetic cooling device, showing (a) XY, (b) XZ, and (c) YZ–plane views. The ferrofluid exhibits temperature dependent susceptibility (χ_m), viz. ferrofluid shown in blue (cold, higher χ_m), green (warm, lower χ_m), red (hot, lowest χ_m). The thermal gradient is provided by the heat load, applied along +ve Z direction by a hot plate, simulating a waste heat load source. The magnetic field is applied by a permanent magnet (PM) along the –ve Z direction. T-type thermocouples, indicated as red dots, were mounted at various positions, as shown in Figure 3.2(b, c). (X_{pm}, Y_{pm}, Z_{pm}) denotes the position of the permanent magnet. All dimensions and coordinate positions are in mm.

Table 3.5. Dimensions of the concentric tori flow channels in the multi-torus magnetic cooling device.

Device Component	Notation	Inner Diameter (mm)	Outer Diameter (mm)
Flow channel 1	FC 1	500	560
Flow channel 2	FC 2	440	500
Flow channel 3	FC 3	380	440

3.3.2 Circular shaped magnetic cooling device

Circular MC devices were developed using copper and silicone tubes. The effect of tube material thermal conductivity on the TM cooling of the heat load was experimentally investigated using these circular devices, the device perimeter (L_D) and heat load arc length (L) of 130 cm and 30 cm, respectively. The schematic of these devices is shown in **Figure 3.3**. The device dimensions and the physical properties of copper and silicone tubes are provided in **Table 3.6**.

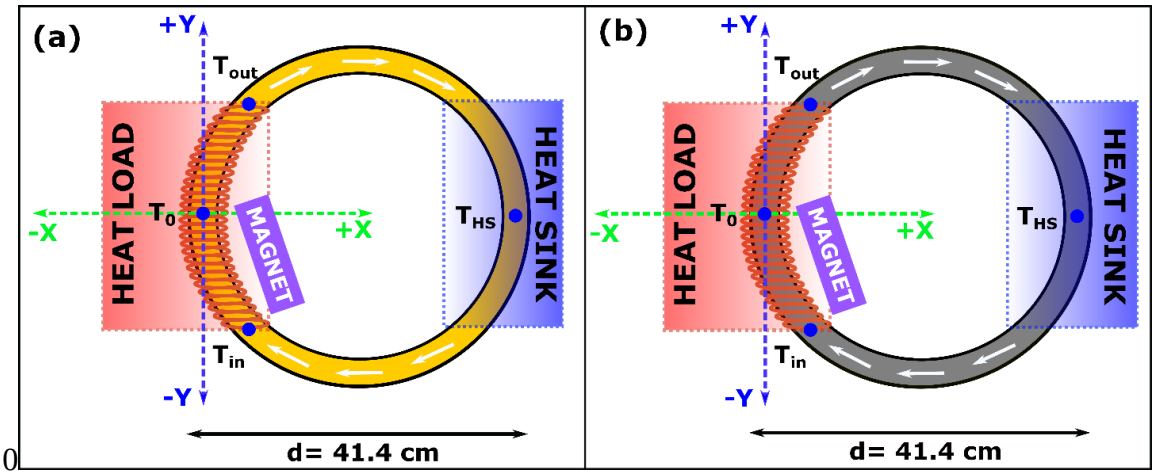

0

Figure 3.3. Schematics of the circular magnetic cooling devices with heat load arc length and perimeter of 30 cm and 130 cm, respectively. The circular devices are made up of (a) copper, and (b) silicone tubes. The heat load is obtained by radial resistive heating wire of nichrome. The magnetic field is applied by a Nd-Fe-B magnet near the heat load region. T-type thermocouples were positioned along the heat load section (blue dots). The origin (0,0,0) is taken at the center of the heat load. White arrows represent the ferrofluid flow direction due to thermomagnetic convection.

Table 3.6. Dimensions and physical properties of circular magnetic cooling devices made from copper and silicone tubes.

Sr.	Tube Material	Thermal Conductivity ($W.m^{-1}.K^{-1}$)	Specific Heat ($J.kg^{-1}.K^{-1}$)	Density ($kg.m^{-3}$)	Internal Diameter (mm)	Device Perimeter (cm)
1.	Copper	400	385	8960	8.1	130
2.	Silicone	0.2	1150	1150	8	130

3.3.3 Racetrack shaped magnetic cooling device

Racetrack shaped MC devices offer lower device footprint compared to circular devices. To study the effect of device geometry on cooling, we developed copper-based circular and racetrack shaped magnetic cooling devices having the same device perimeter (L_D: 130 cm) and heat load arc length (L: 30 cm). The effect of tube material thermal conductivity on the TM cooling was also studied using circular devices of copper and silicone having the same L_D and L as the previous case.

To improve the TM cooling, the thermal gradient near the heat load was enhanced by creating a junction of highly thermally conductive copper tube and the silicone tube having lower thermal conductivity. Due to the dissimilar thermal conductivity, the copper-silicone hybrid hot-cold junction near the heat load region provides relatively larger thermal gradient compared to devices made from a single tube material. Five different hybrid racetrack shaped devices were prepared having the copper tube percentage of 0, 25, 50, 75 and 100 to study the effect of copper to silicone ratio on the TM cooling (**Table 3.7**). The schematics of all racetrack shaped MC devices are shown in **Figure 3.4**. To study the effect of heat load tube material on the TM cooling using the hybrid device, two sets of experiments were performed for Hybrid-25 and Hybrid-75 devices for both copper and silicone heat loads separately (**Table 3.7**).

The heat load was prepared using resistive heating of nichrome wire having a resistivity value of 8.8 Ω/m. The waste heat was simulated by applying a DC voltage across the resistive wire using a DC power supply (Keithley 2231A-30-3 triple channel DC power supply) having a current and voltage rating of 3 A and 30 V, respectively.

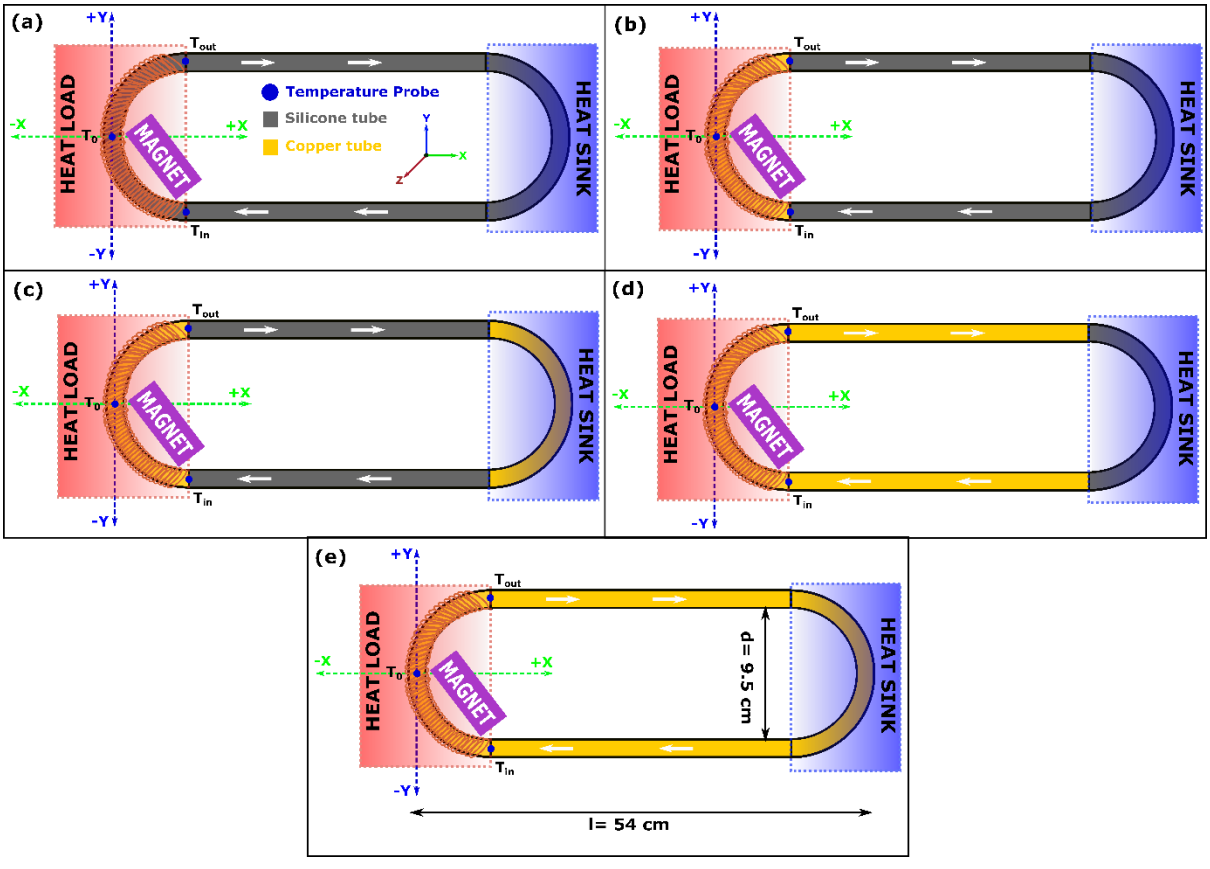

Figure 3.4. Schematics of the racetrack shaped magnetic cooling devices with heat load arc length and perimeter of 30 cm and 130 cm, respectively. The racetrack devices are made up of (a) completely silicone, (b) 25% copper and 75% silicone, (c) 50% copper and 50% silicone, (d) 75% copper and 25% silicone, and (e) completely copper. The heat load is a radial source, simulating a source of waste heat. The magnetic field is applied by a Nd-Fe-B magnet near the heat load region. T-type thermocouples were positioned along the heat load section, blue dots in **Figure 3.4**(b). The origin (0,0,0) is taken at the centre of the heat load. White arrows represent the ferrofluid flow direction due to thermomagnetic convection.

Table 3.7. Developed copper-silicone hybrid magnetic cooling devices, their abbreviations, and heat load material.

Sr.	Copper/Silicone Percentage (%/%)	Abbreviation	Heat Load Material
1	0/100	Silicone-100	Silicone
2	25/75	Hybrid-25	Copper & Silicone
3	50/50	Hybrid-50	Copper
4	75/25	Hybrid-75	Copper & Silicone
5	100/0	Copper-100	Copper

3.3.4 Long magnetic cooling device

The 8 m long MC device was prepared using a copper tube having an internal diameter of 8.1 mm (**Figure 3.5(a)**). The device dimensions are provided in **Table 3.8**. The device was designed in the shape of a racetrack, as shown in **Figure 3.5**. The heat load was prepared using resistive nichrome wire possessing a resistivity value of 8.8 Ω/m. The waste heat was simulated by applying a DC voltage across the resistive wire using a DC power supply having a current and voltage rating of 3 A and 30 V, respectively. The device dimensions are as shown in the schematic of **Figure 3.5(b).** The experimental magnetic field of the magnet was determined using a Gaussmeter (LAKESHORE, model 410).

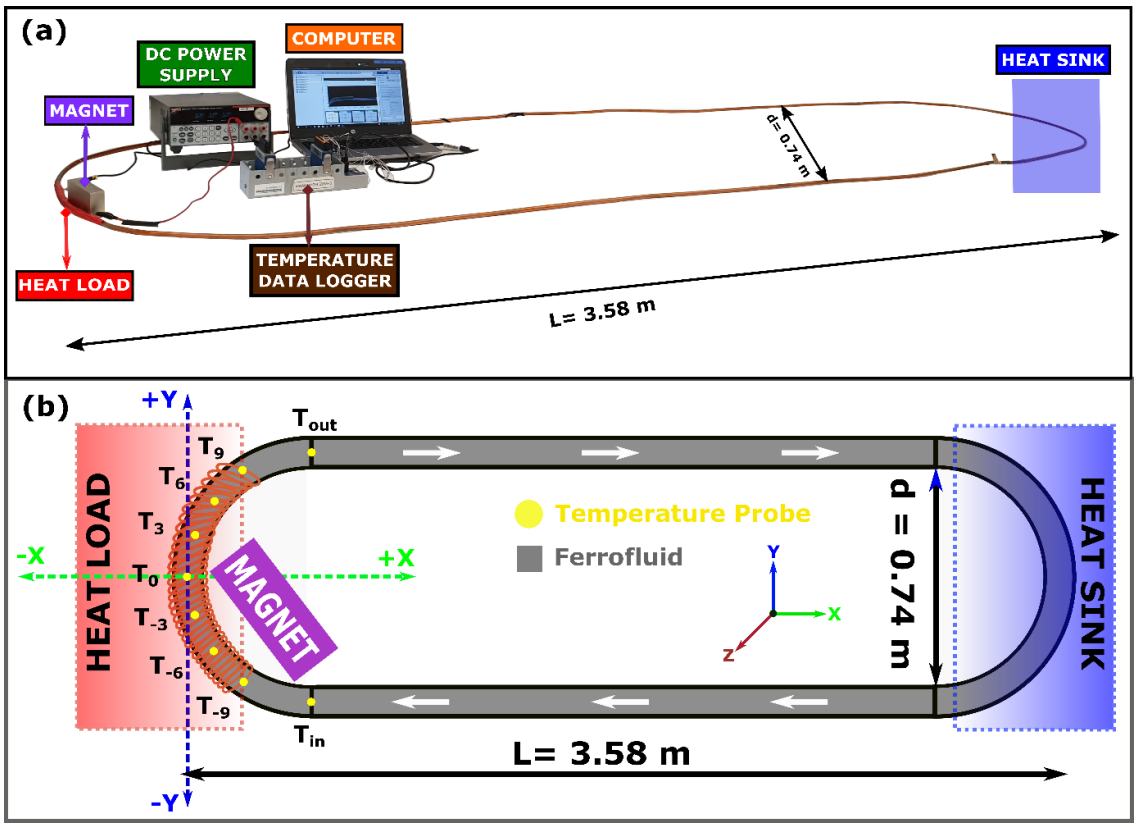

Figure 3.5. Racetrack shaped 8 m long magnetic cooling device, (a) experimental setup, and (b) schematic, XY-plane. The heat load is provided by resistive heating, simulating a source of waste heat. The magnetic field is applied by a Nd-Fe-B magnet, near the heat load region. T-type thermocouples were positioned along the heat load section, yellow dots in Figure 3.5(b). The origin (0,0,0) is taken at the centre of the heat load. The probe positions are denoted by Ti, where i denotes the y-dimension in cm. White arrows represent the ferrofluid flow direction due to thermomagnetic convection.

Table 3.8. Device dimensions of the long racetrack shaped magnetic cooling heat transfer device.

Device Component	Notation	Dimension
Inner diameter of the copper tube	d_i	8.1 mm
Outer diameter of the copper tube	d_o	9.52 mm
Heat load arc length	L	18 cm
Distance between the parallel flow branch	D	0.74 m
Distance between the heat load and the heat sink	L	3.58 m

Total length of the device	L_D	8 m

3.4 Modelling Methodology

The principle for the operation of magnetic cooling device is the non-uniform Kelvin body force experienced by the differentially heated FF near the heat load region in presence of an applied magnetic field. This force leads to force imbalance, attracting the colder FF with a stronger force and the warmer FF with a substantially weaker force towards the higher magnetic field gradient region; the phenomenon is called TMC [1]. To investigate this effect, two-dimensional models were developed using COMSOL Multiphysics simulation software based on the finite element method [2].

Various thermal and fluidic properties of the FF were provided as input to the model. Three physics modules viz., heat transfer, magnetic field, and single-phase laminar flow, were used in the multi-physics model. The magnetic volume force, due to the TM effect, was added as an additional volume force term in the Navier-Stokes equation. The magnetic field distribution due to the Nd-Fe-B magnet was modelled and compared to experimental values of the magnetic field strength. The boundary conditions were specified, consistent with the experimental design.

3.4.1 Governing equations

The governing equations for simulating the TMC effect of the FF in the magnetic cooling device is described in the following sections

3.4.1.1 Equations of magnetic field

Due to the static magnetic field, the Maxell-Ampere's law was used to define the magnetic field distribution [3];

$$\nabla \times \boldsymbol{H} = 0 \qquad (3.1)$$

The displacement current density vector (**J**) was taken to be zero in the above equation by assuming the FF to be electrically non-conductive. Hence, the magnetic field can be derived using the relation,

$$\boldsymbol{H} = -\nabla V_m \qquad (3.2)$$

Gauss's law of magnetism for the continuity of magnetic flux density takes the form [3]

$$\nabla . \boldsymbol{B} = 0 \tag{3.3}$$

The macroscopic magnetic property of the FF medium was described by the constitutive relation between magnetic field (**H**) and magnetic flux density (**B**)

$$\boldsymbol{B} = \mu_0(\boldsymbol{H} + \boldsymbol{M}) = \mu_0(1 + \chi_m)\boldsymbol{H} \tag{3.4}$$

Where, V_m is the magnetic scalar potential, μ_0 and μ_r are the magnetic permeability of free space and FF respectively, and χ_m is the magnetic susceptibility of the FF.

The non-uniform ferrofluid magnetic susceptibility resulting from the spatial variation of temperature and the magnetic field is given by the Langevin equation [4]:

$$\chi_m(H,T) = \frac{\mathbb{C}_0 M_s^{Bulk}}{H} \times \mathcal{L}(\gamma H) \tag{3.5}$$

where $\mathbb{C}_0$ is the magnetic nanoparticle volume fraction in the ferrofluid, M_s^{Bulk} is the bulk saturation magnetization of Fe_3O_4, its value is 446 kA/m [5].

$\mathcal{L}$ is the Langevin function:

$$\mathcal{L}(\gamma H) = coth(\gamma H) - \left({}^{1}/_{\gamma H}\right) \tag{3.6}$$

The Langevin parameter γ is defined as:

$$\gamma(T) = \frac{3\chi_i(T)}{M_s^{Bulk}} \tag{3.7}$$

where χ_i is the initial susceptibility of the Fe_3O_4 nanoparticles at various temperature values.

3.4.1.2 Equations of mass, momentum, and energy conservation

Mass and energy transport in the TMC based magnetic cooling devices is governed by the conservation of mass, momentum, and energy. The governing equations take the form as follows.

Continuity equation:

$$\rho \nabla . \boldsymbol{v} = 0 \tag{3.8}$$

Momentum equation:

$$\rho\left(\frac{\partial \boldsymbol{v}}{\partial t} + (\boldsymbol{v}.\nabla)\boldsymbol{v}\right) = -\nabla p + \nabla.\left(\mu(\nabla \boldsymbol{v} + (\nabla \boldsymbol{v})^T)\right) + \boldsymbol{F_m} \tag{3.9}$$

Energy equation:

$$\rho C_p \left(\frac{\partial T}{\partial t} + \boldsymbol{v}.\nabla T\right) = \nabla.(\kappa \nabla T) \quad (3.10)$$

where **v**, p, and T denote ferrofluid velocity, flow pressure, and temperature, respectively. $\mathbf{F_m}$ represents the net volume magnetic force on the ferrofluid. The ferrofluid properties are the density (ρ), thermal conductivity (κ), dynamic viscosity (μ), and specific heat (C_p).

The significance of the individual terms in Navier-Stokes equation [6] (equation (3.9)) are provided in **Table 3.9**.

Table 3.9. Various volume force terms in the Navier-Stokes equation [6].

Sr.	Volume Force Term	Significance
1	$\rho(\boldsymbol{v}.\nabla)\boldsymbol{v}$	Convective inertial volume force
2	$\rho\frac{\partial \boldsymbol{v}}{\partial t}$	Unsteady inertial volume force
3	∇p	Pressure volume force
4	$\nabla.(\mu(\nabla v + (\nabla v)^T)$	Viscous volume force
5	$\boldsymbol{F_m}$	Magnetic volume force

3.4.1.3 Volume force calculation

The magnetic volume force ($\mathbf{F_m}$) experienced by the ferrofluid in the presence of an applied magnetic field is given by [7]:

$$\boldsymbol{F_m} = \frac{\mathbb{C}_0 \chi_{mnp}}{\mu_0}(\boldsymbol{B}.\nabla)\boldsymbol{B} \quad (3.11)$$

where, $\mathbb{C}_0$ and χ_{mnp} represent the percentage volume concentration and volume magnetic susceptibility of the magnetite nanoparticles, respectively.

3.4.2 Non-dimensional parameters and scaling

To evaluate the TM cooling performance for various device and ferrofluid parameters, we analyzed several non-dimensional parameters. The results of these non-dimensional parameters v/s different parameters can be used to enhance TM cooling.

3.4.2.1 Nusselt number

The heat transfer was investigated using the Nusselt number. Nusselt number (Nu) gives the ratio of the convection to conduction heat transfer in a coolant fluid medium. The value of local convective heat transfer coefficient along the flow direction (h_l) was obtained using the following formula [8],

$$h_l = \frac{Q_{HL}}{(T_w(l) - T_f(l))_l} \tag{3.12}$$

where Q_{HL} is the applied heat flux at the heat load. T_w and T_f are the inner wall temperature of the tube and the bulk FF temperature for a specific position along the flow channel, respectively. The heat flux can be calculated from the applied power (P_{HL}), which is the product of the current (I) and voltage (V), divided by the area of the heat load region,

$$Q_{HL} = \frac{P_{HL}}{l_{HL} d_t \pi} = \frac{VI}{l_{HL} d_t \pi} \tag{3.13}$$

Here, l_{HL} and d_t are the heat load arc length and the internal diameter of the flow channel. The local bulk FF temperature in terms of thermal diffusivity (α) and the thermal conductivity (κ) can be written as,(6.3)

$$T_f(l) = \frac{\alpha Q_{HL} \pi d_t}{\kappa \dot{q}} l + T_{in} \tag{3.14}$$

The local (Nu_L) and average value (Nu_{avg}) of Nusselt number was calculated using equation (3.15) and equation (3.16), respectively.

$$Nu_L(l) = \frac{h_l d_t}{\kappa} \tag{3.15}$$

$$Nu_L(l) = \frac{h_l d_t}{\kappa} \tag{3.16}$$

where, n represents the number of points across the heat load region at which the local Nusselt number was calculated.

3.4.2.2 Peclet number

Convection refers to both advection and diffusion term. Advection is the transport of heat due to bulk fluid motion and diffusion is the heat transfer due to random motion of the molecules [9]. Peclet number (Pe) quantifies the ratio of advection to diffusion during liquid based heat transfer processes and is given as,

$$Pe = \frac{\dot{q}}{\pi d_t \alpha} \quad (3.17)$$

where, q̇ is the volume flow rate of the FF.

3.4.2.3 Stanton number

Stanton number, which is also known as the modified Nusselt number, provides a measure of the amount of heat transferred to the fluid from the heat load to the thermal capacity of the fluid. Stanton number can be represented as [9],

$$St = \frac{Ah\alpha}{\kappa \dot{q}} = \frac{Nu}{Re * Pr} \quad (3.18)$$

Here, Re and Pr represent the Reynolds number and the Prandtl number for the ferrofluid, respectively.

3.4.3 Assumptions and boundary conditions

Two dimensional models were developed using COMSOL Multiphysics simulation software.

Assumptions:

- The FF was treated as a single-phase continuum owing to the continuum model developed by Rosensweig [5] to describe the behavior of a FF in the ferrohydrodynamic regime, in which the FF behaves as a liquid magnet.
- The FF was assumed to be incompressible (constant density), Newtonian (constant viscosity), and electrically non-conductive (zero displacement and surface current density i.e. $J = J_s = 0$) fluid.
- The surface, on which the flow loop was kept, was perpendicular to the direction of gravity, hence the effect of gravity on the net volume force was neglected.
- The cross-sectional area of the flow loop was assumed to be constant throughout the prototype.
- Changes in the density of the FF with respect to temperature were not considered for modelling the thermomagnetic effect, which is known as the Boussinesq approximation.

- Axial conduction due to diffusion process was neglected in comparison to the advection heat transfer process (Peclet number).

3.4.4 Boundary conditions

The following boundary conditions were considered for simulating the TMC effect of the FF in the magnetic cooling devices.

- No-slip boundary condition was applied at the duct walls.
- The initial FF pressure and temperature were set to atmospheric pressure (1 atm.) and room temperature (20°C), respectively.
- For the magnetic field boundary condition, a zero magnetic scalar potential was defined at a distant point from the permanent magnet, where the magnetic field vanishes.
- A pressure point constraint was considered inside the ferrofluid region to obtain a finite number of solutions.
- For thermal boundary condition, a constant surface temperature of 20°C was defined at the heat sink region.
- For the multi-torus magnetic cooling device, the temperature profile at the heat load boundary (T_{HL}, model) was taken to be the same as the experimentally obtained temperature profile at the heat load without applied magnetic field (T_{HL}, exp(B=0 T)).
- For the rest of the magnetic cooling device models, the heat load was simulated by specifying the heat flux value.

References

[1] S. Pal, A. Datta, S. Sen, A. Mukhopdhyay, K. Bandopadhyay, and R. Ganguly, "Characterization of a ferrofluid-based thermomagnetic pump for microfluidic applications," *Journal of Magnetism and Magnetic Materials,* vol. 323, no. 21, pp. 2701-2709, 2011.

[2] C. Multiphysics, "version 5.1, COMSOL AB, Stockholm, Sweden," ed, 2014.

[3] D. J. Griffiths, *Introduction to electrodynamics*. Prentice Hall, 1962.

[4] V. B. Varma, R. G. Wu, Z. P. Wang, and R. V. Ramanujan, "Magnetic Janus particles synthesized using droplet micro-magnetofluidic techniques for protein detection," *Lab Chip,* 10.1039/C7LC00830A vol. 17, no. 20, pp. 3514-3525, Oct 11 2017.

[5] R. E. Rosensweig, *Ferrohydrodynamics*. Courier Corporation, 2013.

[6] J. G. Gutierrez and M. Riccetti, "Analysis and Development of a Magnetocaloric Pump for Electronic Cooling Applications Using a Mn-Zn Ferrite Ferrofluid," in *ASME 2008 International Mechanical Engineering Congress and Exposition*, 2008, pp. 631-636: American Society of Mechanical Engineers.

[7] M. S. Pattanaik, V. Varma, S. Cheekati, G. Prasanna, N. Sudharsan, and R. V. Ramanujan, "A self-regulating multi-torus magneto-fluidic device for kilowatt level cooling," *Energy Conversion and Management,* vol. 198, p. 111819, 2019.

[8] M. A. Khairul, E. Doroodchi, R. Azizian, and B. Moghtaderi, "Thermal performance analysis of tunable magnetite nanofluids for an energy system," *Applied Thermal Engineering,* vol. 126, pp. 822-833, 2017.

[9] T. L. Bergman, F. P. Incropera, D. P. DeWitt, and A. S. Lavine, *Fundamentals of heat and mass transfer*. John Wiley & Sons, 2011.

Chapter 4

A Multi-torus Magneto-fluidic Device for Kilowatt Level Cooling*

Efficiently removing waste heat by novel cooling devices can improve efficiency, reduce material failure, and enhance service life. Magneto-fluidic cooling, which is based on the thermomagnetic convection of a ferrofluid, offers a passive, self-regulating approach for the removal of waste heat. The performance of a novel multi-torus magnetic cooling device for kilowatt level cooling was investigated. Heat load cooling improved from 148˚C to 214˚C when heat load power was increased from 0.5 kW to 1 kW, respectively, demonstrating the self-regulating nature of the device. The heat load cooling performance was assessed for various magnet positions. The temperature profile of the ferrofluid along the axial and radial directions of the flow channel revealed an asymmetric temperature distribution. The transient effect of periodic magnetic field switching on the heat load temperature was simulated using COMSOL Multiphysics and found to be in good agreement with the experimental findings. Simulated surface velocity vector plots revealed ferrofluid vortices near the heat load, these vortices resulted in enhanced mixing of hot and cold ferrofluid, leading to increased cooling. The thermal resistance of our multi-torus magnetic cooling device was determined analytically. The present device offers lower thermal resistance per unit length and lower ferrofluid thermal resistance per unit volume of ferrofluid compared to conventional heat pipes. A self pumping, self regulating passive heat pump, capable of kilowatt level cooling, has been fabricated and its cooling performance assessed.

*The results presented in this chapter is substantially published as "**Pattanaik, M. S.**, Varma, V. B., Cheekati, S. K., Prasanna, G., Sudharsan, N. M., & Ramanujan, R. V. (2019). A self-regulating multi-torus magneto-fluidic device for kilowatt level cooling. *Energy Conversion and Management*, *198*, 111819." (No written permission from Elsevier is required for including self-journal contents in the thesis.)

4.1 Introduction

The Lawrence Livermore National Laboratory energy chart shows that a significant amount of total energy is wasted due to rapid industrial development [1]. In accordance with the second law of thermodynamics, a substantial fraction of the energy input to heat engines is “lost” as waste heat [2]. This waste heat is generated in a wide and diverse range of domains, e.g., power generation and conversion units, industrial devices, data servers, electronic components, and biological processes. Efficient removal of waste heat during device operation increases reliability, service life and can improve device efficiency.

Specifically, there is a need for a better passive heat transfer technique suitable for cooling of heat loads with power output in the kW range. Thermomagnetic convection (TMC) based cooling is a promising technique for this purpose, it utilizes both magnetic and thermal effects [3]. The temperature dependent response of a ferrofluid (FF) in the presence of a magnetic field results in fluid flow, transferring heat from the heat load (HL) to the heat sink (HS). Such magnetic cooling systems are noise-free, exhibit wireless magnetic field control, with no mechanical moving parts. Hence they are free from vibration [4].

A FF is a stable colloidal suspension of magnetic nanoparticles (MNP) dispersed in a suitable carrier medium. The MNPs are coated by a surfactant to prevent particle agglomeration due to dipole-dipole and van der Waals interactions [5]. FF motion can be controlled by an external magnetic field since the ferrofluid possess both fluidic and magnetic characteristics. Magnetic cooling (MC) systems are governed by FF motion due to the combined effect of a thermal gradient and the magnetization gradient of the FF. This motion depends on the heat load temperature and applied magnetic field strength.

Khairul et al. [6] investigated the effect of magnetic field on the TM behavior of a Fe_3O_4 : water FF by analyzing pumping power, friction factor, and exergy loss in both laminar and turbulent flow regimes. Yamaguchi et al. [7] reported a maximum thermal energy transfer of 107 W over a distance of 5 m. They found that the average Nusselt number increases with increasing magnetic field strength. Wang et al. [8] investigated the TMC of Fe_3O_4 : water FF using multiple magnets and their relative positioning at a heat load power of 65 W. Lian et al. [9] performed particle image velocimetry (PIV) measurements to determine the flow velocity of the FF. When two heat loads are used, the flow velocity was higher for

a circular loop compared to both the single heat load case and a square loop. Xuan et al. [10] developed a MC device for electronic chip cooling. They found that placing the magnet near the heat load gave rise to enhanced cooling performance. Li et al. [11] fabricated a rectangular cross section device to investigate the effect of external magnetic field strength and heat load power values on the flow behavior. They observed a linear increase in FF velocity with increasing heat load power. Chaudhary et al [12] studied a Mn-Zn ferrite : water FF based device and investigated its performance by experiments and simulations. The Mn to Zn ratio of the MNP was chosen to achieve the desired Curie temperature and the relevant saturation magnetization. The effect of heat load temperatures on the cooling performance was studied. Cooling was found to increase for larger magnetic field strength and higher MNP volume fraction.

Nomenclature

Abbreviations

FF	Ferrofluid
HL	Heat load
HS	Heat sink
TMC	Thermomagnetic convection
MC	Magnetic cooling
MNP	Magnetic nanoparticle
PM	Permanent magnet
FC	Flow channel
PIV	Particle image velocimetry

Symbols

Magnetic parameters

$\mathbf{H}$	Magnetic field
$\mathbf{B}$	Magnetic flux density
V_m	Magnetic scalar potential
$\mathbf{F_f}$	Magnetic volume force
$\mathbf{M_s}$	Saturation magnetization
μ_0	Permeability of free space
μ_r	Permeability of ferrofluid
χ_m	Magnetic susceptibility of ferrofluid
χ_{mnp}	Magnetic susceptibility of magnetic nanoparticle
Y_{pm}	Y-position of the magnet
Z_{pm}	Z-position of the magnet

Thermal parameters

T	Temperature
κ	Thermal conductivity
C_p	Specific heat
R_D	Device thermal resistance
R_F	Fluid thermal resistance
R_{DL}	Device thermal resistance per unit device length
R_{FV}	Fluid thermal resistance per unit fluid volume

Fluidic parameters

$\mathbf{v}$	Velocity
p	Pressure
ρ	Density
μ/η	Dynamic/static viscosity
κ	Thermal conductivity
$\mathbb{C}_o$	Magnetic nanoparticle volume fraction

Device parameters

A_{fc}	Flow channel area
P_{max}	Max. heat load power
P_{HL}	Heat load power
T_{max}	Max. heat load temperature
ΔT	Heat load cooling

Szabo et al. [13] used infrared thermography to determine the combined effects of buoyancy and magnetic force on the FF. Heat transfer was characterized by determining the Nusselt number and modified Rayleigh number. Zonouzi et al. [14] experimentally studied the role of a magnetic quadrupole field on the device performance. The local heat transfer coefficient and FF pressure drop, for various Reynolds numbers, was studied for different axial positions of the quadrupole magnets. Hekmat et al. [15] numerically investigated the thermomagnetic convection of magnetite : water FF within a 3D annular space for varying MNP volume fraction and magnetic field gradient. Zanella et al. [16] simulated the effect of FF TMC on the cooling of a transformer with and without the ferromagnetic core. The presence of a highly permeable core enhanced the effect of magnetic field near that region, giving rise to stronger TMC. Mousavi et al. [17] numerically investigated the effect of magnetic field on FF flow behavior inside a helical tube. They obtained about 40% increase in Nusselt number with increasing magnetic field strength.

Thus, MC systems provide excellent passive cooling. However, MC systems, which can handle heat load power in the kilowatt range, have not been reported so far. In most cases, the characteristic channel length was limited to less than a few cm, which limits the applications of the device. We simulated the FF velocity for a range of values of device parameters, FF properties, and applied magnetic field. The magnetic field strength and its distribution was found to be the parameter that significantly influences the cooling performance of the MC device. The magnetic field can be altered by either placing several magnets near the heat load, or by suitably altering the position of a single magnet with respect to the heat load. Previous reports on MC devices focused more on heat load cooling using multiple magnets [18, 19]. However, use of multiple magnets results in much larger device footprint and can lead to damage of the HL equipment [20, 21]. The presence of a strong magnetic field near the system to be cooled may affect some electronic systems adversely. Further, if the equipment contains Fe, Co, Ni or their alloys, the magnetic field can attract the components, adversely affecting their motion and stability. In addition, location of the permanent magnet near the heat load may be restricted by the geometry and form factor constraints. The length scale of the heat load region of our device is 250 mm,

which is much larger than previously reported MC devices. Hence, the effect of variation in the position of a permanent magnet on the cooling performance could be explored.

We developed a novel multi-torus magnetic cooling device for the cooling of kilowatt level heat load, with heat load power and temperature up to 1 kW and 580°C, respectively. Cooling was achieved by a three concentric torus configuration device and larger flow channel diameter of 25 mm. This multi-torus device provided larger surface area for waste heat transfer from the heat load to the cooling device. A single NdFeB permanent magnet was used to drive a large volume of FF through all the flow channels. The device performance was studied for a range of magnet positions and heat load power. The temperature profile of the FF at the heat load region was determined. The device performance was studied experimentally and modelled by numerical simulations using COMSOL Multiphysics. The velocity vector plot obtained from the simulations shows FF vortices due to the external magnet; such vortices can improve heat load cooling. The effect of magnetic field switching on the temperature transients of the heat load was studied, the cooling was found to be similar for each cycle. The thermal resistance of the device was also determined for a range of heat load power values.

4.2 Experimental Methodology

The components and the materials used to develop the multi-torus magnetic cooling device and its design are summarized earlier in *section 3.2* and *section 3.3.1*, respectively. The following subsections summarize the experimental FF temperature profile determination setup and the experimental parameters considered to investigate the effects of these parameters on the TM cooling.

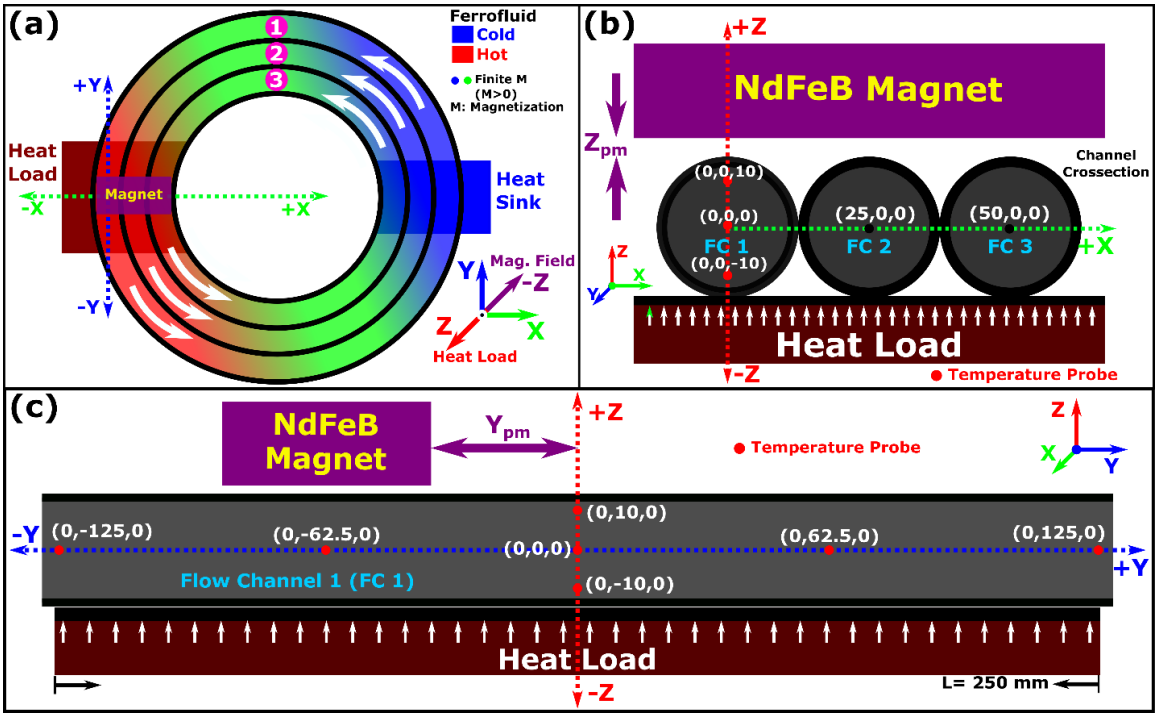

Figure 4.1. Schematic of the multi-torus magnetic cooling device, showing (a) XY, (b) XZ, and (c) YZ–plane views. The ferrofluid exhibits temperature dependent susceptibility (χ_m), viz. ferrofluid shown in blue (cold, higher χ_m), green (warm, lower χ_m), red (hot, lowest χ_m). The thermal gradient is provided by the heat load (HL), applied along +ve Z direction by a hot plate, simulating a waste heat load source. The magnetic field is applied by a permanent magnet (PM) along the –ve Z direction. T-type thermocouples, indicated as red dots, were mounted at various positions, as shown in **Figure 4.1(b, c)**. (X_{pm}, Y_{pm}, Z_{pm}) denotes the position of the permanent magnet. All dimensions and coordinate positions are in mm.

4.2.1 Experimental ferrofluid temperature profile determination setup

The temperature profile of the FF was measured to determine the temperature variation, along the axial and radial directions, due to TMC of FF. Thermocouples were placed along the axial and radial directions of flow channel 1 in the heat load region. Five thermocouples placed along the axial direction of the flow channel (at Z= 0 mm, along ± Y direction) are termed as axial temperature probes (**Figure 4.1**(c)). Three thermocouples placed along the radial direction (at Y= 0 mm, along ± Z-direction), are termed as radial temperature probes (**Figure 4.1**(b, c)). These axial and radial thermocouples were placed at equal distances along the Y- and Z-direction, respectively. The distance between adjacent axial and radial temperature probes are 62.5 mm and 10 mm, respectively.

4.2.2 Experimental parameters

The effect of heat load power (P_{HL}), Y-position of the permanent magnet (Y_{pm}), Z-position of the permanent magnet (Z_{pm}) on the heat load and FF temperature profile was studied. Various temperature profiles were measured, viz., heat load without the multi-torus device (bare HL), heat load without magnet (without TMC), and heat load with magnet (with TMC). These parameters and their range are summarized (**Table 4.1**).

Table 4.1. Parameters, their unit, notation, and their values or range.

Parameter	Unit	Notation	Values/Range
Heat load power	kW	P_{HL}	0.5, 0.67, 0.83, 1
Bare heat load temperature (no cooling device)	°C	Bare HL	320 to 580
Heat load temperature without magnet	°C	Without TMC	211 to 454
Heat load temperature with magnet	°C	With TMC	172 to 366
Y-position of the permanent magnet	Mm	Y_{pm} at Z_{pm}=2	0, 62.5, 125, along −Y
Z-position of the permanent magnet	Mm	Z_{pm} at Y_{pm}= 0	2, 4, 6, 8 along +Z

4.3 Modelling Methodology

A 2D numerical model of the multi-torus magnetic cooling device was developed based on the experimental geometry (**Figure 4.1**(a)) using COMSOL Multiphysics software to investigate the thermomagnetic convection. The FF was taken as a single-phase continuum. The properties of FF (**Table 3.2, section 3.2.2**) were given as input in the model as the fluid phase parameters. The governing equations, basic assumptions and the boundary conditions used for the simulation model were given earlier in **section 3.4**. The magnetic volume force experienced by the FF is added as a source term in the Navier-Stokes equation. The magnetic field distribution of the permanent magnet was simulated and compared with the experimental magnetic field distribution. The boundary conditions were defined in

accordance with the experimental conditions. The developed 2D numerical model was validated to obtain simulation accuracy.

4.3.1 Numerical verification

To ensure the accuracy of the numerical model, a mesh independent test was performed using triangular mesh elements. Prior to the final simulation, the non-dimensional average flow velocity of the FF was plotted against the number of mesh elements (**Figure 4.2**). The FF velocity reached saturation with an error of 6.3% for 415076 number of mesh elements. For the final simulation, 424389 mesh elements were created with maximum element size of 1.1 cm (**Table 4.2**).

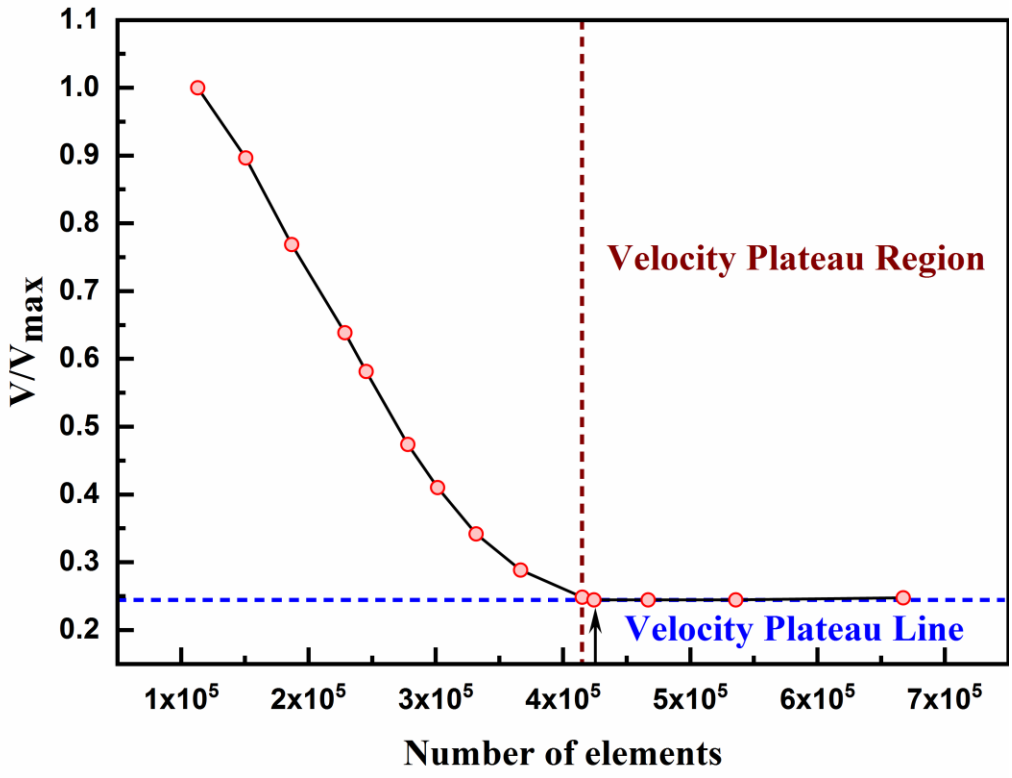

Figure 4.2. Simulated non-dimensional ferrofluid velocity in the multi-torus magnetic cooling device as a function of the number of mesh elements. The black arrow represents the number of mesh elements employed in the present work.

From the mesh independence test, the final meshing condition was determined, which includes 424389 mesh elements having an average mesh quality of 0.8889. The permanent magnet was meshed using quad elements. It is divided into 20000 elements of the same

size. The remaining geometry was meshed using triangular elements. **Table 4.2** summarizes the number of mesh elements and the average mesh quality.

Table 4.2. Mesh details of the modeled multi-torus magnetic cooling device.

Object	Mesh element type	No. of mesh elements	Average mesh quality
Magnet	Quad	20000	1
Ferrofluid flow region	Triangular	219923	0.8739
Tube wall	Triangular	73685	0.8319
Air domain	Triangular	110781	0.8910
Entire device	Triangular & Quad	424389	0.8889

4.3.2 Numerical validation

The numerical model for the simulation of TMC of FF in the multi-torus magnetic cooling device was validated by comparing the steady state magnetic field and temperature results with the experimentally obtained values. The simulated magnetic field along the length and width of the permanent magnet is in good agreement with the experimental values with a maximum error of 6.25% (**Figure 4.6**). Similarly, the simulated temperature profile of the heat load at various magnetic field conditions is consistent with the experimental findings with a maximum error of 8% (*section 4.4.3, section 4.4.4*).

4.4 Results

4.4.1 Determination of Parameters Affecting the Cooling Performance

The cooling of the heat load is due to the TM convective flow of the FF, which results in heat transfer from the heat load to the heat sink. The significant parameters, which can influence FF velocity, were simulated. The heat load cooling is related to the average FF velocity along the flow channel. Hence, we plotted the average non-dimensional FF velocity (V/V_0) against a certain range of each parameter. Here, V_0 denotes the simulated

average FF velocity at a heat load power of 0.5 kW. All parameters were kept the same as the experimental case, except the parameter whose effect is being studied. These parameters are categorized into three different subsections, as stated below.

4.4.1.1 Ferrofluid average velocity as a function of the device parameters

The device parameters are device geometry and device diameter (ΔD_{dev}). The FF velocity was simulated for different device geometries such as circular, elliptical, and rectangular, keeping the device perimeter the same as the experimental case. When the device geometry is changed from circular shape to elliptical and rectangular shape, the FF velocity decreased significantly (**Figure 4.3**(a)). For elliptical and rectangular shapes, the velocity of the FF is reduced by 34% and 74%, respectively, at a heat load power of 0.5 kW. The significant reduction of FF velocity in rectangular geometry is due to the presence of sharp corners. The elliptical geometry can reduce the form factor, however, at the expense of FF velocity. Due to the greater FF velocity in circular geometry, we used circular multi-torus geometry in the present study.

Figure 4.3(b) shows the effect of change in device diameter (ΔD_{dev}), over a range of 0 mm to 50 mm, on the FF velocity. The FF velocity reduces to 65% of V_0 at a ΔD_{dev} of 50 mm. For a constant magnetic field, the FF velocity decreased with increasing device diameter. For the present silicone tube internal diameter and wall thickness, the experimental device diameter is the lowest feasible diameter since the silicone tube tends to kink if the device diameter is lowered further than 38 cm (experimental case, **Table 5, section 3.3.1**).

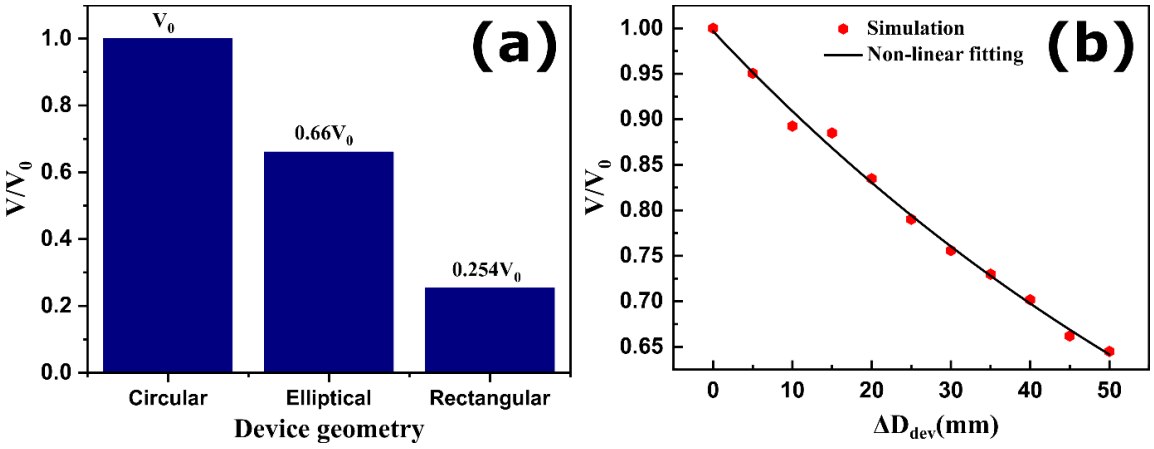

Figure 4.3. Simulated non-dimensional ferrofluid velocity (V/V_0) as a function of (a) device geometry, and (b) change in device diameter (ΔD_{dev}). V_0 denotes the simulated average ferrofluid velocity at a HL power of 0.5 kW, for the same parameter values as the experimental case.

4.4.1.2 Ferrofluid average velocity as a function of ferrofluid property variation

The FF properties that can affect the heat load cooling are thermal conductivity (λ), viscosity (μ), and the MNP volume fraction ($\mathbb{C}_o$). **Figure 4.4** shows the non-dimensional FF velocity for a range of values of these FF properties. The dotted lines represent the properties of APG S11N FF and the corresponding velocity. The effect of FF thermal conductivity on its velocity is provided in **Figure 4.4**(a). The FF velocity increased with an increase in FF thermal conductivity, but the increase is only 0.2% for a 100% change in the FF thermal conductivity. More heat can be transferred to the FF due to its higher thermal conductivity. However, the FF magnetization is lowered when the FF thermal conductivity is increased, reducing the thermomagnetic force experienced by the FF. Hence, the increment in FF velocity is not significant. **Figure 4.4**(b) shows a significant drop in FF velocity with increasing viscosity of the carrier fluid. The fluid velocity can increase by 50% at a FF viscosity value of 60 mPa.s. The viscous drag is less for low viscosity fluids, which increases the average FF velocity. **Figure 4.4**(c) shows the effect of magnetic nanoparticle volume fraction in the FF on the average FF velocity. The velocity increases for higher magnetic nanoparticle volume fraction. The FF velocity increases by ~30% and ~40% for a MNP volume fraction of 10 and 11, respectively. For the commercial FF used in this work, these parameters are constant. Hence, we studied the HL cooling performance, without altering the FF properties.

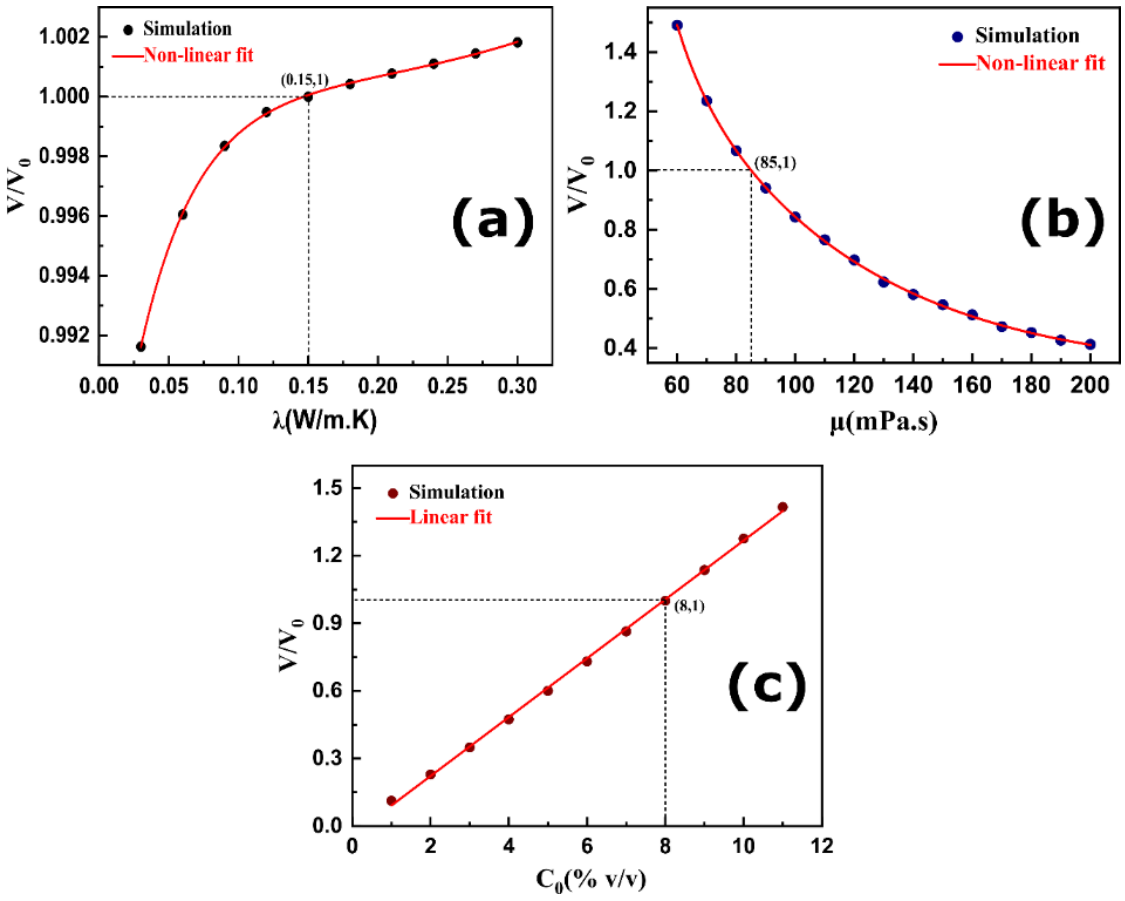

Figure 4.4. Simulated non-dimensional ferrofluid velocity (V/V_0) as a function of ferrofluid (a) thermal conductivity (λ), (b) viscosity (μ), and (c) magnetic nanoparticle volume fraction ($\mathbb{C}_0$). V_0 denotes the simulated average ferrofluid velocity at a HL power of 0.5 kW, for the same parameter values as that of the experimental case.

4.4.1.3 Ferrofluid average velocity as a function of the magnetic field

Figure 4.5 shows the effect of the magnetic field experienced by the ferrofluid on the ferrofluid velocity. The velocity increases sharply with increasing magnetic field. The ferrofluid velocity increases by nearly five times ($5V_0$) for a field increment from 330 mT to 660 mT. The increase in ferrofluid velocity with respect to the magnetic field is very significant compared to the parameters previously considered (*section 4.4.1.1, and section 4.4.1.2*). The magnetic field is varied by altering the position of the permanent magnet with respect to the center of the HL.

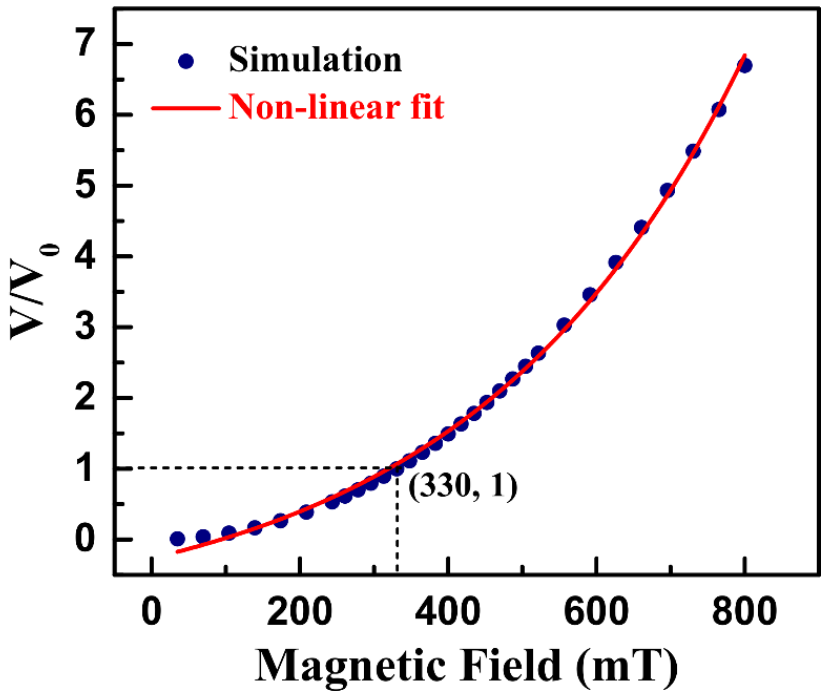

Figure 4.5. Simulated non-dimensional ferrofluid velocity (V/V_0) as a function of the magnetic field experienced by the ferrofluid. V_0 denotes the simulated average ferrofluid velocity at a HL power of 0.5 kW, for the same parameter values as that of the experimental case.

It was found that the increase in FF velocity with increasing magnetic field is very significant. The magnetic field was varied by altering the position of the permanent magnet with respect to the heat load. The device performance and the FF temperature profile were studied as a function of various magnet positions and the heat load power.

4.4.2 Magnetic field distribution

Figure 4.6 shows the magnetic field distribution of the magnet along its length and width. The dotted curves represent the simulated magnetic field distribution. The simulated and experimental magnetic field distribution are in good agreement with a maximum error of 6.25%.

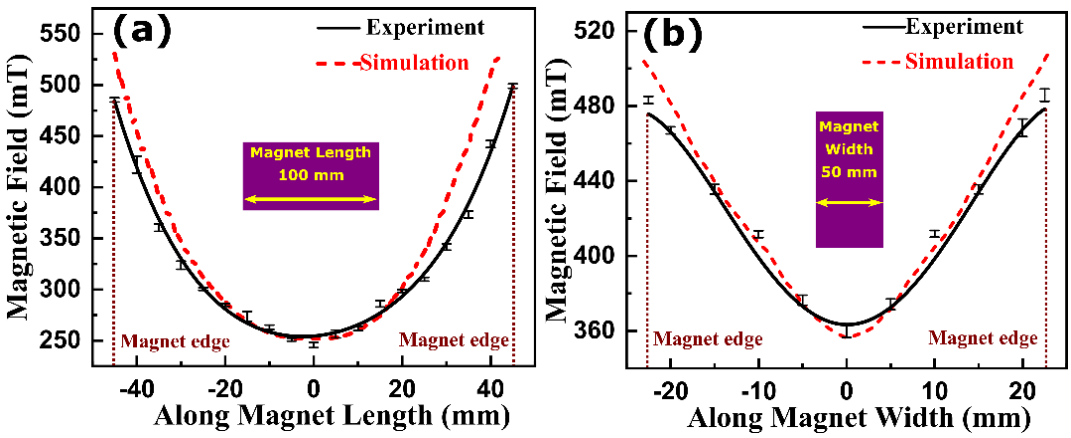

Figure 4.6. Magnetic field distribution of the NdFeB permanent magnet along its (a) length (X-direction), and (b) width (Y-direction). The dotted red curve shows the simulated magnetic field distribution.

4.4.3 Device performance as a function of the Y_{pm} of the magnet

The effect of the magnet distance from the center of the heat load on the cooling of the heat load was studied. For a constant height of the magnet (Z_{pm}= 2mm), the magnet position was varied from the center of the heat load (Y= 0 mm) along the negative Y-direction (Y_{pm}) (**Figure 4.1**(c)).

4.4.3.1 Cooling as a function of Y_{pm} of the magnet

Figure 4.7(a-c) shows the cooling of the heat load as a function of Y-distance of the magnet (Y_{pm}) for a heat load power (P_{HL}) of 0.5 kW. For any fixed heat load power, the temperature of the bare heat load increases to a maximum value and saturates after some time. This saturated bare heat load temperature is shown by the solid brown line. Heat load cooling in the presence of the magnetic field is due to the TMC of FF, as shown by the solid blue line (experiment) and the dotted red line (simulation). The heat load cooling (ΔT) improves from 137˚C for Y_{pm}= 125 mm to 148˚C for Y_{pm}= 0 mm. The FF temperature was the highest at the center of the heat load. A non-zero value of Y_{pm} reduces the magnetic force experienced by the FF in the middle of the heat load section, reducing ΔT. Thus, the coexistence of both higher FF temperature region and stronger magnetic field strength results in greater cooling. Although heat load cooling (ΔT) is reduced from 148˚C to 137˚C, the cooling is still substantial even for Y_{pm}= 125 mm. The simulated profiles are in good agreement with the experimental findings.

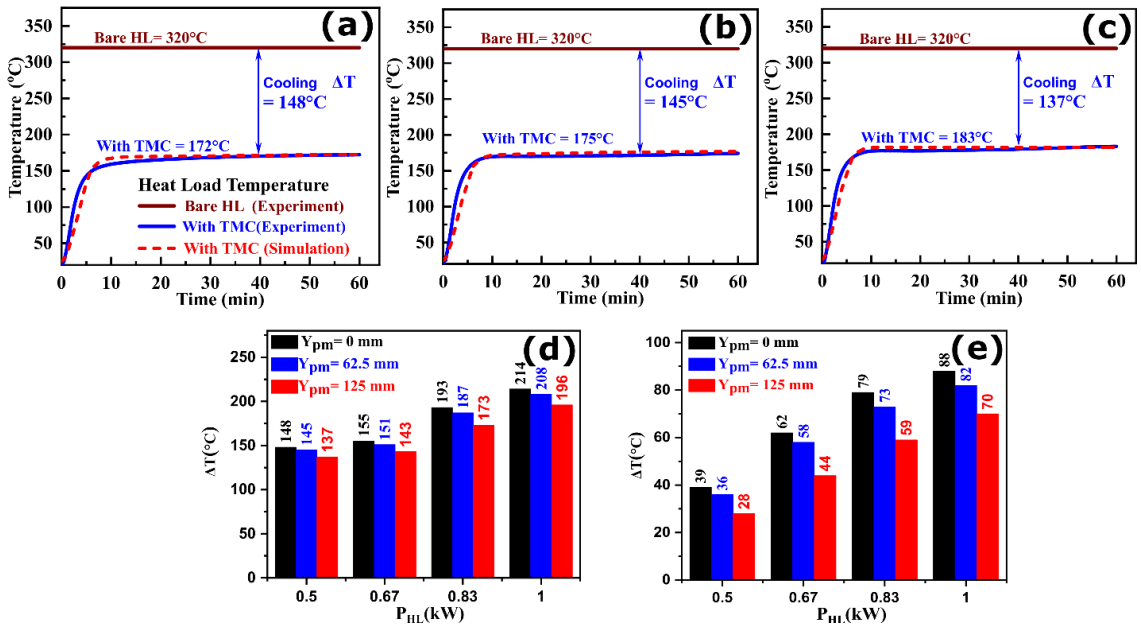

Figure 4.7. Heat load (HL) temperature profile (T) as a function of time (t) for magnet distance of (a) 0 mm, (b) 62.5 mm and (c) 125 mm along the Y-direction (Y_{pm}), at a constant magnet distance of Z_{pm}= 2 mm. The extent of heat load cooling (ΔT) as a function of heat load power (P_{HL}) at various magnet Y-distance (Y_{pm}) due to (d) both thermomagnetic convection (TMC) of the ferrofluid and conduction heat transfer from the heat load to the multi-torus magnetic cooling device, (e) only thermomagnetic convection of the ferrofluid.

4.4.3.2 Cooling as a function of heat load power (P_{HL}) for varying Y_{pm}

Cooling of the heat load was investigated for a range of heat load power (P_{HL}). **Figure 4.7**(d) shows the overall heat load cooling, due to both conduction and TMC, as a function of heat load power, for various Y_{pm} values. Significant ΔT values were observed for all heat load power values. Cooling was the highest when the magnet was placed at Y_{pm}= 0 mm. However, placing the magnet close to the heat load may affect the internal electronics. It may also be challenging to keep the magnet near the center of the heat load due to geometrical and form factor constraints.

Figure 4.7(e) shows the cooling of the heat load due to TMC of the FF, at various heat load power values. For a constant Y_{pm}, the extent of cooling increases as heat load power increases, demonstrating the self-regulating nature of the device. The FF temperature at the heat load region increases with increasing heat load power values, which lowers the magnetic susceptibility of the FF in the heat load region. This results in a larger non-

uniform magnetic force due to the temperature dependent magnetization of the FF. Hence, the FF velocity increases, resulting in greater cooling of the heat load. The temperature profile of the FF was measured and described in the following subsection.

The heat load cooling (ΔT) and percentage drop in ΔT were plotted for a range of heat load power values at various Y_{pm} (**Figure 4.8**). A maximum of 10.3% reduction in cooling was observed for a P_{HL} and Y_{pm} value of 0.83 kW and 125 mm, respectively. For 1 kW heat load power, ΔT value changed from 214°C to 196°C when Y_{pm} was increased from 0 mm to 125 mm. Again, ΔT is substantial even at Y_{pm}= 125 mm.

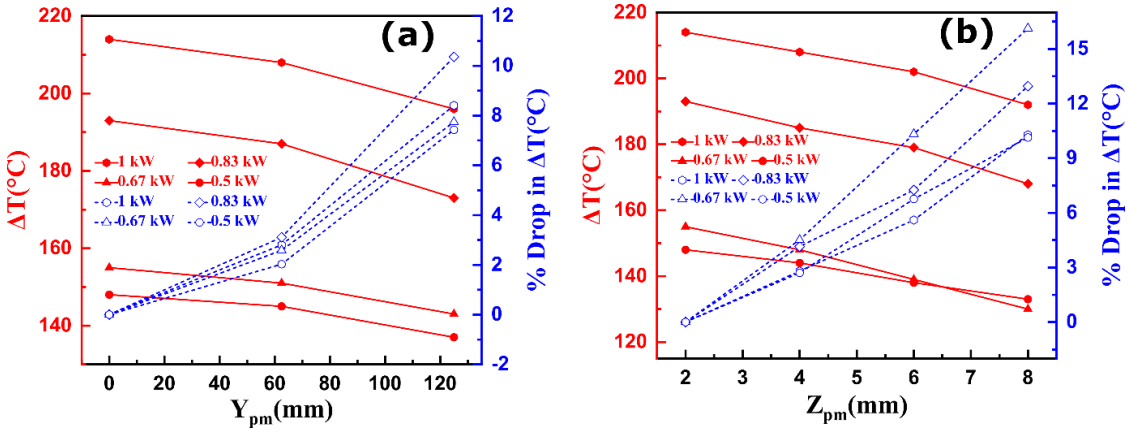

Figure 4.8. Heat load cooling magnitude and its percentage drop as a function of the (a) Y-variation of magnet position (Y_{pm}) at a constant Z_{pm} of 2 mm, and (b) Z-variation of magnet position (Z_{pm}) at a constant Y_{pm} of 0 mm.

4.4.3.3 Ferrofluid temperature profile for a range of Y_{pm}

Figure 4.9(a) shows the FF temperature profile at the axial temperature probe positions, for a heat load power value (P_{HL}) of 0.5 kW and a range of Y_{pm}. In the absence of the magnet, the FF temperature at Y= 0 mm is higher than at other Y-positions. The temperature distribution was found to be symmetrical with respect to the middle of the heat load section (Y= 0 mm). This symmetry breaks down in the presence of the magnetic field (**Figure 4.9**(a)). The temperature asymmetry was altered by changing the Y-position of the permanent magnet (Y_{pm}). The temperature at Y= -125 mm was lower than at Y= 125 mm, indicating counterclockwise FF flow. For Y_{pm}= 0 mm, the temperatures near the magnet, i.e. Y= 0 mm and -62.5 mm were lower than at the other three probe locations. For Y_{pm} = 62.5 mm, the probe temperatures at Y= -62.5 mm and -125 mm were lower compared to

other three probe temperatures since they were closer to the magnet. A similar trend was observed for Y_{pm} = 125 mm. Hence, the position of the magnet does affect the FF temperature profile and the extent of cooling of the heat load.

The temperature at Y= 0 mm increased to a higher value, for magnet positions of Y_{pm}= 62.5 and 125 mm, compared to the case of Y_{pm}= 0 mm. The magnetic field strength at Y= 0 mm decreases with increasing Y_{pm}, resulting in higher FF temperature. Therefore, cooling performance decreases with increasing Y_{pm} for a fixed heat load power (**Figure 4.7**(d,e)). Higher FF temperature at the heat load region leads to a higher difference in the magnetic susceptibility value of the FF in the vicinity of the heat load region compared to the value near the magnet. This results in a larger non-uniform TM force driving the FF. Thus, TM cooling performance improved for higher heat load power for a constant Y_{pm} (**Figure 4.7**(e)).

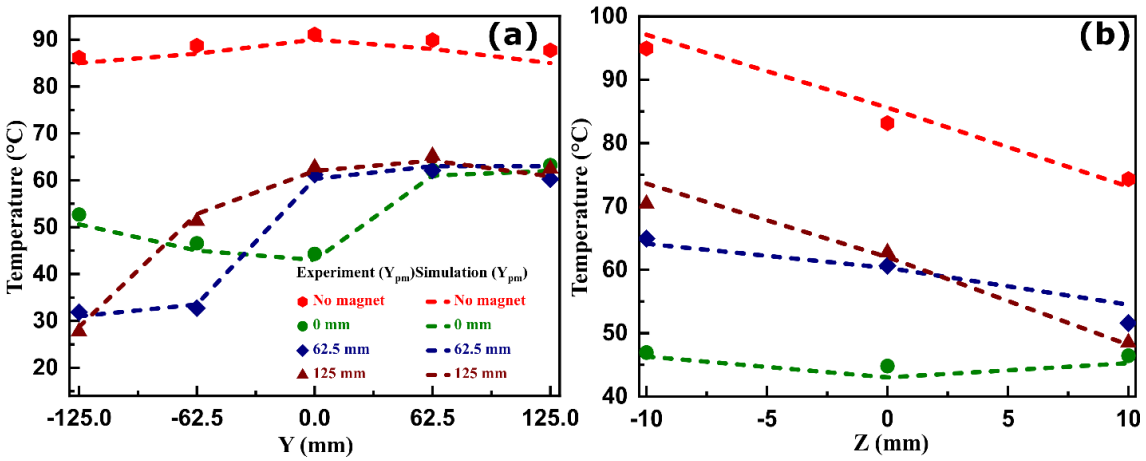

Figure 4.9. Ferrofluid temperature profile at a heat load power value (P_{HL}) of 0.5 kW along (a) the axial temperature probes (Y-direction), and (b) the radial temperature probes (Z-direction). For a constant Z_{pm}= 2 mm, the magnet distance was varied along the Y-direction.

Figure 4.9(b) shows the FF temperature profile along the Z-direction for a heat load power value of 0.5 kW and a range of Y_{pm}. In the absence of the magnet, the temperature decreases along the +Z direction from Z= -10 mm to Z= 10 mm. In the presence of the magnet, lower temperatures were observed for all the probes compared to the no magnet case. At Y_{pm} = 0 mm, the temperatures along the radial directions were similar. Also, at Y_{pm}= 0 mm, the position Z= 0 mm exhibited the lowest temperature due to the synergy between the magnetic field and the thermal field, which gave rise to a strong thermomagnetic

convection effect. For Y_{pm}= 62.5 mm and 125 mm, the radial temperature curves exhibited a similar trend as that of the no magnet case (red curve in **Figure 4.9**(b)). The temperature along the radial direction for Y_{pm}= 62.5 mm and 125 mm was also higher compared to the case of Y_{pm}= 0 mm. This effect is due to the lower magnitude of the magnetic force with increasing Y_{pm}. For higher Y_{pm}, the magnetic field strength experienced by the FF at Y= 0 mm was weaker compared to the case when the magnet was placed at Y_{pm}= 0 mm. Therefore, the cooling is less. The permanent magnet position at Y_{pm}= 0 mm, (green curve in **Figure 4.9**(a)) is the position for maximum cooling. Hence, all subsequent experiments were carried out at Y_{pm} of 0 mm.

4.4.4 Device performance as a function of the Z_{pm} of the magnet

The effect of magnet elevation from the top of the magnetic cooling device on the cooling of the heat load was studied. At constant Y_{pm} of 0 mm, the magnet elevation was varied from the top surface of the device (Z= 15 mm, **Figure 4.1**(b, c)), along the positive Z-direction.

4.4.4.1 Cooling as a function of Z_{pm} of the magnet

Figure 4.10(a-d) shows the cooling of the heat load for a range of Z-distance of the magnet (Z_{pm}) at a constant heat load power (P_{HL}) of 0.5 kW. The heat load cooling (ΔT) improved from 137˚C for Z_{pm}= 8 mm to 148˚C for Z_{pm} = 2 mm. This observation can be attributed to the stronger magnetic force experienced by the FF as the magnet was moved closer to the device. As expected, the stronger the magnetic field experienced by the FF at the heat load region, the greater the magnetic force on the FF, resulting in higher FF velocity and better cooling.

4.4.4.2 Cooling as a function of heat load power (P_{HL}) for varying Z_{pm}

The device performance was investigated for different heat load power values. **Figure 4.10**(e) depicts the overall heat load cooling, due to both conduction and TMC, as a function of heat load power for various magnet position along the Z-direction. For all the heat load power values, Z_{pm}= 2 mm gives the maximum cooling. However, the stronger magnetic field may affect the electronics of the equipment. Also, due to the geometrical constraints or form factor restrictions, the magnet may adversely affect ferromagnetic

metals and alloys in the device. Therefore, it may be necessary to keep the magnetic field strength low or the magnet physically away from the heat load. We plotted the ΔT value and its percentage drop as a function of Z_{pm} at various heat load power values (**Figure 4.8**(b)). A maximum of 16.1% ΔT drop was observed for a P_{HL} and Z_{pm} value of 0.67 kW and 8 mm, respectively. For 1 kW heat load power, ΔT value decreased from 214°C to 192°C when Z_{pm} increased from 2 mm to 8 mm. Hence, a permanent magnet can be placed away from the heat load region and at a reasonable height from the top of the heat load surface without much compromise on the heat load cooling. **Figure 4.10**(f) presents the cooling due to TMC of the FF at various heat load power values. Cooling increases with increasing P_{HL}. The increase in the TMC effect of the FF results in higher ΔT at lower Z_{pm}.

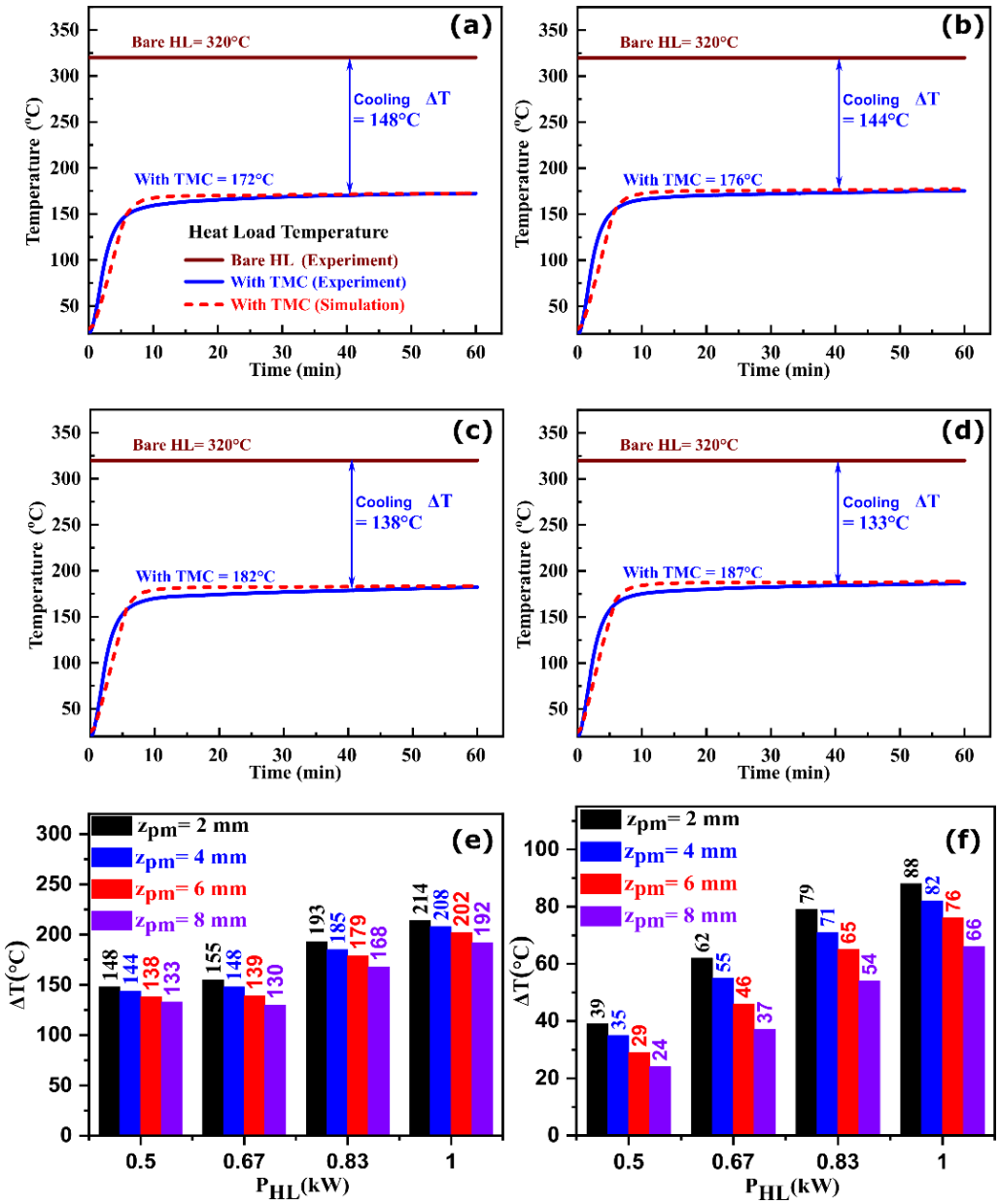

Figure 4.10. Heat load (HL) temperature profile (T) as a function of time (t) for a magnet distance of (a) 2 mm, (b) 4 mm, (c) 6 mm and (d) 8 mm along the Z-direction (Z_{pm}), at a constant Y_{pm}= 0 mm. The extent of heat load cooling (ΔT) as a function of heat load power at various magnet Z-distance (Z_{pm}) due to (d) both thermomagnetic convection (TMC) of the ferrofluid and conduction heat transfer from the heat load to the multi-torus magnetic cooling device, (e) only thermomagnetic convection of the ferrofluid.

4.4.4.3 Ferrofluid temperature profile for a range of P_{HL} and Z_{pm}

Figure 4.11(a) shows the FF temperature profile due to TMC, for various axial probe positions, at a heat load power (P_{HL}) of 0.5 kW and a range of Z_{pm}. Under an external magnetic field, the FF temperatures were lower compared to the no magnet case (red curve in **Figure 4.9**(a)). The temperature drop was higher at positions closer to the magnet (Y= 0 mm, -62.5 mm) compared to positions further away (**Figure 4.11**(a)). This is due to the stronger magnetic field experienced by the FF in those regions resulting in greater thermomagnetic force in the FF. The flow of colder FF from the heat sink region leads to lower temperatures in the negative Y-direction (Y= -62.5 mm, -125 mm) compared to their equivalent probes in the positive Y-direction.

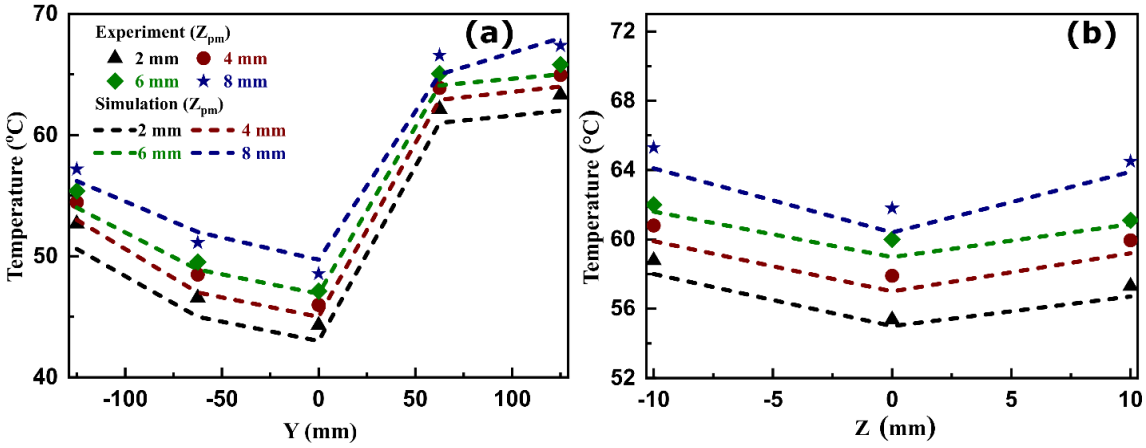

Figure 4.11. Ferrofluid temperature profile at a heat load power value (P_{HL}) of 0.5 kW (a) along the axial temperature probes (Y-direction), (b) along the radial temperature probes (Z-direction). For a constant Y_{pm}= 0 mm, the magnet distance was varied along the Z-direction.

Figure 4.11(b) illustrates the FF temperature profile along the Z-direction (radial probes), for varying Z_{pm} and a heat load power value of 0.5 kW. At a fixed power, the temperatures were similar for a constant Z_{pm}. The effect can be attributed to the strong TMC effect due to the presence of the magnet near the higher thermal gradient region (Y= 0 mm). The temperature at Z= -10 mm was slightly higher compared to Z= 0 mm and Z= 10 mm since it was closer to the heat load. With decreasing value of Z_{pm}, TMC of the FF and cooling are greater due to the higher magnetic field strength experienced by the FF.

The experimental results were in good agreement with the simulation. The small difference in temperatures between experiment and simulation could be due to errors in the positioning of the temperature probes.

4.4.5 Cooling for magnet position of Y_{pm}= 0 mm and Z_{pm}= 2 mm

From section **4.4.3** and **4.4.4**, it can be inferred that maximum heat load cooling occurs for Y_{pm}= 0 mm, and small magnet elevation above the device (Z_{pm}= 2 mm). For this position of the magnet, the extent of cooling increases from 148°C to 214°C, with an increase in heat load power from 0.5 kW to 1 kW, respectively (**Figure 4.12**). However, in the case of magnetic field sensitive devices, the magnet can be placed at certain distance and height from the middle of the heat load.

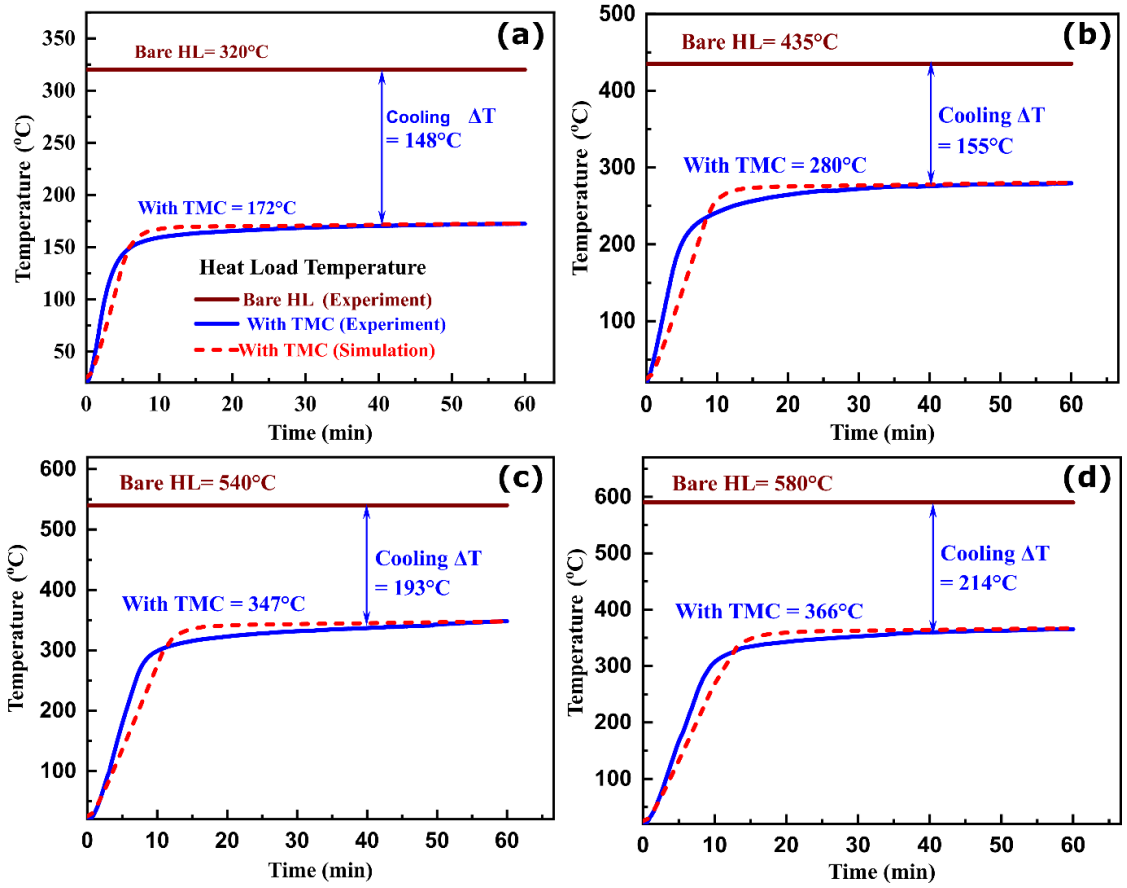

Figure 4.12. HL temperature (T) as a function of time (t), both in the presence (with TMC) and absence (bare heat load) of the multi-torus magnetic cooling device at varying heat load power (P_{HL}) of (a) 0.5 kW, (b) 0.67 kW, (c) 0.83 kW and (d) 1 kW, for an optimized magnet position of Y_{pm}= 0 mm and Z_{pm}= 2 mm. Dotted red curves represent the simulated heat load temperature at all powers.

4.4.6 Multiphysics modelling results

Multiphysics modeling of the multi-torus magnetic cooling device was performed, using a 2-D planar model, as described in **section 3.4** and **section 4.3**.

4.4.6.1 Simulated surface temperature

The combined effect of thermal gradient and magnetic field on FF flow can be inferred from the surface temperature plot, with and without the magnetic field (**Figure 4.13**(a, b)). Without the magnet, a uniform temperature distribution was obtained across the heat load section, whereas in the presence of the magnetic field, the temperature distribution became non-uniform. The uniform temperature distribution across the heat load section is due to the absence of FF flow. The temperature distribution under the external magnetic field also revealed the FF flow to be anticlockwise. It can also be observed that the thermal boundary layer was distorted near the heat load region due to FF thermomagnetic convection (**Figure 4.13**(b)).

4.4.6.2 Simulated surface velocity vectors

To study the combined effect of the magnetic field gradient and the thermal gradient on the FF flow direction and the nature of the flow, surface velocity vectors of the FF were plotted (**Figure 4.13**(d, e)). Far away from the magnetic field, the FF flow was laminar (**Figure 4.13**(e)). Interestingly, FF vortices were formed near the strong magnetic field region (**Figure 4.13**(d)). Vortex formation can be attributed to the combined effect of the magnetic field and thermal field on the FF flow. Near the heat load, the hotter FF, due to its smaller magnetization, gets attracted towards the magnetic field region with a small magnetic force. Simultaneously, the incoming colder FF, with higher magnetization experiences higher magnetic force, pushing it forward, resulting in the formation of a vortex.

Vortex formation helps in efficient mixing of the hotter and colder FF near the magnet. Hence, the FF temperature in the radial direction was similar (**Figure 4.11**(b)). The drop in FF temperatures near the magnet can also be attributed to these vortices (**Figure 4.9**(b), **Figure 4.11**(b)). Therefore, cooling is due to both the flow of FF through the flow channels across the heat load, and the vortices, which enhance thermal transport at the heat load

region. The vortices also disrupt the thermal boundary layer near the magnet (**Figure 4.13**(b)), enhancing heat transfer. Similar effects were reported by Bahiraei et al.[22] for the two-phase simulation of the FF flow in a square duct.

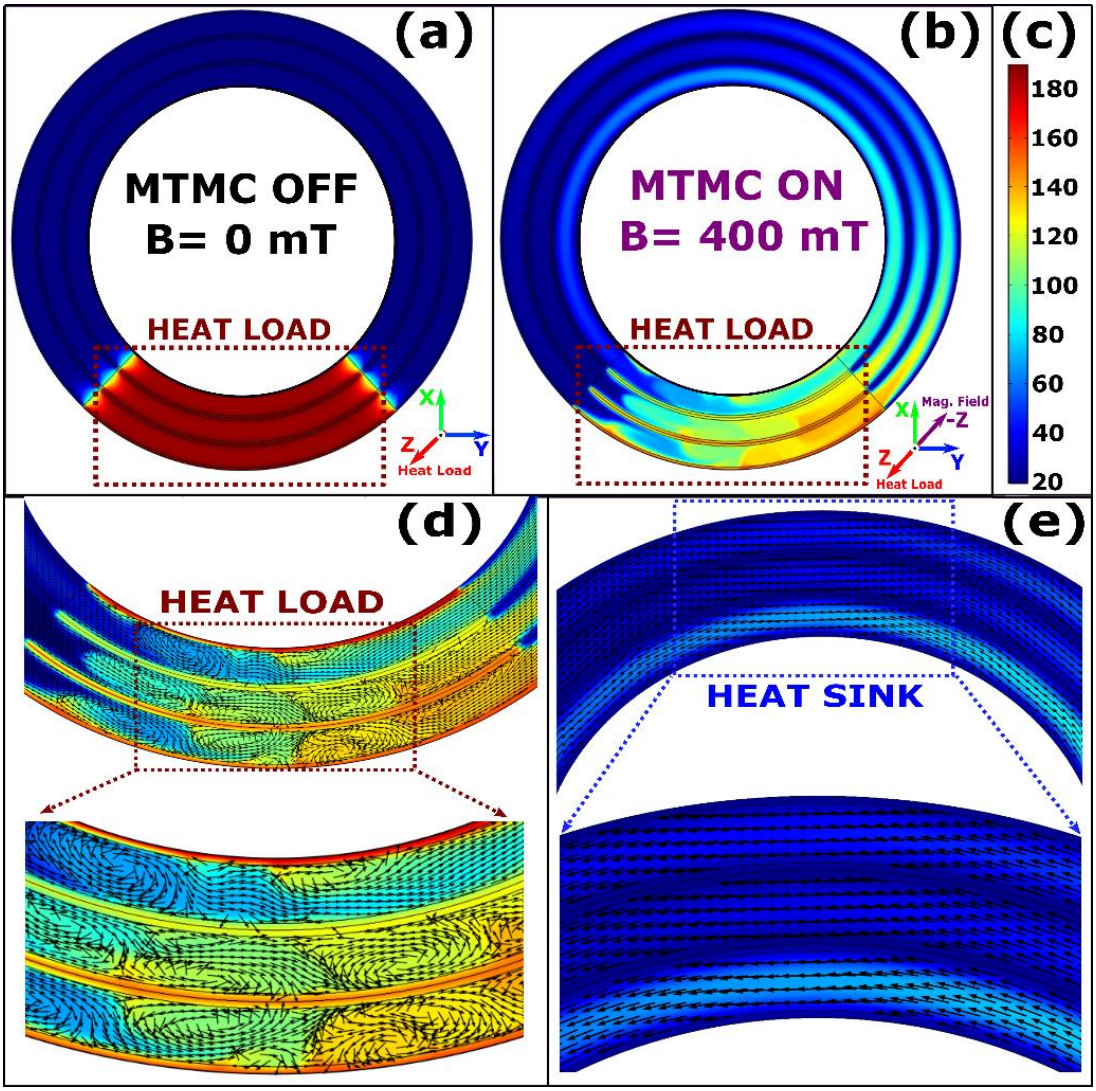

Figure 4.13. Simulation results showing the surface temperature profile of the multi-torus magnetic cooling device, temperature plots (a) without, and (b) with the magnetic field, (c) temperature color scale bar. Simulated velocity vector plots of the ferrofluid (d) near the magnet at the heat load region, and (e) far away from the magnet at the heat sink region.

4.4.6.3 Simulated velocity profile

The velocity profile was plotted for different heat load powers (**Figure 4.14**). The FF velocity increases with increasing heat load power. The velocity profile at the heat load region is not parabolic (**Figure 4.14**(a)). Rather, it is asymmetric with respect to the flow axis, which is due to the non-uniform magnetic field distribution along the flow channel axis and FF vortices (**Figure 4.13**(d)). At the heat sink region, the velocity profile is parabolic (**Figure 4.14**(b)) as the flow was laminar (**Figure 4.13**(e)) and the magnetic field effect is negligible.

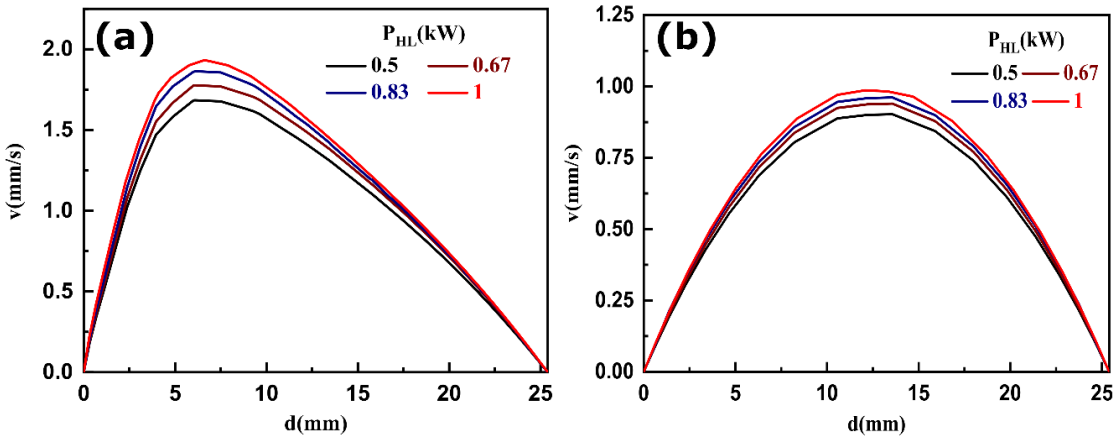

Figure 4.14. Simulated velocity profile of the ferrofluid as a function of the channel diameter (a) near the magnet at the HL region, (b) away from the magnet at the HS region.

4.4.7 Temperature transient effect

The effect of magnetic field switching between 0 mT and 400 mT on the heat load temperature transient effects was investigated for 0.5 kW heat load power (**Figure 4.15**). Initially, the heat load was allowed to attain a steady state temperature without the application of the magnetic field. Then, the magnet was brought near the device at the heat load region. A sudden drop in temperature was observed. The magnetic field switching cycle was repeated several times. The heat load temperature starts to increase and attains its maximum value over a duration of time after removing the magnetic field. The transient effect can be significant if the magnetic field is applied using an electromagnet. Some amount of the external energy can be saved by switching off the electromagnet for a particular time duration, when the heat load temperature rises. Once the heat load reaches

its critical temperature, the electromagnet can be switched on to commence the heat load cooling.

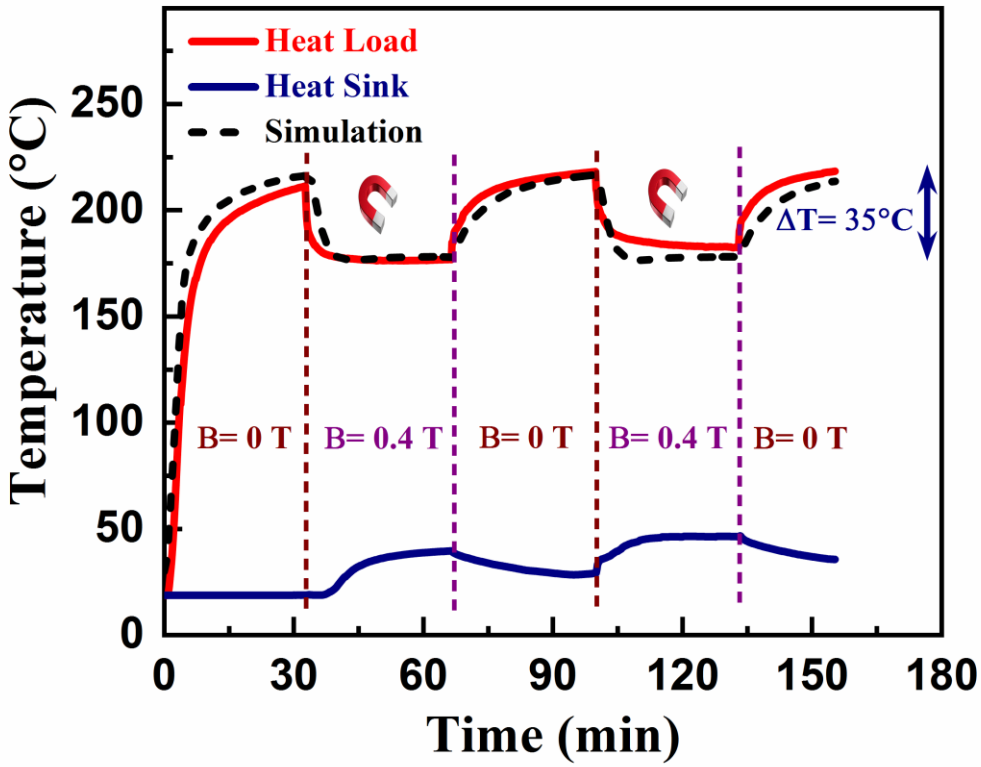

Figure 4.15. Effect of magnetic field switching between 0 mT and 400 mT on the heat load temperature profile and the ferrofluid temperature at the heat sink, at 0.5 kW heat load power.

The transient effect has been simulated by periodically removing and applying the magnetic field using a permanent magnet. For the simulation of transient effect, the total simulation time was 160 min, the same as that of the experiment. Each magnetic field switching cycle was maintained for ~30 min. The simulation time step size was taken to be 1 s. Smaller time steps are required for transient simulation [23]. For every cycle, the temperature drop due to FF thermomagnetic convection (ΔT) was found to be almost constant. At a heat load power of 0.5 kW, a drop in temperature of 35°C was obtained due to FF thermomagnetic convection. The simulated transient effect with magnetic field switching was in good agreement with the experiments with a maximum error of 4%. The FF temperature at the heat sink region was also found to change due to cycling. For the initial heating cycle, the temperature of the FF at the heat sink was constant. After

application of the magnetic field at t= 31 min, the hotter FF from the heat load started to flow and reached the HS region after 5 min, resulting in an increase in heat sink temperature. After removing the magnet at t= 64 min, the heat sink temperature reduced. The inflow of hotter FF to the heat sink region stopped and heat transfer to the ambient resulted in lower FF temperature at the heat sink. A similar trend was observed for further heating and cooling cycles.

4.4.8 Thermal resistance of the magnetic cooling device

Heat pipes are devices for thermal transport operating by the principle of an evaporation-condensation cycle. One important parameter to evaluate their thermal performance is by calculating the thermal resistance for a given input power [24, 25]. To compare the heat transfer of our device with a heat pipe, we calculated the device thermal resistance (R_D) and the FF thermal resistance (R_F). R_D is defined as the ratio of the temperature difference between the average heat load temperature (T_{HL}) and the heat sink average wall temperature (T_{HS}) to the applied heat load power. R_F is defined as the ratio of the average FF temperature difference at the heat load (T_{FF}^{HL}) and the HS (T_{FF}^{HS}) to the applied heat load power.

$$R_D = \frac{T_{HL} - T_{HS}}{P_{HL}} \quad (1)$$

$$R_F = \frac{T_{FF}^{HL} - T_{FF}^{HS}}{P_{HL}} \quad (2)$$

The device thermal resistance and the FF thermal resistance was plotted in **Figure 4.16**. For 1 kW heat load power, R_D and R_F were 0.26°C/W and 0.0187°C/W, respectively. The thermal resistances decrease with increasing heat load power. As heat load power increases, efficient heat transfer was observed. These thermal resistance results are consistent with the FF flow velocity behavior (**Figure 4.14**). For heat transport over a long distance, the overall device thermal resistance per unit length (R_{DL}) should be small. The fluid thermal resistance per unit volume of the fluid (R_{FV}) should also be low for better cooling performance. We compared R_{DL} and R_V for our device and conventional heat pipes.

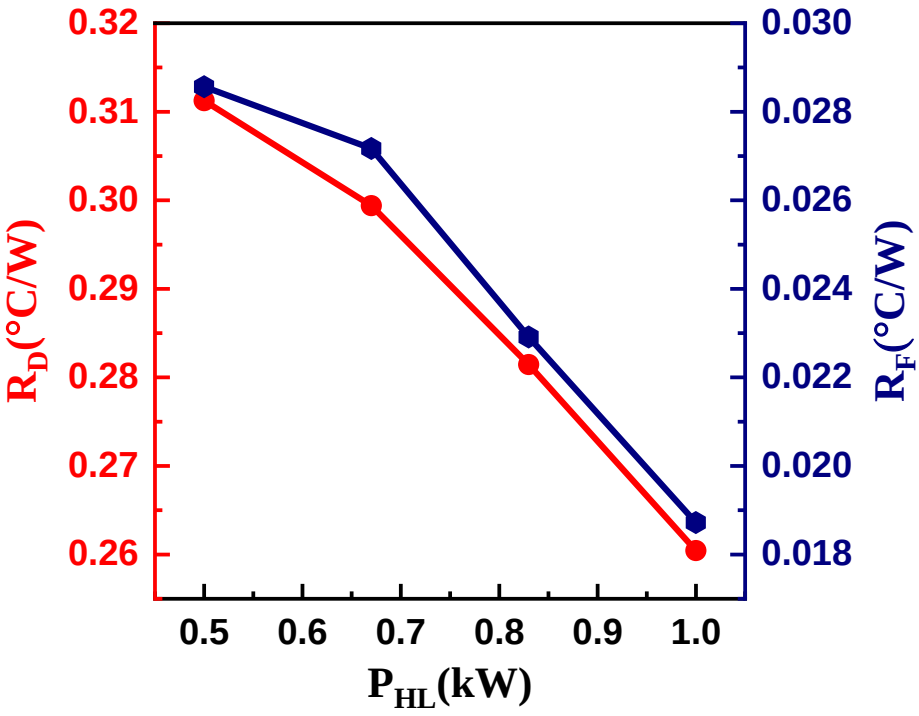

Figure 4.16. The thermal resistance of the device and the ferrofluid thermal resistance due to thermomagnetic convection in the presence of a permanent magnet at Y_{pm}= 0 mm and Z_{pm}= 2 mm.

Table 4.3 shows that the thermal resistance of our device and that of the FF are of the same order of magnitude as conventional heat pipes. Interestingly, the R_{DL} and R_{FV} values for our device are better than conventional heat pipes (**Table 4.3**). The multi-torus magnetic cooling device offers lower thermal resistance per unit length and lower fluid thermal resistance per unit volume of the FF. Hence, for the same device length, higher heat load cooling can be achieved using multi-torus magnetic cooling device than by conventional heat pipes, if the distance between the heat load and heat sink of the cooling device is large. Hence, the multi-torus magnetic cooling device can be more useful for cooling over large distances.

Table 4.3. Comparison of the thermal resistance of our multi-torus magnetic cooling device with conventional heat pipes. Notation: R_F = thermal resistance due to fluid flow at highest heat load power, R_D= device thermal resistance at highest heat load power, R_{FV}=R_{fluid}/fluid volume= volume thermal resistance of the fluid, R_{DL}= R_D/device length =device thermal resistance per unit length, NA= data not available.

Reference	R_F (°C W^{-1})	R_D (°C W^{-1})	R_{FV} (°C·W^{-1}·L^{-1})	R_{DL} (°C·W^{-1}·m^{-1})
This work	0.0187 (R_{FF})	0.26 (R_{MTD})	0.0085	0.18
[26]	NA	1.2 (15% Water)	NA	0.7384
		1.2 (20% Ethanol)		0.7384
		1.4 (50% R-123 special fluid)		0.8615
[27]	0.09 (Evaporator)	0.3 (Sink temp: 25ºC)	32.14	0.267
	0.23 (Condenser)		82.14	
[24]	NA	0.008 (0° inclination angle)	NA	0.0266
[25]	0.01	0.182	0.0535	0.1892

4.5 Discussion

Our multi-torus magnetic cooling device can be used for cooling of the heat load with power values and temperature upto 1 kW and 580°C, respectively. The extent of cooling (ΔT) of the heat load was 214°C at 1 kW heat load power, which is by far the maximum ΔT obtained using such device. The multi-torus device utilizes no external energy for driving the FF along the flow channels. Previously developed magnetic cooling devices mostly use small channel length of the flow channels and small volume of FF, which limits the overall heat transfer capacity of the device. A planar heat load source (250 mm*250 mm) with large dimensions was considered for the first time and cooled using our magnetic cooling device. A single permanent magnet was used to provide the thermomagnetic driving force to a large volume of FF along multiple flow channels, enhancing the heat transfer capacity. The lower value of thermal resistance per unit length of our magnetic cooling device and the FF thermal resistance per unit volume of the fluid makes it suitable

for heat transport over larger distance. The present multi-torus magnetic cooling device can be used for kW level heat loads at high temperatures. Various examples include industrial systems such as battery cabinets, compressors, data servers etc.

4.6 Conclusion

A multi-torus magnetic cooling device based on thermomagnetic convection of a FF was designed, fabricated, and tested for waste heat removal from a heat load in the kilowatt level power range. No external power was utilized for pumping the FF through the flow channel. Cooling of 148°C was achieved at a heat load power of 0.5 kW, which increased to 214°C at 1 kW. The temperature profile of the FF was recorded at the heat load section along both axial and radial directions. A 10.3 % and 16.1 % drop in heat load cooling magnitude from its maximum value was observed when the magnet was positioned at Y_{pm}= 125 mm and Z_{pm}= 8 mm, respectively.

The simulated results from the multiphysics model were in good agreement with the experimental findings. The surface velocity vector plot revealed the formation of FF vortices, which disrupt the thermal boundary layer and enhance cooling. The effect of magnetic field switching on the heat load temperature was studied and the effect was also simulated. The cooling was similar during each cooling cycle. Our device can operate at higher heat load power over greater lengths and higher fluid content because of the lower thermal resistance per unit length of the device and thermal resistance per unit volume of the fluid used. Hence, this self-pumping and self-regulating magnetic cooling device will be useful for kW level cooling.

References

[1] B. Insider. *The world wastes more energy than it uses every year*. Available: https://www.businessinsider.com/worlds-dirty-energy-comes-from-oil-wasted-2015-11?IR=T, [Accessed on: 3 January 2019].

[2] R. K. Das and C. Subramanian, "Thermal Analysis of Waste Heat Recovery Unit Using the Exhaust Gas Emitted From Internal Combustion Engine," *International Journal of Advances in Science Engineering and Technology*, vol. 4, no. 2, pp. 28-33, 2016.

[3] V. Sharma, S. Pattanaik, H. Parmar, and R. V. Ramanujan, "Magnetocaloric properties and magnetic cooling performance of low-cost Fe 75− x Cr x Al 25 alloys," *MRS Communications*, vol. 8, no. 3, pp. 988-994, 2018.

[4] G. Karimi-Moghaddam, R. Gould, and S. Bhattacharya, "Thermomagnetic liquid cooling: A novel variable speed motor drives thermal management solution," in *Electric Machines & Drives Conference (IEMDC), 2015 IEEE International*, 2015, pp. 1768-1773: IEEE.

[5] R. E. Rosensweig, *Ferrohydrodynamics*. Courier Corporation, 2013.

[6] M. Khairul, E. Doroodchi, R. Azizian, and B. Moghtaderi, "Thermal performance analysis of tunable magnetite nanofluids for an energy system," *Applied Thermal Engineering*, vol. 126, pp. 822-833, 2017.

[7] H. Yamaguchi and Y. Iwamoto, "Energy transport in cooling device by magnetic fluid," *Journal of Magnetism and Magnetic Materials*, vol. 431, pp. 229-236, 2017.

[8] J. Wang, G. Li, H. Zhu, J. Luo, and B. Sundén, "Experimental investigation on convective heat transfer of ferrofluids inside a pipe under various magnet orientations," *International Journal of Heat and Mass Transfer*, vol. 132, pp. 407-419, 2019.

[9] W. Lian, Y. Xuan, and Q. Li, "Characterization of miniature automatic energy transport devices based on the thermomagnetic effect," *Energy Conversion and Management*, vol. 50, no. 1, pp. 35-42, 2009.

[10] Y. Xuan and W. Lian, "Electronic cooling using an automatic energy transport device based on thermomagnetic effect," *Applied Thermal Engineering*, vol. 31, no. 8-9, pp. 1487-1494, 2011.

[11] Q. Li, W. Lian, H. Sun, and Y. Xuan, "Investigation on operational characteristics of a miniature automatic cooling device," *International Journal of Heat and Mass Transfer*, vol. 51, no. 21-22, pp. 5033-5039, 2008.

[12] V. Chaudhary, Z. Wang, A. Ray, I. Sridhar, and R. Ramanujan, "Self pumping magnetic cooling," *Journal of Physics D: Applied Physics*, vol. 50, no. 3, p. 03LT03, 2016.

[13] P. S. Szabo, M. Beković, and W.-G. Früh, "Infrared thermography of wall temperature distribution caused by convection of magnetic fluid," *International Journal of Thermal Sciences*, vol. 134, pp. 129-139, 2018.

[14] S. A. Zonouzi *et al.*, "Experimental investigation of the flow and heat transfer of magnetic nanofluid in a vertical tube in the presence of magnetic quadrupole field," *Experimental Thermal and Fluid Science*, vol. 91, pp. 155-165, 2018.

[15] M. H. Hekmat and K. K. Ziarati, "Effects of nanoparticles volume fraction and magnetic field gradient on the mixed convection of a ferrofluid in the annulus between vertical concentric cylinders," *Applied Thermal Engineering*, vol. 152, pp. 844-857, 2019.

[16] R. Zanella, C. Nore, F. Bouillault, J.-L. Guermond, and X. Mininger, "Influence of thermomagnetic convection and ferrofluid thermophysical properties on heat transfers in a cylindrical container heated by a solenoid," *Journal of Magnetism and Magnetic Materials*, vol. 469, pp. 52-63, 2019.

[17] S. Mousavi, N. Jamshidi, and A. Rabienataj-Darzi, "Numerical investigation of the magnetic field effect on the heat transfer and fluid flow of ferrofluid inside helical tube," *Journal of Thermal Analysis and Calorimetry*, pp. 1-11.

[18] M. Asfer, B. Mehta, A. Kumar, S. Khandekar, and P. K. Panigrahi, "Effect of magnetic field on laminar convective heat transfer characteristics of ferrofluid flowing through a circular stainless steel tube," *International Journal of Heat and Fluid Flow*, vol. 59, pp. 74-86, 2016.

[19] M. Goharkhah and M. Ashjaee, "Effect of an alternating nonuniform magnetic field on ferrofluid flow and heat transfer in a channel," *Journal of Magnetism and Magnetic Materials*, vol. 362, pp. 80-89, 2014.

[20] M. Bahiraei and M. Hangi, "Flow and heat transfer characteristics of magnetic nanofluids: A review," *Journal of Magnetism and Magnetic Materials*, vol. 374, pp. 125-138, 2015.

[21] A. Kumar and S. Subudhi, "Preparation, characteristics, convection and applications of magnetic nanofluids: A review," *Heat and Mass Transfer*, vol. 54, no. 2, pp. 241-265, 2017.

[22] M. Bahiraei, M. Hangi, and A. Rahbari, "A two-phase simulation of convective heat transfer characteristics of water–Fe3O4 ferrofluid in a square channel under the effect of permanent magnet," *Applied Thermal Engineering*, 2018.

[23] A. Lin, Q. Zheng, Y. Jiang, X. Lin, and H. Zhang, "Sensitivity of air/mist non-equilibrium phase transition cooling to transient characteristics in a compressor of gas turbine," *International Journal of Heat and Mass Transfer*, vol. 137, pp. 882-894, 2019.

[24] H. Tang, Y. Tang, B. S. Zhuang, G. Chen, and S. W. Zhang, "Experimental investigation of the thermal performance of heat pipes with double-ended heating and middle-cooling," (in English), *Energy Conversion and Management*, vol. 148, pp. 1332-1345, Sep 15 2017.

[25] G. H. Zhou and J. Li, "Two-phase flow characteristics of a high performance loop heat pipe with flat evaporator under gravity," (in English), *International Journal of Heat and Mass Transfer*, vol. 117, pp. 1063-1074, Feb 2018.

[26] S. Khandekar, N. Dollinger, and M. Groll, "Understanding operational regimes of closed loop pulsating heat pipes: an experimental study," (in English), *Applied Thermal Engineering*, vol. 23, no. 6, pp. 707-719, Apr 2003.

[27] N. S. Ramasamy, P. Kumar, B. Wangaskar, S. Khandekar, and Y. F. Maydanik, "Miniature ammonia loop heat pipe for terrestrial applications: Experiments and modeling," (in English), *International Journal of Thermal Sciences*, vol. 124, pp. 263-278, Feb 2018.

Chapter 5

High Conductivity, Low Footprint, High Cooling, Passive Magneto-fluidic Devices

Waste heat management by a passive magnetic cooling device can improve the reliability, efficiency, and life span of a plethora of systems. A magnetic cooling device is governed by the thermomagnetic convection of a ferrofluid. We investigated the effect of device characteristics and properties on the cooling performance. The effect of thermal conductivity of the tube of the device and device geometry on the cooling profile was determined. We developed for the first time several racetrack shaped magnetic cooling devices with low device footprint and high thermal conductivity. Copper-silicone hybrid magnetic cooling devices having a range of copper/silicone content were studied. The effects of this variation on cooling were examined. The effect of magnet position along the device periphery was evaluated. The all copper device cooled the heat load even when the magnet was placed close to the heat sink region. A hybrid copper-silicone device exhibited highest cooling of 123°C for a heat flux value and initial heat load temperature of 3.47 kW/m^2 and 197°C. Interestingly, the extent of cooling was higher for a hybrid device with higher silicone content. The hybrid magnetic cooling device is more useful for cooling of magnetic field insensitive devices, whereas an all copper device is useful for faster cooling of magnetic field sensitive devices.

5.1 Introduction

Efficient cooling solutions for the removal of waste heat are the need of the hour for modern industrial, electronic, and household devices. A magnetic nanofluid, also known as a FF, is a class of nanofluid consisting of coated superparamagnetic/soft ferromagnetic nanoparticles in a carrier fluid. The suspended MNP are typically 5-15 nm in diameter [1]. A ferrofluid possesses both fluidic and magnetic behavior [2]. Hence, the flow behavior of the ferrofluid can be controlled and manipulated by an external magnetic field. The thermal gradient due to the difference in heat load and heat sink temperatures results in a magnetization gradient in the FF. The FF at the heat load exhibit low magnetization. Near the heat sink, FF possesses higher magnetization. Under the influence of an external magnetic field, this differentially heated FF experiences a non-uniform magnetic volume force, giving rise to FF flow. This phenomenon is called thermomagnetic convection of the FF [2]. The FF continuously circulates in the flow channel under the combined effect of the waste heat and the external magnetic field. **Figure 5.1** shows the schematic of our passive MC device.

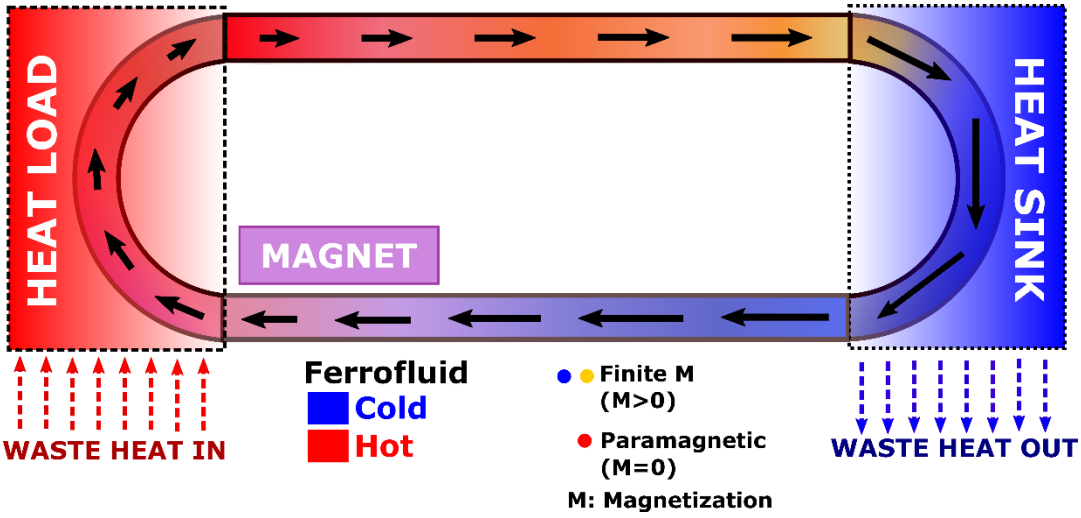

Figure 5.1. Schematic of a magnetic cooling device governed by the principle of thermomagnetic convection of a ferrofluid. A differentially heated ferrofluid flows around the closed loop under the effect of thermal gradient from the waste heat and an applied magnetic field. The color of the fluid inside the flow loop represents its thermal state, red being hot and blue being cold ferrofluid. The direction of arrows indicated the ferrofluid flow direction, and the length of the arrow represents the relative magnetization of the corresponding ferrofluid region.

Abbreviations

MC	Magnetic cooling
MEMS	Micro-electromechanical systems
LOC	Lab-on-a-chip
MNP	Magnetic nanoparticles
HL	Heat load
HS	Heat sink
PFA	Perfluoroalkoxy alkane
PMMA	Polymethyl methacrylate

Notation: Magnetic parameters

$\mathbf{H}$	Magnetic field
$\mathbf{M}$	Magnetization
$\mathbf{B}$	Magnetic flux density
M_S^{Bulk}	Bulk saturation magnetization of iron oxide
$\mathbf{M_s}$	Saturation magnetization
V_m	Magnetic scalar potential
$\mathbf{F_m}$	Magnetic volume force
μ_0	Permeability of the free space
χ_m	Ferrofluid magnetic susceptibility
χ_i	Initial magnetic susceptibility of the iron oxide nanoparticle

Notation: Thermal & fluidic parameters

T	Temperature
T_0	Heat load temperature without magnet
T_m	Heat load temperature with magnet
T_0'	Heat sink temperature without magnet
T_m'	Heat sink temperature with magnet
T_w	Inner tube wall temperature
T_f	Bulk ferrofluid temperature
$T_{f,in}$	Ferrofluid inlet temperature
h_y	Local convective heat transfer coefficient
P_{HL}	Power applied to the heat load
Q_{HL}	Heat flux at the heat load
Nu_L	Local value of Nusselt number
Nu_{avg}	Average value of Nusselt number
K	Thermal conductivity
C_p	Specific heat
$\mathbf{v}$	Velocity
P	Density
P	Pressure
M	Dynamic viscosity
$\mathbb{C}_o$	Magnetic nanoparticle volume fraction

Other parameters

L_D	Device length
L	Distance between the heat load and the heat sink
d_i	Inner diameter of the tube
d_o	Outer diameter of the tube
L	Heat load arc length
D	Distance between the parallel flow branch
V	Voltage
I	Current
Γ	Langevin parameter
$\mathcal{L}$	Langevin function
N	Number of points across the heat load

The salient properties of magnetic cooling systems are given below [2].

- FF flow is due to the waste heat from the device which needs to be cooled and the external magnetic field produced by either a permanent magnet or an electromagnet.
- It is self-pumping and self-regulating.
- The MC device does not require a wicking structure or actuator system.
- The MC device is noise-free, vibration-free, and requires low/no maintenance. Hence, it can be used in remote areas for cooling.

Several MC devices were developed and investigated for their TM cooling performance. They can be categorized as microscale, small-scale, and large-scale devices. Initial studies focused mainly on the cooling of microscale devices, e.g., for micro electromechanical system (MEMS) and lab-on-chip (LOC) applications [3-6]. Hatch et al. [6] developed a micropump based on magnetic actuation of FF for both pumping and valving, intended for LOC applications. Love et al. [3] designed and investigated a magnetocaloric pump for LOC applications. They synthesized oil-based magnetite, and water and oil-based Mn-Zn ferrite FF and compared their cooling in a magnetic cooling system. Ghasemian et al. [5] numerically examined forced laminar convection based heat transfer of a magnetite FF in a mini channel

Recent studies have focused more on large-scale cooling for long-distance and high-power waste heat transfer. Pattanaik et al. [2] investigated the cooling performance of kW level heat loads using a large-scale multi-torus MC device having an effective flow channel length and diameter of 1.8 m and 25 mm, respectively. They achieved a heat load temperature drop of 214°C at 1 kW heat load power using oil-based magnetite FF. Yamaguchi et al. [7] experimentally studied the performance of a 5 m long MC system using a temperature-sensitive binary magnetic fluid. For a horizontal orientation of the device, they reported a heat transfer of 35.8 W employing liquid-gas boiling two-phase flow.

All these reports investigated MC as a function of FF properties, heat load power/power density and temperature, device orientation, magnetic field strength, position, and orientation of the applied magnetic field. However, very few reports examined the effect of MC device geometry on the TM cooling [8]. Previous reports investigated cooling of a single tube material type e.g., glass [4], copper [7, 9], aluminum [10], stainless steel [11, 12], polymeric PFA [13], PMMA [14], or silicone [2]. However, there was no investigation of the effect of thermal conductivity of the tube material on the cooling of the heat load. The influence of FF parameters [3, 13, 15, 16] and magnetic field conditions [2, 7] on cooling was studied . However, the effect of thermal gradient on the cooling has not been studied. The effect of magnet position from the heat load all the way to the heat sink on the cooling was not studied.

Hence, the scope of the present study is to investigate the cooling with respect to device parameters and characteristics. We studied the effect of flow tube thermal conductivity, i.e., highly thermally conductive copper tube and less thermally conductive silicone tube on the cooling. To investigate the effect of device form factor on cooling, we developed, and investigated for the first time, racetrack geometry-based MC devices with a low device footprint. We fabricated hybrid racetrack MC devices to enhance the thermal gradient, and hence cooling by creating a junction of two materials with dissimilar thermal conductivity along the flow channel. A thermally conductive copper tube was joined to a lower thermal conductivity silicone tube to form a hybrid device. This results in a copper-silicone hybrid hot-cold junction near the heat load region, increasing the thermal gradient region.

The heat load temperature profile, cooling magnitude, heat sink temperature, and the simulated average FF velocity were investigated as a function of copper percentage in the hybrid MC device. We report superior cooling performance using racetrack MC devices. The cooling is maximized for lower copper content hybrid racetrack device. High cooling by 111°C, and 123°C was observed using an all copper and a hybrid MC device with 25% copper content, respectively, for a heat flux value and initial heat load temperature of 3.47 kW/m^2 and 197°C, respectively. The effect of magnet position on cooling for both copper and hybrid devices were analyzed. The heat load was cooled down using an all-copper racetrack device even when the magnet was placed at the heat sink region, which was the farthest point from the heat load. The cooling performance was studied over a heat flux and heat load temperature range of 0.49-3.47 kW/m^2 and 50-200°C, respectively. Based on the cooling results as a function of magnet position, we present potential applications of copper and hybrid MC devices to cool magnetic field sensitive and magnetic field insensitive devices systems, respectively.

Our racetrack MC devices are versatile and offer an environmentally friendly passive cooling solution without the need of external energy input. The heat load can be cooled to a certain extent by placing a magnet away from the heat load using an all-copper MC device, which can significantly cool magnetic field sensitive industrial, electronic, and household devices and systems, e.g., gaming laptops, CPUs and data servers. On the other hand, for systems that are not affected by magnetic fields, such as solar panels, compressors,

automobiles, high power LEDs and battery cabinets, a hybrid MC device can be used the waste heat removal.

5.2 Experimental Methods

All the technical details and the dimensions of the experimental setup of the developed circular and racetrack devices are summarized in detail in section 3.3.2 and section 3.3.3, respectively. The schematics of the circular and racetrack devices are shown in **Figure 5.2** and **Figure 5.3**, respectively. The properties of the fluid material used for this study is also provided in section 3.2.2. The following subsection covers the experimental parameters, which are considered for the cooling performance investigation of racetrack devices.

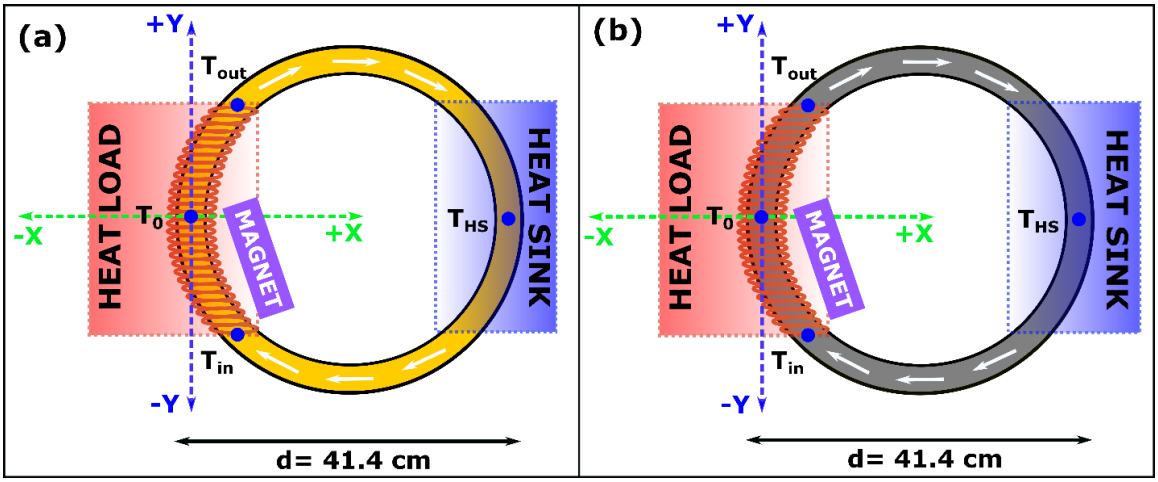

Figure 5.2. Schematics of the circular magnetic cooling devices with heat load arc length and perimeter of 30 cm and 130 cm, respectively. The circular devices are made up of (a) copper, and (b) silicone tubes. The heat load is obtained by radial resistive heating wire of nichrome. The magnetic field is applied by a Nd-Fe-B magnet near the heat load region. T-type thermocouples were positioned along the heat load section (blue dots). The origin (0,0,0) is taken at the center of the heat load. White arrows represent the ferrofluid flow direction due to thermomagnetic convection.

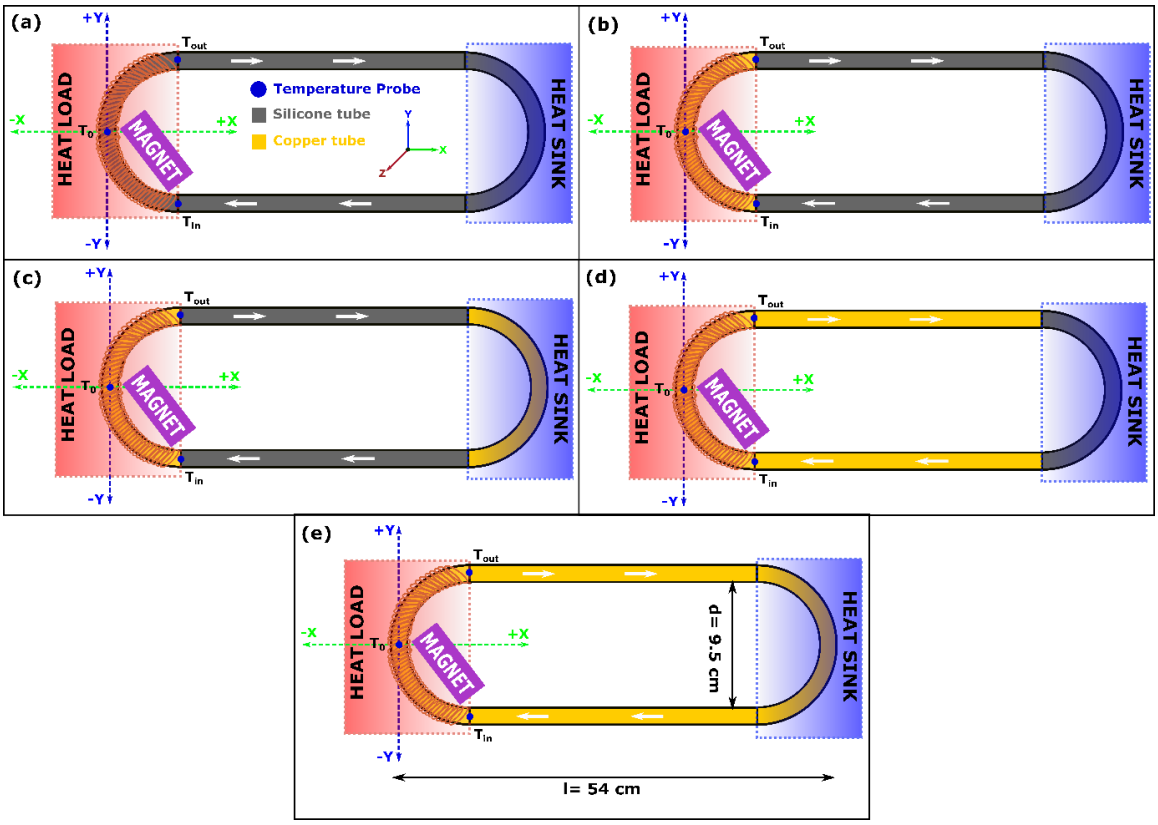

Figure 5.3. Schematics of the racetrack magnetic cooling devices with heat load arc length and perimeter of 30 cm and 130 cm, respectively. The racetrack devices are made up of (a) all silicone, (b) 25% copper and 75% silicone, (c) 50% copper and 50% silicone, (d) 75% copper and 25% silicone, and (e) all copper. The heat load is a radial resistive heating wire of nichrome, simulating a source of waste heat. The magnetic field is applied by a Nd-Fe-B magnet near the heat load region. T-type thermocouples were positioned along the heat load section (blue dots). The origin (0,0,0) is taken at the center of the heat load. White arrows represent the ferrofluid flow direction due to thermomagnetic convection.

5.2.1 Experimental parameters

The effect of device parameters, magnet position, and heat flux on the cooling was examined both experimentally and numerically. The device parameters considered for this study are tube material thermal conductivity, device geometry, and the copper to silicone ratio in the hybrid MC device. The experimental parameters, notation, and the range of these parameters studied are given in **Table 5.1**.

Table 5.1. Parameters, their notation, range, and the measurement sets.

Parameters	Unit	Notation	Performed Sets
Tube thermal conductivity	W/m.K	κ_{tube}	0.2 & 400
Device geometry	-	-	Circular & Racetrack
Copper to silicone ratio in hybrid device	%/%	-	0, 25, 50, 75, 100
Magnet position	Cm	d_m	0 to 55
Heat load heat flux	kW/m^2	Q	0.49-3.47
Heat load temperature without magnet	°C	T_0	50-200
Heat load temperature with magnet	°C	T_m	43-121

5.3 Modeling Methods

The details of the numerical model, governing equations, and the boundary conditions used for the numerical simulation of the circular and racetrack MC devices are summarized in section 3.4. The numerical verification and validation details are provided in the following subsections.

5.3.1 Numerical verification

For numerical verification of the 2D model, a mesh independence test was performed over a range of 2D triangular mesh elements. The final simulation of the racetrack MC device consists of 173918 triangular mesh elements with an average mesh quality of 0.8895. The mesh independence test was performed considering the non-dimensional FF velocity as a function of the number of mesh elements (graph not provided) [2].

5.3.2 Numerical validation

The 2D model for the FF TMC based heat transfer in the MC device was numerically validated by comparing the simulated magnetic field distribution (**Figure 5.4**) and heat

load temperature profile (**Figure 5.5**) results with experimental findings. The simulated value of the surface magnetic field of the NdFeB magnet along its length and width is in good agreement with the experimental value, with a maximum absolute error of 6.2%. The simulated heat load temperature profiles for a heat flux value and initial heat load temperature of 3.47 kW/m^2 and 197°C, respectively, are also in accordance with the experimental results.

5.4 Results and Discussions

5.4.1 Magnetic field distribution

Figure 5.4 shows the distribution of the magnetic field along the length and width of the NdFeB permanent magnet. The pink curves represent the simulated value of the magnetic field distribution. The experimental and simulated results are in good agreement, with a maximum absolute error of 6.2%.

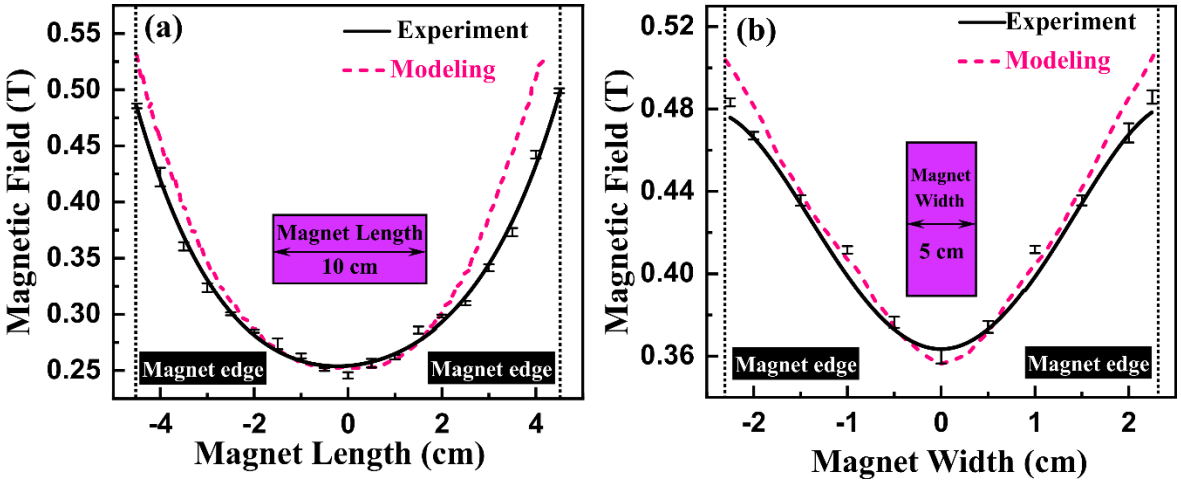

Figure 5.4. Surface magnetic field distribution of the NdFeB permanent magnet (a) along its length, and (b) width. The pink dotted curve represents the simulated magnetic field distribution.

5.4.2 Effect of tube material thermal conductivity on cooling

Two circular MC devices with the same tube internal diameter and device perimeter but different thermal conductivity values were developed using copper and silicone tubes (**Figure 5.2**). The dimensions and the physical properties of both the devices are provided in **Error! Reference source not found.** Initially, the heat load was allowed to reach a s aturation temperature (T_0) without an external magnetic field. A magnetic field was applied

near the heat load region after the heat load temperature reached a saturation value. **Figure 5.5** depicts the effect of tube material thermal conductivity on magnetic cooling of the heat load. The heat load was cooled from 197°C to 84°C (**Figure 5.5**(a)) and 114°C (**Figure 5.5**(b)) for copper and silicone-based circular MC devices, respectively. For the same initial heat load temperature T_0, the amount of cooling obtained in the copper-based device was 36% higher than its silicone counterpart. After the application of the magnetic field, the initial rate of change of heat load temperature ($\partial T/\partial t$) was 40°C/min for the copper-based device, whereas it was only 18°C/min for the silicone-based device.

These observations signify the strong effect of tube material thermal conductivity on the cooling. In addition to the ferrofluid thermomagnetic convection, the greater thermal conductivity of copper enhanced the cooling due to the additional effect of conductive heat transfer from the heat load to the heat sink. Effective heat transfer from the tube surface to the bulk of the FF can also contribute to the enhanced cooling. In the case of the copper-based device, heat transfer from the tube surface to the bulk of the FF results in a higher thermal gradient and higher magnetization gradient near the heat load region. This results in a larger magnetic force field across the heat load region, enhancing the cooling. On the other hand, due to the lower thermal conductivity of silicone, the transfer of heat from the surface to the FF bulk takes place slowly. Hence, we observed a gradual change in the heat load temperature profile in the silicone-based device, whereas for the copper case, the change is quite rapid (**Figure 5.5**).

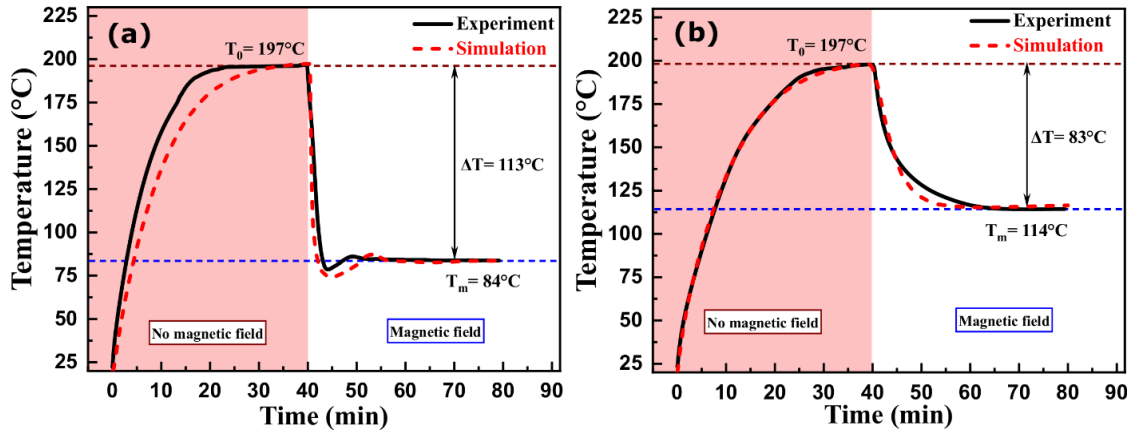

Figure 5.5. Heat load temperature profile as a function of time without and with the applied magnetic field for (a) copper, and (b) silicone tube material based circular magnetic cooling devices.

T_0 and T_m denote the heat load temperature without and with the magnetic field, respectively. Brown and blue dashed lines represent the heat load saturation temperature before and after the application of the magnetic field, respectively.

Figure 5.6 shows the heat sink temperature profiles of both copper and silicone-based circular MC devices. The heat sink temperature profile of a copper-based circular magnetic cooling device can be subdivided into four different points (**Figure 5.6**(a)). A constant heat sink temperature of 21°C was observed until point A. Subsequently, the heat sink temperature slightly increased to 22.5°C and saturated thereafter. This increase in heat sink temperature can be attributed to thermal conduction through the copper tube. At 40 min, the heat sink temperature from point B increased at a rapid rate and reached a peak value of 86°Cat point C. This steep rise in the heat sink temperature is due to the inflow of hot FF from the heat load region immediately after placing the permanent magnet. From point C, the heat sink temperature started to reduce again and saturated near point D at 58°C. A sharp drop in the heat sink temperature after point C (t~50 min.) may be ascribed to the completion of the initial half cycle of the FF flow (inflow of the FF from the heat load to the heat sink) and equilibration thereafter. The simulated heat sink profile (orange dashed line in **Figure 5.6**(a)) also exhibited a similar temperature trend. The sharp peaks in both the heat load (**Figure 5.6**(a)) and heat sink (**Figure 5.6**(a)) temperature profiles of the copper device are mainly due to effective conductive heat transfer and enhanced TMC based heat transfer due to efficient transfer of heat from the copper surface to the bulk of the FF.

Unlike the copper case, the heat sink temperature profile of a silicone-based circular MC device can be subdivided into only three different points instead of four (**Figure 5.6**(b)). Due to the lower thermal conductivity of silicone, the heat sink temperature was the same as the ambient temperature of 21°C even after the application of the magnetic field at 40 minutes. The heat sink temperature started to rise at point A, 10 minutes after the application of the magnetic field. The rise in heat sink temperature is also not as sharp as the copper case. At point B, the heat sink temperature reached its maximum and then started to drop. At point C, the heat sink temperature tended towards a saturation value of 51°C unlike copper, where the temperature was already saturated. Efficient heat transfer through the copper-based device gave rise to higher cooling compared to the silicone-based MC

device. For both the heat sink simulated profiles, some differences were observed with respect to the experimental profiles.

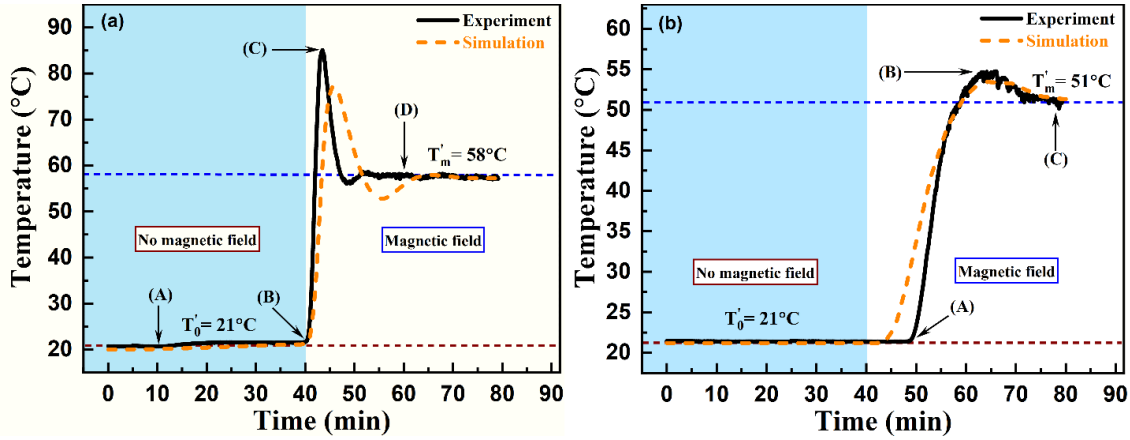

Figure 5.6. Heat sink temperature profile as a function of time without and with the applied magnetic field for (a) copper, and (b) silicone tube material based circular magnetic cooling devices. T_0' and T_m' denote the heat sink temperature without and with the magnetic field, respectively. Brown and blue dashed lines represent the heat load saturation temperature before and after the application of the magnetic field, respectively.

5.4.3 Effect of device geometry on cooling

To study the effect of device geometry on cooling, circular and racetrack devices were developed, and their cooling performance was studied. A magnetic field was applied near the heat load region after the heat load temperature saturated. **Figure 5.7** shows the temperature profile of the heat load before and after the application of the magnetic field for both the geometries. Though the amount of cooling was significant for both the geometries, slightly higher cooling was achieved for circular geometry than the racetrack geometry. In the case of the racetrack geometry, the FF velocity is slightly lower than the circular geometry due to higher curvature near the heat load and the heat sink. However, the device footprint for the racetrack geometry (390 cm^2) is considerably lower compared to the circular geometry (1345 cm^2). The device dimensions, device footprints, and the cooling performance for both the copper-based circular and racetrack devices are provided in **Table 5.2**. The rest of the work investigates the cooling performance of racetrack MC devices.

Table 5.2. Device dimensions, footprints, and the cooling performance of copper-based circular and racetrack magnetic cooling devices.

Device type	Device Perimeter (cm)	Device Footprint (cm^2)	Cooling(°C)
Circular copper	130	1345	113
Racetrack copper	130	390	111

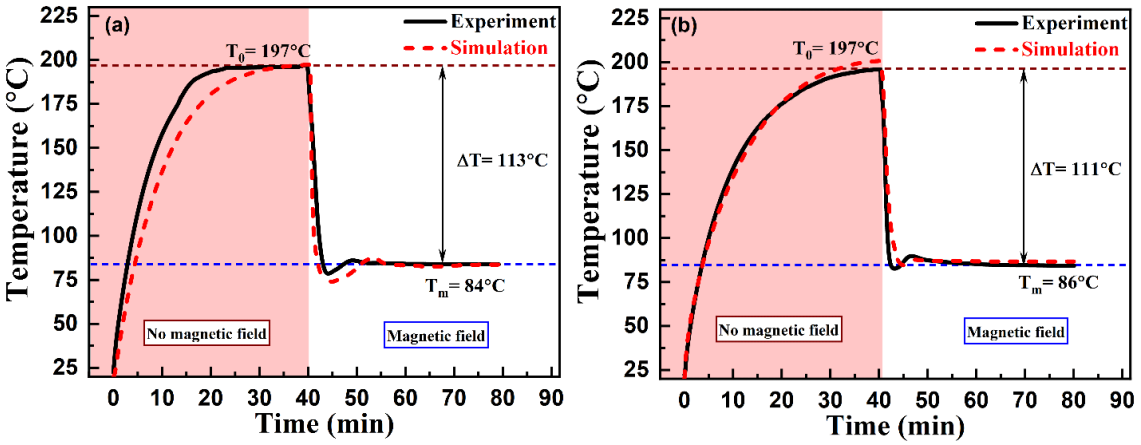

Figure 5.7. Heat load temperature as a function of time without and with the applied magnetic field for copper-based magnetic cooling devices of (a) circular and (b) racetrack design. T_0 and T_m denote the heat load temperature without and with the magnetic field, respectively. Brown and blue line represent the saturation temperature before and after the application of the magnetic field, respectively.

5.4.4 Racetrack copper-silicone hybrid thermomagnetic cooling device

The combined effect of thermal gradient and magnetic field gradient gives rise to the TMC of FF. The magnetic field gradient can be controlled by changing the position and orientation of the permanent magnet with respect to the heat load. Similarly, the thermal gradient can be enhanced by creating a junction of two materials having dissimilar thermal conductivity along the flow channel. In the present study, a highly thermally conductive copper tube was joined to a silicone tube having a relatively lower thermal conductivity, thus creating a copper-silicone hybrid hot-cold junction near the heat load region. This gives rise to a larger thermal gradient region. A magnetic field gradient near this large

thermal gradient region in the hybrid copper-silicone device can improve cooling compared to the all copper device counterpart. In addition, the use of silicone reduces both the cost and weight of the device.

5.4.4.1 Effect of copper percentage variation in the racetrack magnetic cooling device

Effect on the heat load temperature profile

To study the effect of copper to silicone ratio in the hybrid MC device on the cooling, five different race-track geometry devices were prepared to have the copper tube percentage of 0, 25, 50, 75, and 100 (**Table 3.7**) and their cooling performance was tested. The cooling performance was investigated for all five racetrack devices at a constant heat flux value (**Figure 5.8**). The heat load temperature profiles for all the cases were simulated and are in good agreement with the experimental findings. The cooling was inferior for the silicone-100 device due to the reasons stated in section 5.4.2. The highest cooling by 123°C was achieved for the copper-25 hybrid racetrack device. For the copper-50 device, the cooling magnitude was slightly lower than the copper-25 device. Interestingly, it was observed from **Figure 5.8** that the extent of cooling reduced with an increase in the percentage of copper in the racetrack device. A cooling of 111°C was obtained using copper-100 racetrack device. This effect of the reduction in the heat load cooling performance with increasing copper percentage can be described as follows.

The percentage increase of copper in the magnetic cooling device affects:

(A) Reduction in ferrofluid magnetization due to higher thermal conductivity of copper, and (B) reduction in thermal gradient within the ferrofluid column in the vicinity of the heat load due to more uniform temperature distribution across the device and the ferrofluid.

These two factors directly impact the thermomagnetic volume force. Lower magnetization and lower temperature gradient results in lower volume force. Hence, the flow velocity of the ferrofluid decreases resulting in lower heat load cooling for higher copper percentage.

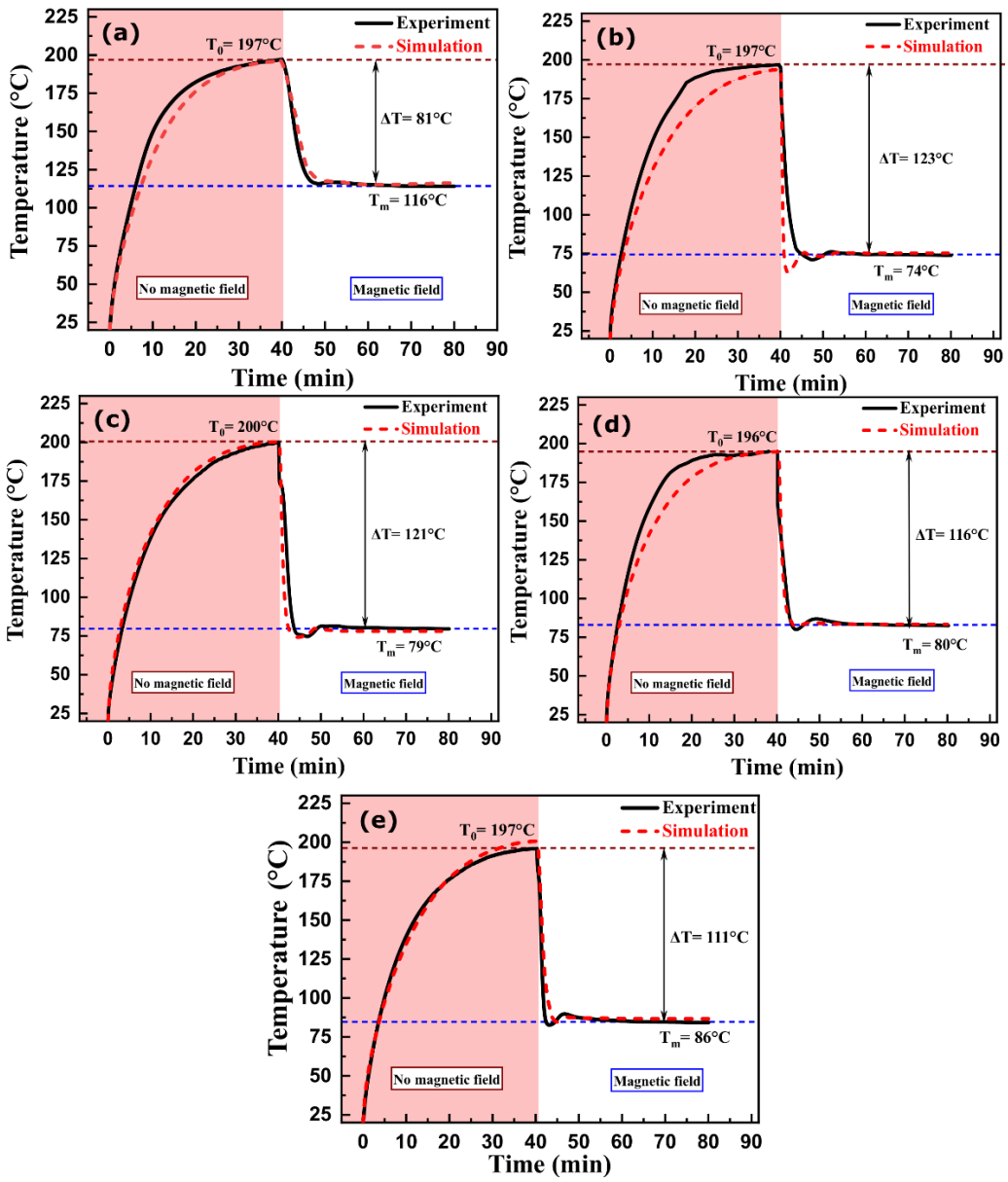

Figure 5.8. Heat load temperature profile as a function of time without and with applied magnetic field for (a) silicone-100, (b) hybrid-25, (c) hybrid-50, (d) hybrid-75, and (e) copper-100 racetrack magnetic cooling devices for a heat flux value of 3.49 kW/m^2. T_0 and T_m denote the heat load temperature without and with the magnetic field, respectively. Brown and blue dashed lines represent the heat load saturation temperature before and after the application of magnetic field, respectively.

Effect on cooling, and simulated ferrofluid velocity

Figure 5.9(a) shows the extent of cooling for all the racetrack devices with non-zero copper percentage. As can be seen in **Figure 5.9**(a), when the copper percentage was below 50%, the heat load exhibits highest cooling for both the magnet positions. This is due to the enhanced TM force experienced by the FF column at the heat load section in the hybrid MC device compared to the copper-100 device. The hybrid device has a hot-cold junction due to the dissimilar thermal conductivities of copper and silicone, resulting in a higher thermal gradient region in the ferrofluid. The temperature dependent magnetization of FF results in a large magnetization gradient in the FF near to the heat load region. However, due to the higher thermal conductivity of copper, no such larger thermal gradient region exists for the copper-100 device, giving rise to a lower cooling. The cooling was lower for all the cases when the magnet position was changed from 0 cm to 15 cm with respect to the center of the heat load. This is due to a reduction in the magnetic volume force experienced by the FF as the magnet is moved away from the heat load region.

Effect on rate of temperature change and time to achieve minimum heat load temperature

The rate of change of temperature of the heat load ($\partial T/\partial t$) and the extent of time (Δt) required to attain the minimum heat load temperature versus percentage copper, immediately after the application of an external magnetic field was shown in **Figure 5.9**(b). $\partial T/\partial t$ showed an increasing trend with higher copper percentage. The higher initial cooling rate of the heat load for copper rich racetrack cooling device may be attributed to the higher thermal conductivity of copper. The faster cooling rate of the heat load was also inferred from the curve of time duration required to attain the minimum temperature (blue curve). The Δt value was the lowest for copper-100 device.

Hence, the cooling rate increases with thermal conductivity of the device, whereas the extent of cooling is a strong function of the thermal gradient and reduces beyond 25 % copper. **Table 5.3** summarizes the cooling results for all the racetrack MC devices.

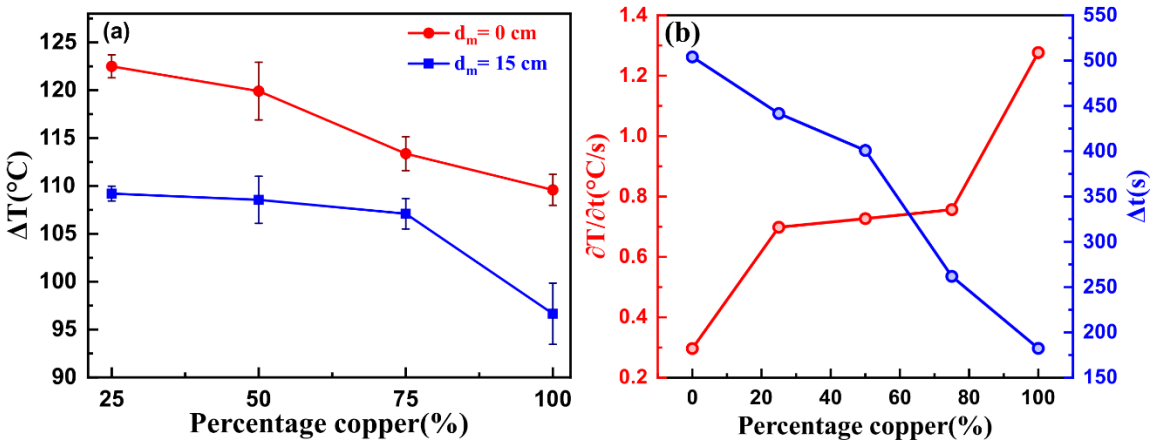

Figure 5.9. Initial rate of change of temperature (red curve) and the time required to reach the lowest heat load temperature (blue curve) as a function of percentage of copper tube in the racetrack magnetic cooling device.

Table 5.3. Extent of cooling as a function of the variation in copper/silicone ratio in the racetrack magnetic cooling devices for a heat flux value of 3.47 kW/m^2. Symbols used: T_0- heat load temperature without a magnetic field, Tm- heat load temperature with a magnetic field, ΔT- cooling, $\partial T/\partial t$- rate of temperature change of the heat load immediately after the application of the magnetic field.

Sr.	Copper/Silicone Percentage (%/%)	Abbreviation	Heat Load Temperature		ΔT= T_0- T_m, (°C)	**$\partial T/\partial t$** (°C/s)
			T_0 (°C)	T_m (°C)		
1	0/100	Silicone-100	197	116	81	0.29667
2	25/75	Hybrid-25	197	74	123	0.69833
3	50/50	Hybrid-50	200	79	121	0.72667
4	75/25	Hybrid-75	196	80	116	0.75667
5	100/0	Copper-100	197	86	111	1.27667

Effect on simulated ferrofluid temperature profile along the device perimeter

Figure 5.10 shows the simulated FF temperature as a function of the probe positions along the device perimeter for all the racetrack MC devices. The FF temperatures were measured

along the middle of the flow channel axis. Dashed line A represents the center of the heat load, whereas dashed lines C and B represent the start and end of the heat load region, respectively. The magnet was placed asymmetrically from the bottom side of the racetrack device with respect to the center of the heat load (**Figure 5.3**), which corresponds to the dashed line C in **Figure 5.10**. As is evident from **Figure 5.10**, the silicone-100 device showed maximum FF temperatures. This is due to the lowest cooling and smallest average FF velocity for the silicone-100 device case (**Table 5.3**). For all other racetrack devices involving non-zero copper tubing, the FF temperature is lower than the silicone-100 case.

The FF temperature profile was in accordance with the extent of cooling as a function of copper percentage (**Figure 5.8**, **Figure 5.9**(a)). In the C-A region of the heat load from 115 min to 130 min, the FF temperature first increased, then decreased and then increased again due to the strong magnetic field gradient. This non-uniformity in the FF temperature profile can be attributed to the formation of FF vortices near the strong magnetic field gradient and thermal gradient region [2]. However, the FF temperature tends to increase from dashed line A (0 cm, middle of the heat load region) to dashed line B (15 cm, end of the heat load region). The continuous increase in FF temperature in the A-B region indicates a weaker effect of FF vortices. Subsequently, the FF temperature reduced from the end of the heat load region (15 cm) to the start of the heat load region (120 cm). These trends signify the strong effect of copper tube percentage on the cooling performance. Hence, the hybrid-25 device offered enhanced cooling performance.

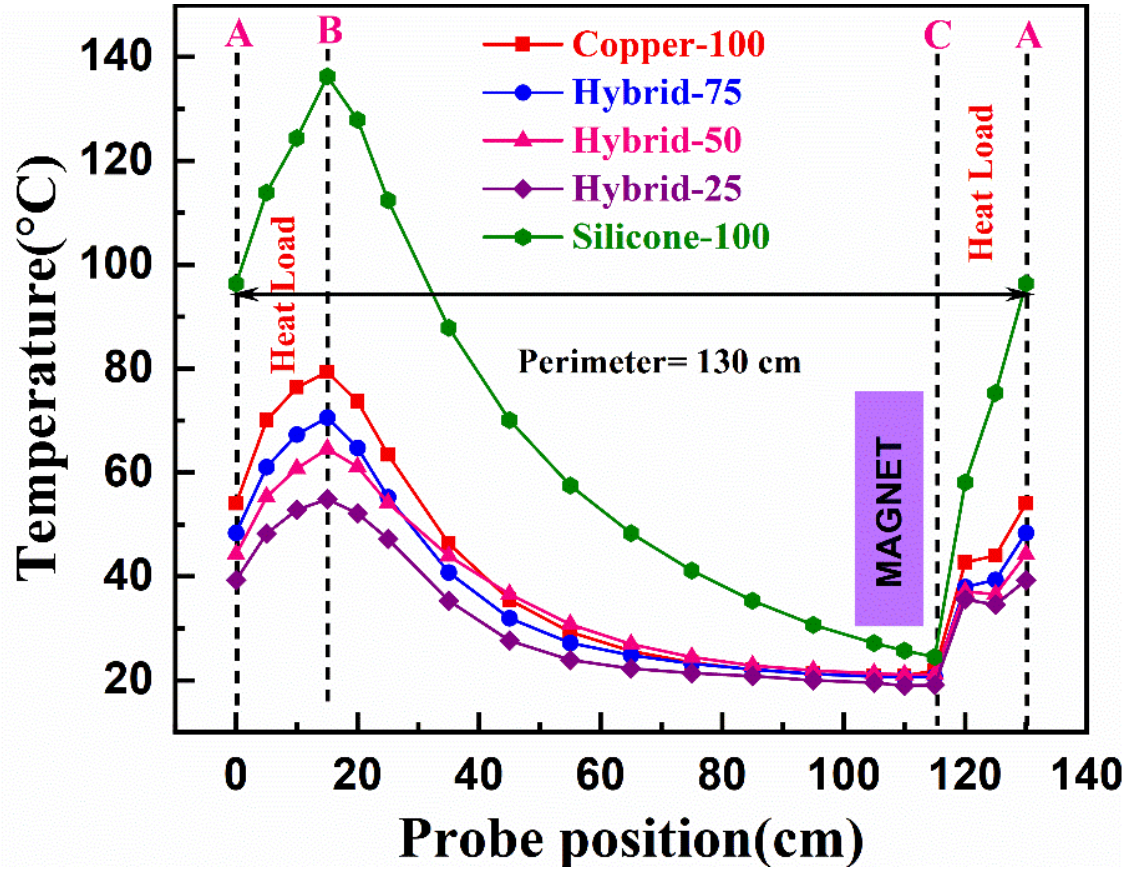

Figure 5.10. Simulated ferrofluid temperature curve at the end of the cooling cycle as a function of probe position along the device perimeter for all the developed racetrack-magnetic cooling devices. Dotted lines A at 0 cm and 130 cm mark the middle of the heat load region. Dotted lines B and C are the end and the start of the heat load region with respect to the ferrofluid flow direction, respectively. Magnet is applied at the C side of the heat load.

5.4.4.2 Effect of heat load tube material on cooling

To study the effect of heat load tube material in the hybrid racetrack device on the cooling, hybrid-25 and hybrid-75 devices were considered with copper and silicone as the heat load material, respectively. These two hybrid devices were chosen to maintain the percentage of the heat load and non-heat load section at 25% and 75%, respectively (**Table 3.7**). **Figure 5.11** shows the heat load and heat sink temperature profile of hybrid-25 and hybrid-75 devices with copper and silicone heat load tube material, respectively. Significant cooling of 123°C was obtained for hybrid-25 device with copper heat load (**Figure 5.11**(a)). For hybrid-75 device with silicone heat load, the heat load was cooled by 102°C (**Figure 5.11**(b)). The reason for such a notable difference in the cooling with different heat load

tube material can be due to the significant difference in the copper and silicone tube thermal conductivity. Also, for the copper-silicone hybrid junction, the thermal gradient can be higher with copper as the heat load material compared to the case of silicone as the heat load material. Hence, higher cooling was achieved for hybrid device with copper as the heat load material.

In **Figure 5.8**(d), hybrid-75 device with copper as the heat load material exhibited a cooling by 116°C, higher than the 102°C obtained for the same device with silicone heat load (**Figure 5.11**(b)). This is due to the higher thermal conductivity of copper and the development of greater thermal gradient region for the copper heat load case. The saturation heat sink temperature was 42°C and 53°C for copper and silicone heat load, respectively (**Figure 5.11**). The higher thermal gradient in the case of the copper heat load resulted in more TM force to push the ferrofluid along the hybrid-25 device with a greater velocity compared to the silicone heat load case with the hybrid-75 device. Hence, it can be inferred that the hybrid device with less than 50% copper tubing gives superior cooling performance with copper as the heat load material.

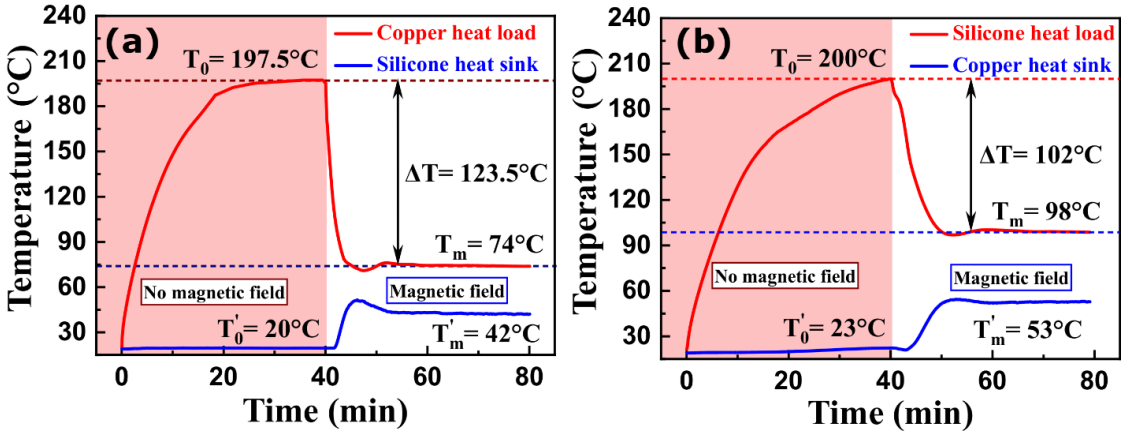

Figure 5.11. Heat load and heat sink temperature profile as a function of time without and with the applied magnetic field for (a) hybrid-25 device with copper heat load, and (b) hybrid-75 device with silicone heat load, for a heat flux value of 3.49 kW/m^2. T_0 and T_m denote the heat load temperature without and with the magnetic field, respectively. Brown and blue dashed lines represent the heat load saturation temperature before and after the application of magnetic field, respectively.

5.4.4.3 Effect of variation in the magnet position on cooling

The effect of variation in the magnet position along the perimeter of the racetrack copper-100 and hybrid-50 devices on the amount of cooling was examined (**Figure 5.12**). The magnet position with respect to the heat load center along the perimeter of the racetrack device was varied over a range of 0-55 cm from the heat load all the way to the heat sink. **Figure 5.12**(a) and **Figure 5.12**(b) show the extent of cooling for copper-100 and hybrid-50 racetrack devices, respectively. As expected, the extent of cooling reduced when the magnet was moved away from the heat load region due to the reduction of magnetic volume force experienced by the differentially heated FF at the heat load region.

The reduction in ΔT was gradual when the magnet was placed in the heat load region for both copper-100 and hybrid-50 devices. However, the magnitude of ΔT was higher for hybrid-50 case as compared to the copper-100 case for the reasons stated in section 5.4.4. Interestingly, the ΔT value showed a gradual decrease as a function of magnet position (0-55 cm) over all the regions for copper-100 device (**Figure 5.12**(a)). A lower non-zero value of cooling (ΔT= 6°C) was obtained, even when the magnet was placed at the heat sink region, at 55 cm away from the center of the heat load section. For the copper-100 device, the superior thermal conductivity of copper resulted in efficient heat distribution from the heat load to the heat sink. In the intermediate region, the copper-100 device exhibited a linear reduction in ΔT with a slope of -2.73°C/cm. The change of slope from the heat load to the intermediate region is due to the reduction of thermal gradient, which resulted in lower magnetization gradient and magnetic volume force experienced by the FF.

However, unlike the copper-100 device, the hybrid-50 device revealed a sharp reduction in the ΔT value when the magnet was moved away from the heat load region. Away from the heat load region, the device and the FF does not possess higher thermal gradient due to the absence of copper tubing. Hence, the magnetic volume force is not sufficient enough to drive the FF. The ΔT diminishes and becomes zero when the magnet is moved further away. Hence, hybrid devices are not suitable to cool systems when the magnet is placed away from the hot spot. However, for the copper-100 device, the cooling can be controlled by suitably placing the permanent magnet with respect to the heat load center.

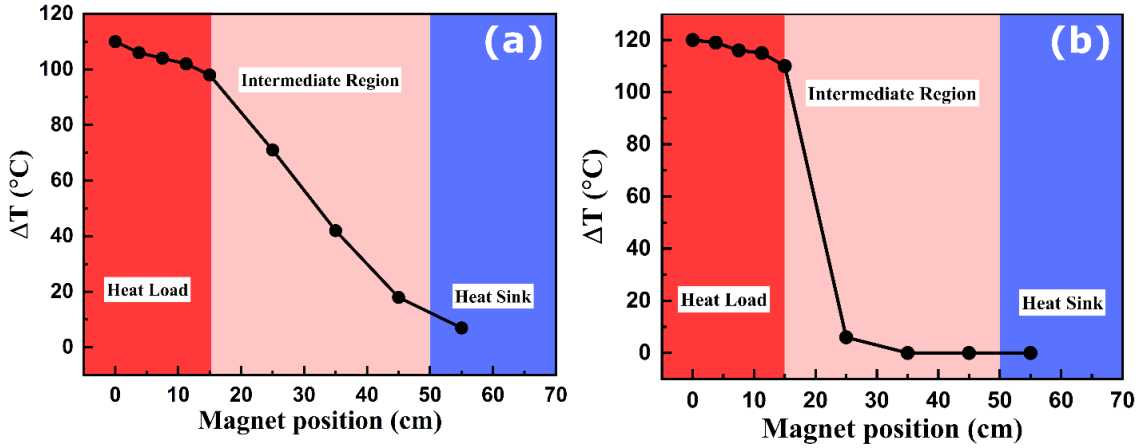

Figure 5.12. cooling magnitude as a function of magnet position along the perimeter of the racetrack(a) copper-100, and (b) hybrid-50 magnetic cooling device for a heat flux value (Q) and bare heat load temperature (T_0) of 3.47 kW/m^2 and 197°C, respectively.

5.4.5 Racetrack Copper Thermomagnetic Cooling Device

Racetrack copper based TM cooling devices have several advantages. Though the amount of cooling provided by copper-100 device was not the best (**Figure 5.8**, **Table 5.3**), they do offer a finite thermal gradient region throughout the magnetic cooling device (**Figure 5.12**(a)). Hence, cooling can be controlled by placing the magnet away from the heat load region, providing safe operation of magnetic field sensitive devices and systems such as CPUs and data servers.

5.4.6 Effect of heat flux value on cooling

The applied heat flux at the heat load of copper-100 MC device was varied over a range of 0.49-3.47 kW/m^2 to study the effect on cooling. **Figure 5.13**(a) shows the effect of heat flux variation on the heat load temperature profile without (red shaded area) and with (non-shaded area) the application of magnetic field. At higher heat flux values, the heat load temperature profiles revealed a sharp minimum immediately after the application of magnetic field. This decrease in temperature was rather gradual for low heat flux values. These observations manifest the strong dependence of magnetic cooling on the magnitude of thermal gradient. An improvement in thermal gradient with increasing heat flux value resulted in improved cooling (**Figure 5.13**(b)). As can be seen in **Figure 5.13**(b), the cooling increased almost linearly as a function of applied heat flux, demonstrating the self-

regulating nature of MC device. For a heat flux value of 3.47 kW/m^2, the estimated cooling using linear fit was slightly higher than the experimental results.

Figure 5.13(c) delineates the rate of change of heat load temperature as a function of time for various heat flux conditions. Initially, at t= 0 min, a sharp rise in the $\partial T/\partial t$ was observed. This positive rise is due to the heat load ON condition without a magnetic field. At t= 40 min, a sharp negative drop in $\partial T/\partial t$ was observed (dotted rectangular region) due to the application of the magnetic field. This point indicates the commencement of TMC. This negative drop at t=40 min is not as broad as the heating case. The inset shows the rate of change of heat load temperature and the time duration during which the heat load was cooled, and the temperature was significantly reduced. This indicates a shift in the minimum towards the left of the time axis (as indicated by the dotted curved arrow). The magnitude of the minimum increased for higher heat flux values. Cooling performance improved for higher heat load temperatures and heat flux values. The trough of $\partial T/\partial t$ also narrowed as the heat flux value increased. However, for 3.47 kW/m^2 heat flux, the trough broadened, and some kinks in the curve were observed. This may be due to the formation of air columns at a high heat load temperature of ~200°C. Nevertheless, the amount of cooling and the magnitude of $\partial T/\partial t$ was the highest for 3.47 kW/m^2 heat flux value.

The extent of cooling and the rate of cooling decreases and increases, respectively as a function of copper percentage in the hybrid magnetic cooling device. Cooling depends strongly on both the thermal gradient and the magnetic field gradient, whereas the cooling rate depends strongly on the thermal conductivity of the device. Hence, copper based magnetic cooling devices can be used in industrial and electronic systems which need faster cooling rate in the event of temperature spikes. In copper-based devices, the thermal gradient is non-zero far away from the heat load. Thus, the heat load can be cooled to a certain extent even by placing a magnet away from the heat load. This can be useful in waste heat management of magnetic field sensitive industrial, electronic, and household. systems such as gaming laptops, CPUs, and data servers. However, for other devices and systems that are not affected by magnetic fields such as solar panels, compressors, automobiles, high power LEDs and battery cabinets, hybrid MC device can be used.

From the results, although silicone tubes offer design flexibility, they are not as effective in cooling heat loads at a fast rate. On the other hand, copper tube-based devices are more thermally stable and have better mechanical properties. Copper tube-based MC device exhibited higher cooling than its silicone counterpart due to the superior thermal conductivity of copper.

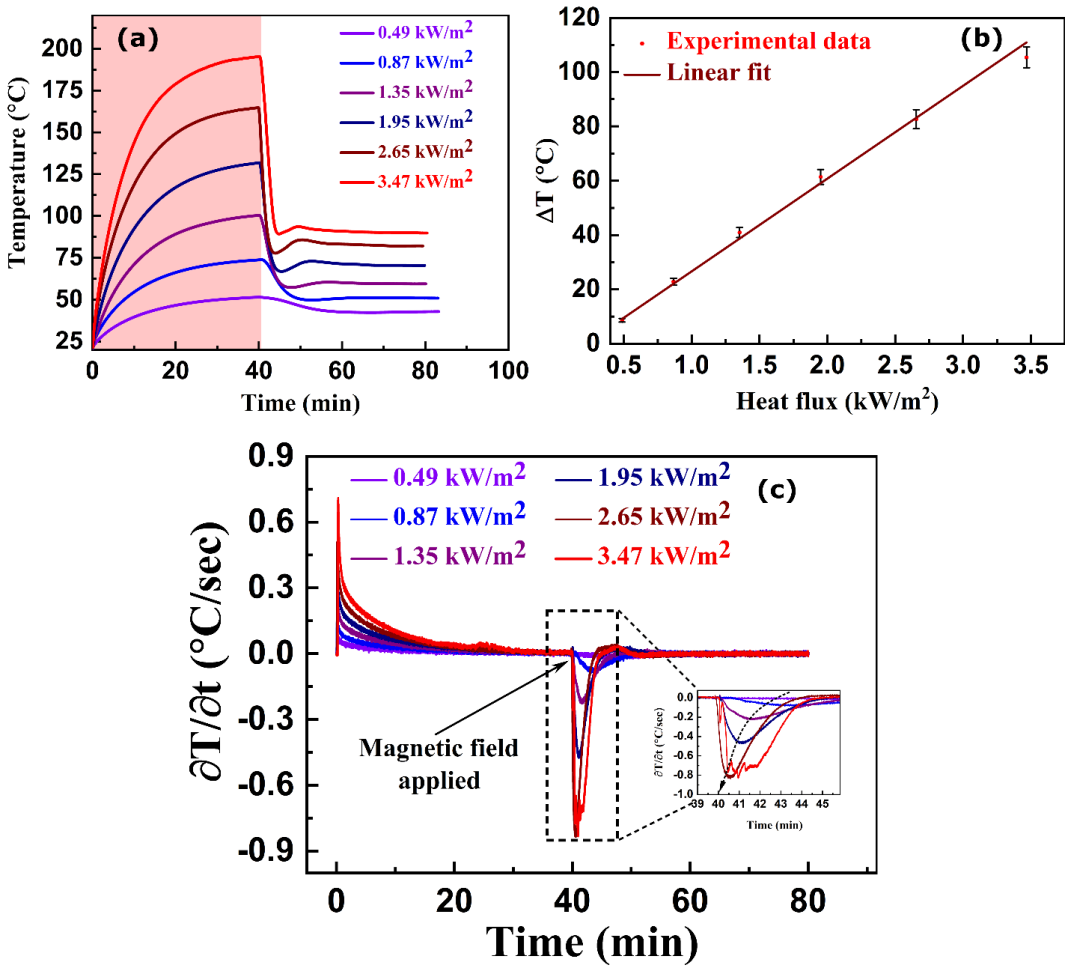

Figure 5.13. Effect of applied heat flux on (a) heat load temperature profile, (b) cooling magnitude, and (c) the rate of change of temperature of the heat load as a function of time for copper-100 magnetic cooling device. Inset in subfigure (c) shows the enlarged rate of change of temperature profile immediately after the application of the magnetic field.

5.5 Conclusions

Several magnetic cooling devices of circular and racetrack shapes were developed using copper, silicone, and copper-silicone hybrid tubing to examine the effect of device

properties and parameters on the thermomagnetic cooling performance of the heat load. The cooling performance was assessed using experiments and validated using 2D numerical simulations. We developed and investigated the cooling performance of racetrack shaped magnetic cooling device for the first time. The effect of copper tube percentage, and the heat load tube material in the hybrid magnetic cooling device on the cooling was investigated. The effect of varying magnet position and a range of heat flux values on the thermomagnetic cooling was examined using developed racetrack devices. The conclusions are:

- The study on the effect of device material revealed that the circular copper device exhibited a cooling by 113°C, whereas the circular silicone device provided a cooling by 83°C for a heat flux value of 3.47 kW/m^2 and a heat load temperature of 197°C.
- The hybrid-25 magnetic cooling device exhibited maximum temperarture drop of 123°C due to enhanced thermal gradient, resulting in higher ferrofluid velocity. The cooling tends to reduce with increasing copper percentage from 25% to 100%. However, the rate of cooling increased with increasing copper percentage. Hence, the amount of cooling depends strongly on the thermal gradient and the magnetic field gradient, whereas the cooling rate depends strongly on the thermal conductivity of the device.
- The effect of magnet position on the thermomagnetic cooling for all copper and hybrid-50 devices was evaluated. The all copper device exhibited cooling for all magnet positions along the device perimeter. However, the hybrid-50 device provided superior cooling when the magnet was placed near the heat load region and reduced to zero with increasing magnet distance from the heat load region.
- The increasing heat flux value for all copper device resulted in higher cooling, demonstrating self-regulation.
- The racetrack devices offer superior cooling with low footprint. Copper based racetrack device could be used to cool magnetic field sensitive devices and systems. Hybrid device, on the other hand, could be effective in cooling magnetic field insensitive devices and systems.

- The developed self-regulating, and passive racetrack shaped magnetic cooling device can be a solution for industrial and household cooling needs without consuming external energy, thereby increasing efficiency, service life and reliability.

References

[1] A.Shahsavar, M.Saghafian, M.R.Salimpour, and M.B.Shafiic, "Experimental investigation on laminar forced convective heat transfer of ferrofluid loaded with carbon nanotubes under constant and alternating magnetic fields," *Experimental Thermal and Fluid Science*, vol. 76, pp. 1-11, 2016.

[2] M. S. Pattanaik, V. Varma, S. Cheekati, G. Prasanna, N. Sudharsan, and R. V. Ramanujan, "A self-regulating multi-torus magneto-fluidic device for kilowatt level cooling," *Energy Conversion and Management*, vol. 198, p. 111819, 2019.

[3] L. J. Love, J. F. Jansen, T. McKnight, Y. Roh, and T. J. Phelps, "A Magnetocaloric Pump for Microfluidic Applications," *IEEE Transactions on Nanobioscience*, vol. 3, no. 2, pp. 101-110, 2004.

[4] S. Pal, A. Datta, S. Sen, A. Mukhopdhyay, K. Bandopadhyay, and R. Ganguly, "Characterization of a ferrofluid-based thermomagnetic pump for microfluidic applications," *Journal of Magnetism and Magnetic Materials*, vol. 323, no. 21, pp. 2701-2709, 2011.

[5] M. Ghasemian, Z. N. Ashrafi, M. Goharkhah, and M. Ashjaee, "Heat transfer characteristics of Fe3O4 ferrofluid flowing in a mini channel under constant and alternating magnetic fields," *Journal of Magnetism and Magnetic Materials*, vol. 381, pp. 158-167, 2015.

[6] A. Hatch, A. E. Kamholz, G. Holman, P. Yager, and K. F. Bohringer, "A ferrofluidic magnetic micropump," *Journal of Microelectromechanical systems*, vol. 10, no. 2, pp. 215-221, 2001.

[7] H. Yamaguchi and Y. Iwamoto, "Energy transport in cooling device by magnetic fluid," *Journal of Magnetism and Magnetic Materials*, vol. 431, pp. 229-236, 2017.

[8] W. Lian, Y. Xuan, and Q. Li, "Characterization of miniature automatic energy transport devices based on the thermomagnetic effect," *Energy Conversion and Management*, vol. 50, no. 1, pp. 35-42, 2009.

[9] H. Yamaguchi and T. Bessho, "Long distance heat transport device using temperature sensitive magnetic fluid," *Journal of Magnetism and Magnetic Materials*, vol. 499, p. 166248, 2020.

[10] M. Goharkhah, A. Salarian, M. Ashjaee, and M. Shahabadi, "Convective heat transfer characteristics of magnetite nanofluid under the influence of constant and alternating magnetic field," *Powder Technology*, vol. 274, pp. 258-267, 2015.

[11] M. Khairul, E. Doroodchi, R. Azizian, and B. Moghtaderi, "Thermal performance analysis of tunable magnetite nanofluids for an energy system," *Applied Thermal Engineering*, vol. 126, pp. 822-833, 2017.

[12] M. Asfer, B. Mehta, A. Kumar, S. Khandekar, and P. K. Panigrahi, "Effect of magnetic field on laminar convective heat transfer characteristics of ferrofluid flowing through a circular stainless steel tube," *International Journal of Heat and Fluid Flow*, vol. 59, pp. 74-86, 2016.

[13] V. Chaudhary, Z. Wang, A. Ray, I. Sridhar, and R. V. Ramanujan, "Self pumping magnetic cooling," *Journal of Physics D: Applied Physics*, vol. 50, no. 3, p. 03LT03, 2016.

[14] Y. Xuan and W. Lian, "Electronic cooling using an automatic energy transport device based on thermomagnetic effect," *Applied Thermal Engineering*, vol. 31, no. 8-9, pp. 1487-1494, 2011.

[15] V. Sharma, S. Pattanaik, H. Parmar, and R. V. Ramanujan, "Magnetocaloric properties and magnetic cooling performance of low-cost Fe 75− x Cr x Al 25 alloys," *MRS Communications*, vol. 8, no. 3, pp. 988-994, 2018.

[16] V. Chaudhary and R. V. Ramanujan, "Magnetocaloric properties of Fe-Ni-Cr nanoparticles for active cooling," *Scientific reports*, vol. 6, no. 1, pp. 1-9, 2016.

Chapter 6

Magnetic Cooling Device for Long Distance Heat Transfer by Thermomagnetic Convection of Ferrofluid

Effective removal of waste heat is a major challenge in a plethora of industrial and commercial systems and devices. Lower operating temperatures can reduce system failure and enhance the performance, reliability, and service life of such systems. The use of conventional heat pipes for waste heat removal is limited by the short distance of heat transfer and complex geometrical requirements. On the other hand, simple form factor magnetic cooling devices, based on ferrofluid thermomagnetic convection, can transfer heat over long distances. An 8 m long racetrack-shaped magnetic cooling device was developed for the first time, and its thermomagnetic cooling performance was studied. The extent of heat load cooling was examined over a wide range of heat flux values. This device transported heat from devices with heat flux values of up to 8.85 kW/m^2. The drop in temperature is up to 41°C for a heat load temperature of 197 °C. The local Nusselt number exhibited a maximum near the magnet, enhancing heat load cooling. The simulated velocity vectors and the temperature isotherms revealed vortex formation and disruption of the thermal boundary layer, leading to enhanced cooling. Thus, our device is a promising passive long-distance heat pipe.

6.1 Introduction

Many modern technological applications e.g., industrial systems, data servers, battery cabinets, and solar panels require long distance transport of waste heat. However, there are very few reports of heat transfer over long distance using FF based MC devices. Pattanaik et al. [1] developed a multi-torus MC device having an effective flow channel length and diameter of 1.8 m and 25 mm, respectively. Using an oil based Fe_3O_4 ferrofluid, they found a heat load temperature drop from initial temp 580°C to final temp.366°C at 1 kW heat load power. Khairul et al. [2] studied the TMC of a Fe_3O_4/water ferrofluid under laminar and turbulent flow conditions as a function of the external magnetic field. The channel length of this system was more than 3 m. The thermal performance was investigated by studying the effect of pumping power, friction factor, and exergy loss. Yamaguchi et al. [3] experimentally studied the performance of a 5 m long magnetic heat transfer system using a temperature-sensitive binary magnetic fluid. They reported heat transfer from a 35.8 W heat load using liquid-gas boiling two-phase flow for a horizontal orientation of the device. Recently they developed a 10 m long-distance thermal transport device based on liquid-gas two-phase boiling of a temperature-sensitive magnetic fluid [4].

Nomenclature

Abbreviations

MC	Magnetic cooling
MEMS	Micro-electromechanical systems
LOC	Lab-on-a-chip
MNP	Magnetic nanoparticles

Symbols

Thermal & fluidic parameters

T	Temperature
T_0	Heat load temperature without magnet
T_m	Heat load temperature with magnet
T_w	Inner tube wall temperature
T_f	Bulk ferrofluid temperature
$T_{f,in}$	Ferrofluid inlet temperature
h_y	Local convective heat transfer coefficient
P_{HL}	Power applied to the heat load
Q_{HL}	Heat flux at the heat load
Nu_L	Local value of Nusselt number
Nu_{avg}	Average value of Nusselt number

Magnetic parameters

H	Magnetic field
M	Magnetization
B	Magnetic flux density
M_S^{Bulk}	Bulk saturation magnetization of iron oxide
$\mathbf{M_s}$	Saturation magnetization
V_m	Magnetic scalar potential
$\mathbf{F_m}$	Magnetic volume force
μ_0	Permeability of the free space
χ_m	Ferrofluid magnetic susceptibility
χ_i	Initial magnetic susceptibility of the iron oxide nanoparticle

Other parameters

L_D	Device length
L	Distance between the heat load and the heat sink
d_i	Inner diameter of the tube
d_o	Outer diameter of the tube
L	Heat load arc length
D	Distance between the parallel flow branch

K	Thermal conductivity	V	Voltage
C_p	Specific heat	I	Current
v	Velocity	Γ	Langevin parameter
ρ	Density	**ℒ**	Langevin function
P	Pressure	N	Number of points across the heat load
M	Dynamic viscosity		
$\mathbb{C}_o$	Magnetic nanoparticle volume fraction		

The previous reports on long-distance heat transfer focused mainly on heat transfer below 100°C. Most of these studies focused only on experiments, with very few simulation and modeling investigations. The experiments used either (a) two-phase boiling heat transfer of a mixture of temperature-sensitive MF and a low boiling point organic liquid or (b) a miniature pump to maintain flow inside the flow channel. Some previous work used flow tubes with small cross-sectional area, limiting the heat transfer capability of the MC device. Moreover, the effect of waste heat flux and heat load temperature values on cooling were not investigated in detail.

Hence, the scope of this work is to study the cooling performance and thermal transport characteristics of a 8 m long racetrack MC device (**Figure 6.1**). The cooling performance was examined over a wide range of heat flux values. We used single-phase TM convective flow of an iron oxide-based FF below its boiling point. The cooling performance was also simulated using COMSOL Multiphysics. The local and average value of the Nusselt number at the heat load section was determined for a range of heat flux values. The simulated temperature contour plots of the FF at the heat load section were plotted at various time durations before and after applying an external magnetic field to elucidate the temperature distribution due to the TMC effect. We report for the first time an 8 m long race track geometry MC device based on single-phase ferrofluid flow, capable of cooling a heat load with heat flux values of up to 8.85 kW/m^2, and with a temperature drop of up to 41°C.

6.2 Experimental Methods

The experimental setup and the schematic of developed 8 m long racetrack MC device is shown in **Figure 6.1**. The details of the experimental setup is provided in section 3.3.4. The device dimensions are tabulated in **Table 3.8**. A commercial oil based Fe_3O_4 FF is used as the coolant fluid (section 3.2.2). The properties of the FF are given in **Table 3.2**.

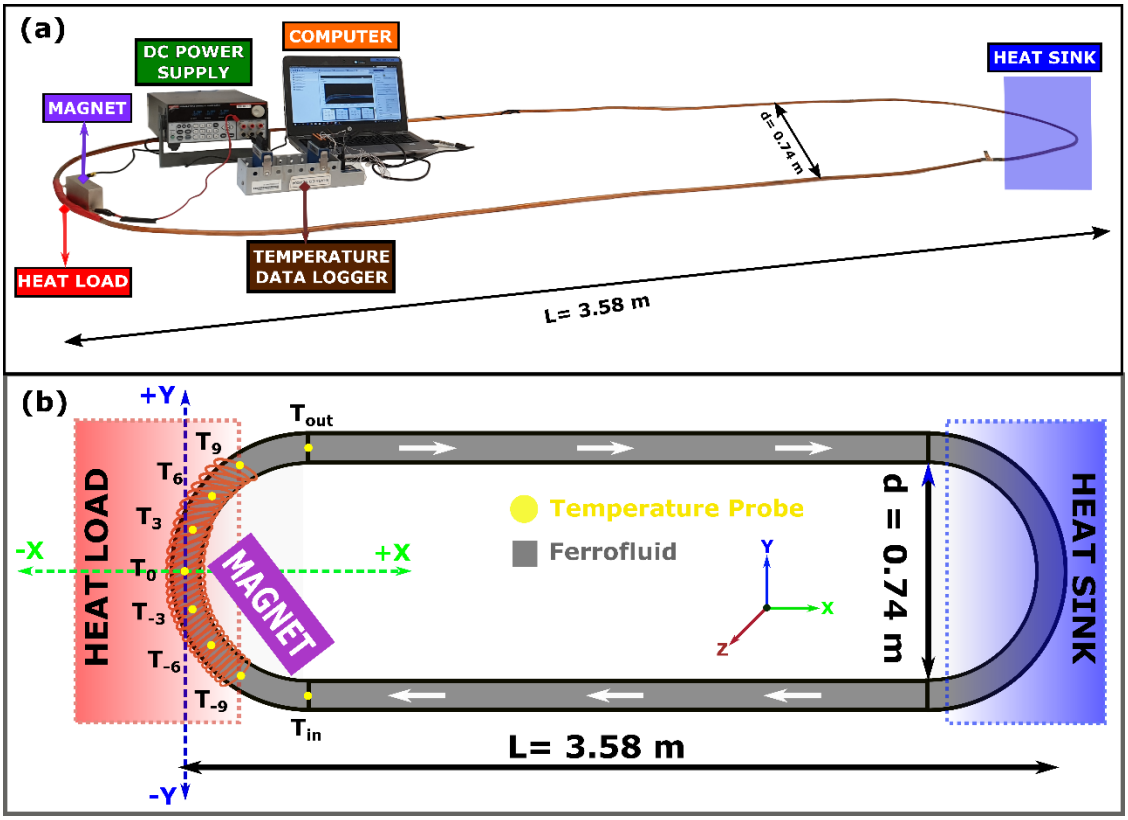

Figure 6.1. Racetrack shaped 8 m long magnetic cooling device, (a) experimental setup, and (b)schematic, XY-plane. The heat load is provided by resistive heating, simulating a source of waste heat. The magnetic field is applied by a NdFeB magnet, near the heat load region. T-type thermocouples were positioned along the heat load section, yellow dots in Figure 1(b). The origin (0,0,0) is taken at the center of the heat load. The probe positions are denoted by Ti, where i denotes the y-dimension in cm. White arrows represent the ferrofluid flow direction due to thermomagnetic convection.

6.2.1 Experimental Nusselt number determination

The local and average Nusselt number were determined to elucidate the nature of the convective heat transfer arising from FF TMC. The local and average Nusselt number was obtained by seven T-type thermocouples connected along the wall of the heat load region (**Figure 6.1**(b)). The thermocouples were denoted by T_i, where i denotes the y-position of the temperature probe (in cm) with respect to the origin. Two T-type thermocouples were connected just before (T_{in}) and after (T_{out}) the heat load region to monitor the inlet and outlet temperatures of the ferrofluid.

6.2.2 Experimental parameters

The effect of heat flux at the heat load, over a range of 1.87 kW/m^2-8.85 kW/m^2, on the temperature profile of the heat load and the local and average Nusselt number was studied. **Table 6.1** summarizes the parameters, their units, notation, and experimental sets considered in this work.

Table 6.1. Parameters, their notation, range, and the measurement sets.

Parameters	Unit	Notation	Performed Sets
Heat flux at the heat load	kW/m^2	Q_{HL}	1.87-8.85
Heat load temperature without magnet	°C	T_0	67 to 197
Heat load temperature with magnet	°C	T_m	64 to 156

6.3 Modelling Methods

The details of the developed 2D numerical model, governing equations, and the boundary conditions to simulate the thermomagnetic convection effect are detailed in section 3.4. The formulae to calculate the Nusselt number, numerical verification, and validation of the long magnetic cooling device are discussed in the following subsections.

6.3.1 Nusselt number calculation

The value of local convective heat transfer coefficient along the flow direction (h_y) was obtained using the following formula [2],

$$h_y = \frac{Q_{HL}}{(T_w(y) - T_f(y))_y} \qquad (6.1)$$

where Q_{HL} is the heat flux value applied at the heat load. $T_w(y)$ and $T_f(y)$ are the inner wall temperature of the copper tube and the bulk ferrofluid temperature for a specific y position, respectively. The heat flux can be calculated from the applied power (P_{HL}), which is the product of the current (I) and voltage (V), divided by the area of the heat load region,

$$Q_{HL} = \frac{P_{HL}}{l d_i \pi} = \frac{VI}{l d_i \pi} \qquad (6.2)$$

l and d_i are the length of the heat load region and the flow tube inner diameter, respectively. The local bulk FF temperature is in equation (6.3),

$$T_f(y) = \frac{Q_{HL}\pi d_i}{\rho A v C_p} y + T_{f,in} \quad (6.3)$$

In equation (6.3), ρ and Cp denote the density and specific heat of the FF, respectively. A and v represent the flow tube cross-sectional area and the velocity of the FF, respectively. $T_{f,in}$ denotes the bulk inlet temperature of the FF.

The local (Nu_L) and average value (Nu_{avg}) of Nusselt number was calculated using equation (6.4) and equation (6.5), respectively.

$$Nu_L(y) = \frac{h_y d_i}{\kappa_f} \quad (6.4)$$

$$Nu_{avg} = \sum_{i=1}^{n} \frac{Nu_L(y)}{n} \quad (6.5)$$

Where, n represents the number of points across the heat load region at which the local Nusselt number was calculated.

6.3.2 Numerical verification and mesh independency test

For numerical verification of the developed 2D model, mesh independence test was carried out using 2D triangular mesh elements. The non-dimensional FF average velocity (**v/v_{max}**) for a heat flux value of 4.07 kW/m^2 at the heat load region was plotted as a function of the number of mesh elements (**Figure 6.2**). The velocity converged with 7% absolute error for 579538 mesh elements (black arrow in **Figure 6.2**) with respect to the highest number of mesh elements. A total of 579538 mesh elements were considered in the final model (**Table 6.2**). The entire geometry of the long magnetic cooling device was divided into small discrete regions using triangular mesh elements. **Table 6.2** gives the corresponding number of mesh elements and their average quality.

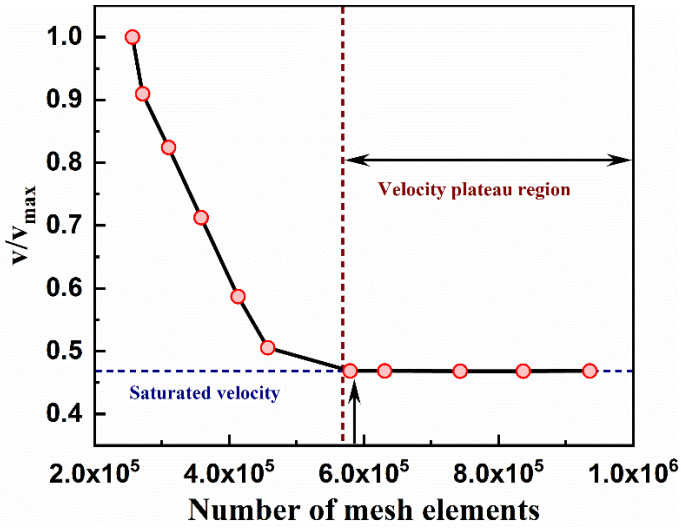

Figure 6.2. Simulated values of non-dimensional velocity of the ferrofluid as a function of the number of mesh elements. The black arrow at the bottom shows the number of mesh elements considered for the simulation.

Table 6.2. Mesh details for the simulation of 8 m long magnetic cooling device.

Object	Mesh element	Number of mesh elements	Average quality of the mesh
Magnet	Triangular	1362	0.852
Fluid domain	Triangular	190042	0.9006
Tube wall	Triangular	46997	0.7761
Air domain	Triangular	341137	0.8554
Entire device	Triangular	579538	0.8636

6.3.3 Numerical validation

The developed 2D model for the FF TM heat transfer in the 8 m long MC device was numerically validated by comparing the simulated magnetic field distribution (**Figure 6.3**) and heat load temperature profile (**Figure 6.5**) results with experimental findings. The simulated value of the surface magnetic field of the NdFeB magnet along its length and

width is in agreement with the experimental value with a maximum absolute error of 6.2%. The simulated heat load temperature profile for a heat flux value of 8.85 kW/m^2 is also accordance with the experimental results.

6.4 Results and Discussion

6.4.1 Magnetic field distribution

Error! Reference source not found. shows the distribution of the magnetic field along the l ength and width of the NdFeB permanent magnet. The pink curves represent the simulated value of the magnetic field distribution. The experimental and simulated results are in good agreement with a maximum absolute error percentage of 6.2%.

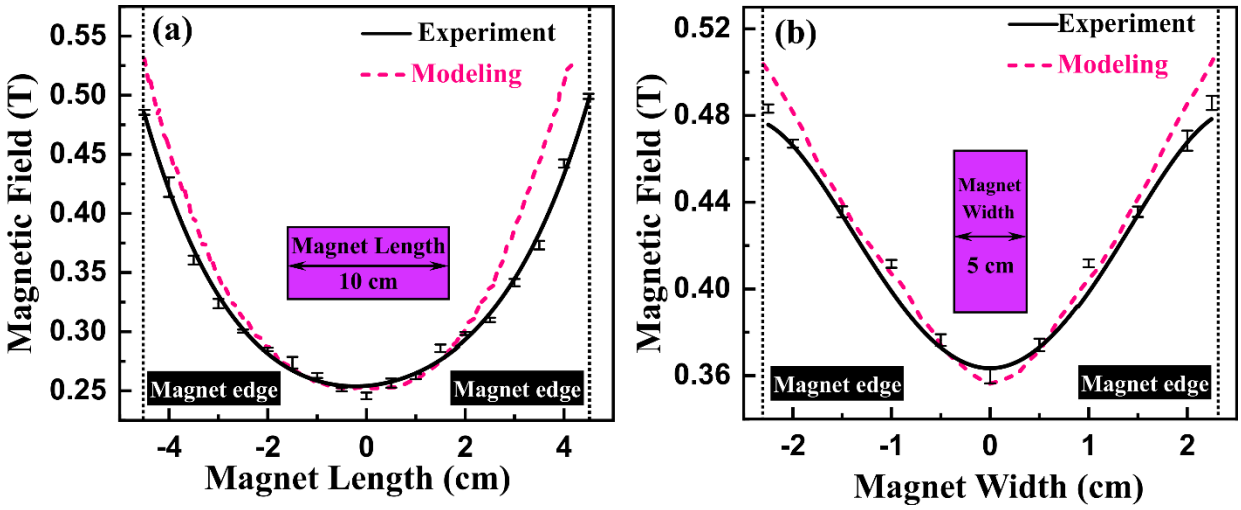

Figure 6.3. Surface magnetic field distribution of the NdFeB permanent magnet (a) along its length, and (b) width. The pink dotted curve represents the simulated magnetic field distribution.

6.4.2 Simulated heat load cooling as a function of device perimeter

Small passive magnetic cooling devices have been previously investigated [5, 6]. However, there is an urgent need for magnetic cooling devices with heat transport capability over longer distance. Hence, we investigated the effect of device perimeter over a wide range, on the heat load cooling performance using our developed simulation model. In the simulation model, other factors such as heat load arc length, heat load temperature, applied magnetic field strength and its distribution, and other initial conditions were kept the same as the developed 8 m long magnetic cooling device.

The device perimeter was varied over a substantial range of 1 m to 20 m. **Figure 6.4** shows the variation of heat load cooling magnitude (ΔT) as a function of the device perimeter. As expected, the heat load cooling decreased with increasing device perimeter. Interestingly, ΔT tends to saturate at higher device perimeter. This result suggests that a local cooling effect near the heat load persists. This observation can be attributed to the formation of ferrofluid vortices (**section 6.4.6**). Hence, ferrofluid mixing also contributes to cooling, apart from the bulk motion of the ferrofluid. At a device perimeter as large as 20 m, we predict a heat load cooling by 17°C. The above result suggests that our device is capable of transporting heat over longer distance without the aid of any external pumping power. Hence, such longer passive magnetic cooling devices can be the potential solution to transfer waste heat from air conditioner compressors, energy storage systems, heat exchangers, and electric vehicle battery cooling etc.

For this work, we carried out all the experimental studies for an 8 m device perimeter. That was the maximum available lab space for us to design this racetrack device. The dotted lines parallel to the x- and the y-axis in **Figure 6.6** represent the experimental case of 8 m device perimeter.

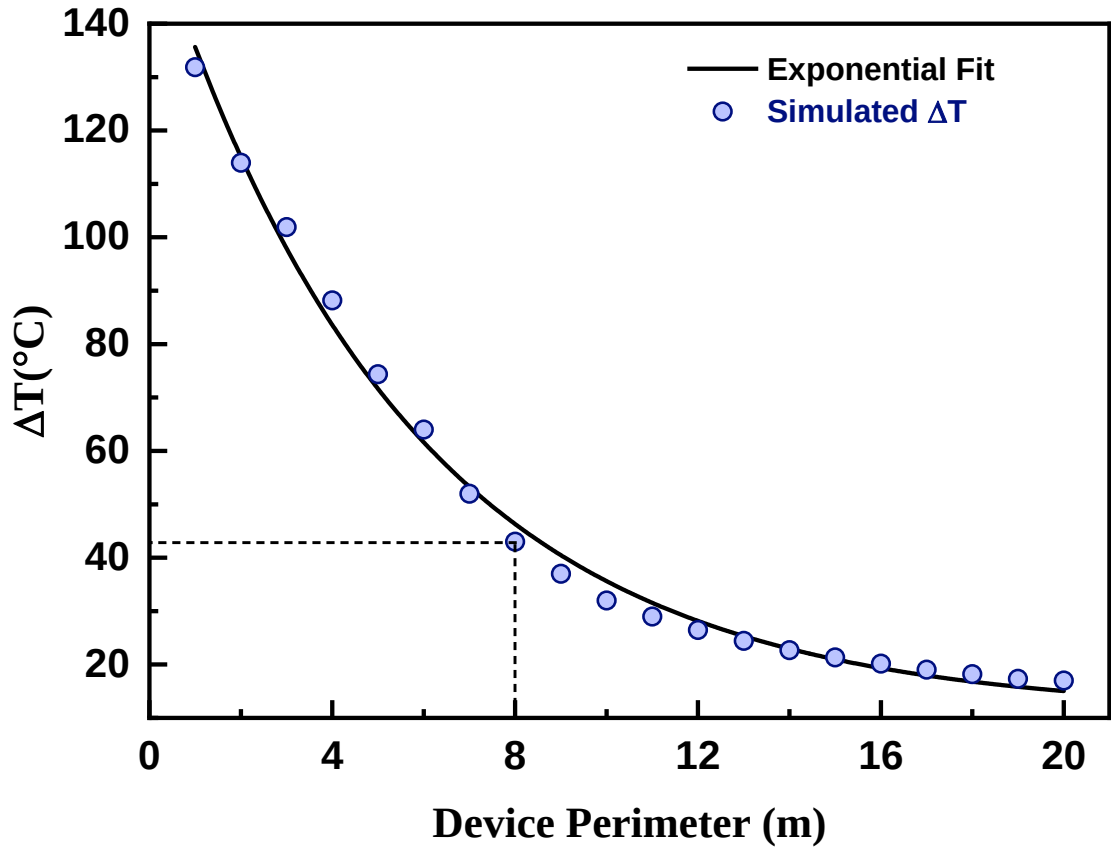

Figure 6.4. Simulated heat load cooling versus total perimeter of the magnetic cooling device for a fixed heat load temperature, heat load arc length, and magnetic field strength of 197°C, 18 cm, and 0.41 T, respectively.

6.4.3 Heat load temperature and the heat load cooling as a function of heat flux

The effect of the applied heat flux on the heat load cooling performance was studied. In our previous work, we showed that placing the magnet close to the middle portion of the heat load section results in maximum heat load cooling [1]. Hence, for all the experimental sets, the magnet was placed asymmetrically from the middle of the heat load section and 2 mm away from the copper tube, as shown in **Figure 6.1(b)**.

Figure 6.5 shows the heat load temperature profile versus time without and with an external magnetic field at a heat flux value of 8.85 kW/m^2. Initially, without the magnetic field, the heat load temperature reached a saturation value of 197°C (temperature T_0 in the red shaded area). At 30 min, a permanent magnet with a surface magnetic field strength of 0.41 T was placed near the heat load. An immediate drop in heat load temperature was

observed. The heat load temperature reached a minimum steady state temperature of 156°C in the presence of the magnet (temperature T_m in the blue shaded area). Thus, at a heat flux value of 8.85 kW/m^2, the heat load was cooled by 41°C by TMC. This heat load cooling was simulated using our 2D numerical model and plotted as the red dotted curve in **Figure 6.5**. The total simulation time was taken as 60 min, the same as that of the experiment. A simulation time step of 1 s was taken. The simulated heat load temperature profile was in agreement with the experimental results with a maximum error of 8.9%. The final heat load cooling obtained from the simulated temperature profile was 42.3°C.

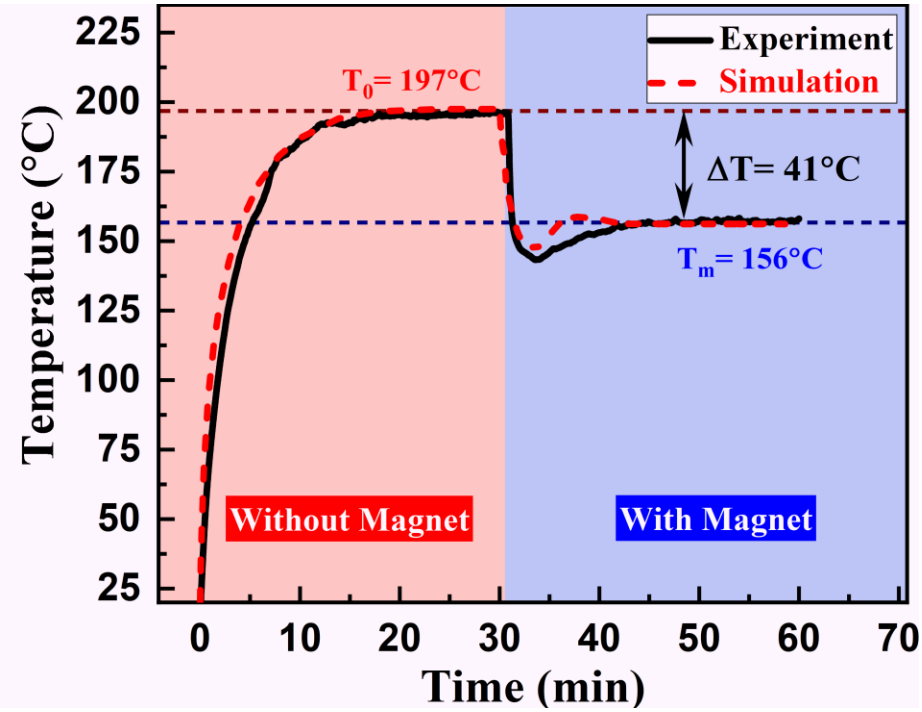

Figure 6.5. Heat load temperature versus time curve without and with the application of an external magnetic field for a heat flux value of 8.85 kW/m^2.

Figure 6.6 represents the heat load cooling (ΔT) as a function of the heat flux (Q_{HL}) and the heat load temperature without the magnetic field, T_0. The heat load cooling increases almost linearly as a function of heat flux. Even for low applied heat flux of 1.86 kW/m^2, a small value of ΔT was obtained. Therefore, this long MC device is capable of transferring waste heat over a significant range of heat flux values. The present device is also self-regulating and self-pumping. The increase in heat load cooling with increasing heat flux is due to temperature-dependent FF magnetization. The magnetization of the FF column at

the heat load section is low due to the higher heat load temperature. The FF adjacent to the heat load region has higher magnetization due to its lower temperature. This difference in the magnetization values of the FF is higher for larger heat flux values, since higher heat flux results in larger initial heat load temperatures. The higher difference in magnetization values creates a greater non-uniform magnetic volume force. This magnetic volume force drives the FF along the flow tube with higher velocity, resulting in improved cooling.

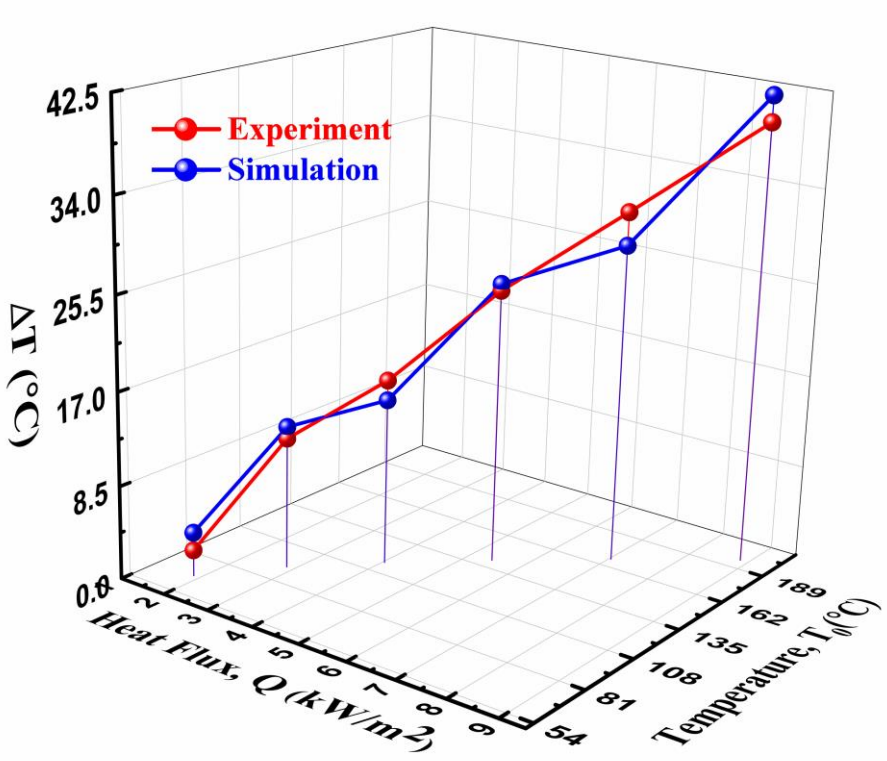

Figure 6.6. Experimental and simulated heat load cooling as a function of heat flux and the initial heat load temperature.

The heat load cooling values obtained from the simulations (red curve) at various heat flux values are in excellent agreement with the experimental findings (blue curve). The rate of change of temperature of the heat load ($\partial T/\partial t$) immediately after application of the magnetic field was due to the sudden inflow of colder FF due to TM effect (**Figure 6.7**). This rate follows an exponential growth (fitting of **Figure 6.7** as per the equation in **Table 6.3**) as a function of increasing applied heat flux value. This exponential rise in the value of $\partial T/\partial t$ also manifests as a faster rate of heat transfer, hence, higher ΔT is observed with

increasing value of heat flux. The value of constants and fitting parameters for the fitting curve in **Figure 6.7** is provided in **Table 6.3**.

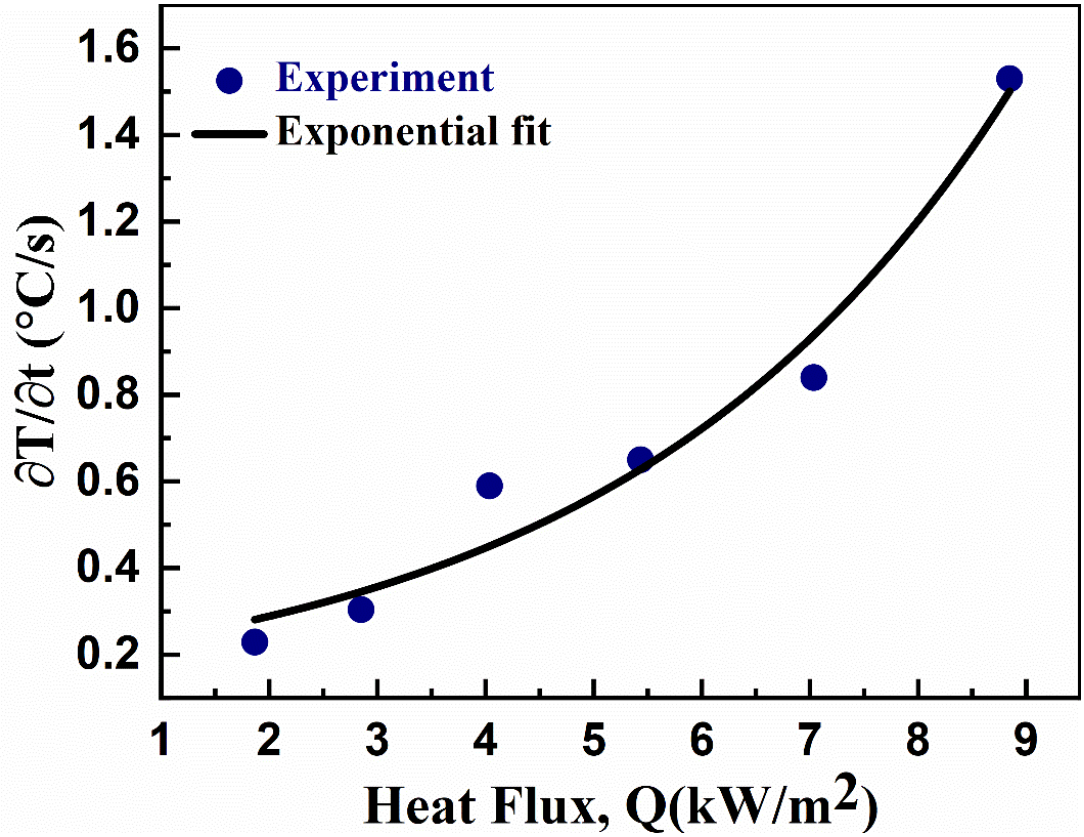

Figure 6.7. Initial rate of change of temperature immediately after the application of an external magnetic field (t= 30 min., Error! Reference source not found.) as a function of the applied heat f lux value. The solid curve represents the exponential growth fitting to the observed trend.

Table 6.3. Fitting parameters for the fit of the rate of change of temperature as a function of applied heat flux (Figure 6.7).

Fitting details	Particulars
Fitting type	Exponential growth
Equation	$y = y_0 + ae^{(x/t)}$
y_0	0.076 ± 0.26
A	0.12 ± 0.14
T	3.59 ± 1.53
Reduced χ-square	0.011
Adjacent R-square	0.95

6.4.4 Local and average Nusselt number as a function of applied heat flux

The nature of heat transfer at the heat load region was investigated by calculating the average value (Nu_{avg}) and the local value (Nu_L) of the Nusselt number. The average value of the Nusselt number at the heat load section was plotted as a function of applied heat flux under the effect of an external magnetic field (**Figure 6.8**). The average Nusselt number increases for larger heat flux values, implying better convective heat transfer from the heat load region by TMC of the ferrofluid. This observation is also consistent with the increase in the magnitude of cooling (ΔT) of the heat load for larger heat flux values. The average Nusselt number is less than 10 for heat flux values below 7 kW/m^2, suggesting the ferrofluid flow is laminar. However, for heat flux values above 7 kW/m^2, the FF flow can be thought of as a transition flow between the laminar and turbulent flow regime. The red curve in **Figure 6.8** is a non-linear cubic polynomial fitting curve for the average value of the Nusselt number.

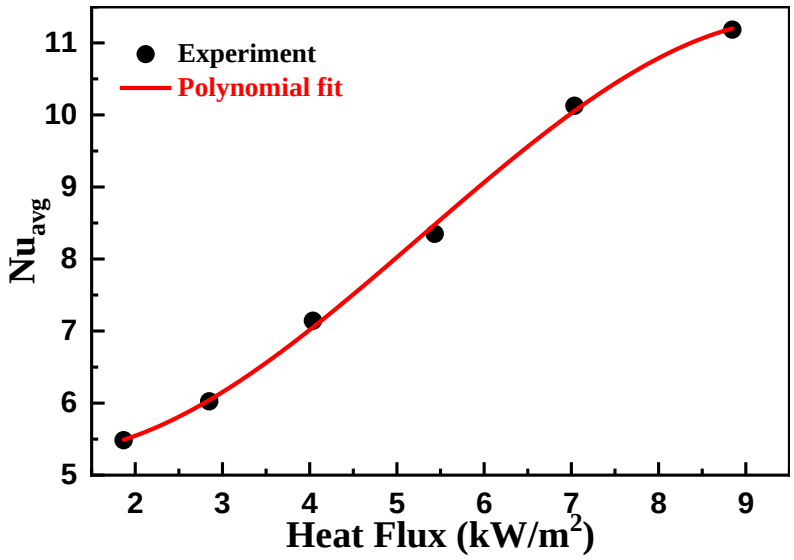

Figure 6.8. Average Nusselt number of the ferrofluid as a function of applied heat flux at the heat load. Solid red curve is the non-linear polynomial fitting of the average Nusselt number.

Figure 6.9 is a plot of local Nusselt number of the FF along the axial flow direction (y-direction) at the heat load section for a range of applied heat flux values, under an applied magnetic field. Significant peaks, as shown by the black dotted ellipse, of the local Nusselt number values were observed around the axial position of y= 3 cm (T_3 sensor) for all heat flux values. For a given heat flux value, Nu_L increased by almost 20% in comparison to the

value at y= 0 cm due to the presence of the permanent magnet at that position. This effect can be attributed to the enhancement in convection due to the TM effect of the FF in the presence of an external magnetic field. The peaks are sharper for higher heat flux values compared to lower heat flux values, indicating a stronger TM effect in the larger thermal gradient and stronger magnetic field gradient region [1].

The sudden increase in convective heat transfer near the stronger magnetic field region may be attributed to chain formation due to agglomeration of magnetite nanoparticles in the direction of the applied magnetic field [7]. These chains may offer lower thermal resistance for heat transfer and enhance local convective heat transfer by its interaction with the bulk motion of the FF. The interactions between the nanoparticle chains and the fluid flow can be thought of as a local perturbation which increases heat transfer along the flow tube from the heat load region to the heat sink region [8]. After y= 3 cm, the local Nusselt number again reduced and reached saturation as it entered the fully developed flow region. It can be inferred from **Figure 6.8** and **Figure 6.9** that the increase in both local and average Nusselt number with increasing heat flux is responsible for the self-regulating nature of the long MC device.

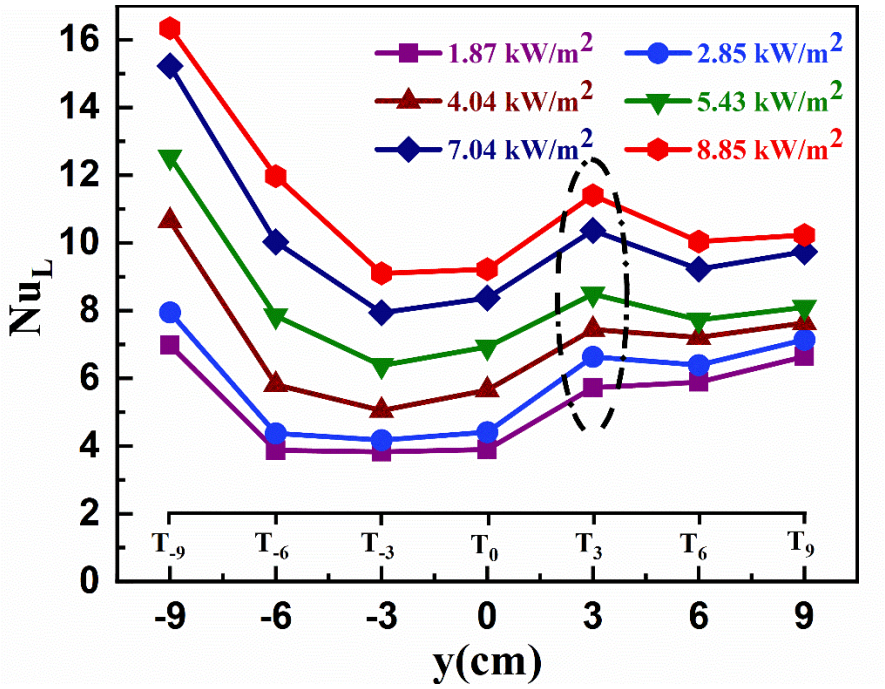

Figure 6.9. Local Nusselt number of the ferrofluid at various heat flux values as a function of axial position of the heat load region along the flow direction of the ferrofluid. y= 0 cm is the center of

the heat load region. The dashed ellipse represents the stronger magnetic field region. T_i (9 cm ≥ i ≥ -9 cm) shows the position of the T-type thermocouples along the copper tube wall(**Figure 6.1**(b)).

6.4.5 Simulated isothermal temperature contour plots

Contours of temperature isotherms were plotted at various time durations after the application of an external magnetic field at an applied heat flux value of 8.85 kW/m^2 (**Figure 6.10**). At t= 0 s, the temperature distribution was symmetric with respect to the heat load center. Therefore, the temperature isotherms are nearly parallel to each other on either side of the middle of the heat load section. However, after applying the magnetic field, the FF started to flow due to the TMC effect, hence the isothermal contours started to develop along the flow direction (for t≠ 0 *s*). At t= 2 s, a blue isothermal contour loop started to grow along with a small green contour just to its left, which further increased in size for higher time of magnetic field application (zone 1). The blue contour represents the lower FF temperature region (20-100°C), the green contour represents the intermediate temperature region (110-130°C). The difference in the temperature distribution of these two isothermal contours is due to the gradient in the magnetic field strength experienced by the FF in those regions.

From t=2-10 s, the other end of the heat load exhibited similar temperature isotherm profiles (zone 3). However, the flow started to develop gradually as the parallel isotherms became more and more parabolic along the ferrofluid flow direction. After a duration of magnetic field application of ~1800 s, the ferrofluid flow was fully developed at the end of the heat load region (zone 3). Surprisingly, fewer isothermal contours were observed in zone 2 which can be due to the combined effect of stronger thermal and magnetic field regions (**Figure 6.10**), resulting in significant distortion of the thermal boundary layer. After 1800 s of magnetic field application, the temperature at the heat load was reduced by ~ 40°C, which can be inferred by comparing the temperature color scale bar at t= 0 s.

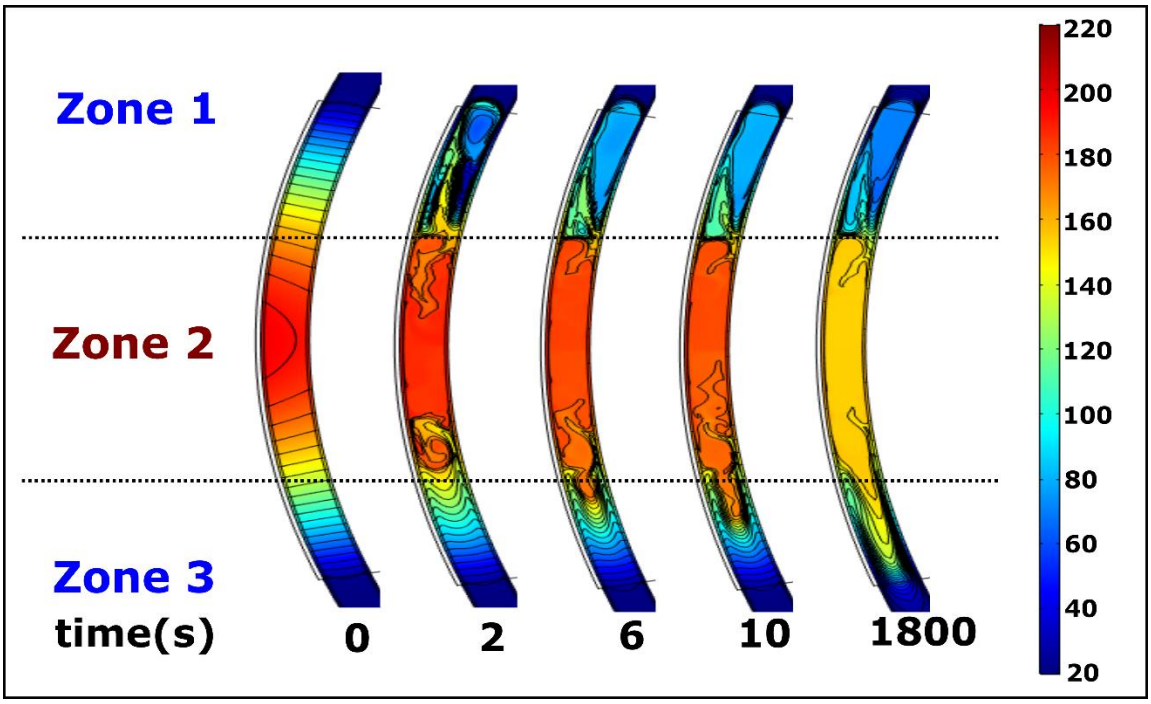

Figure 6.10. Simulation results showing the time dependence of (from 0 s to 1800 s) isothermal temperature contours and surface temperature profiles at an applied magnetic field of 0.4 T and heat flux value of 8.85 kW/m^2. The colored scale bar shows the temperature with values in degrees Celsius. Different zones represent different thermal energy, magnetic energy and ferrofluid magnetization states.

The thermal boundary layer was distorted at some regions of the heat load section due to the FF TM effect and the formation of FF vortices under the applied magnetic field, as can be seen from **Figure 6.10** and **Figure 6.11(a)**. The temperature gradient along the tube diameter at zone 1 and zone 2 increased with time duration of magnetic field application (from t=2 to 1800 s), as can be inferred from the densely packed isothermal contours along the tube wall (**Figure 6.10**). However, the temperature gradient increased at zone 3 compared to zone 1 and 2 due to differences in the strength of the magnetic field, the thermal gradient and the gradient in the FF magnetization in a given zone (**Table 6.4**).

6.4.6 Simulated velocity vector and ferrofluid velocity profile

Simulated 2D FF velocity vectors were plotted at the heat load section (**Figure 6.11(a)**) to investigate the effect of a magnetic field and thermal gradient on the FF flow. To understand the TMC of the FF, the heat load section was subdivided into three zones along the mean FF flow direction. Zone 1 refers to the inlet zone of the colder FF to the heat load.

Two counter-orienting FF vortices were formed in this zone, as shown in the enlarged section of zone 1. The orientation of the larger vortex in the blue temperature region was clockwise. The orientation of the smaller vortex in the green temperature region just above the blue region was counterclockwise. The size of the vortices strongly depends on the strength of the magnetic field at these regions.

Zone 2 is the middle of the heat load region. The temperature is maximum in this zone. The FF is in a minimum magnetization state. Due to the higher temperature at zone 2, the velocity vectors are randomly oriented. The random orientation of the velocity vectors is a result of strong domination of the thermal energy over magnetic energy. The vortices were less distinct than zone 1 due to the lower magnetization of the FF compared to zone 1.

Zone 3 represents the final portion of the heat load section. As can be seen in the enlarged image of zone 3, the temperature of the FF was higher due to the inflow of hot FF from the middle portion (zone 2) of the heat load section, hence the FF was in a lower magnetization state. Since it is further away from the magnetic field region compared to zones 1 and zone 2, small weak vortices were observed and later entered a fully developed flow region. **Table 6.4** summarizes the three zones with their temperature, magnetic field strength, and magnetization states. The FF formed vortices throughout the heat load section because of the external magnetic field. The formation of the FF vortices can be attributed to the simultaneous effect of the magnetic field gradient and temperature gradient [1]. Importantly, vortex formation results in effective intermixing of the hotter and colder ferrofluid.

The simulated velocity profile of the FF was plotted as a function of applied heat flux values in the middle of the heat load region, as shown in **Figure 6.11(b)**. The velocity profile does not exhibit the characteristics of a fully developed flow. The velocity profile, for any given heat flux value, has two distinct maxima near the edge of the flow tube. Moreover, the velocity maximum at x= 1 mm is higher than the maximum value at x= 6.5 mm. This is due to the placement of the permanent magnet close to the inner tube surface (x= 0 mm) and the higher magnetization state of the FF close to the inner tube surface.

The velocity maxima can be attributed to the formation of the FF vortices at the heat load region. **Figure 6.12** represents the temporal variation of the temperature and the velocity

vector field of the FF before and after application of an external magnetic field. At t=0 s, due to the absence of a magnetic field, the FF velocity was zero. The mode of heat transfer was conduction both across and along the flow tube through the copper tube and FF. Vortices were developed immediately after application of the magnetic field. With time, the vortices traversed along the heat load section, hence the FF and the heat load temperature continued to decrease. After 30 minutes of magnetic field application, the heat load was cooled by 41°C, which resulted in significantly lower temperature in the middle of the heat load section (change in color from red to yellow).

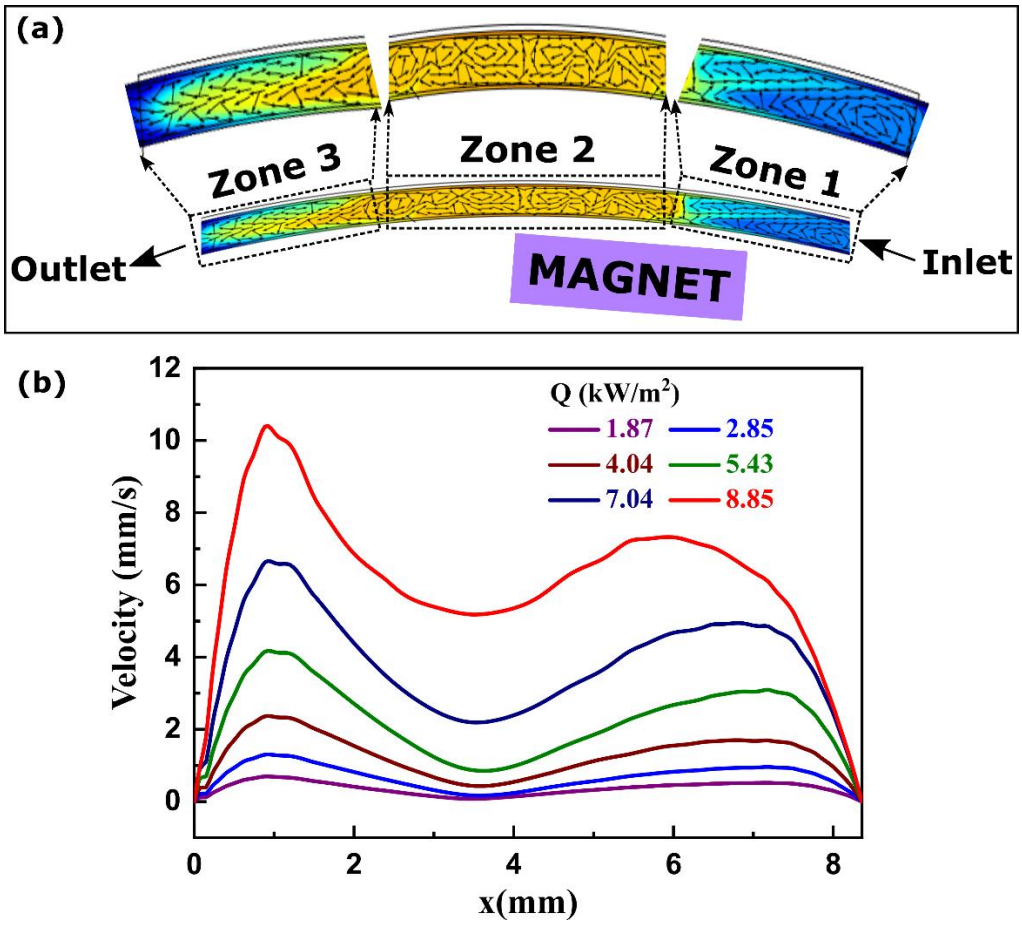

Figure 6.11. Simulated (a) velocity vectors with the background as the temperature distribution at the heat load section, and (b) velocity profile of the ferrofluid as a function of the heat flux in the middle of the heat load region across the tube diameter. The zones show different magnetization states and velocity of the ferrofluid along the heat load section.

Table 6.4. Summary of the temperature, magnetic field, magnetization, and vortex state of the ferrofluid at different zones of the heat load section.

Heat load zones	Temperature	Magnetic field	Magnetization state	Vortex strength
Zone 1	Colder	Stronger	Higher	Strong
Zone 2	Hotter	Stronger	Lower	Weak
Zone 3	Hotter	Weaker	Lower	Weak

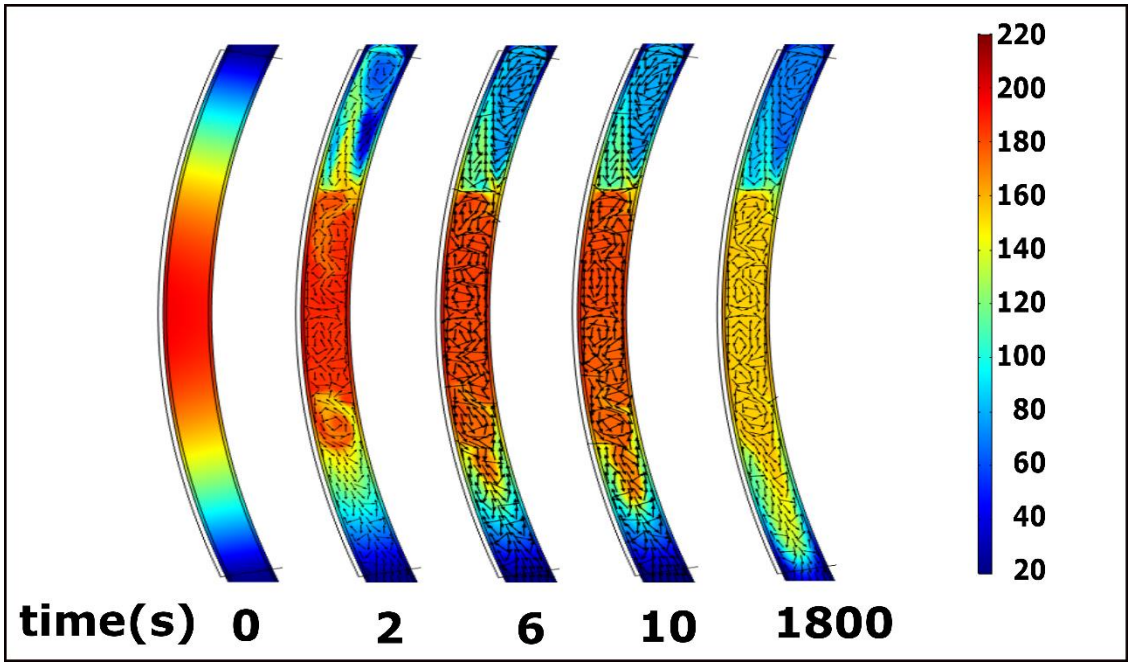

Figure 6.12. Simulation results showing both transient and steady state behavior (from 0 s to 1800 s) temperature surface profiles and velocity vector plots before and after applying an external magnetic field of 0.4 T and heat flux value of 8.85 kW/m^2. The colored scale bar shows the temperature scale with their values in degree Celsius.

6.5 Conclusions

A racetrack-shaped 8 m long magnetic cooling device, based on the principle of thermomagnetic convection of a ferrofluid, was developed. Our device is the longest magnetic cooling heat pipe developed and tested so far, which utilizes a single-phase flow of ferrofluid to cool the heat load over a wide range of heat flux values. The device performance was tested for its ability to remove waste heat from a heat load over a range of heat flux values. The device was self-pumping, no pump was used to drive the ferrofluid

along the tube. Heat load cooling by 41°C was obtained for heat flux and heat load temperature value of 8.85 kW/m^2 and 197°C, respectively. The simulated multi-physics results were in good agreement with the experimental values. The average Nusselt number increases with an increase in heat flux value, consistent with the self-regulating nature of the device. The local Nusselt number exhibited a maximum near the strong magnetic field strength region, indicating better heat transfer. The surface temperature contours showed the effect of thermal boundary layer disruption on enhanced cooling performance. The surface velocity vector plots revealed the formation of ferrofluid vortices, which increase mixing of hotter and colder ferrofluid, leading to thermal boundary disruption. Our magnetic cooling device can operate over a wide range of heat load temperatures and heat flux values and is a better candidate for passive long-range thermal transport compared to conventional heat pipes used in industry.

References

[1] M. S. Pattanaik, V. Varma, S. Cheekati, G. Prasanna, N. Sudharsan, and R. V. Ramanujan, "A self-regulating multi-torus magneto-fluidic device for kilowatt level cooling," *Energy Conversion and Management*, vol. 198, p. 111819, 2019.

[2] M. A. Khairul, E. Doroodchi, R. Azizian, and B. Moghtaderi, "Thermal performance analysis of tunable magnetite nanofluids for an energy system," *Applied Thermal Engineering*, vol. 126, pp. 822-833, 2017.

[3] H. Yamaguchi and Y. Iwamoto, "Energy transport in cooling device by magnetic fluid," *Journal of Magnetism and Magnetic Materials*, vol. 431, pp. 229-236, 2017.

[4] H. Yamaguchi and T. Bessho, "Long distance heat transport device using temperature sensitive magnetic fluid," *Journal of Magnetism and Magnetic Materials*, vol. 499, p. 166248, 2020.

[5] V. Chaudhary, Z. Wang, A. Ray, I. Sridhar, and R. V. Ramanujan, "Self pumping magnetic cooling," *Journal of Physics D: Applied Physics*, vol. 50, no. 3, p. 03LT03, 2016.

[6] V. Varma, M. Pattanaik, S. Cheekati, and R. Ramanujan, "Superior cooling performance of a single channel hybrid magnetofluidic cooling device," *Energy Conversion and Management*, vol. 223, p. 113465, 2020.

[7] A.Shahsavar, M.Saghafian, M.R.Salimpour, and M.B.Shafiic, "Experimental investigation on laminar forced convective heat transfer of ferrofluid loaded with carbon nanotubes under constant and alternating magnetic fields," *Experimental Thermal and Fluid Science*, vol. 76, pp. 1-11, 2016.

[8] M. Khairul, E. Doroodchi, R. Azizian, and B. Moghtaderi, "Thermal performance analysis of tunable magnetite nanofluids for an energy system," *Applied Thermal Engineering*, vol. 126, pp. 822-833, 2017.

Chapter 7

Performance Metrics and Ranking of Ferrofluids for Magnetic Cooling

The performance metrics, non-dimensional parameters, and heat load cooling were calculated to analyze the thermomagnetic cooling performance of various ferrite and metallic based ferrofluids. The resultant magnetic pressure, friction factor, power transferred, and the exergy loss were derived as a function of magnetic and thermophysical parameters to predict the performance of ferrofluid based magnetic cooling devices. Numerical simulations were performed to investigate the effect of magnetic properties of the nanoparticles viz., bulk saturation magnetization, Curie temperature, pyro magnetic coefficient, and initial magnetic susceptibility on the cooling performance. Ferrite ferrofluids prepared from γ-Fe_2O_3, Fe_3O_4, and $CoFe_2O_4$ exhibited superior cooling. For metallic/alloy-based ferrofluids, FeCo ferrofluid exhibited the best cooling performance followed by Fe and FeNi ferrofluids. Bulk saturation magnetization of the suspended magnetic nanoparticles in the ferrofluid was found to be a significant parameter which enhanced the passive convective heat transfer and the heat load cooling significantly. These results can be used to select the optimum ferrofluid for enhanced thermomagnetic cooling.

7.1 Introduction

Magnetic cooling (MC), which is governed by the thermomagnetic convection (TMC) of a ferrofluid (FF), is a promising passive cooling system [1]. The schematic of a passive MC device is represented in **Figure 7.1**.

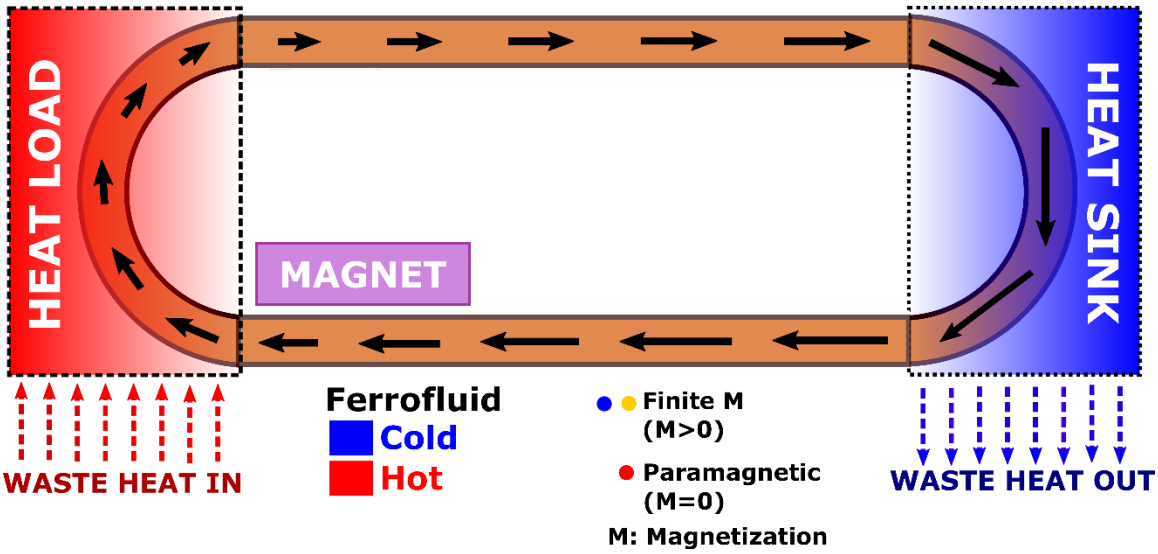

Figure 7.1. Schematic of a copper-based racetrack magnetic cooling device governed by the principle of thermomagnetic convection of a ferrofluid. A differentially heated ferrofluid flows along the closed channel under the combined effect of thermal gradient and the magnetization gradient, under an applied magnetic field. The direction of arrows indicated the flow direction, and the length of the arrow represents the relative magnetization of the corresponding ferrofluid region.

Nomenclature

Symbols

Magnetic parameters

$\mathbf{H}$	Magnetic field
$\mathbf{M}$	Magnetization
$\mathbf{B}$	Magnetic flux density
M_S^{Bulk}	Bulk saturation magnetization of MNP
M_s	Saturation magnetization
V_m	Magnetic scalar potential
$\mathbf{F_m}$	Magnetic volume force
$\mathbf{H_{min}}$	Minimum magnetic field strength
$\mathbf{H_{max}}$	Maximum magnetic field strength
μ_0	Permeability of the free space
χ_m	Ferrofluid magnetic susceptibility
χ_i	Initial magnetic susceptibility of the MNP
χ_{mnp}	Volume magnetic susceptibility of MNP
Δp_m	Magnetic pressure
$\mathbb{C}_o$	Magnetic nanoparticle volume fraction

Other parameters

l_D	Device length
d_t	Inner diameter of the tube
L	Flow channel length parameter
l’	Length of the side channel wall
l_{max}	Position with respect to $\mathbf{H_{max}}$
l_{min}	Position with respect to $\mathbf{H_{min}}$
A	Flow channel cross sectional area
l_{HL}	Heat load arc length
l_{HS}	Heat sink arc length
V	Voltage
I	Current
Γ	Langevin parameter
$\mathcal{L}$	Langevin function
N	Number of points across the heat load

Thermal & fluidic parameters

T	Temperature
T_{amb}	Ambient temperature
T_0	Heat load temperature without magnet
T_m	Heat load temperature with magnet
T_{HS}	Heat sink temperature
T_w	Inner tube wall temperature
T_f	Bulk ferrofluid temperature
T_{in}	Ferrofluid inlet temperature
T_{out}	Ferrofluid outlet temperature
h_l	Local convective heat transfer coefficient
h_{HS}	Avg. convective heat transfer coefficient at heat sink
P_{HL}	Power applied to the heat load
Q_{HL}	Heat flux at the heat load
Nu_L	Local value of Nusselt number
A	Thermal diffusivity
Nu_{avg}	Average value of Nusselt number
Nu_{HS}	Average value of Nusselt number at the heat sink
Pe	Peclet number
St	Stanton number
Re	Reynolds number
Pr	Prandtl number
$\dot{q}$	Volume flow rate
P’	Total rate of heat transfer
P”	Exergy loss
K	Thermal conductivity
C_p	Specific heat
$\mathbf{v}$	Velocity
ρ	Density
P	Pressure
M	Dynamic viscosity

Abbreviations

MC	Magnetic cooling
MNP	Magnetic nanoparticles
PIV	Particle image velocimetry
HL	Heat load
HS	Heat sink

Earlier reports on MC extensively investigated the TM heat transfer as a function of device properties, heat load parameters, and the strength, position, and orientation of applied magnetic field. Most of the literature utilized certain ferrite-based commercial FF for the evaluation of cooling performance. For enhanced heat load cooling, Aursand et al. [2] numerically investigated the cooling performance based on their optimization results for

the solenoid geometry, power consumption in the solenoid, TM pumping, and MNP size. However, there are no numerical studies or ranking to predict the TM cooling performance of various ferrites- and metallic/alloy-MNP based FF as a function of their magnetic and thermophysical parameters.

Hence, the scope of the present study is to investigate the cooling performance of the MC device with respect to the magnetic and thermophysical properties of the FF. For the first time, we evaluated numerically and analytically the performance metrics, the non-dimensional parameters, and the heat load cooling to rank various ferrite and metallic based FF. The resultant magnetic pressure term was derived and found to be a function of bulk saturation magnetization, MNP volume fraction, temperature dependent initial magnetic susceptibility curve, and the magnetic field strength. The friction factor, power transferred from the heat load to the heat sink, and the exergy loss were derived as function of magnetic, thermal, and thermophysical parameters to investigate the performance of various FF. Numerical simulations were performed to examine the effect of magnetic parameters of the nanoparticles viz., bulk saturation magnetization, Curie temperature, pyro magnetic coefficient, and initial magnetic susceptibility on the cooling performance. Several ferrite and metallic/alloy FF were simulated to evaluate the TM cooling performance. Ferrite ferrofluids of γ-Fe_2O_3, Fe_3O_4, and $CoFe_2O_4$ exhibited superior cooling performance at various range of heat flux values. For the case of metallic/alloy-based FF, FeCo FF exhibited the best cooling performance, followed by Fe and FeNi FF. Bulk saturation magnetization of the suspended MNP in the FF was found to be a parameter which significantly enhanced heat transfer and cooling.

Maximum heat load cooling was predicted for Fe-Co nanoparticle-based FF. However, the cooling was not significantly different for the best ferrite FFs at lower heat load temperatures and heat load power density. Hence, for lower heat load temperatures, ferrite materials can exhibit similar cooling as the metallic case. The effect of thermophysical parameters of the FF on the heat load cooling revealed that a FF possessing higher thermal conductivity and lower viscosity gives rise to higher cooling performance. We also analyzed the non-dimensional quantities viz., Nusselt number, Peclet number, and Stanton number as a function of bulk saturation magnetization of the soft MNP. The Nusselt number and the Peclet number increased significantly for higher bulk saturation

magnetization, implying better heat transfer. Our simulation results for the ranking of various FFs can be used to select the optimum FF for enhanced TMC.

7.2 Analytical and Modelling Methods

7.2.1 Numerical model

2D numerical simulations were developed using COMSOL Multiphysics software to investigate the TM cooling performance of various ferrite- and metallic-based FF using a racetrack MC device. The ferrofluids were treated as single-phase continuum owing to Rosensweig's continuum hypothesis [3]. Thermal, fluidic, and magnetic properties of the FF were used as inputs to the numerical model. Three physics modules viz., magnetic field, heat transfer, and single-phase flow in the laminar regime, were used in this model. The magnetic volume force resulting from the TMC effect was added as an additional volume force term in the momentum conservation equation. The magnetic field distribution due to the NdFeB magnet was simulated and compared to the experimentally obtained values of the magnetic field strength. The boundary conditions were specified, which are consistent with the experimental design. The 2D numerical model was validated to obtain better simulation accuracy.

7.2.2 Derivation of the performance metrics

The volume flow rate (q̇) of a FF within a closed circulation flow loop can be written as;

$$\dot{q} = A\vartheta \tag{7.1}$$

where A is the cross-section area of the flow loop. Using equation (7.1), the conservation equations in terms of flow loop length l can be rewritten as,

$$\frac{\partial \dot{q}}{\partial l} = 0 \tag{7.2}$$

$$\frac{\rho}{A^2}\frac{\partial \dot{q}^2}{\partial l} = -\frac{\partial p}{\partial l} + \frac{\mu}{A}\frac{\partial^2 \dot{q}}{\partial l^2} + F_m \tag{7.3}$$

$$\dot{q}\frac{\partial T}{\partial l} = \alpha A \frac{\partial^2 T}{\partial l^2} \tag{7.4}$$

Here, l represents the flow direction and α is the thermal diffusivity of the FF. The energy conservation equations for the heat load section, heat sink section, and the inflow and outflow channels can be written as,

$$\kappa\dot{q}\frac{dT}{dl} = \alpha\frac{P_{HL}}{l_{HL}} \tag{7.5}$$

$$\kappa\dot{q}\frac{dT}{dl} = -\alpha\frac{h_{HS}A\left(T_f - T_w\right)}{l_{HS}} \tag{7.6}$$

$$\dot{q}\frac{dT}{dl} = 0 \tag{7.7}$$

Here, P_{HL} is the applied heat load power, and h_{HS} is the heat transfer coefficient at the heat sink. The length of the heat load and the heat sink is denoted as l_{HL} and l_{HS}, respectively. T_f and T_w denote the temperature of the bulk FF and the flow channel wall, respectively. The right-hand side of equation (7.7) is zero because of negligible temperature difference between the FF and the flow channel wall.

$$T(l) = \frac{P_{HL}}{l_{HL}\rho C_p\dot{q}}l + T_{in} \tag{7.8}$$

$$T(l) = T_{in}, \left(\frac{l_{HL}}{2} \le l \le \frac{l_{HL}}{2} + l'\right) \tag{7.9}$$

$$T(l) = T_{HS} + (T_{out} - T_{HS})exp\left\{-\frac{\pi Nu_{HS}\alpha}{\dot{q}}l\right\} \tag{7.10}$$

$$T(l) = T_{out}, \left(-\frac{l_{HL}}{2} - l' \le l \le -\frac{l_{HL}}{2}\right) \tag{7.11}$$

The above temperature expressions analytically give the FF temperature at any point along the flow channel. T_{in}, T_{out}, and T_{HS} are the FF inlet temperature, the outlet temperature, and the heat sink temperature, respectively. *l*' represents the length of the inflow (bottom straight channel from the heat sink to the heat load) and outflow channels (top straight channel from the heat load to the heat sink) in the racetrack MC device (**Figure 7.1**).

The 1D momentum equation (equation (7.3)) can be integrated around the racetrack flow channel to obtain the friction factor as a function of the resultant magnetic pressure due to the TMC effect. Integration of the steady-state momentum equation takes the form,

$$\oint\left(\frac{\rho}{A^2}\frac{\partial\dot{v}^2}{\partial l}\right)dl = -\oint\left(\frac{\partial p}{\partial l}\right)dl + \oint\left(\frac{\mu}{A}\frac{\partial^2\dot{v}}{\partial l^2}\right)dl + \oint\left(\mu_0 M(T,H)\frac{\partial H}{\partial l}\right)dl \tag{7.12}$$

The integration of convective acceleration term (1st term in equation (7.12)) is zero owing to the continuity equation (equation (7.2)), under the assumption of constant density of the ferrofluid and constant cross-section of the flow channel. The pressure gradient term around the flow channel vanishes as the pressure difference along a closed loop is zero. Integration of viscous drag term (3rd term in equation (7.12)) leads to equation (7.13) [4].

$$\int \frac{\mu}{A}\frac{\partial^2 \dot{q}}{\partial l^2} = -\frac{f l_d}{d_t}\frac{\rho \dot{q}^2}{2A^2} \tag{7.13}$$

where, f is the friction loss associated with the MC device. l_d and d_t are the total perimeter and the internal diameter of the flow channel. Integrating the added magnetic volume force term in the Navier-Stokes equation gives rise to the resultant magnetic pressure (Δp_m) due to the TMC effect.

$$\Delta p_m = \oint F_m dl = \oint \left(\mu_0 M(T,H)\frac{\partial H}{\partial l}\right) dl \tag{7.14}$$

Using equation (3.5) and (3.6) in equation (7.14), we obtain Δp_m as a function of T, H, bulk Ms, and $\mathbb{C}_0$.

$$\Delta p_m = \mu_0 \mathbb{c}_0 M_s^{bulk}\left[\left\{ln\left(\frac{|sinh(\gamma H_{max})|}{\gamma H_{max}}\right)^{1/\gamma}\right\}_{T(l_{max})} - \left\{ln\left(\frac{|sinh(\gamma H_{min})|}{\gamma H_{min}}\right)^{1/\gamma}\right\}_{T(l_{min})}\right] \tag{7.15}$$

H_{max} and H_{min} corresponds to the maximum and the minimum field experienced by the FF in the vicinity of the heat load region. l_{max} and l_{min} are the corresponding positions along the flow channel with respect to the maximum and minimum applied magnetic field. In the limit of zero magnetic field,

$$\lim_{H\to 0} ln\left(\frac{|sinh\,(\gamma H)|}{\gamma H}\right)^{1/\gamma} = 1 \tag{7.16}$$

Hence, the magnetic pressure term is negligible at very low applied magnetic field and vanishes at zero magnetic field. The magnetic pressure term is directly proportional to the

bulk saturation magnetization and the MNP volume fraction in the ferrofluid. However, the temperature dependence comes from the Langevin parameter (γ).

After substitution of equation (7.14) and equation (7.16) to equation (7.13), we obtain the friction factor (f) [5],

$$f = \frac{\Delta p_m \pi^2 d_t^5}{8 l_{HL} \rho \dot{q}^2} \tag{7.17}$$

Total rate of heat transfer (P') between the heat load and the heat sink can be given as,

$$P' = \frac{\dot{q} C_p (T_{out} - T_{in})}{\rho} \tag{7.18}$$

Exergy refers to the maximum possible work during a thermodynamic process under the equilibrium condition with the heat load. Exergy is the available energy under entropy maximum condition. Exergy loss is one of the major parameter that defines efficient heat transfer between the system and the surrounding [5]. For a TMC based MC device, exergy loss can be given as,

$$P'' = T_{amb} \left[\frac{\dot{q} C_p}{\rho} ln \left(\frac{T_{out}}{T_{in}} \right) \right] \tag{7.19}$$

7.2.3 Numerical verification and mesh independency test

The developed 2D simulation model was numerically verified by performing mesh independency test to ensure better simulation accuracy using 2D triangular mesh elements. The non-dimensional heat load cooling ($\Delta T/\Delta T_{max}$) for a heat flux value of 1.6 kW/m^2 was plotted as a function of the number of mesh elements (**Figure 7.2**(a)). A total of 249554 triangular mesh elements were considered in the final model. The entire racetrack geometry of the MC device was divided into discrete regions using triangular mesh elements. The overall average mesh quality was 89.67%.

7.2.4 Numerical validation

The developed 2D simulation model was numerically validated by comparing the simulated magnetic field distribution along the length and the width of the magnet with the experimentally measured values (**Figure 7.2**(b, c)). Hence, the developed numerical model

was used to predict the performance for various ferrites-, and metallic/alloy-based FF for different magnetic and thermophysical properties of the FF.

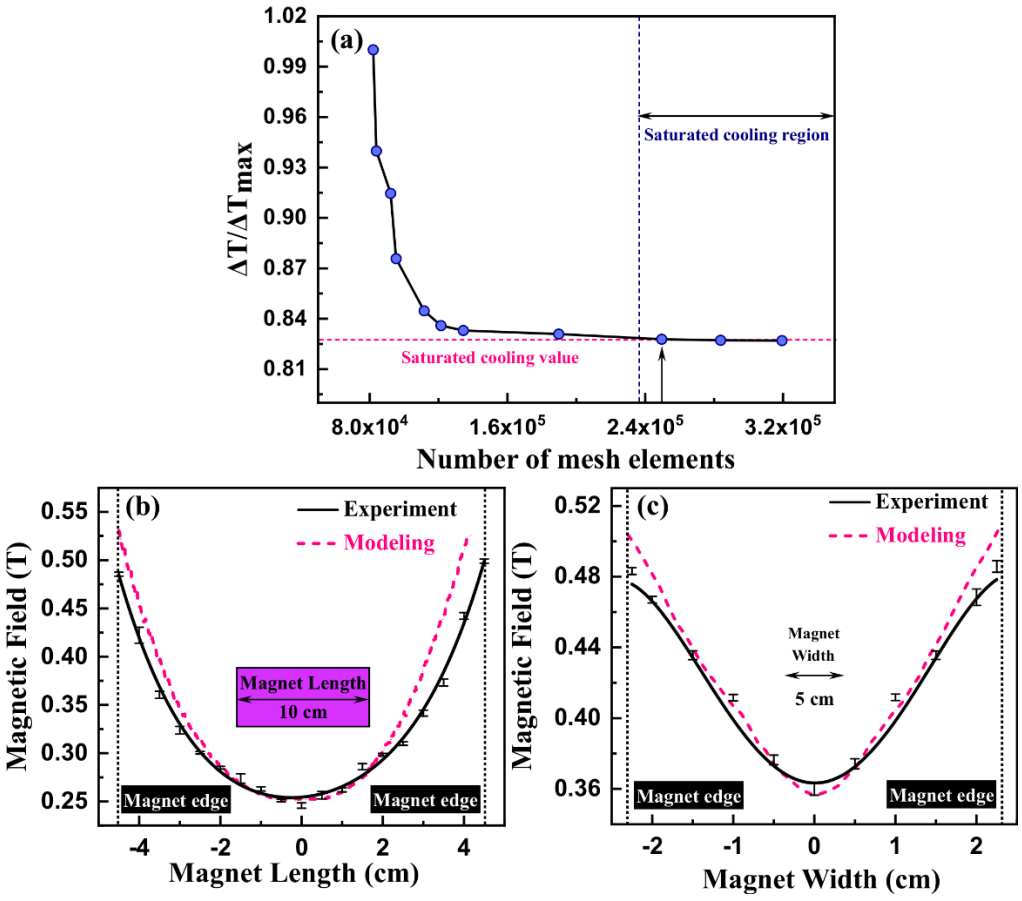

Figure 7.2. (a) Simulated non-dimensional heat load cooling as a function of the number of mesh elements. Experimental and simulated magnetic field distribution along the (b) length, and the (c) width of the NdFeB magnet.

7.2.5 Parameters considered

The effect of magnetic parameters of the ferrofluid, viz., bulk saturation magnetization, initial magnetic susceptibility, pyro magnetic coefficient, and Curie temperature on the heat load cooling was evaluated. The heat flux was also varied over a certain range to study its effect on heat load cooling. The bulk saturation magnetization and initial magnetic susceptibility curves for various ferrite and metallic/alloy-based FF were considered to rank the FF. Various performance metrics and non-dimensional numbers were studied as a function of bulk saturation magnetization of the MNP. **Table 7.1** summarizes the parameters, their units, notation, and experimental sets considered in this work.

Table 7.1. Summary of Parameters, their notation, range, and the measurement sets.

Parameters	Unit	Notation	Performed Sets
Bulk saturation magnetization	kA/m	M_s^{bulk}	50-2002
Initial magnetic susceptibility	Unitless	χ_i(T=0°C)	1.75-14
Ratio of pyro magnetic coefficient	Unitless	(dχ”/dT)/(dχ’/dT)	64 to 156
Curie temperature	°C	Tc	75-200
Heat flux	kW/m^2	Q	0.6-4.3
Initial heat load temperature	°C	T_0	60-200

7.3 Results and Discussions

7.3.1 Experimental and simulated heat load cooling for magnetite ferrofluid

Before performing numerical investigation for various FF, the numerical simulation was validated against the experimental heat load cooling result using a copper racetrack shaped MC device (**Figure 7.1**) having a device perimeter and internal tube diameter of 130 cm, and 0.81 cm, respectively. The experimentally obtained heat load temperature profile was compared with the simulated profile for an initial heat load temperature of 197°C using commercial Fe_3O_4 FF in a copper-based racetrack MC device. The experimental and simulated temperature profiles are in good agreement (**Figure 7.3**). The developed 2D numerical simulation was then used to simulate the effect of ferrofluidic thermophysical and magnetic properties for enhanced cooling performance.

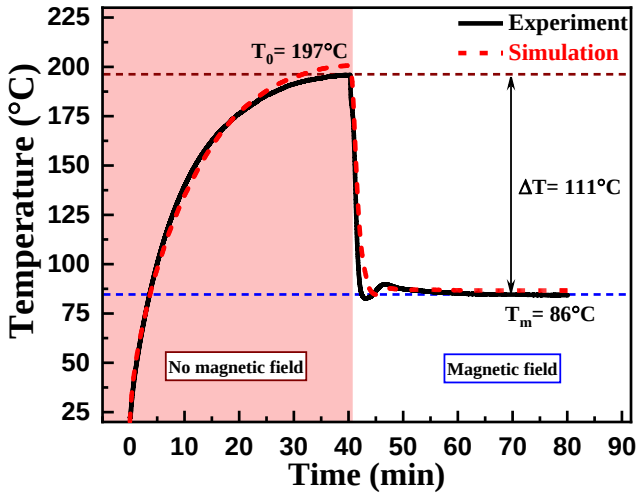

Figure 7.3. Heat load temperature versus time curve without and with the application of an external magnetic field for an initial heat load temperature of 197°C.

7.3.2 Effect of ferrofluid magnetic parameters on heat load cooling

The effect of various magnetic parameters of the ferrofluid viz., initial magnetic susceptibility (χ_i), pyro magnetic coefficient ($d\chi/dT$), bulk saturation magnetization (M_s^{bulk}), and the Curie temperature (T_c) on cooling was numerically investigated. For these investigations, virtual susceptibility vs temperature profiles were taken to understand the effects of various magnetic parameters on cooling. The initial susceptibility versus temperature behavior of magnetite nanoparticles was taken as the reference susceptibility curve ($\chi'(T)$) with a modified Curie temperature of 200°C (**Figure 7.4**(a)). The results are described below.

7.3.2.1 Effect of change in bulk saturation magnetization on heat load cooling

For the reference susceptibility curve, and an initial heat load temperature of 100°C, the effect of the bulk saturation magnetization of MNP in the FF on heat load cooling performance and FF average velocity was investigated (**Figure 7.4**(b, c)). As can be seen, ΔT increased significantly from 2°C to 52°C with an increase in Ms from 50 kA/m to 500 kA/m. It followed a polynomial behavior. The average FF velocity also increased significantly in a linear manner as a function of Ms. Higher value of bulk saturation magnetization results in higher magnetic pressure (equation (7.15)), which gives rise to higher FF velocity, and hence better cooling.

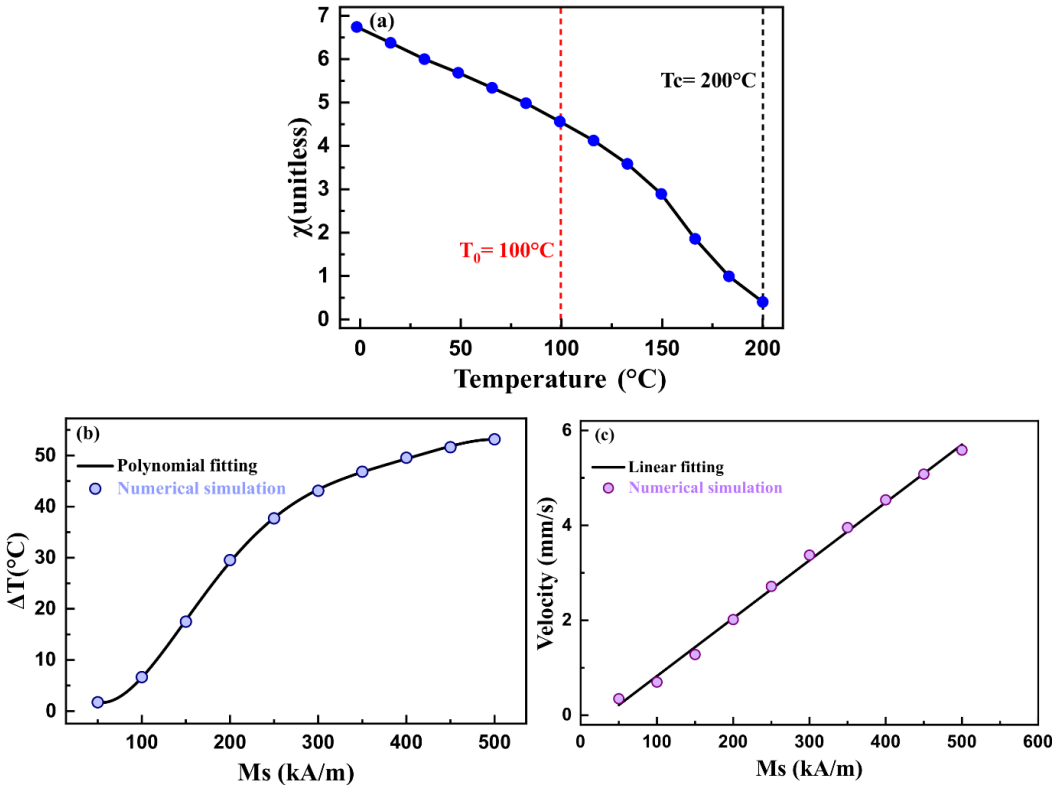

Figure 7.4. (a) Virtual initial magnetic susceptibility curve (reference χi curve); (b) the heat load cooling magnitude, and (c) the average ferrofluid velocity as a function of the bulk saturation magnetization of the magnetic nanoparticles in the ferrofluid.

7.3.2.2 Effect of change in initial susceptibility on heat load cooling

To investigate the effect of magnitude of initial magnetic susceptibility (χ_i) on the heat load cooling, two different χ_i profiles were considered with the same pyro magnetic coefficient and same Curie temperature of 200°C (**Figure 7.5**). These susceptibility profiles were provided as input to the numerical model. Subsequently, the effects of heat flux and the bulk saturation magnetization on cooling were investigated for a heat load temperature of 200°C.

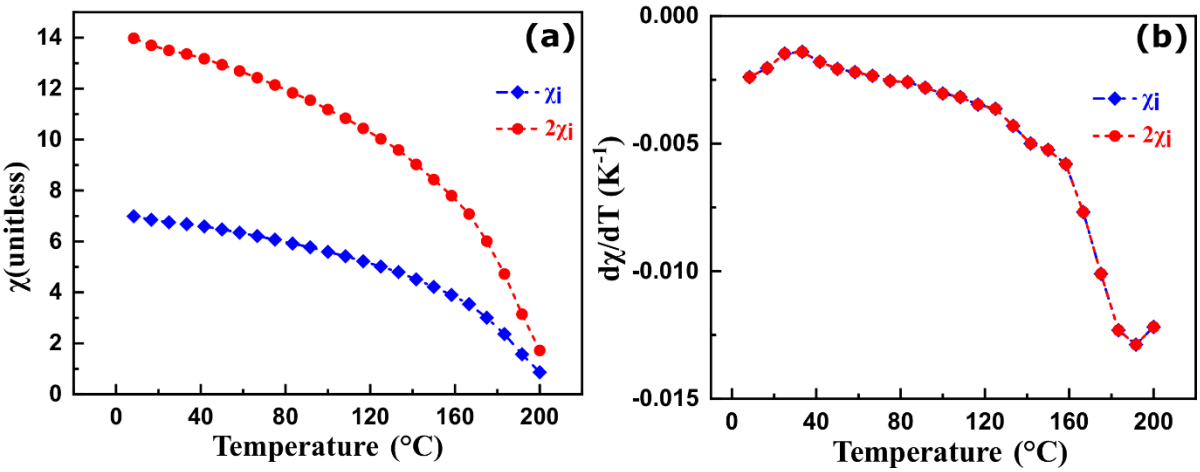

Figure 7.5. (a) Virtual initial magnetic susceptibility curves with different magnitudes, and (b) the corresponding pyro magnetic coefficient curves having a Curie temperature of 200°C.

Figure 7.6(a, b) show the effect of heat flux on the heat load cooling and the average FF velocity for two different initial susceptibility profiles considering a bulk saturation magnetization value of 446 kA/m. The heat load temperature was 200°C. Both the cooling and FF average velocity profiles tend to increase for higher heat flux value slightly beyond the Tc point of the FF. However, the cooling and the velocity started to reduce significantly beyond Tc. This reduction in the cooling performance is due to the overall reduction in the TM force as the FF reached the paramagnetic regime. The increasing value of heat load cooling for higher heat flux values demonstrates the self-regulating nature of the MC device. Moreover, MC devices are self-pumping as the pumping force arises from the combined effect of the temperature gradient and applied magnetic field on the magnetic susceptibility of the FF. The effect of bulk saturation magnetization of the MNP showed negligible difference in the cooling for both the susceptibility profiles (**Figure 7.6**(c, d)).

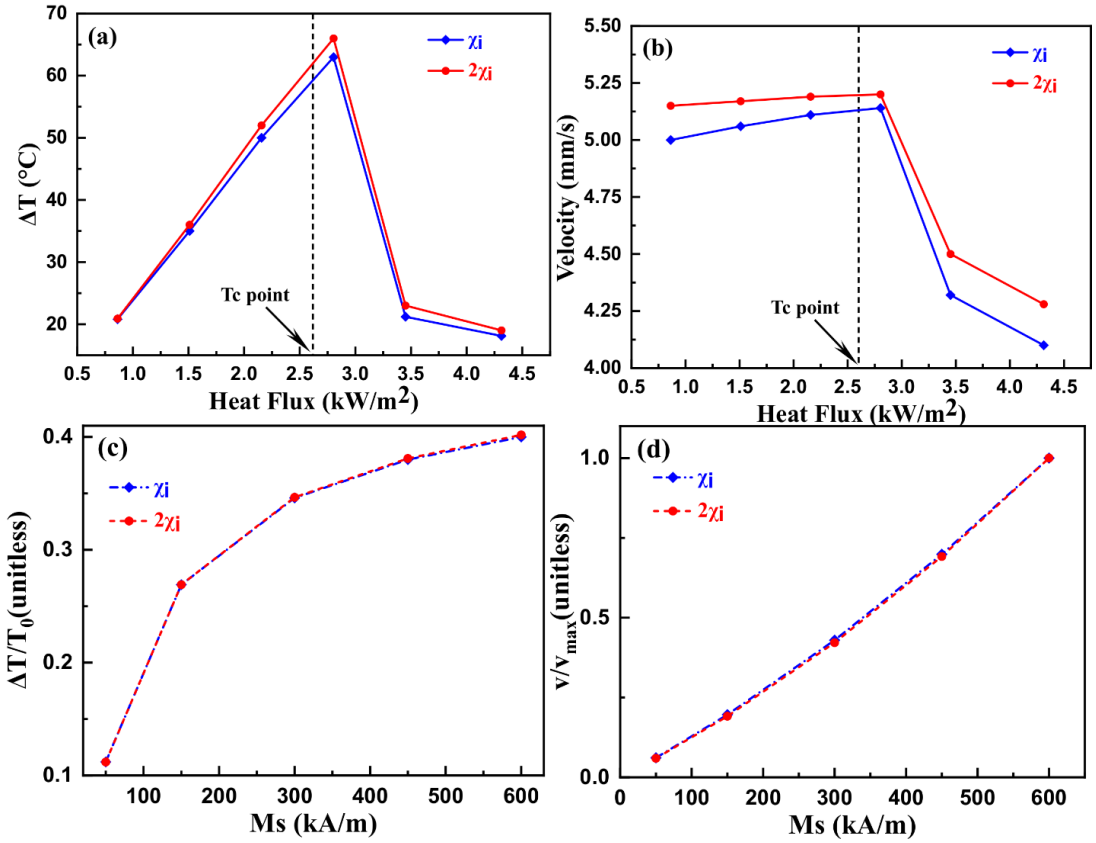

Figure 7.6. (a) The extent of cooling, and (b) the average ferrofluid velocity as a function of applied heat flux for the virtual magnetic susceptibilities as shown in Figure 7.5, for a bulk saturation magnetization value of 446 kA/m. (c) The non-dimensional heat load cooling, and (d) the non-dimensional average ferrofluid velocity as a function of the bulk saturation magnetization, for the same magnetic susceptibilities.

We also investigated the effect of the ratio of initial magnetic susceptibilities to the reference susceptibility profile on the cooling (**Figure 7.7**(b, c)). The χ_i profiles considered for this investigation are shown in **Figure 7.7**(a). Both the heat load cooling and the FF velocity exhibited a small increase of 10.6% and 29%, respectively, with 700% increase in χ''/χ' (χ' being the reference χ curve). Hence, the initial magnetic susceptibility is not a significant parameter.

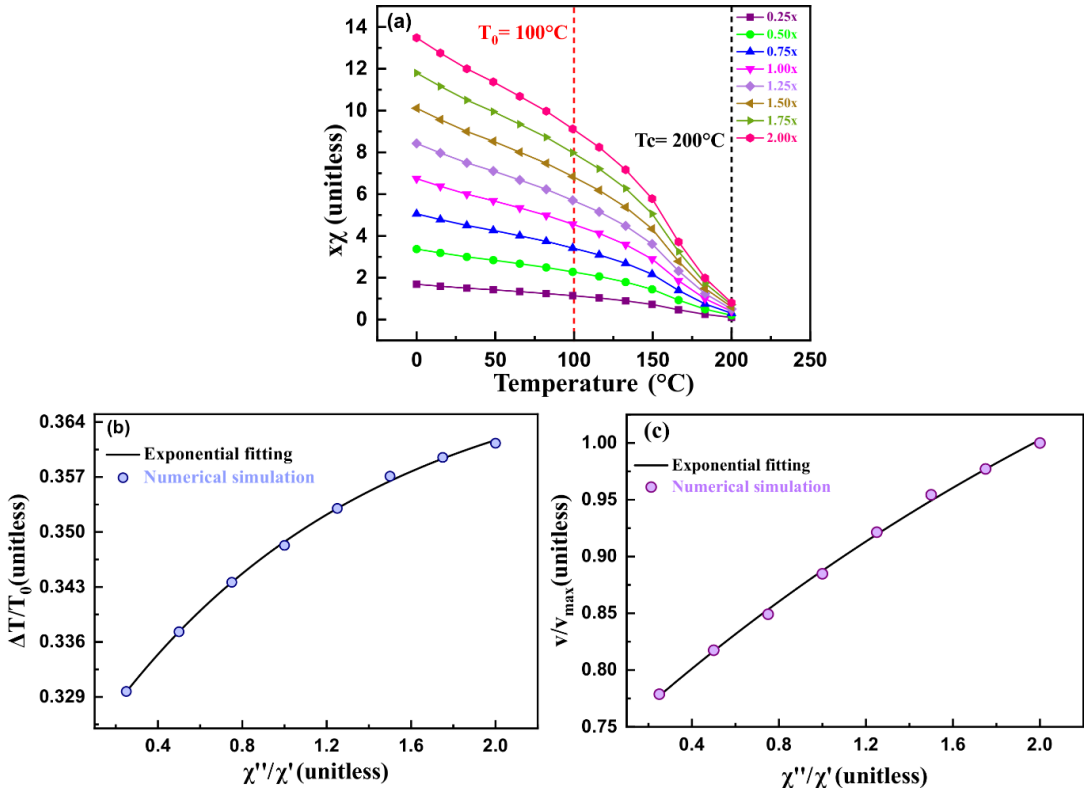

Figure 7.7. (a) Initial magnetic susceptibility profiles with varying magnitudes with respect to the reference susceptibility curve (pink curve); (b) the non-dimensional heat load cooling, and (d) the non-dimensional average ferrofluid velocity as a function of the ratio of the magnitude of susceptibility to the reference susceptibility curve.

7.3.2.3 Effect of change in pyro magnetic coefficient on heat load cooling

To study the effect of pyro magnetic coefficient on the cooling performance, several virtual susceptibility curves were considered with increasing pyro magnetic coefficient ratio, as shown in **Figure 7.8**(a). The corresponding pyro magnetic coefficient curves are shown in **Figure 7.8**(b).

The effect of pyro magnetic coefficient ratio on the heat load cooling magnitude and the average FF velocity were plotted in **Figure 7.8**(c, d). Both the curves exhibited an increasing trend and showed similar behavior as a function of ratio of the pyro magnetic coefficient. However, the cooling performance tends to saturate for higher ratio of the pyro magnetic coefficient. The heat load cooling magnitude increased by only 4°C with respect to a 200% increase in the pyro magnetic coefficient. Hence, pyro magnetic coefficient is also not a significant parameter.

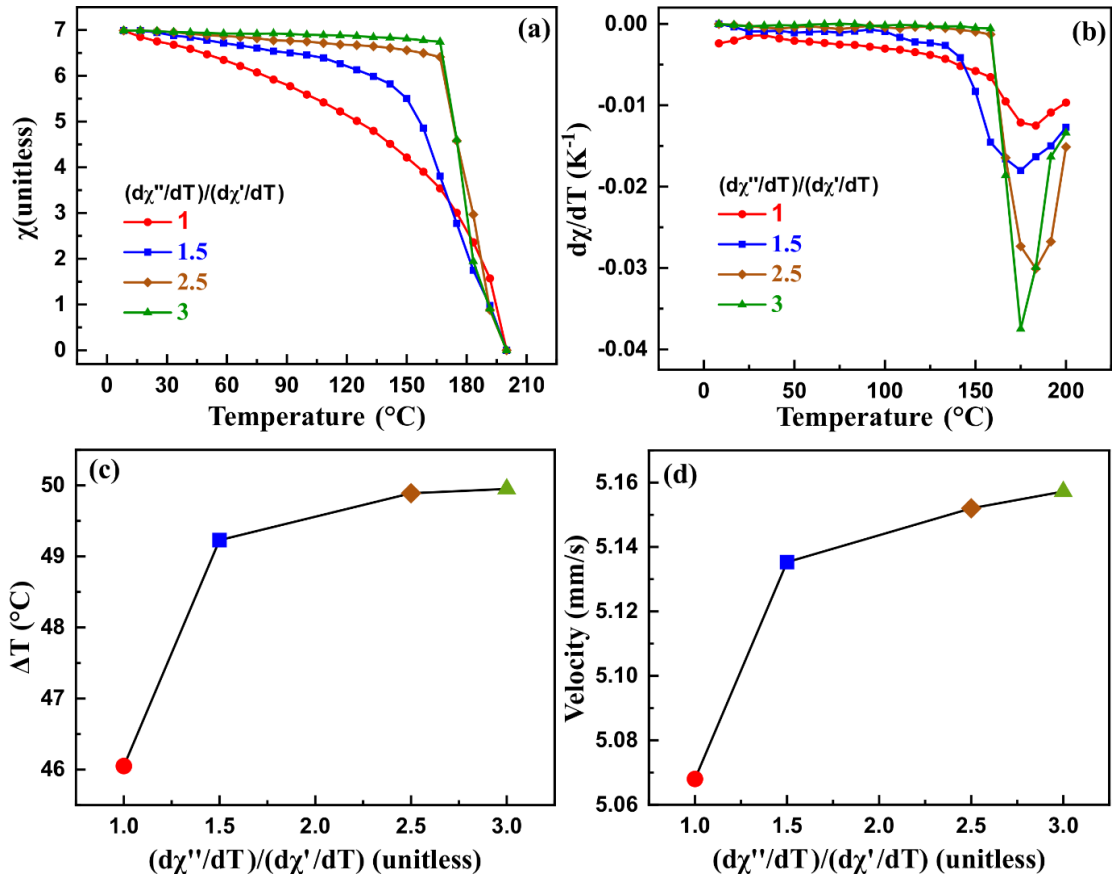

Figure 7.8. (a) Virtual initial magnetic susceptibility curves with different pyro magnetic coefficient ratio, and (b) the corresponding pyro magnetic coefficient curves having a Curie temperature of 200°C. (c) The heat load cooling magnitude, and (d) the average ferrofluid velocity as a function of ratio of pyro magnetic coefficients with respect to the reference susceptibility curve, for the virtual magnetic susceptibility curves in Figure 7.8(a, b), for a bulk saturation magnetization value of 446 kA/m.

7.3.2.4 Effect of Curie temperature on heat load cooling

To study the effect of Curie temperature (Tc) of the susceptibility curve on MC of the heat load, we considered several virtual χ_i curves with the same Ms value and same initial χ_i (**Figure 7.9**(a)). The effect of Tc on the heat load cooling and the FF velocity profile was studied for a heat load temperature of 60°C for a range of bulk saturation magnetization values (**Figure 7.9**(b, c)). Both the parameters exhibited an increase in the cooling performance for the values of Tc closer to the heat load temperature curves. In the present case, a Tc value of 75°C is the closest to the heat load temperature, hence it exhibited maximum cooling performance. These results for the effect of Tc can be attributed to the

enhancement of pyro magnetic coefficient ($d\chi/dt|_{T=60°C}$) when the Tc is close to the heat load temperature. This result is consistent with the obtained results for the effect of pyro magnetic coefficient (**Figure 7.8**).

From these results, it was clear that the bulk saturation magnetization is the significant parameter that affects the cooling performance. For constant bulk saturation magnetization, pyro magnetic coefficient and Curie temperature affect the TM cooling. Initial magnetic susceptibility has the least impact. The effects of these parameters can also be understood from the derived expression of magnetic pressure (equation (7.15)).

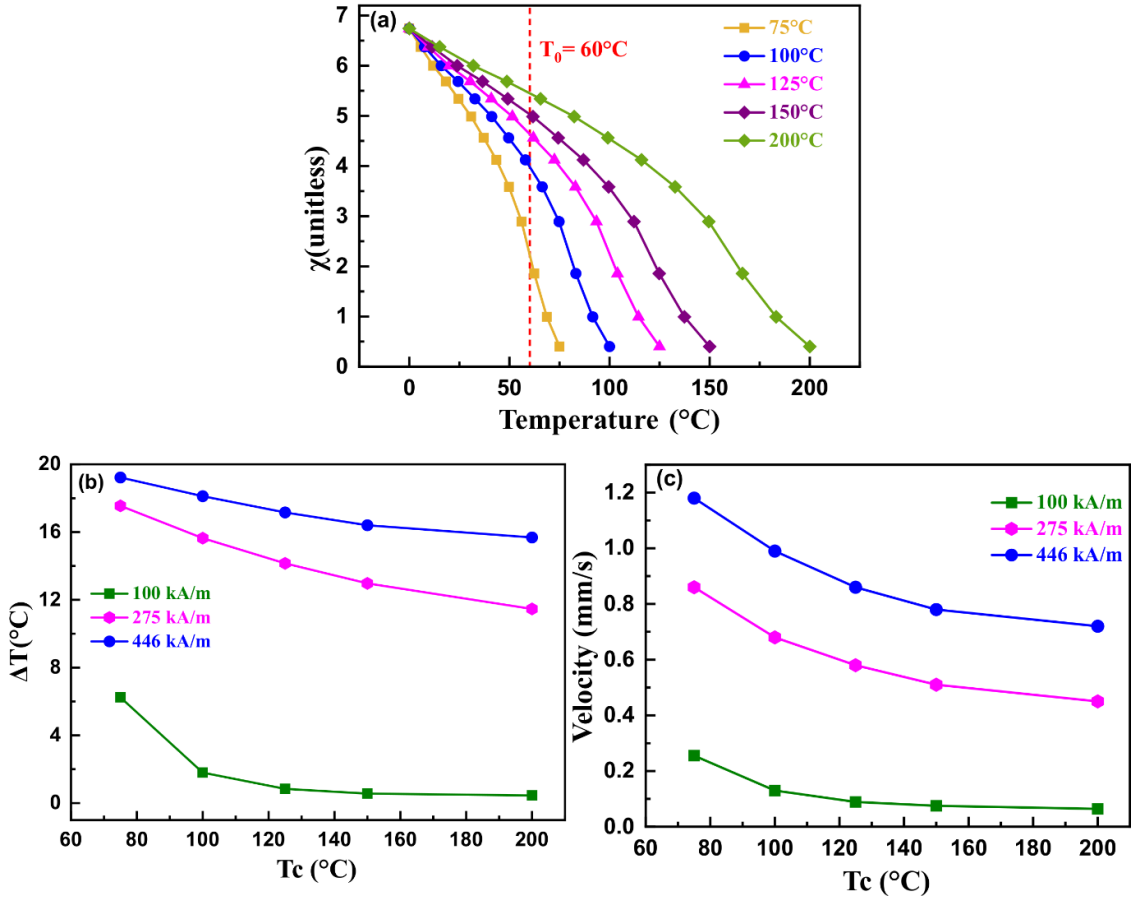

Figure 7.9. (a) Virtual initial magnetic susceptibility curves with varying Curie temperature but same initial susceptibility; (b) the heat load cooling magnitude, and (c) the average ferrofluid velocity as a function of Curie temperature for a heat load temperature of 60°C and a bulk saturation magnetization value of 446 kA/m.

7.3.3 Heat load cooling for ferrite and metallic nanoparticle based ferrofluids

To rank ferrite and metallic nanoparticle-based FF in accordance with their TM cooling performance, several numerical simulations were performed for several initial susceptibility versus temperature curves, and the bulk saturation magnetization of the nanoparticles as input to the model. **Figure 7.10**(a, b) show the heat load cooling and the average FF velocity of various ferrite-based FF as a function of the bulk saturation magnetization of the corresponding MNP.

Figure 7.10(c, d) is the heat load cooling and the average FF velocity curves for the MNP based FF. The general trend shows an increase in cooling and FF velocity with increasing bulk saturation magnetization for both the cases. For low heat flux and heat load temperature values, the magnitude of ΔT increase is not so significant. However, for higher heat flux and heat load temperature values, the cooling as well as the FF velocity enhanced significantly for FF having higher bulk Ms.

However, certain anomalies were observed for the ΔT and the velocity curves (yellow shaded area) in the case of ferrite-based FF. Nonetheless, the increase in bulk saturation magnetization of the suspended MNP in the FF results in an increase in both heat load cooling and the average FF velocity. Hence, the anomalies are not related to the increase in bulk Ms. They can be attributed both to the pyro magnetic coefficient and the Curie temperature of the materials whose Ms values are falling in the shaded region. For lower heat flux values, the anomalies are not so sharp. However, the effect intensifies for higher heat flux values. In general, at lower temperatures which corresponds to lower heat flux value, the magnetic susceptibility curve has a lower pyro magnetic coefficient. However, for higher temperature regions, the pyro magnetic coefficient tends to be higher. Hence, the anomalies are significant at higher heat load temperatures at higher heat flux values. A decrease (1^{st} and 3^{rd} yellow shaded regions) or increase (2^{nd} and 3^{rd} yellow shaded regions) in cooling and the velocity corresponds to a decrease or increase in the $d\chi/dT$ value for higher magnetization, respectively. A slight anomaly is observed in the lower bulk Ms region for the metallic FF case. However, due to much higher bulk saturation magnetization of metallic FF, the obtained value of ΔT and average velocity is significantly larger than

ferrite FF. **Table 7.2** and **Table 7.3** summarizes the cooling performance for various ferrite-based and metallic/alloy-based FF, respectively.

In practical applications, it is challenging to synthesize stable metallic MNP based FF due to oxidation issues and the higher density of the nanoparticles. These problems lead to particle agglomeration and settling. It can be inferred from the above discussion that, for lower heat load temperatures, ferrite FF having moderate volume magnetization can exhibit similar cooling performance as the metallic case. However, for higher heat load temperatures, utilizing stable metallic FF can be advantageous.

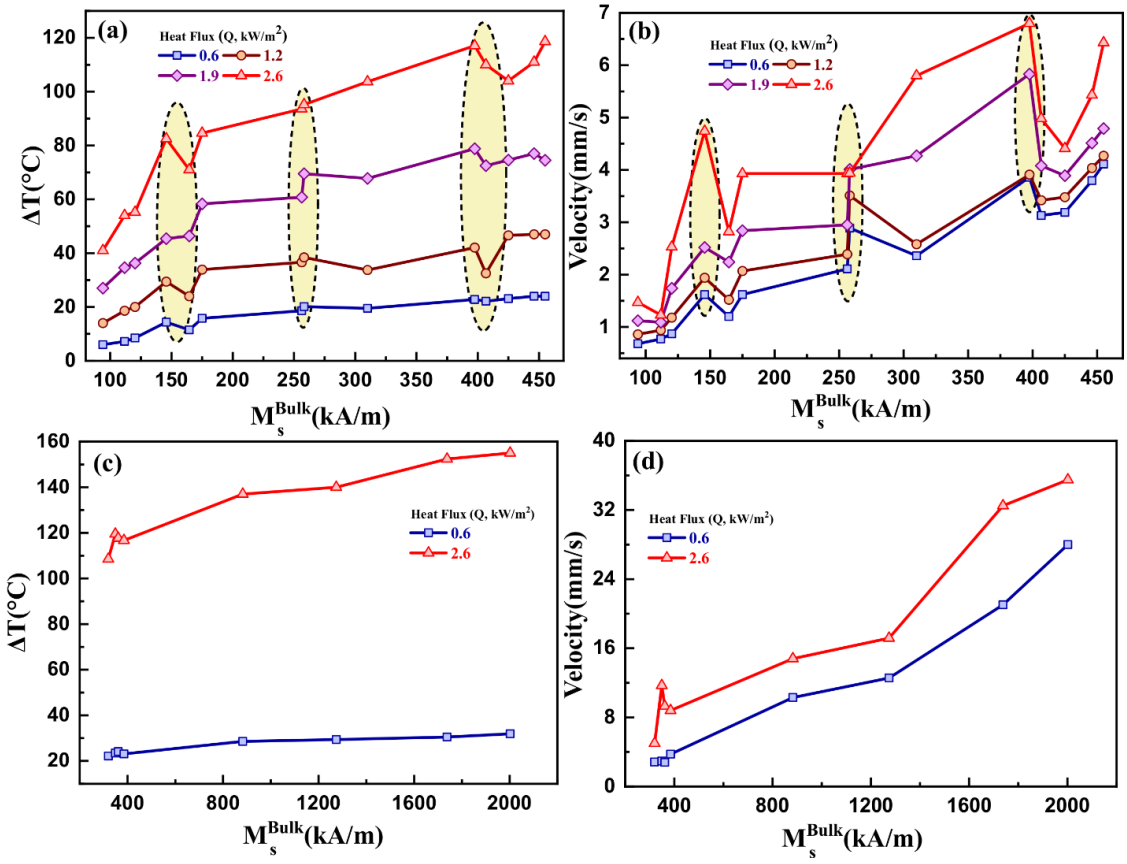

Figure 7.10. (a/c) The heat load cooling magnitude, and (b/d) the average ferrofluid velocity as a function of bulk saturation magnetization values of various ferrite/metallic nanoparticle-based ferrofluids.

Table 7.2. Magnitude of heat load cooling and average ferrofluid velocity for various ferrite nanoparticle based ferrofluids. Notation: HL= heat load, T_0= bare heat load temperature, Q= applied heat flux, ΔT= heat load cooling, v= average ferrofluid velocity.

HL Temp(T_0)/He at flux(Q)	Bulk Ms	T_0= 60°C, Q= 0.6 kW/m^2		T_0= 100°C, Q= 1.2 kW/m^2		T_0= 150°C, Q= 1.9 kW/m^2		T_0= 200°C, Q= 2.6 kW/m^2	
Materials	Bulk Ms (kA/m)	ΔT (°C)	v (mm/s)	ΔT (°C)	V (mm/s)	ΔT (°C)	v (mm/s)	ΔT (°C)	v (mm/s)
$Mn_{0.3}Zn_{0.7}Fe_2O_4$	94.0	6.0	0.7	14.0	0.8	27.0	1.2	41.0	1.5
$ZnFe_2O_4$	111.7	7.2	0.8	18.6	0.9	34.6	1.1	54.0	1.2
$MgFe_2O_4$	120.2	8.5	0.9	20.0	1.2	36.3	1.7	55.2	2.5
$Mn_{0.4}Zn_{0.6}Fe_2O_4$	145.7	11.5	1.2	24.0	1.5	46.4	2.2	71.0	2.8
$Mn_{0.5}Zn_{0.5}Fe_2O_4$	164.5	14.3	1.6	29.4	1.9	45.4	2.5	82.5	4.7
$NiFe_2O_4$	175.0	15.7	1.7	33.9	2.1	58.3	2.8	84.6	3.6
$CuFe_2O_4$	256.3	18.6	2.1	36.6	2.4	60.8	2.9	93.6	3.8
$CuNiFe_2O_4$	258.2	20.1	2.9	38.4	3.5	69.5	4.0	95.2	3.9
$Co_{0.6}Zn_{0.4}Fe_2O_4$	310.0	19.5	2.4	33.7	2.6	67.7	4.3	103.7	5.8
γ-Fe_2O_3	397.5	22.8	3.9	42.0	3.9	78.8	5.8	117.1	6.8
$MnFe_2O_4$	406.7	22.1	3.1	32.5	3.4	72.5	4.1	110.0	4.9
$Co_{0.8}Zn_{0.2}Fe_2O_4$	425.0	23.1	3.2	46.6	3.5	74.5	3.9	104.0	4.4
Fe_3O_4	446.0	24.0	3.8	47.0	4.0	77.0	4.5	111.0	5.4
$CoFe_2O_4$	455.0	24.0	4.1	47.0	4.3	74.5	4.8	118.6	6.4

Table 7.3. Extent of heat load cooling and the average ferrofluid velocity for various metallic/alloy magnetic nanoparticle based ferrofluids. Notation: T_0= bare heat load temperature, Q= applied heat flux, ΔT= heat load cooling, v= average ferrofluid velocity.

HL Temp(T_0)/Heat flux(Q)	Bulk saturation magnetization	T_0= 60°C, Q= 0.6 kW/m^2		T_0= 200°C, Q= 2.6 kW/m^2	
Materials	Bulk Ms(kA/m)	ΔT(°C)	v(mm/s)	ΔT(°C)	v(mm/s)
HEA-AlCoFeNiCr	320.0	22.2	2.8	108.5	5.0
$FeNi_{0.7}Cr_{0.3}$	349.0	23.5	2.9	119.5	11.7
$Fe_{0.5}Cu_{0.5}$	361.2	24.1	2.8	117.6	9.3
$FeNi_{0.9}Cr_{0.1}$	385.0	23.1	3.7	116.7	8.8
HEA-AlCoFeNi	882.5	28.6	10.3	137.0	14.8
$Fe_{0.3}Ni_{0.7}$	1274.0	29.4	12.5	140.0	17.2
Fe	1738.0	30.5	21.0	152.4	32.5
$Fe_{0.5}Co_{0.5}$	2002.0	31.9	28.0	155.0	35.5

7.3.4 Effect of thermophysical properties of ferrofluid on average flow velocity

Figure 7.11 shows the effect of thermophysical properties of the FF on the normalized average FF flow velocity for a range of parameters. FF velocity tends to increase for higher thermally conductive FF (**Figure 7.11**(a)). A reason for the enhancement of average FF velocity and cooling (not shown) with increasing thermal conductivity can be due to enhanced heat transfer by the MNP. This process distorts the thermal boundary layer, giving rise to better flow mixing due to the random motion of MNP. For a 50% increase in the value of FF thermal conductivity, the flow velocity increased by a mere 5.2%.

Figure 7.11(b) shows the effect of viscosity of FF on the average FF velocity. The average velocity decreased exponentially as a function of viscosity. The TM cooling performance is higher for lower viscosity due to low viscous drag between the ferrofluid layers. The FF velocity tends to decrease exponentially for an increase in the specific heat of the FF

(**Figure 7.11**(c)). However, the reduction in the flow velocity is not so significant with respect to the specific heat capacity as the viscosity case. From all the three curves, it can be inferred that viscosity has a significant effect on the TM cooling performance. For a 116% increase in the value of FF viscosity, the flow velocity reduced by 42%. *Hence, amongst all the thermophysical properties of the ferrofluid, viscosity is the significant parameter which affects the cooling performance*. An ideal FF should have higher thermal conductivity, lower viscosity, and lower specific heat capacity for enhanced heat load cooling performance.

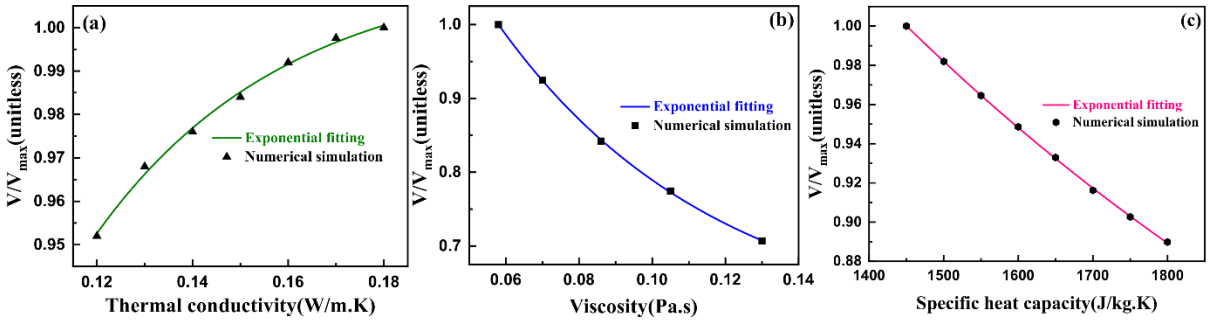

Figure 7.11. Normalized average flow velocity of the ferrofluid as a function of its (a) thermal conductivity, (b) viscosity, and (c) specific heat capacity.

7.3.5 Non-dimensional parameters and figure of merit of ferrofluids

7.3.5.1 Transferred power and exergy loss versus bulk saturation magnetization

The amount of heat transported from the heat load to the heat sink by the TMC of FF using a MC device was plotted as a function of bulk saturation magnetization of the MNP (**Figure 7.12**(a)). It is evident from the figure that more heat can be removed using highly magnetic FF. This is due to the higher volume flow rate of FF possessing larger magnetization for a given magnetic field strength.

Figure 7.12(b) shows the exergy loss curve versus the bulk saturation magnetization. It exhibits similar exponentially decaying trend as the power curve. The exergy loss also tends to increase with bulk Ms. Exergy loss represents higher randomness. Hence, the entropy is more at higher exergy loss. Both the power and the exergy loss are directly proportional to the volume flow rate of the FF, which is larger for higher bulk Ms due to the greater TM volume force experienced by the FF. The FF forms vortices near the heat load region due to the combined effect of thermal gradient and the magnetization gradient

[6]. The increase in entropy can also be attributed to the formation of these strong vortices when the FF possess higher magnetization.

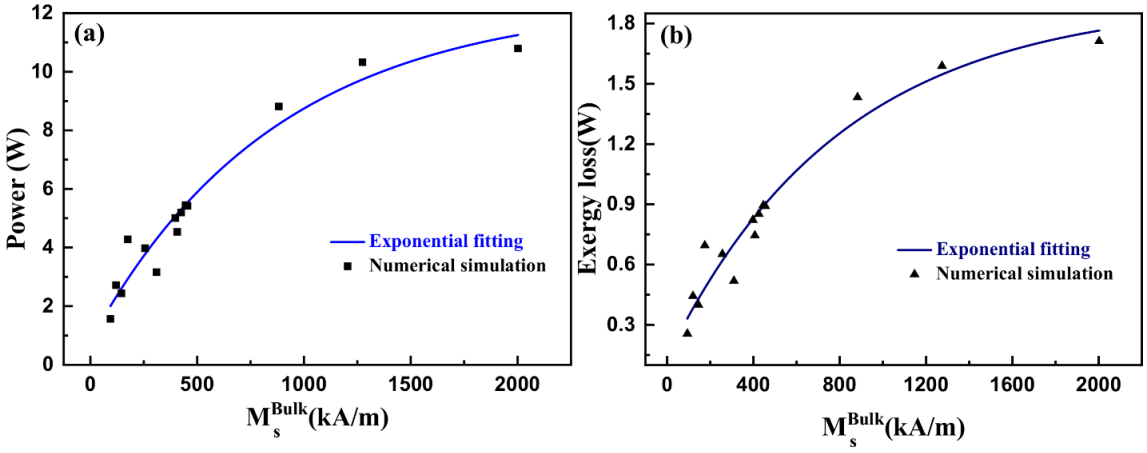

Figure 7.12. (a) The amount of power transferred from the heat load to the heat sink, and (b) the exergy loss, as a function of bulk saturation magnetization of various ferrite and metallic nanoparticle based ferrofluids, for a heat flux value of 1.6 kW/m2.

7.3.5.2 Non-dimensional parameters versus bulk saturation magnetization

To better understand the TMC heat transfer in FF-based MC devices, we examined the behavior of several non-dimensional parameters as a function of the bulk saturation magnetization of MNP.

The nature of heat transfer at the heat load region was investigated by calculating the average (Nu_{avg}). **Figure 7.13**(a) shows the variation in the average Nusselt number versus bulk Ms. The average Nusselt number increases for larger bulk Ms, implying better TMC heat transfer from the heat load region. This observation is also consistent with the increase in the magnitude of cooling (ΔT) of the heat load for larger bulk Ms (**Figure 7.10**). The average Nusselt number is below 10 for Ms values below 250 kA/m, suggesting the FF flow is laminar. However, for Ms values above 250 kA/m, the FF flow can be thought of as a transition between the laminar and turbulent flow regime. The red curve in **Figure 7.13** suggests a linear increase in the average value of the Nusselt number with Ms. Hence, the passive TMC heat transfer increases for F having higher saturation magnetization.

Figure 7.13 (b) shows the Peclet number as a function of bulk Ms. The linear increase in Pe with increasing bulk Ms suggests greater advection heat transfer than the diffusion-

based heat transfer. Thus, convective motion of the bulk fluid carries significant amount of heat away from the heat load region compared to conductive heat transfer through the nanoparticle chains.

Figure 7.13 (c) shows the effect of Stanton number as a function of bulk Ms. The non-linear reduction in St with an increase in bulk Ms signifies a reduction in the thermal capacity of the FF. The thermal capacity tends to increase for higher volume flow rate of the FF.

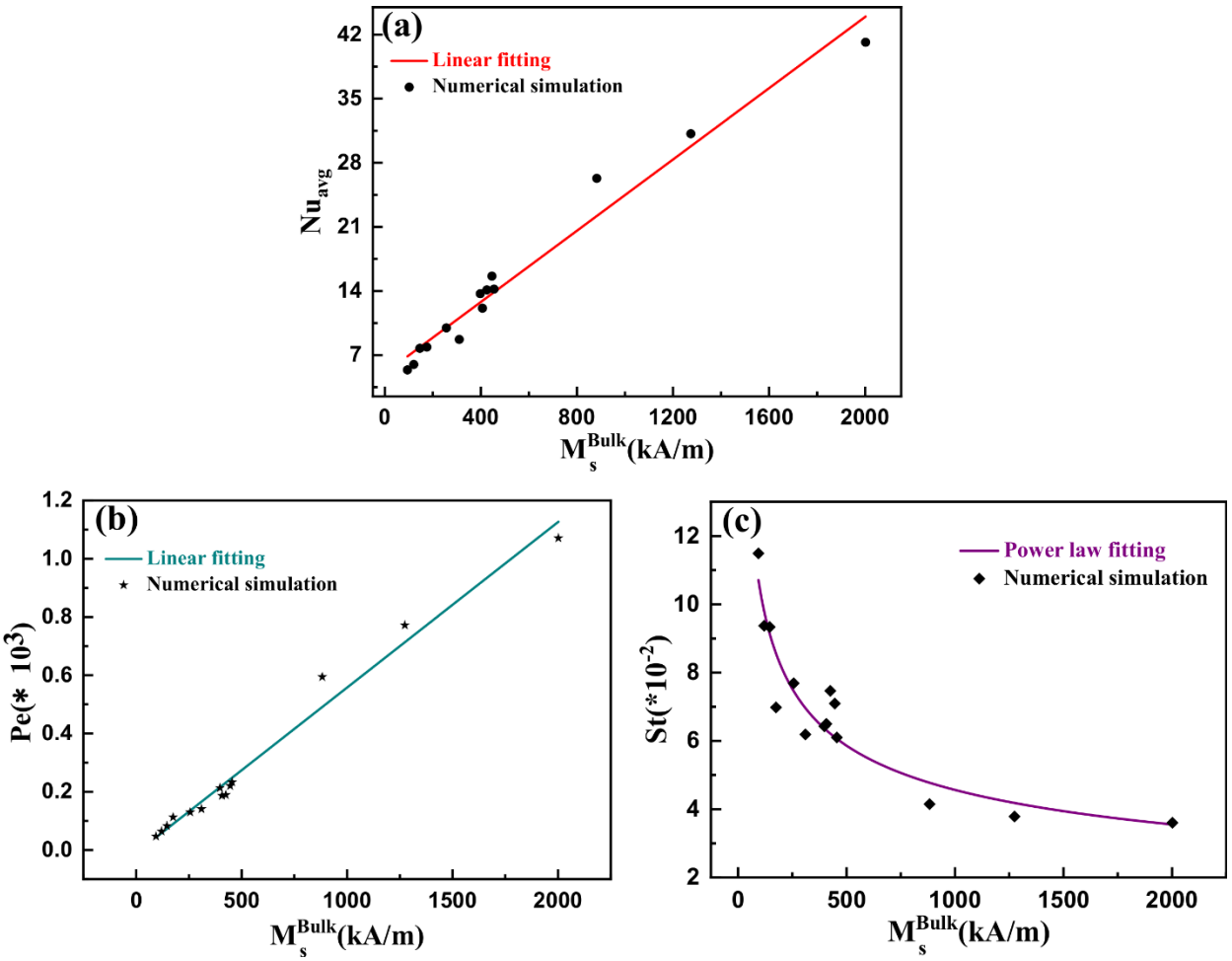

Figure 7.13. (a) The average Nusselt number (Nuavg), (b) the Peclet number (Pe), and (c) the Stanton number (St) as a function of bulk saturation magnetization of various ferrite and metallic nanoparticle based ferrofluids.

7.4 Conclusions

The cooling performance of the thermomagnetic convection based magnetic cooling device was numerically assessed with respect to the magnetic properties of various ferrite- and metallic/alloy-nanoparticle based ferrofluids. For the first time, we ranked the ferrofluids based on their thermomagnetic cooling performance. The effect of bulk saturation magnetization, initial magnetic susceptibility, pyro magnetic coefficient, and the Curie temperature on the heat load cooling was evaluated. Several ferrites- and metallic/alloy-based ferrofluids were simulated to investigate their thermomagnetic cooling performance. Various performance metrics and the non-dimensional parameters were used to evaluate the heat transfer as function of magnetic properties of the ferrofluid. The conclusions are as follows.

- The bulk saturation magnetization significantly enhances the heat load cooling. Heat load cooling increases to a lesser extent with increasing magnitude of initial magnetic susceptibility and higher pyro magnetic coefficient material.
- Maximum cooling performance is obtained when the Curie temperature is near the heat load temperature.
- For the case of thermophysical properties, viscosity significantly affected the heat load cooling. Cooling increases significantly for low viscous ferrofluid.
- γ-Fe_2O_3, Fe_3O_4 and $CoFe_2O_4$ ferrite based ferrofluids displayed higher heat load cooling performance.
- For the case of metallic/alloy-based ferrofluids, FeCo ferrofluid exhibited the best cooling performance followed by Fe and FeNi ferrofluids.
- Power transport capability and the exergy loss increased for higher bulk saturation magnetization of magnetic nanoparticles.
- The non-dimensional average Nusselt number and Peclet number also revealed the enhancement in heat transfer for strongly magnetic ferrofluids.

References

[1] V. Sharma, S. Pattanaik, H. Parmar, and R. V. Ramanujan, "Magnetocaloric properties and magnetic cooling performance of low-cost Fe 75− x Cr x Al 25 alloys," *MRS Communications,* vol. 8, no. 3, pp. 988-994, 2018.

[2] E. Aursand, M. A. Gjennestad, K. Y. Lervåg, and H. Lund, "Potential of enhancing a natural convection loop with a thermomagnetically pumped ferrofluid," *Journal of Magnetism and Magnetic Materials,* vol. 417, pp. 148-159, 2016.

[3] R. E. Rosensweig, *Ferrohydrodynamics*. Courier Corporation, 2013.

[4] G. Karimi-Moghaddam, R. D. Gould, and S. Bhattacharya, "A Nondimensional analysis to characterize thermomagnetic convection of a temperature sensitive magnetic fluid in a flow loop," *Journal of Heat Transfer,* vol. 136, no. 9, 2014.

[5] M. Khairul, E. Doroodchi, R. Azizian, and B. Moghtaderi, "Thermal performance analysis of tunable magnetite nanofluids for an energy system," *Applied Thermal Engineering,* vol. 126, pp. 822-833, 2017.

[6] M. S. Pattanaik, V. Varma, S. Cheekati, G. Prasanna, N. Sudharsan, and R. V. Ramanujan, "A self-regulating multi-torus magneto-fluidic device for kilowatt level cooling," *Energy Conversion and Management,* vol. 198, p. 111819, 2019.

Chapter 8

Conclusions and Recommendations

This chapter is the summary of the present work stating the significant results of the thesis. We developed several magnetic cooling devices based on the principle of thermomagnetic convection of a ferrofluid and investigated their cooling performance, both experimentally and numerically. The cooling performance was investigated for a range of heat load temperatures, heat load power/heat flux values, magnet positions, and device parameters viz., thermal conductivity of the tube material, geometrical shape, form factor, and hybrid tube assembly. We also ranked various ferrites-, and metallic/alloy-based ferrofluids using numerical simulations as a function of their magnetic and thermophysical parameters. For the first time, we developed a multi-torus magnetic cooling device, which is capable of cooling kW level heat loads. We also developed and tested the performance of a 8 m magnetic cooling device based on single-phase thermomagnetic heat transfer for long distance thermal transport. The notable conclusions and major findings of this work are given in this chapter. Based on the obtained experimental and simulation results, the future perspective of this research work is discussed.

8.1 Summary

This section points out the major findings of this research work. The cooling performance of passive MC device governed by the principle of TMC of a ferrofluid was investigated for several MC devices. All the developed MC devices can cool the heat load significantly over a range of heat load power/power density and initial heat load temperatures. The main objective of the present work was to develop high performance MC devices, capable of large-scale cooling high power heat loads, and transfer the waste heat over longer distance. The work also experimentally and numerically optimized various device designs and position of the magnetic field application for enhanced cooling.

The first results focused on the development of a multi-torus magneto-fluidic cooling device to cool kW level heat loads. The permanent magnet position was optimized with respect to the thermal gradient to obtain maximum cooling performance. A 1 kW heat load with an initial heat load temperature of 580°C, was cooled down to 366°C. The performance of MC device was optimized with respect to the device parameters in the next chapter. The effect of various device parameters such as thermal conductivity of the tube, shape, form factor, and footprint of the MC device on the cooling performance was investigated. Further enhancement in cooling was achieved using hybrid MC device having greater thermal gradient interface points. The following chapter focused on the development and investigation of cooling performance of an 8 m long MC device for long range heat transfer. The effect of heat flux variation over a wide range on the heat load cooling was examined. The final chapter gave an insight into the effect of FF parameters on the heat lad cooling. Various ferrites- and metallic/alloy-based FF were ranked in accordance with their cooling performance.

Hence, the present research work provides a detailed cooling performance analysis of passive magnetic cooling devices for large-scale thermal transport to cool high-power heat loads and transfer the waste heat over a longer distance. The thesis also provides a comprehensive experimental and numerical analysis of the effect of device, and ferrofluid parameters on the enhanced cooling performance of a passive magnetic cooling device.

The important findings of the thesis are summarized below.

1. A multi-torus MC device based on TMC of a FF was designed, fabricated, and tested for waste heat removal from a heat load in the kilowatt level power range.
2. Cooling of 148°C was achieved at a heat load power of 0.5 kW, which increased to 214°C at 1 kW. Our device can operate at higher heat load power over greater lengths and higher fluid content because of the lower thermal resistance per unit length of the device and thermal resistance per unit volume of the fluid used.
3. Several MC devices of circular and racetrack shapes were developed using copper, silicone, and copper-silicone hybrid tubing to examine the effect of device properties and parameters on the TM cooling performance of the heat load. We developed and investigated the cooling performance of racetrack shaped MC device for the first time. The effect of copper tube percentage, and the heat load tube material in the hybrid MC device on the cooling was investigated.
4. The hybrid-25 MC device exhibited maximum cooling performance of 123°C due to enhanced thermal gradient, resulting in higher FF velocity. The cooling reduced with increasing copper percentage from 25% to 100%. However, the rate of cooling increased with increasing copper percentage. The all copper device exhibited cooling for all magnet positions along the device perimeter. However, the hybrid-50 device provided superior cooling when the magnet was placed near the heat load region and reduced to zero with increasing magnet distance from the heat load region.
5. A racetrack-shaped 8 m long MC device was developed. Our device is the longest MC heat pipe developed and tested so far, which utilizes a single-phase flow of FF to cool the heat load over a wide range of heat flux values. Heat load cooling of 41°C was obtained for heat flux and heat load temperature value of 8.85 kW/m^2 and 197°C, respectively. The surface temperature contours showed the effect of thermal boundary layer disruption on enhanced cooling performance.
6. The cooling performance of the TMC based MC device was numerically assessed with respect to the magnetic properties of various ferrite- and metallic/alloy-nanoparticle based FF. For the first time, we ranked the FF based on their TM cooling performance. The effect of bulk saturation magnetization, initial magnetic susceptibility, pyro magnetic coefficient, and the Curie temperature on the heat load

cooling was evaluated. Several ferrites- and metallic/alloy-based FF were simulated to investigate their TM cooling performance.

7. The bulk saturation magnetization significantly enhances the heat load cooling. Maximum cooling performance was obtained when the Curie temperature is near the heat load temperature.
8. For the case of thermophysical properties, viscosity significantly affected the heat load cooling. Cooling increases significantly for low viscous ferrofluid.
9. γ-Fe_2O_3, Fe_3O_4 and $CoFe_2O_4$ ferrite-based FF displayed higher heat load cooling performance. For the case of metallic/alloy-based ferrofluids, FeCo FF exhibited the best cooling performance followed by Fe and FeNi ferrofluids.

8.2 Future Work

The future perspectives of the present work are categorized according to the developed MC devices and the ranking of FF to further enhance the cooling performance of such devices.

8.2.1 Multi-torus magnetic cooling device

Multi-torus MC devices are capable of transferring waste heat from kW level heat loads due to their higher surface area of heat transfer and higher volume of FF. To further improve the performance, a detailed investigation of the flow behavior of FF is required at various regions of the flow channel with varying magnetic field position and strength. As the flow channels with lower inner diameter give rise to higher flow velocity, the performance of these multi-torus devices can be improved further by using flow tubes with lower internal diameter. To cool vertically oriented high-power heat loads, the individual flow loops can be stacked on top of each other, instead of joining them in concentric tori fashion, as in the present study. To further improve the capability of the device for even more high-power heat load cooling, multi-torus devices can be cascaded to one another. The performance of the multi-torus device can be enhanced by incorporating hybrid aspect, where high thermal conductivity tube materials can be used in the heat load and heat sink region to improve the conduction and convection heat transfer, respectively. **Figure 8.1** shows one possible potential application of the multi-torus MC device to cool large battery cabinets dissipating at higher power.

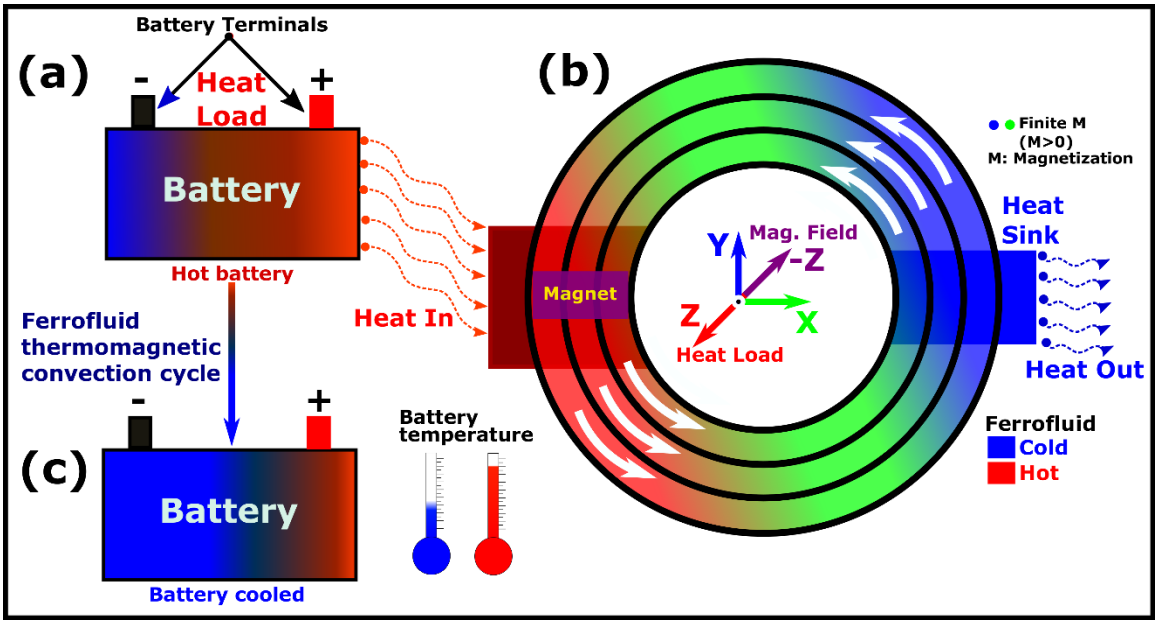

Figure 8.1. Potential application of the multi-torus magnetic cooling device for cooling a battery heat load, which is a three step process, (a) the waste heat transfer from the battery to the magnetic cooling device, (b) in presence of an external magnetic field, the thermomagnetic convection cycle starts and the ferrofluid carries the heat from the battery and rejects it at the heat sink region, (c) depending on the battery temperature, ferrofluid flow self-regulates, cooling the battery down to a safer working limit, enhancing its service life [1].

8.2.2 Racetrack magnetic cooling device

Racetrack MC device offers significantly lower device footprint with comparable performance in comparison to the circular MC device. The all copper racetrack MC device offers thermal gradient throughout the perimeter of the device. Hence, copper-based racetrack device could be used to cool magnetic field sensitive devices and systems. Hybrid device, on the other hand, could be effective in cooling magnetic field insensitive devices and systems. One of the potential applications of an all copper racetrack device is shown in **Figure 8.2**. The all copper racetrack device can also be incorporated inside an external cooling box, which can be attached to high speed gaming laptops for the waste heat removal. Racetrack shaped long MC device are capable of transferring the waste heat over longer distances. However, the cooling magnitude can be improved further by artificially generating local turbulence effect at the heat load region for higher amount of waste heat transfer. The all copper long racetrack device can be useful in cooling data servers owing

to the rapid increase in the market size with an estimated compound growth rate of 13.5% between the year 2019-2025 [2, 3]. The performance of long device in such applications can be further enhanced using multi-phase flow of FF, which involves latent heat.

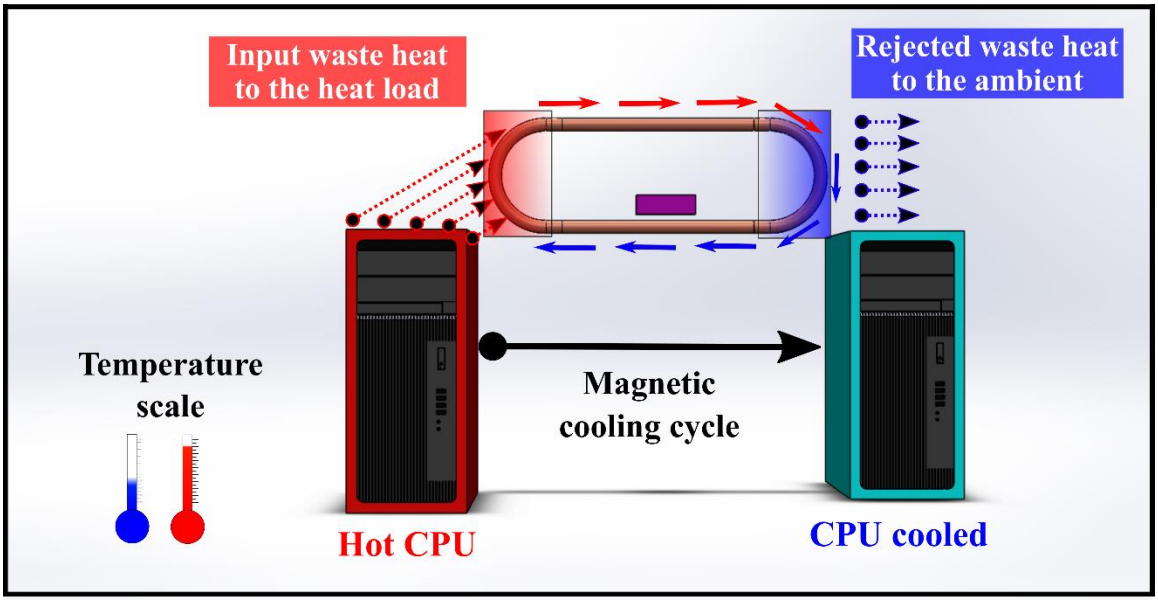

Figure 8.2. Potential application of an all copper magnetic cooling device for cooling of high-power CPUs. The magnet is kept at a farther distance from the magnetic field sensitive CPU because of the presence of thermal gradient region at any point along the device perimeter.

8.2.3 Ferrofluid performance

As evident from the results of Chapter 7 , FF with improved magnetic and thermophysical properties can improve the cooling performance of MC devices significantly.

8.2.3.1 Synthesis of ferrofluid with optimal magnetic properties

It can be inferred from the results of Chapter 7 that the saturation magnetization of the FF is the most significant magnetic parameter that improves the cooling. Metallic/alloy FF with higher saturation magnetization can improve the cooling. Moreover, these FF can enhance the cooling capacity of the MC device due to rapid heat transfer through the highly thermally conductive chains. It is difficult to prepare a stable FF from metallic/alloy nanoparticles due to their higher particle density as compared to ferrite nanoparticles. These nanoparticles tend to settle down under gravity. Hence, it is difficult to obtain a stable colloidal dispersion for practical application.

Earlier studies mostly used commercial ferrite FF for the MC systems. Very few reports investigated the effect of alloy based FF on TM cooling performance [4, 5]. However, synthesis of stable metallic/alloy-based FF with higher Ms and κ is still a challenge. Still there is scope to make stable metallic/alloy FFs for TM cooling. Bönnemann et al. [6] synthesized air stable iron and iron-cobalt FFs using thermolysis of carbonyl compounds of these metal ions under argon atmosphere. Controlled chemical synthesis can be performed under inert atmosphere followed by necessary heat treatments and surface capping to synthesize highly magnetic alloy-based FF.

8.2.3.2 Synthesis of ferrofluid with optimal thermophysical properties

Flow behavior and the cooling performance of a FF greatly depends on its thermophysical properties, such as viscosity and thermal conductivity. Low thermal conductivity is a major constraint for the development of reliable heat transfer fluids for industrial applications [7]. Several attempts have been made to prepare hybrid FF by increasing the thermal conductivity of the FF through the addition of highly conductive nanoparticles [7-11]. However, the extensive TM cooling performance analysis of hybrid FF based MC devices is still lacking. Highly thermal conductive materials such as graphene, reduced graphene oxide, carbon nanotubes, Al naopowder, and Cu nanopowder can be added to the FF to increase its thermal conductivity. However, the addition of these particles results in increasing the viscosity of the FF, which results in slight reduction in the cooling performance. Therefore, the volume fraction of highly thermal conductive materials need to be optimized for enhanced cooling performance. Similarly, a low viscous FF can improve the cooling by manifold. However, not much attempts have been made to play with the viscosity of FF. A stable low viscous FF even with lower saturation magnetization can provide higher heat load cooling than a high viscous FF with very high saturation magnetization.

8.3 Publications & Conferences

Following articles are related to the thesis work.

[1] **Pattanaik, M. S.**, Varma, V. B., Cheekati, S. K., Prasanna, G., Sudharsan, N. M., & Ramanujan, R. V. (2019). A self-regulating multi-torus magneto-fluidic device for kilowatt level cooling. Energy Conversion and Management, 198, 111819.

[2] Sharma, V., **Pattanaik, S.**, Parmar, H., & Ramanujan, R. V. (2018). Magnetocaloric properties and magnetic cooling performance of low-cost Fe 75− x Cr x Al 25 alloys. MRS Communications, 8(3), 988-994.

[3] Deepak, K., **Pattanaik, M. S.**, & Ramanujan, R. V. (2019). Figure of merit and improved performance of a hybrid thermomagnetic oscillator. Applied Energy, 256, 113917.

The research work was presented/accepted in the following conferences/summer schools/symposiums:

1. "Thermomagnetic Convection based Magnetic Cooling Heat Pipe for Long Distance Heat Transfer", **M. S. Pattanaik**, S. K. Cheekati, V. B. Varma, and R. V. Ramanujan, Oral presentation, INTERMAG 2020, Montreal, Canada.
2. "Ferrofluid Based Heat Transfer in a Kilowatt Level Thermomagnetic Cooling Device", **M. S. Pattanaik**, V. B. Varma, S. K. Cheekati, G. Prasanna, N. M. Sudarshan, and R. V. Ramanujan, Flash oral presentation, ICMAT 2019, Singapore.
3. "Ferrofluid Based Heat Transfer in a Kilowatt Level Thermomagnetic Cooling Device", **M. S. Pattanaik**, V. B. Varma, S. K. Cheekati, and R. V. Ramanujan, Poster presentation- "***Best poster award***", MRS Summer School 2019, Singapore.
4. "Multi-torus Magneto-fluidic Device for Kilowatt Level Cooling Applications", **M. S. Pattanaik**, V. B. Varma, S. K. Cheekati, G. Prasanna, and R. V. Ramanujan, Poster presentation- IEEE Magnetic Summer School 2019, Richmond, VA, USA.
5. "Self-regulating Kilowatt Level Magneto-fluidic Cooling", **M. S. Pattanaik**, V. B. Varma, S. K. Cheekati, G. Prasanna, and R. V. Ramanujan, Poster presentation- MRS Summer School 2018, Singapore.

6. "Self-regulating Magneto-fluidic Device for Large-scale Cooling Applications", **M. S. Pattanaik**, V. B. Varma, and R. V. Ramanujan, Oral presentation- "***Best presentation award***", IEEE Magnetic Symposium 2018, Singapore.
7. "Self-regulating Kilowatt Level Magneto-fluidic Cooling", **M. S. Pattanaik**, V. B. Varma, G. Prasanna, and R. V. Ramanujan, Poster presentation- Asia-Pacific Energy Conference-2018, Singapore.

References

[1] M. S. Pattanaik, V. Varma, S. Cheekati, G. Prasanna, N. Sudharsan, and R. V. Ramanujan, "A self-regulating multi-torus magneto-fluidic device for kilowatt level cooling," *Energy Conversion and Management*, vol. 198, p. 111819, 2019.

[2] K. Matthews. *The Future of Data Center Cooling: Five Trends to Follow*. Available: https://www.vxchnge.com/blog/the-future-of-data-center-cooling, [Accessed on: 30 July 2020].

[3] G. V. Research. *Data Center Cooling Market Size & Share Report, 2019-2025*. Available: https://www.grandviewresearch.com/industry-analysis/data-center-cooling-market, [Accessed on: 30 July 2020].

[4] V. Chaudhary and R. V. Ramanujan, "Magnetocaloric properties of Fe-Ni-Cr nanoparticles for active cooling," *Scientific reports*, vol. 6, no. 1, pp. 1-9, 2016.

[5] V. Sharma, S. Pattanaik, H. Parmar, and R. V. Ramanujan, "Magnetocaloric properties and magnetic cooling performance of low-cost Fe 75− x Cr x Al 25 alloys," *MRS Communications*, vol. 8, no. 3, pp. 988-994, 2018.

[6] H. Bönnemann *et al.*, "Air stable Fe and Fe Co magnetic fluids—synthesis and characterization," *Applied organometallic chemistry*, vol. 19, no. 6, pp. 790-796, 2005.

[7] S. U. Choi and J. A. Eastman, "Enhancing thermal conductivity of fluids with nanoparticles," Argonne National Lab., IL (United States)1995.

[8] M. H. Aghabozorg, A. Rashidi, and S. Mohammadi, "Experimental investigation of heat transfer enhancement of Fe2O3-CNT/water magnetic nanofluids under laminar, transient and turbulent flow inside a horizontal shell and tube heat exchanger," *Experimental Thermal and Fluid Science*, vol. 72, pp. 182-189, 2016.

[9] E. Sadeghinezhad *et al.*, "Experimental study on heat transfer augmentation of graphene based ferrofluids in presence of magnetic field," *Applied Thermal Engineering*, vol. 114, pp. 415-427, 2017.

[10] A. Shahsavar, M. Saghafian, M. Salimpour, and M. Shafii, "Experimental investigation on laminar forced convective heat transfer of ferrofluid loaded with carbon nanotubes under constant and alternating magnetic fields," *Experimental Thermal and Fluid Science*, vol. 76, pp. 1-11, 2016.

[11] A. Shahsavar, M. Salimpour, M. Saghafian, and M. Shafii, "An experimental study on the effect of ultrasonication on thermal conductivity of ferrofluid loaded with carbon nanotubes," *Thermochimica Acta*, vol. 617, pp. 102-110, 2015.